1987

Direct detection of optical radiation through a sampling orifice for inductively coupled plasma atomic emission spectroscopy

Bryant Robert LaFreniere
Iowa State University

INFORMATION TO USERS

While the most advanced technology has been used to photograph and reproduce this manuscript, the quality of the reproduction is heavily dependent upon the quality of the material submitted. For example:

- Manuscript pages may have indistinct print. In such cases, the best available copy has been filmed.
- Manuscripts may not always be complete. In such cases, a note will indicate that it is not possible to obtain missing pages.
- Copyrighted material may have been removed from the manuscript. In such cases, a note will indicate the deletion.

Oversize materials (e.g., maps, drawings, and charts) are photographed by sectioning the original, beginning at the upper left-hand corner and continuing from left to right in equal sections with small overlaps. Each oversize page is also filmed as one exposure and is available, for an additional charge, as a standard 35mm slide or as a 17"x 23" black and white photographic print.

Most photographs reproduce acceptably on positive microfilm or microfiche but lack the clarity on xerographic copies made from the microfilm. For an additional charge, 35mm slides of 6"x 9" black and white photographic prints are available for any photographs or illustrations that cannot be reproduced satisfactorily by xerography.

Order Number 8721902

Direct detection of optical radiation through a sampling orifice for inductively coupled plasma atomic emission spectroscopy

LaFreniere, Bryant Robert, Ph.D.

Iowa State University, 1987

U·M·I
300 N. Zeeb Rd.
Ann Arbor, MI 48106

PLEASE NOTE:

In all cases this material has been filmed in the best possible way from the available copy. Problems encountered with this document have been identified here with a check mark __✓__.

1. Glossy photographs or pages _____
2. Colored illustrations, paper or print _____
3. Photographs with dark background _____
4. Illustrations are poor copy _____
5. Pages with black marks, not original copy _____
6. Print shows through as there is text on both sides of page _____
7. Indistinct, broken or small print on several pages ✓
8. Print exceeds margin requirements _____
9. Tightly bound copy with print lost in spine _____
10. Computer printout pages with indistinct print _____
11. Page(s) _____ lacking when material received, and not available from school or author.
12. Page(s) _____ seem to be missing in numbering only as text follows.
13. Two pages numbered _____. Text follows.
14. Curling and wrinkled pages _____
15. Dissertation contains pages with print at a slant, filmed as received _____
16. Other _____

_____

_____

University
Microfilms
International

Direct detection of optical radiation through a sampling orifice for inductively coupled plasma atomic emission spectroscopy

by

Bryant Robert LaFreniere

A Dissertation Submitted to the
Graduate Faculty in Partial Fulfillment of the
Requirements for the Degree of
DOCTOR OF PHILOSOPHY

Department: Chemistry
Major: Analytical Chemistry

Approved:

Signature was redacted for privacy.
In Charge of Major Work

Signature was redacted for privacy.
For the Major Department

Signature was redacted for privacy.
For the Graduate College

Iowa State University
Ames, Iowa

1987

TABLE OF CONTENTS

CHAPTER I. INTRODUCTION†

Although inductively coupled plasma-atomic emission spectroscopy (ICP-AES) has become a powerful tool for trace analysis in the industrial analytical community, it has limitations for the determination of the nonmetal elements. The resonance lines of many of the nonmetals lie in the vacuum ultraviolet (VUV) region (<200 nm). Observation of these resonance lines with conventional instrumentation is complicated by absorption of radiation by oxygen in the atmosphere and by mirrors and/or windows employed in conventional optical transfer systems.

In this dissertation, a novel approach to observing the VUV lines excited in ICPs and the application of this approach to the detection and determination of those non-metallic and other elements whose resonance lines lie in the VUV region will be presented. Also included are the results of diagnostic studies of plasma excitation and ionization processes. The extension of ICP-AES analysis to the determination of nonmetals, metalloids, and/or selected metals in aqueous and gaseous samples will illustrate the value of this optical sampling approach for the detection of VUV radiation.

Table I was compiled to summarize the detection limits for the nonmetals and metalloids which have been reported for the emission spectra excited by Ar microwave-induced plasmas (MIP), He MIPs, He inductively coupled plasmas (ICP), afterglows, direct current plasmas (DCP), and Ar ICPs. The reader should refer to this table during subsequent discussion of the AES techniques listed above for the determination of nonmetals and

---

†Definitions of acronyms and abbreviations are given in Appendix A.

Table I. Detection limits of nonmetals by atomic emission spectroscopy with various emission sources

Mode of Sample Introduction	Elements	Wavelength (nm)	Detection Limit	Comments	Ref. #
Ar Inductively Coupled Plasma-Near Infrared-Atomic Emission Spectroscopy					
GC	Br I Cl I F I	700.57 725.67 634.85	200 μg 7 μg 1000 μg	First published accounts of the determination of these halogens by ICP-AES	(1)
Gaseous	N I N I	821.67 868.03	1 ppm (v/v) 300 ng	Continuous sample introduction 157 μL gas loop injection	(2)
Gaseous	O I	777.19	500 ng	10 μL sample volume	(3)
Gas Loop Injection	O I	777.19	25 ng	GC-ICP also reported	(4)
Gaseous	F I	685.60	350 ng 1000 ng	43 μL gas loop injection. GC-ICP-AES. Off center view.	(5)
Gas loop Injection (8 μL)	Br I Cl I	827.24 837.60	50 ng 50 ng	Observation height: 6 mm above load coil.	(6)
Gas loop Injection (8 μL)	S I C I	921.29 909.48	6 ng 130 ng	Observation height: 6 mm above load coil.	(7)
Pneumatic Nebulization	F I Cl I Br I	685.60 725.66 700.52	2000 μg mL^{-1} 100 μg mL^{-1} 500 μg mL^{-1}	First published F determination by solution nebulization with ICP-AES.	(8)
Pneumatic Nebulization	S I	921.7	20 μg mL^{-1}	10 % O_2/Ar mixture as plasma gas.	(9)

Table I. (Continued)

Mode of Sample Introduction	Elements	Wavelength (nm)	Detection Limit	Comments	Ref. #
Ar Inductively Coupled Plasma-Ultraviolet-Atomic Emission Spectroscopy					
Heated Injection Block w/ Split	B I	249.77	1 ng	Heated analyte transported with a 0.05 L min^{-1} flow of Ar and introduced into the plasma with makeup Ar gas for a total flow rate of ~0.9 L min^{-1}.	(10)
	C I	247.86	12 ng		
	I I	206.16	4 ng		
	P I	213.62	0.6 ng		
	S I	190.03	250 ng		
	Si I	251.61	0.8 ng		
Pneumatic Nebulization	P I	213.62	16 ng mL^{-1}	Ar purge, VUV lines also observed. Steel analyses.	(11)
	B I	249.77	3 ng mL^{-1}		
Pneumatic Nebulization	B I	249.77	4.8 ng mL^{-1}	- - - -	(12)
	Bi I	223.06	34 ng mL^{-1}		
	Ga I	294.36	46 ng mL^{-1}		
	Ge I	209.43	40 ng mL^{-1}		
	In II	230.61	63 ng mL^{-1}		
	P I	213.62	76 ng mL^{-1}		
	Sb I	206.83	32 ng mL^{-1}		
	Si I	251.61	12 ng mL^{-1}		
	Te I	214.28	41 ng mL^{-1}		
Pneumatic Nebulization	P I	214.9	60 ng mL^{-1}	HPLC-ICP also attempted.	(13)
	C I	247.8	200 ng mL^{-1}		
	Se I	203.9	80 ng mL^{-1}		
Ultrasonic Nebulization	B I	208.95	16 ng mL^{-1}	Side-arm tube purge (Ar)	(14)
	I I	206.16	920 ng mL^{-1}		
	P I	213.62	6 ng mL^{-1}		

Table I. (Continued)

Mode of Sample Introduction	Elements	Wavelength (nm)	Detection Limit	Comments	Ref. #
Ar Inductively Coupled Plasma-Vacuum Ultraviolet-Atomic Emission Spectroscopy					
Pneumatic Nebulization	As I	189.04	13 ng mL^{-1}	Optical path extension tube purged with Ar. Fused silica refractor plate and PMT window.	(15)
		193.76	25 ng mL^{-1}		
	B I	182.64	3 ng mL^{-1}		
	Bi II	190.24	60 ng mL^{-1}		
	Br I	163.34	3000 ng mL^{-1}		
	Ge II	164.92	50 ng mL^{-1}		
	I I	178.28	50 ng mL^{-1}		
	P I	177.50	15 ng mL^{-1}		
	S I	180.73	15 ng mL^{-1}		
	Se I	196.09	30 ng mL^{-1}		
	Si I	185.07	30 ng mL^{-1}		
	Tl II	190.86	35 ng mL^{-1}		
Pneumatic Nebulization	As I	193.76	53 ng mL^{-1}	- - - -	(12)
	Se I	196.03	75 ng mL^{-1}		
	Tl II	190.86	40 ng mL^{-1}		
Ultrasonic Nebulization	As I	193.76	2 ng mL^{-1}	- - - -	(16)
	Se I	196.09	40 ng mL^{-1}		
Pneumatic Nebulization	As I	189.04	110 ng mL^{-1}	Side-arm tube and monochromator purged with Ar.	(17)
		193.76	160 ng mL^{-1}		
	Br I	154.07	800 ng mL^{-1}		
	Cl I	134.72	6000 ng mL^{-1}		
	I I	178.28	200 ng mL^{-1}		
	P I	177.50	60 ng mL^{-1}		
	S I	180.73	50 ng mL^{-1}		
	Se I	196.09	200 ng mL^{-1}		

Table I. (Continued)

Mode of Sample Introduction	Elements	Wavelength (nm)	Detection Limit	Comments	Ref. #
Pneumatic Nebulization	S I	182.04	2000 ng mL^{-1}	Glass side-arm tube purged with N_2, silica lens.	(18-19)
	P I	185.92	400 ng mL^{-1}		
	I I	183.04	800 ng mL^{-1}		
	Hg I	184.96	1 ng mL^{-1}		
	As I	193.69	100 ng mL^{-1}		
	Se I	196.09	110 ng mL^{-1}		
Ultrasonic Nebulization	As I	189.04	15 ng mL^{-1}	Side-arm tube purged with Ar.	(14)
		193.76	5 ng mL^{-1}		
	S I	182.04	3000 ng mL^{-1}		
	Se I	196.09	40 ng mL^{-1}		
	Tl II	190.86	10 ng mL^{-1}		
Pneumatic Nebulization	As I	189.04	13 ng mL^{-1}	Polychromator under vacuum; Ar purge tube employed.	(20)
	B I	182.64	6 ng mL^{-1}		
	I I	178.28	16 ng mL^{-1}		
	P I	177.50	8 ng mL^{-1}		
	S I	180.73	24 ng mL^{-1}		
Pneumatic Nebulization	As I	189.04	15 ng mL^{-1}	HPLC-ICP also attempted.	(13)
	S I	180.73	60 ng mL^{-1}		
Pneumatic Nebulization	As I	189.04	70 ng mL^{-1}	- - - -	(21)
	P I	178.3	53 ng mL^{-1}		
	S I	180.73	4 ng mL^{-1}		
Pneumatic Nebulization	Cl I	133.57	10000 ng mL^{-1}	Optical path extension evacuated and purged with Ar.	(8)
	Br I	163.34	3000 ng mL^{-1}		
	I I	178.28	50 ng mL^{-1}		
Pneumatic Neb.	Br,I	?	500 ng mL^{-1}	Abstract did not specify lines.	(22)

Table I. (Continued)

Mode of Sample Introduction	Elements	Wavelength (nm)	Detection Limit	Comments	Ref. #
Pneumatic Nebulization	Ge II In II	164.92 158.64	10 ng mL^{-1} 3 ng mL^{-1}	N_2 purge	(23)
Pneumatic Nebulization	S I	180.73	50 ng mL^{-1}	N_2 purge	(24)
Pneumatic Nebulization	S I	180.7	10 ng mL^{-1}	- - - -	(25)
Hydride Generation	As Se Sb	? ? ?	0.3 ng mL^{-1} 0.3 ng mL^{-1} 0.8 ng mL^{-1}	- - - -	(26)
Ar Microwave Induced Plasma-Emission Spectroscopy					
GC	I I Br II Cl (Cl_2)	206.2 470.5 256	22.4 ng 159 ng 42 ng	Atmospheric pressure Ar MIP at 80 W.	(27)
Pneumatic Nebulization	Various Metal-loids	Various	sub-ppm	- - - -	(28)
Br_2 Generation	Br (Br_2)	291	50 ng	Br_2 generated by addition of $K_2Cr_2O_7$ in conc. H_2SO_4.	(29)

Table I. (Continued)

Mode of Sample Introduction	Elements	Wavelength (nm)	Detection Limit	Comments	Ref. #
He Microwave Induced Plasma-Atomic Emission Spectroscopy					
GC	Br II	478.55	20 pg s^{-1}	Low pressure He-MIP	(30)
	Cl II	479.45	60 pg s^{-1}		
	I II	533.82	50 pg s^{-1}		
	P I	253.57	9 pg s^{-1}		
	S II	545.38	50 pg s^{-1}		
GC	C I	247.86	80 pg s^{-1}	Low pressure He-MIP; FID also used for atomic ratios	(31)
	H I	486.13	30 pg s^{-1}		
	D I	656.10	90 pg s^{-1}		
	F I	685.60	60 pg s^{-1}		
	Cl II	479.45	60 pg s^{-1}		
	Br II	470.49	91 pg s^{-1}		
	I II	516.12	50 pg s^{-1}		
	S II	545.39	90 pg s^{-1}		
	N I	746.88	2900 pg s^{-1}		
	O I	777.19	3000 pg s^{-1}		
Injection into an Exponential Dilutor	C I	193.1	0.4 pg s^{-1}	First analytical results from an atmosphere pressure He-MIP.	(32)
	H I	486.1	2 pg s^{-1}		
	Cl II	479.5	7 pg s^{-1}		
	Br II	470.5	5 pg s^{-1}		
	I II	516.1	3 pg s^{-1}		
	S II	545.4	25 pg s^{-1}		

Table I. (Continued)

Mode of Sample Introduction	Elements	Wavelength (nm)	Detection Limit	Comments	Ref. #
Injection into an Exponential Dilutor	C I	247.86	350 pg s^{-1}	Low pressure He-MIP for determination of elemental ratios of organic compounds.	(33)
	Cl II	479.45	1000 pg s^{-1}		
	Br II	470.49	1800 pg s^{-1}		
	I II	516.12	1400 pg s^{-1}		
	S II	545.38	7200 pg s^{-1}		
	C I	247.8	7 to 50 pg s^{-1}	Beenakker cavity used.	(33)
	Cl II	479.5	150 to 230 pg s^{-1}		
	S I	190.0	140 pg s^{-1}		
Gaseous	C I	247.9	8 pg s^{-1}	New low-flow, laminar flow torch for atmospheric pressure He-MIP; polychromator; plasma power: 80 W.	(34)
	H I	656.3	4.9 pg s^{-1}		
	Br II	470.5	62 pg s^{-1}		
	Cl II	479.5	40 pg s^{-1}		
	F I	685.6	3.6 pg s^{-1}		
Br_2 Generation	Br II	470.5, 478.6	1000 pg	130 W He-MIP; electrothermal vaporization also employed.	(35)
GC	Br II	470.5	33 pg s^{-1}	45 to 75 W He-MIP	(36)
	Cl II	479.5	43 pg s^{-1}		
	F I	685.5	20 pg s^{-1}		
	I I	206.2	21 pg s^{-1}		
	C I	247.9	2.7 pg s^{-1}		
	P I	253.6	3.3 pg s^{-1}		
	As I	228.8	6.5 pg s^{-1}		
	Se I	204.0	5.3 pg s^{-1}		

Table I. (Continued)

Mode of Sample Introduction	Elements	Wavelength (nm)	Detection Limit	Comments	Ref. #
GC	H I	656.28	6.2 pg s^{-1}	Atmospheric pressure He-MIP at 75 W.	(37)
	C I	193.09	8.8 pg s^{-1}		
	F I	685.60	1.8 pg s^{-1}		
	Cl II	479.45	5.4 pg s^{-1}		
	Br II	470.49	6.3 pg s^{-1}		
	I I	206.24	6.6 pg s^{-1}		
	S II	545.39	39 pg s^{-1}		
GC	C I	247.96 x 2	2.4 pg s^{-1}	Atmospheric pressure He-MIP at 60 to 70 W.	(38)
	H I	656.3	6.0 pg s^{-1}		
	Cl II	479.5	56 pg s^{-1}		
GC	F I	685.6	36 pg s^{-1}	Atmospheric pressure He-MIP at 75 W; gas purge and trap method also employed.	(39)
	Cl II	479.5	32 pg s^{-1}		
	Br II	470.5	28 pg s^{-1}		
	I I	206.2	6.7 pg s^{-1}		
GC	F I	685.6	7.5 pg s^{-1}	Atmospheric pressure He-MIP at 75 W.	(40)
GC	Br II	478.5	98 to 380 pg s^{-1}	He-MIP at 50 to 60 W; rapid scanning spectrometer and polychromator were employed.	(41)
	Cl II	479.5	53 to 150 pg s^{-1}		
GC	C I	247.9	700 pg s^{-1}	Tangential flow torch with atmospheric pressure He-MIP at 115 W	(42)
	S ?	469.4	10000 pg s^{-1}		
	Br II	478.5	40000 pg s^{-1}		

Table I. (Continued)

Mode of Sample Introduction	Elements	Wavelength (nm)	Detection Limit	Comments	Ref. #
GC	C I	247.86 x 2	200 pg s^{-1}	Low pressure He-MIP	(43)
	H I	486.13	200 pg s^{-1}		
	D I	656.1	10 pg s^{-1}		
	O I	777.19	3000 pg s^{-1}		
	N I	746.88	4000 pg s^{-1}		
	F I	685.6	200 pg s^{-1}		
	Cl II	479.45	100 pg s^{-1}		
	Br II	470.49	300 pg s^{-1}		
	I II	516.12	100 pg s^{-1}		
	S II	545.39	200 pg s^{-1}		
	P I	253.56 x 2	120 pg s^{-1}		
	Hg ?	365.0 x 2	50 pg s^{-1}		
GC	C I	247.9	76 pg s^{-1}	He-MIP at 190 W	(44)
	Cl II	479.5	120 pg s^{-1}		
	H I	656.3	50 pg s^{-1}		
GC	C I	247.9	30 pg s^{-1}	Tangential flow torch; 115 W	(45)
	I II	516.6	150 pg s^{-1}		
	P I	253.6	300 pg s^{-1}		
GC	C I	247.9	8 pg s^{-1}	New laminar flow, atmospheric pressure He-MIP; polychromator; partial empirical formulae of pyrethroids and dioxins.	(46)
	H I	656.3	5 pg s^{-1}		
	Br II	470.5	62 pg s^{-1}		
	Cl II	479.5	40 pg s^{-1}		
	F I	685.6	4 pg s^{-1}		
GC	Cl II	481.0	5 pg s^{-1}	Atmospheric pressure He-MIP; packed and capillary GC used.	(47)
	P I	214.9	0.3 pg s^{-1}		
	Br II	478.6	- -		
	S II	216.9	50 pg s^{-1}		

Table I. (Continued)

Mode of Sample Introduction	Elements	Wavelength (nm)	Detection Limit	Comments	Ref. #
GC & TLC	F I Cl II	685.6 479.5	95 pg s^{-1} 105 pg s^{-1}	30 W He-MIP	(48)
Chemical Vapor-ization from aqueous soln.	Cl II Br II	479.5 478.6	0.2 $\mu g\ mL^{-1}$ 0.3 $\mu g\ mL^{-1}$	500 W He-MIP; halogen converted to hydrogen halide	(49)
Pneumatic Nebulization	Cl II	479.5	7 $\mu g\ mL^{-1}$	500 W He-MIP	(50)
Pneumatic Nebulization	Cl II Br II I I	479.45 478.55 206.16	2 $\mu g\ mL^{-1}$ 60 $\mu g\ mL^{-1}$ 7 $\mu g\ mL^{-1}$	480 W He-MIP	(51)
Ultrasonic Nebulization	Cl II Br II I I	479.45 478.55 206.16	0.4 $\mu g\ mL^{-1}$ 3 $\mu g\ mL^{-1}$ 0.8 $\mu g\ mL^{-1}$	480 W He-MIP; large matrix effects	(51)
He Inductively Coupled Plasma-Atomic Emission Spectroscopy					
Gaseous	Cl	- -	ng mL^{-1} range for volatile organic chloride	Reduced pressure He-ICP at < 300 W.	(52)
Ultrasonic Nebulization	Cl I Br I	725.67 734.85	13 $\mu g\ mL^{-1}$ 18 $\mu g\ mL^{-1}$	Improvement in LODs of 63- and 34-fold for Cl and Br, respectively, in comparison to Ar-ICP; 1 kW power; 57 L min^{-1} He gas required to sustain plasma.	(53)

Table I. (Continued)

Mode of Sample Introduction	Elements	Wavelength (nm)	Detection Limit	Comments	Ref. #
Ultrasonic Nebulization	Br I	827.24	5 μg mL^{-1}	Only 8 L min^{-1} He required to sustain plasma.	(54)
Afterglows with Subsequent Detection by Emission Spectroscopy					
Hydride generation or direct introduction into N_2-APAG	Br (Br_2)	674.2	5 ng s^{-1}	Molecular bands used for non-metal detection	(55)
	Cl (NCl)	664.6	30 ng s^{-1}		
	S (S_2)	374.0	5 ng s^{-1}		
	I I	183.0	10 ng s^{-1}		
GC w/ Ar-APAG	P I	213.6	0.04 ng	80 W; organic compounds determined	(56)
	S I	182.0	0.1 ng		
	C I	193.1	0.1 ng		
	I I	183.0	0.5 ng		
	Cl I	725.6	2 ng		
	Br I	734.9	10 ng		
GC w/ He-APAG	F I	739.9	20 pg	45 W	(57)
	Cl I	837.6	8 pg		
	Br I	827.2	15 pg		
	I I	183.0	2 pg		
	C I	193.1	10 pg		
	P I	253.5	30 pg		
	S I	182.0	5 pg		
	As I	189.0	20 pg		
	Hg I	253.6	0.5 pg		

Table I. (Continued)

Mode of Sample Introduction	Elements	Wavelength (nm)	Detection Limit	Comments	Ref. #
Direct Current Plasma-Atomic Emission Spectroscopy					
Aqueous Nebulization	Hg II Se I As I I I P I S I	184.96 196.09 228.81 183.04 213.62 180.7	0.1 $\mu g\ mL^{-1}$ 1 $\mu g\ mL^{-1}$ 0.2 $\mu g\ mL^{-1}$ 4 $\mu g\ mL^{-1}$ 0.1 $\mu g\ mL^{-1}$ 0.5 $\mu g\ mL^{-1}$	Ar purge system; S determination in organic solvents yielded LODs of 1 to 15 $\mu g\ mL^{-1}$	(58)
Aqueous Nebulization	Hg II Se I As I S I P I I I C I	184.96 196.09 193.69 180.7 185.92 183.04 165.69	0.1 $\mu g\ mL^{-1}$ 1 $\mu g\ mL^{-1}$ 0.2 $\mu g\ mL^{-1}$ 0.05 $\mu g\ mL^{-1}$ 0.4 $\mu g\ mL^{-1}$ 2 $\mu g\ mL^{-1}$ 5 $\mu g\ mL^{-1}$	Ar purge between plasma and monochromator	(59)
H_2S Generation	S I	180.7	10 ng	Ar purge system; inorganic sulfur reduced to H_2S.	(60-61)
GC	S I	180.7	5 to 10 ng	Organic sulfur into GC.	(61)
GC	S I	180.7	300 pg s^{-1}	Ar purge system.	(62)

metalloids. The detection limits obtained by the work accomplished in this dissertation have been compared to the ICP-VUV-AES literature in Chapter III. The compilation of detection limits is not all inclusive, but represents an overview of nonmetal, metalloid, and selected metals determinations with a plasma or afterglow emission source and subsequent emission spectroscopic detection.

Detection of Nonmetals by Argon Inductively Coupled Plasma-Atomic Emission Spectroscopy (ICP-AES)

Conventional ICP-AES

Inductively coupled plasma-atomic emission spectroscopy was initiated with the landmark papers of R. Wendt and V. A. Fassel (63) at the Ames Laboratory and S. Greenfield et al. (64) in Britain in the 1960s. The plasma is comprised of Ar gas, raised to a high temperature, with a significant fraction of its atoms ionized. A schematic diagram of an ICP, within the confines of a quartz torch, is shown in Figure 1A. A high frequency current flows through the induction coil. Oscillating magnetic fields are generated and their lines of force are axially oriented inside the coil. These induced magnetic fields cause charged particles within the coil to flow in closed annular paths, which result in collisions that release energy (which in some way provide for analyte interaction and excitation). The primary Ar flow (plasma gas) sustains the plasma, cools the quartz walls, and creates the doughnut-shape configuration of the plasma. The auxiliary Ar flow prevents meltdown of the inner tube of the plasma torch. The nebulizer gas flow (also called the aerosol gas) transports the sample (analyte) into the center of the plasma, which is called the axial channel (the hole in the doughnut-shaped plasma). As the

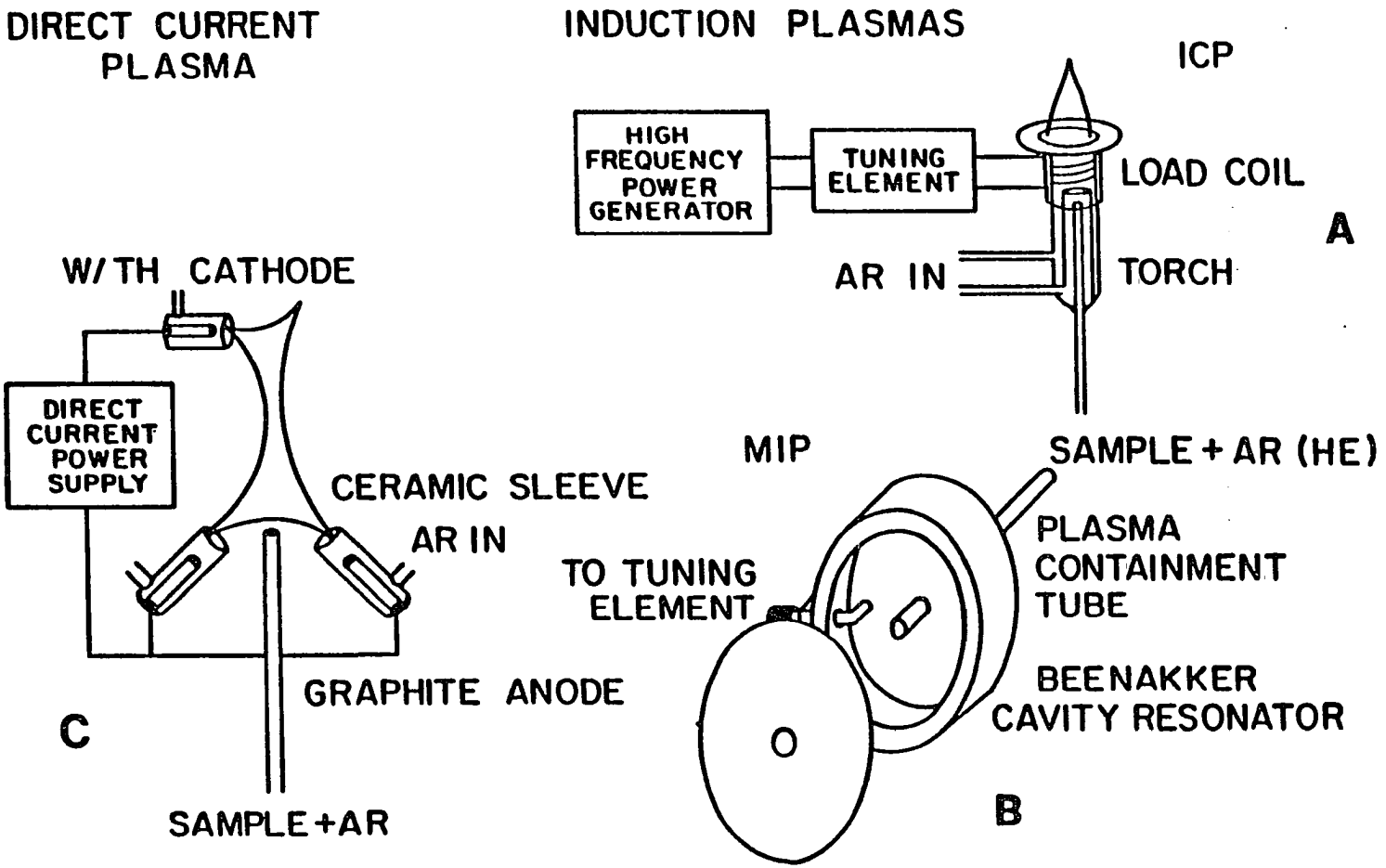

Figure 1. Plasma sources for emission spectroscopy
(A) inductively coupled plasma, ICP; (B) microwave induced plasma, MIP; (C) direct current plasma, DCP (Figure reprinted from Reference 65)

analyte flows through the axial channel, it is vaporized, atomized, excited, and/or ionized and the resulting atom or ion emits light at its characteristic wavelengths. Sample can be introduced into the ICP as a liquid, gas, or solid. The two most popular methods of introduction for liquids are pneumatic and ultrasonic nebulization. These nebulization techniques will be discussed later in the experimental section. Gases can be directly introduced into the nebulizer gas flow stream and then into the axial channel of the ICP. One way in which solids are introduced into the ICP is by sweeping the atoms generated by a graphite furnace into the ICP. Generally, liquid samples comprise greater than 90% of all analyses. A historical aspect of ICP-AES can be found elsewhere (66).

From 1965 to the present day, ICP-AES has made great strides as a useful analytical method for the determination of metals. The optical detection systems for conventional ICP-AES usually consist of a lens that focuses an image of the vertically oriented plasma upon the entrance slit of a spectrometer. The line emission from the ICP continues through the spectrometer to the detector. The spectrometer can either be a polychromator, in which many analytical lines are detected simultaneously, or a monochromator, in which the grating is adjusted so that a particular line of interest is detected. A lens is usually necessary in order to maximize the collection of light from a particular volume of the plasma. A similar collection efficiency can be obtained without lenses by the placement of the plasma close to the entrance slit, but the configuration, intense heat, and electrical characteristics of the ICP make this placement a difficult task. The mathematical treatment of light collection will be discussed later in order to clarify the above discussion.

The commonly viewed wavelength regions in ICP-AES are the ultraviolet (UV) and visible (VIS) regions, because most of the metallic elements in the periodic table have their prominent lines in these regions. Unfortunately, the ICP does not possess the same analytical figures of merit for nonmetals. Although the near infrared (NIR) region is easily accessible with ICR-AES, the nonmetal emission lines in this region are usually too weak for trace analysis. The nonmetals, especially the halogens, have their most intense analytical lines in or near the VUV region, usually defined as the wavelength region from 10 to 200 nm.

Windsor and Denton (10) have employed the UV lines for the determination of B, C, H, I, P, S, and Si in the ICP. Limits of detection (LODs) were in the ng range. As a logical follow-up of their previous work, Windsor and Denton (1) reported a GC-ICP-AES system that allowed for the detection of the IR lines of halogens that were introduced into the plasma. Detection limits for Br, Cl, and F were 200, 7, and 1000 μg, respectively. Although these LODs were poor, the work of Windsor and Denton was one of the first published accounts of the determination of these halogens by ICP-AES.

Fry and associates have published a series of papers (2-7,67-69) on the detection and tabulation of nonmetal emission lines in the infrared (IR) region emitted by an Ar ICP. Their studies were limited to low observation heights (<=6 mm above the load coil), low sample carrier gas flow rates (usually < 0.3 L min^{-1}), small sample gas flow rate of < 100 mL min^{-1}, and analysis of gaseous samples only. Off center viewing was employed for nitrogen (2) and fluorine detection (5). Detection limits of 50, 50, 6, and 130 ng were achieved for Br, Cl, S, and C, respectively (6,7). The LODs for Br and Cl were 2 to 4 orders of magnitude better than

those reported by Windsor and Denton (1). Hughes et al. (68) employed a photodiode array detector for the determination of C, H, N, and O at a 6 mm observation height. Instrumental modifications made more efficient use of the photodiode array for the determination of C, H, N, and O (67) and F, Cl, Br, I, and S (69). These latest determinations took advantage of the optimum emission observed between the top 2 turns of the load coil. Also, studies of the IR region coupled with detection by Fourier transform spectroscopy (FTS) with an Ar ICP source have been accomplished (70,71). In general, the maximum emission from the nonmetals occurred at an observation height that was within the turns of the load coil, but most of Fry's work used an observation height that was a few mm above the load coil due to the inability of their optical configuration to fully sample the emission between the turns of the load coil.

Nygaard et al. (8) observed the IR emission lines of F, Cl, and Br in an Ar ICP after introduction of solutions of the potassium salts of these elements by pneumatic nebulization. Detection limits were 2000, 100, and 500 $\mu g\ mL^{-1}$ for F, Cl, and Br, respectively. These results were the only ones published on the detection of halogens by ICP-IR-AES with pneumatic nebulization and the only report of a detection limit value for a F I emission line with aqueous sample introduction into an Ar ICP.

Mautz et al. (72) introduced various gaseous nonmetallic species into an Ar ICP. Many atomic and molecular emission lines and bands were observed but no LODs were listed. Stubley and Horlick (9) have also studied the NIR region for the spectral emission characteristics of Ar, N, C, O, and S.

ICP-vacuum ultraviolet (VUV)-AES

There are some advantages to the employment of the VUV region rather than the near IR for AES. One advantage is that the sensitivity of the VUV lines is superior to the IR lines due to the higher transition probabilities and lower excitation energies for the VUV with respect to the IR lines. Secondly, the background intensity is lower in the VUV than the IR region. The combination of the increased sensitivity of the VUV lines and the lower background intensity associated with the VUV region should therefore enhance the detectability of the nonmetals, metalloids, and selected metals in the VUV region. If the VUV region could be made accessible for Ar ICP-AES studies, all of the elements in the periodic table, except Ar, He, and Ne, could be detected at trace levels, barring impurities in the plasma gas and/or contamination in samples.

Unfortunately, the observation of spectra in the VUV region poses several problems. First, because oxygen absorbs optical radiation below about 180 nm, air must be eliminated from the optical path between the ICP and the detector. Evacuation of the optical path to the ICP is not practical, but purging with a VUV transparent noble gas can eliminate the air present in the optical path. Second, there is no known window or lens material, with any significant thickness (i.e., excluding thin metal films), that is sufficiently transparent in the 50 to 108 nm region. The common window materials used in the VUV region are LiF, MgF_2, CaF_2, sapphire, and fused quartz whose lower transparency limits are 108, 115, 122, 145, and 155 to 185 nm, respectively (73). These materials leave the analyst with few choices in the construction of an optical system. An obvious solution to these problems is to utilize an illumination system without lenses or windows in which the total optical path is filled with a

transparent noble gas, such as helium, which is transparent down to 58 nm. This gas is also chemically inert, nonflammable, and has no atomic emission lines in the VUV region above 58 nm. Such a system will be described later.

The choices of detectors that are useful in the VUV region are also limited. Two VUV detectors that are reported extensively in the literature are the solar blind photomultiplier tube (PMT) and the wavelength-shifter-PMT combination.

Because there is no known solid that can transmit light below 110 nm, no window on a conventional PMT detector is suitable for transmission of light below this wavelength. Either a windowless detector or a means to transfer radiation through an opaque surface is needed. If windowless detectors are considered, such as an electron multiplier, one must be aware of exposure to the air, vacuum, or inert gas during the analysis along with damage done by the consecutive vacuum and atmospheric pressure exposures. Lincke (74) mentioned a fluorescence-sensitized photomultiplier tube as a detector for VUV radiation below 105 nm. This PMT can be called a wavelength shifter-PMT combination. An fluorescent organic molecule was coated on a glass plate and placed on a PMT window. The material was irradiated by wavelength-resolved VUV photons and fluoresced in the visible region of 380 to 530 nm, thereby "converting" VUV radiation into visible light that is transmitted through the glass plate. The fluorescence spectrum was registered at the conventional PMT with a current output proportional to the VUV radiation from the source. The wavelength-shifter-PMT combination will be denoted as scintillator PMT throughout this dissertation.

Kumar and Datta (75) compared the two common scintillators, sodium salicylate and p-terphenyl, for VUV work. Although sodium salicylate has been the choice of the majority of VUV spectroscopists, Kumar and Datta found that p-terphenyl had a higher absolute fluorescent efficiency than sodium salicylate and was not hygroscopic like sodium salicylate. Thus it appears that a choice of two good scintillators for VUV work is available, but use of sodium salicylate dominates the literature.

The other choice for a VUV detector is a solar blind PMT. The solar blind PMT is relatively insensitive to radiation above 300 nm due to the higher work function of the photocathode material with respect to the photocathodes used for PMTs in the visible region. The higher work function of the photocathode material results in a very low dark current because detection of stray, visible light is prevented. Therefore, much weaker UV radiation can be detected by the solar blind PMT with respect to the scintillator PMT. The window material of the solar blind PMT dictates the low wavelength limit, whereas there is no lower wavelength limit for the scintillator PMT.

The first reported observation of VUV lines from an ICP occurred in 1972, when Kirkbright et al. (18,19) employed an ICP source for atomic emission spectrometry in the VUV region for the elements S, P, I, Hg, As, and Se. Detection limits were 2, 0.4, 0.8, 0.001, 0.1, and 0.11 $\mu g\ mL^{-1}$, respectively, for those elements. The apparatus consisted of a side arm perpendicular to the plasma (an air gap exists between the torch and sidearm) and fused silica lenses to focus the radiation. The side arm, which was connected to the monochromator, was purged with nitrogen to eliminate absorption of oxygen. This arrangement permitted observations

in the spectral region of 170 to 200 nm, the low wavelength limit being due to absorption by fused silica.

In 1975, Wohlers et al. (17) constructed a special plasma torch that eliminated the air gap associated with that of Kirkbright et al. (18). The special plasma torch had a side arm that was attached to the monochromator, and focused radiation with a MgF_2 lens. The entire optical path was purged with Ar from the plasma to the photomultiplier tube. Wohlers observed slightly superior detection limits than Kirkbright for S, P, and I and comparable detection limits for As and Se. Wohlers recorded spectra down to 115 nm, which enabled him to detect Br and Cl emission lines. His LODs for Br and Cl of 0.8 and 6 $\mu g\ mL^{-1}$, respectively, were the best LODs for pneumatic nebulization of these halogens in ICP-AES until the work accomplished in this dissertation.

In 1980, Denton et al. (76) designed an experimental apparatus similar to Wohlers et al. (17) in which an ICP torch had a side arm connected to a VUV spectrometer. Denton used CaF_2 windows that limited his studies to greater than 120 nm. The optical path from the CaF_2 window and the plasma was purged with He instead of Ar, because helium had a greater optical transparency. Denton appeared to be the first to publish a study of the resonance lines of O, N, C, S, Cl, and Br from an ICP-VUV system for wavelengths as low as 120 nm. Denton found many VUV lines for the nonmetals, but did not perform any trace analysis studies.

Nygaard et al. (11), of Allied Analytical Systems (now Thermo-Jarrell Ash), applied a commercial ICP instrument (IL Plasma-200) to the detection of P, B, and S in the analysis of steel. An optical path extension from the vacuum monochromator was placed so its end was flushed with the inside diameter of the outer tube of the ICP torch. The extension arm was purged

with Ar gas. The monochromator was evacuated and purged with Ar. Nygaard and coworkers (8) extended their work to Br, Cl, and I. They stated that a CaF_2 lens was used between the extension arm and monochromator, reflecting surfaces were coated with MgF_2, and the refractor plate and window at the PMT were fabricated from fused silica. With this system, VUV radiation below 160 nm could not be detected. Improvements in the LOD for Br and Cl due to the utilization of VUV instead of NIR emission lines were 170-fold for Br and 10-fold for Cl. The LODs for Br, Cl, and I were 3, 10, and 0.05 $\mu g\ mL^{-1}$ for their VUV lines, respectively. These detection limits for Br and Cl had been the best published values for ICP-AES with aqueous nebulization prior to the work that is stated in this dissertation. An extensive atlas of emission lines by element and wavelength from 160 to 200 nm has been compiled by Nygaard and Leighty (15). Relative intensities for each line and approximate LODs for the significant lines were stated alongside the corresponding emission lines.

Recently, Carr and Blades (77) were the first to describe an ICP-spectrometer system capable of observing radiation down to 85 nm. A direct He gas path, without windows and/or lenses, from the plasma through the spectrometer and to the detector enabled these investigators to observe radiation down to 85 nm. Radiation transfer from the plasma to the spectrometer was accomplished via a 40 cm long sidearm extension to the ICP torch that effectively coupled the plasma to the entrance slit of the monochromator. According to Carr and Blades, plasma emission from the 5 to 25 mm region above the load coil entered the monochromator. A scintillator PMT was used as the detector. The Ar I resonance lines and ICP background spectra from 90 to 195 nm with and without aqueous aerosol introduced into the axial channel were observed. No LODs were reported.

Most of the work performed in the NIR region involved the analysis of gases. The enhanced detectability of the nonmetals, metalloids, and selected metals in the VUV allowed trace analysis to be performed on aqueous samples. Undoubtedly, the VUV region is the choice for nonmetal analysis, although the obstacles to the construction of an optical detection system that observes VUV radiation need to be overcome.

Detection of Nonmetals by Other AES Techniques

Microwave induced plasma (MIP)

An introduction into this spectroscopic source can be found in Carnahan (78) and a schematic drawing of a MIP is shown in Figure 1B. Briefly, power is transferred from a generator to the plasma and plasma containment device (at 2450 MHz) through a coaxial cable. A tuning device is usually needed to match the impedance of the load to the generator. The plasma containment device, i.e., the cavity resonator, maintains a standing electromagnetic wave with the maximum electric field situated in the center of the cavity and oriented perpendicular to the face of the plasma containment tube (78). Due to the efficient power transfer of the resonant cavity, the plasma is maintained within the containment tube. MIPs with power around 100 W are generally used, although powers up to 500 W have been explored.

Beenakker (79) developed a cavity for MIPs at atmospheric pressure with either He or Ar gas. Previously, the cavities used for He MIPs produced stable plasmas only at reduced pressures. The new cavity (TM_{010} cylindrical resonance cavity) was used for Ar MIP with cross-flow pneumatic nebulization of aqueous solutions without desolvation (28). Prior to this work, aqueous nebulization with desolvation had been

employed. With the Beenakker's cavity, LODs were in the sub-ppm range for some metal and metalloids, although nonmetals were not studied at that time.

The use of He instead of Ar gas for the MIP allowed more efficient excitation of higher energy levels of the nonmetals that resulted in emission from atom and ion energy levels that were never attained or efficiently populated within an Ar MIP. A comparison of the observed emission from a He, Ne, and Ar MIPs (80) indicated that higher energy levels were populated by the He and Ne MIP with respect to the Ar MIP. Many emission lines from S II, Br II, Cl II, and I II were observed in He and Ne (the He MIP had slightly more ionic lines present) but were not present in the Ar MIP. Higher energy excitation has also been observed for a He MIP with respect to an Ar or air MIP (81).

The first significant analytical result from an atmospheric pressure He MIP was reported by Beenakker (32) in 1977. Detection limits improved dramatically with the utilization of He gas with this MIP versus the reduced pressure He MIP or Ar MIP. LODs ranged from 0.4 to 25 pg s^{-1} for C, H, Cl, Br, I, and S. Dingjan and DeJong (33) acquired better detection limits for C, Cl, and S with a modified Beenakker cavity than their own cavity.

Detection of GC effluents has been extensively studied with He MIPs. Detection limits of nonmetals for GC effluents have been attained in the range of 1 to hundreds of pg s^{-1} (36-47) as noted in Table I. Preliminary studies concerning detection of sample separated by GC and thin layer chromatography (TLC) with subsequent detection by He MIP have been performed (48).

The wavelengths of the nonmetals (H, C, N, O, F, Cl, P, S, Br, and I) from 190 to 850 nm emitted from a He MIP have been tabulated by Tanabe et al. (82). The NIR emission lines from 700 to 1200 nm for C, N, O, F, S, Cl, and Br have been compiled by Freeman and Hieftje (83). Some IR spectra and wavelength tables of various nonmetals excited in a He MIP with detection by Fourier transform spectroscopy (FTS) have been collected (84-87).

Extinguishment of the plasma by aerosol produced by aqueous sample nebulization had been a problem for MIP. Recently, Michlewicz and Carnahan (50) overcame this problem with a higher power (500W) generator; demountable, slotted torch; and a modified TM_{010} cavity that provided stability to the He MIP during aqueous nebulization without desolvation. Detection limits for Cl, Br, and I of 0.4, 3, and 0.8 $\mu g\ mL^{-1}$ for ultrasonic nebulization with desolvation and 2, 60, and 7 $\mu g\ mL^{-1}$ for pneumatic nebulization, respectively, were obtained in later studies (51). These results were the best detection limits for aqueous nebulization into a He MIP.

The He MIP excited the nonmetal, especially the halogen, emission lines more efficiently than the analogous counterpart, the Ar MIP. Extinguishment of the plasma and large interference effects reduced the potential of the He MIP as a halogen-specific detector. The use of higher powers (~500 W) has allowed the introduction of aerosol into the plasma, and more studies should be completed in order to access the impact of He MIPs upon trace nonmetal analysis of solutions.

He ICP

Initial studies have been conducted on a reduced pressure He ICP at low powers (< 300 W) by Seliskar and Warner (52). The utilization of He

gas in lieu of Ar gas increased the excitation energy used for energy transfer to the halogens so more analytical emission could be attained. Atomic and ionic emission from Br and Cl within a He ICP from low-molecular weight organohalogens has been compiled from 250 to 750 nm, although detection limits were not reported (88).

The first reported instance of an annular-shaped atmospheric pressure He ICP developed for analytical work was reported by Chan and Montaser (53). Helium gas did not create efficient aerosol formation and transportation with a pneumatic nebulizer, so an ultrasonic nebulizer was used for their work. Nebulization of 0.1 M HCl and HBr resulted in detection limits of 13 and 18 $\mu g\ mL^{-1}$ for Cl and Br, respectively, and improvements over an Ar ICP by factors of 63 and 34 for Cl and Br, respectively. Initially, the He gas flow rate was 57 L min^{-1}, although recent refinements in the torch design have lowered the gas requirement to ~8 L min^{-1} (54). With ultrasonic nebulization of aqueous bromide, the detection limit for Br was 5 $\mu g\ mL^{-1}$ vs. 26 $\mu g\ mL^{-1}$ with an Ar ICP.

Afterglows and other emission sources

An atmospheric pressure nitrogen afterglow (N_2-APAG), sometimes called atmospheric pressure active nitrogen (APAN) discharge, was used by Rice et al. (55) to observe molecular spectra for compounds containing Br, Cl, and S, and atomic iodine emission. Detection limits from 5 to 40 ng s^{-1} were acquired for Br, Cl, S, and I. Analyte species were introduced by hydride generation into the N_2-APAG and energy transfer from long-lived excited states of atomic and molecular nitrogen resulted in dissociation and excitation of the analyte. The employment of Ar gas instead of N_2 resulted in atomic emission of the halogens due to the higher excitation

energies of Ar. LODs for P, S, C, I, Cl, and Br were from 0.04 to 10 ng for an Ar-APAG system (56).

Just as He gas increased the amount of emission seen by a MIP with respect to Ar gas, He gas also improved the efficiency of the afterglow source in excitation of the halogens. Rice et al. (57) have developed a He discharge-afterglow that achieved detection limits in the range of 0.5 to 30 pg for F, Cl, Br, I, S, C, P, As, and Hg for GC effluents. These LODs were quoted as superior to Estes et al. (36) by factors of 3 to 120 over those obtained from He MIP, except for C for which similar values were obtained, although more recent LODs for He MIPs (see Table I) gave comparable results. When excessive solvent loads were introduced, the stability of the He discharge-afterglow was maintained after temporary quenching of the afterglow region in contrast to the extinguishment behavior of most MIPs. However, the He discharge-afterglow has only been adapted for GC effluents and vapor generation products, and analysis of aqueous solutions has not been possible. The system was simple, easy to use, and with low gas consumption.

Direct current plasma (DCP)

A DCP is comprised of two graphite anodes and a thoriated tungsten cathode (65). The anodes and cathode are arranged as an inverted "Y" as shown in Figure 1C. Sample is introduced at the bottom of the plasma by Ar gas. The plasma is maintained by an electrical discharge through the Ar support gas.

In 1977, Ellebracht et al. (58) utilized a DCP source to detect S in solutions that contained organic compounds; and Hg, Se, As, I, P, and S in aqueous solutions at the ppm level with their near UV and VUV emission lines. Ellebracht et al. (60-62) determined sulfur by two methods: 1)

inorganic sulfur was reduced to H_2S, and 2) organic sulfur compounds were fractionated by a gas chromatograph and introduced into a DCP to observe the sulfur VUV atomic emission resonance lines by a complicated version of the spectrometer used earlier (59). Ellebracht did not observe spectra below 165 nm. Detection of 10 ng (60,61) and 300 pg s^{-1} (62) were obtained for S.

Carr and Blades (89) observed spectra down to 95 nm for a DCP. Dilute acids containing the elements P, S, and Cl were introduced into the DCP and analyte and background spectra were taken from 120 to 200 nm. Observation of emission at low wavelength was obtained through a ~35 cm long purge tube connected to a VUV monochromator. No LODs were reported with this system.

Summary

As shown in Table I, the LODs of the nonmetals and metalloids for the techniques of MIP-AES and He-APAG with He gas were in the low pg s^{-1} range for the analysis of gaseous samples and were superior to those same techniques with the use of N_2 and Ar gases. Usually, NIR or near UV atomic lines and NIR atomic or visible ion lines were used for He-APAG and He MIP-AES, respectively. Recent developments have allowed the use of aqueous nebulization introduction into the MIP resulting in LODs in the μg mL^{-1} range, which were comparable to those obtained with He ICP-AES for the elements, Br and Cl. When Ar ICP-AES was employed for Br and Cl determinations, μg mL^{-1} detection limits were achieved, although ng mL^{-1} detection limits were prevalent for the other nonmetals and metalloids. An advantage of Ar ICP-AES was that aqueous sample nebulization could be conveniently employed without extinguishment problems. Higher powers (500W) were needed to maintain the He MIP during aqueous nebulization (50)

and only ultrasonic nebulization could be used with the He ICP (53). The DCP-AES systems did not fare as well as Ar ICP-AES as the LODs for nonmetals and metalloids were in the sub-μg mL^{-1} range for solutions and ng to sub-ng range for gases.

Argon ICP-AES is the method of choice for analysis of solutions for which it is extensively used within the industrial community. There has not been routine employment of aqueous sample introduction into the He MIP, APAG, and He ICP. More research is needed before these techniques can be considered alternative sources of atomic emission for nonmetals, metalloids, and selected metals in solution. If aqueous nebulization with a He source can be successfully demonstrated, the advantage of trace nonmetal analysis with the use of He gas with this source may be important, because the He gas should result in excitation of the nonmetal emission lines to a higher degree than an Ar source.

Purpose of Proposed Research

There have been several deficiencies in the ICP-VUV-AES research done in the past. First, except for Carr and Blades (77), all previous ICP-VUV-AES work has been limited to wavelengths greater than about 120 nm. Various VUV transparent materials, such as MgF_2, have been used as windows for solar blind PMTs or as barriers between vacuum and gaseous atmosphere or between two gaseous atmospheres. Second, because of the intense heat of the plasma, the spectrometer must be placed at a considerable distance from the plasma, making it necessary to utilize a condensing lens to fill the optical aperture of the spectrometer. The limitations imposed by the lack of transparency of lens materials have already been discussed above. Third, ICP-VUV-AES researchers have used horizontally oriented optics for

light collection at a particular observation height. The height above the load coil that was observed by the monochromator system was not the optimum emission position for every element that was introduced into the plasma. Fourth, spatial studies of the ICP for emission lines in the VUV region have been ignored.

Birth from ICP-mass spectrometry (MS)

An experimental approach that has the potential of solving these deficiencies is based on the insertion of a water-cooled sampling probe directly into the plasma. An orifice in the probe provides the means of optical sampling. Several research groups have recently demonstrated the feasibility and analytical value of extracting ions from an inductively coupled plasma (ICP) into a mass spectrometer (90-92), as shown in Figure 2. This extraction process is accomplished by immersing a water-cooled, metal cone directly into the ICP. Plasma gas is sampled through an orifice in the cone into a vacuum system housing a mass spectrometer. In an ICP mass spectrometer, photons from the plasma also travel through the sampling orifice and can yield an undesirable background unless care is taken to screen them from the electron multiplier. These background photons are a nuisance in mass spectrometry but the fact that they are observable may be turned to advantage for optical spectroscopy, namely as an effective way to observe VUV emission spectra at wavelengths not accessible with conventional optical transfer systems. The configuration of a plasma impinging upon a cone assembly that is attached to a monochromator creates a novel optical sampling system. The purging of the monochromator and interface with a transparent inert gas would permit photon emission from the ICP to enter the monochromator for detection.

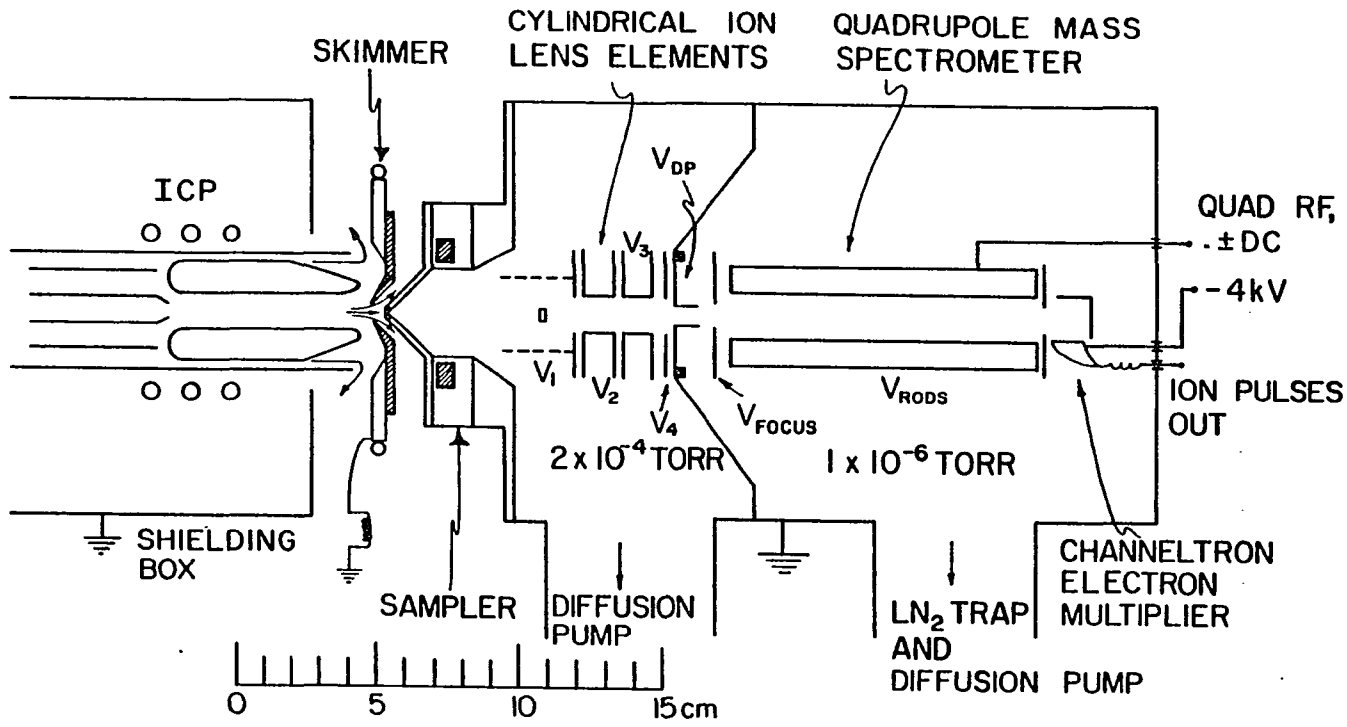

Figure 2. Schematic diagram of ICP, interface, and vacuum system for ICP-MS

There have been instrument designs discussed in the literature that had similarities to the copper cone interface used in this research. In 1972, Muller et al. (93) observed Ar lines in the VUV region using a cascade arc with a differential pumping system interfaced with a monochromator. Emission was extracted from the arc through a 0.6 mm orifice drilled into a copper and tungsten anode that was attached to the differential pumping system. A vacuum optical path was employed. Also, in 1985, Rogoff (94) discussed the theory of the use of an optical probe, i.e., an optical fiber, for obtaining 3-D resolution of emission and absorption from a hypothetical plasma. No experimental data were published. Present fiber optic materials would prevent the transmission of VUV radiation.

Solutions to VUV problems

The water-cooled, metal cone used for the extraction of VUV photons has several properties. The ICP can be positioned very close to the monochromator in order to improve the collection of analyte emission from the plasma. The cone keeps the monochromator cool. The monochromator and cone assembly are purged with He to preserve the transparency of the entire optical path from the plasma to the detector. The He purge gas deflects the plasma stream around the cone tip, impedes contaminates from entering the monochromator, and prevents solid deposition near the orifice of the cone. No windows or lenses are necessary between the plasma and detector when this mode of sampling is used.

Another advantage of the collection of analyte emission from the plasma with the cone assembly is the ability to view end-on through the axial channel. The benefits of axial channel viewing have been documented by Apel et al. (95,96). Light was directed from the axial channel of the

plasma to a spectrograph by placement of a mirror above the plasma. Covering the image of the plasma torus at the entrance slit of the spectrograph with a mask greatly reduced the high background intensity that was received from the brilliant plasma. The mirror was protected from the high temperature of the plasma by a jet stream of air that flowed across the mirror. Apel et al. stated that improved sensitivity, lower detection limits, better signal to background ratios, and a better compromise viewing position for multielemental analysis are some advantages of axial channel over side-on viewing.

Also, the constrained viewing field of the probe-monochromator interface facilitates obtaining spatial profiles of the plasma. The spatial resolution that is attained using the cone assembly and monochromator will be discussed in a later section. With the utilization of spatial resolution, important diagnostic studies can be performed on the argon resonance lines and other VUV lines in order to compile data about the physical structure of an ICP and further understand the energy transport processes occurring therein.

CHAPTER II. EXPERIMENTAL FACILITIES AND OPERATING PROCEDURES

The ICP-VUV-AES instrumental layout is shown schematically in Figures 3-5. Instrumental components and operating conditions are listed in Table II.

Instrumentation

Overall configuration of instrumentation

A schematic diagram of the overall configuration of instrumentation in the ICP-VUV-AES system is shown in Figure 3 and will be discussed in brief detail in this section. A more detailed description of the individual components and their relationship to the operation of the ICP-VUV-AES instrumentation will be described in subsequent sections. Ar gas [A] was delivered to the nebulizer [B] and the plasma torch [C]. Power was supplied for the plasma by the radiofrequency (RF) generator [D]. The Tesla coil [E] was needed to create the initial spark at the torch so the plasma could be ignited. The ICP impinged upon the cone assembly [F], which was positioned on the entrance slit chamber of a monochromator [G]. The monochromator was initially evacuated by a vacuum pump [H] by way of a pumping adapter [I], and then filled with purge gas [J], usually He. Photons were detected by a PMT [K] and the current generated was converted to voltage by a picoammeter [L] and sent to a recorder [M]. The voltage signal may also be diverted to an Apple IIe computer and ISAAC software module [N] where it was manipulated and sent to a printer [O]. An active filter [P] was employed between the picoammeter and recording electronics when electronic filtering of the emission signal was required.

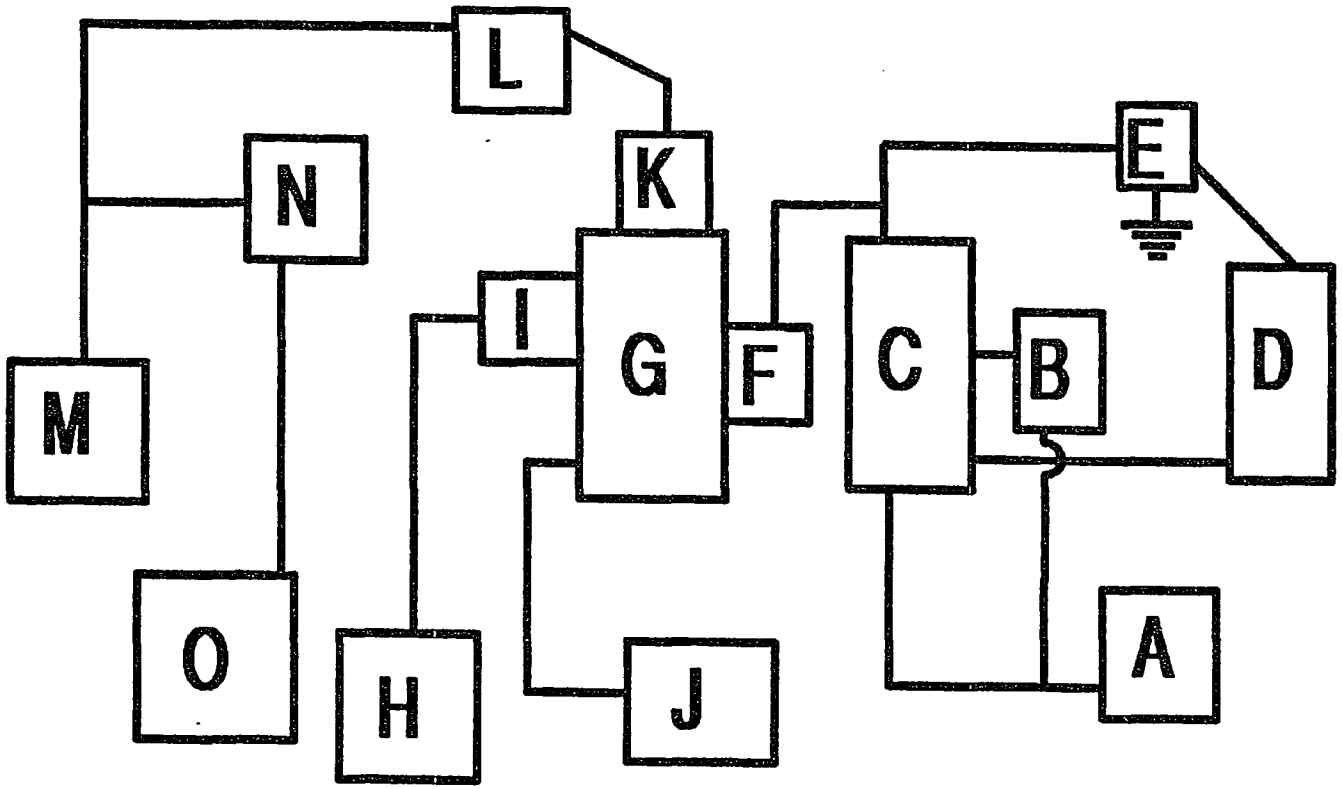

Figure 3. Schematic diagram of the entire ICP-VUV-AES instrumentation
[A] Ar gas cylinder, [B] nebulizer, [C] ICP, [D] RF generator, [E] ground, [F] cone assembly, [G] monochromator, [H] vacuum pump, [I] pumping port, [J] He gas cylinder, [K] photomultiplier tube, [L] picoammeter [M] recorder, [N] ISAAC-Apple IIe computer, [O] printer, [P] active filter

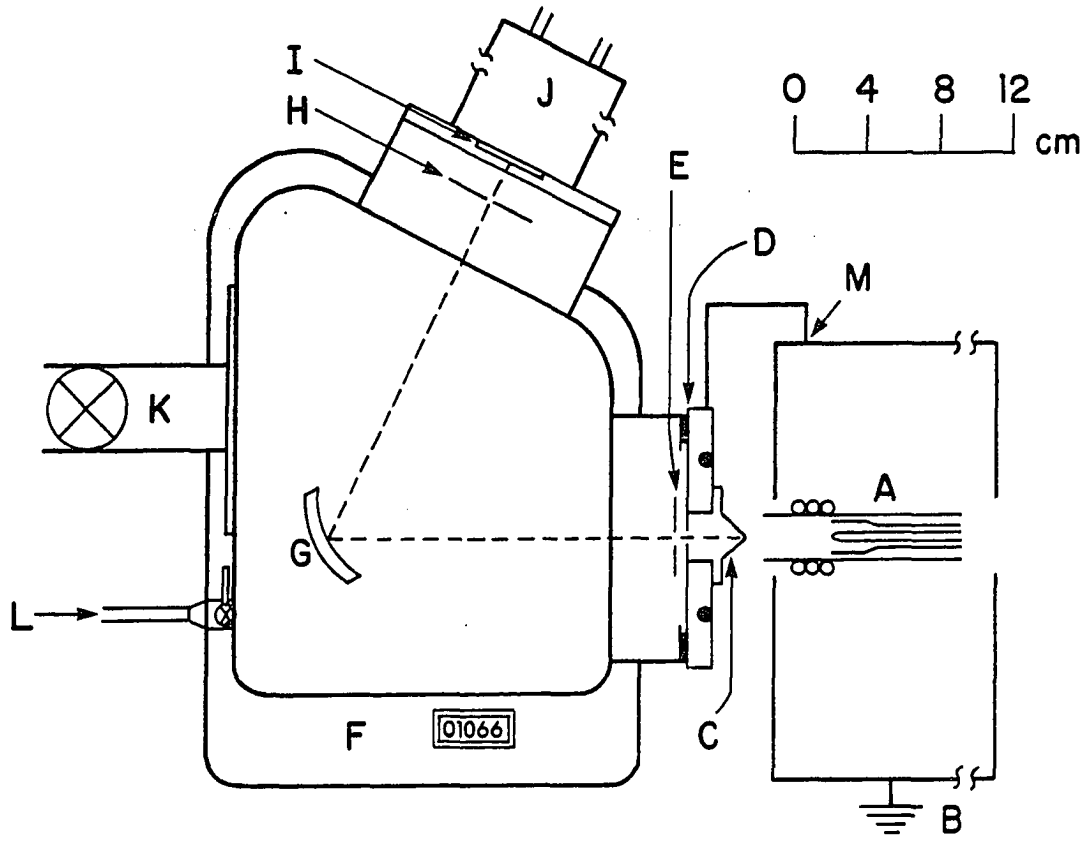

Figure 4. Top view of ICP, optical sampler, and VUV monochromator:
[A] ICP torch and load coil
[B] Copper shielding box
[C] Copper cone with sampling orifice drilled in tip
[D] Optical mask
[E] Variable entrance slit
[G] Grating
[H] Variable exit slit
[I] Scintillator
[J] Photomultiplier
[K] Piping and valve to mechanical vacuum pump for initial evacuation of spectrometer. The sampling orifice (C) is plugged with a piece of Viton during evacuation. The valve is closed when purge gas is added
[L] Piping and valve for He purge gas
[M] Copper strap connecting flange and cooling jacket with grounded shielding box

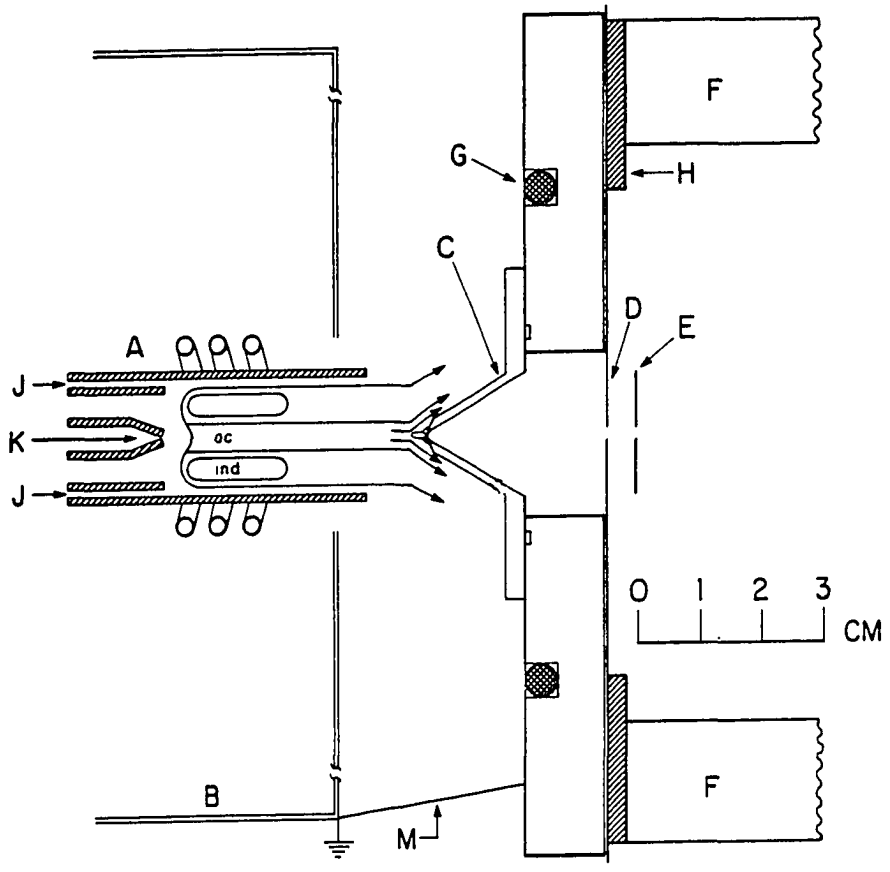

Figure 5. Side view of ICP and Mode 1 cone assembly [A-F,M] same legend as Figure 4, [G] cooling coils, [H] Viton gasket, [J] plasma gas, [K] nebulizer gas, [ac] axial channel, [ind] induction region

Table II. Instrumental components and plasma operating conditions

Plasma (general):	Plasma-Therm, Inc., Kresson, NJ (now RF Plasma Products)
RF Generator:	Model HFS3000D; 27.12 MHz
Power (forward):	see Nebulizer
Power (reflected):	<20 W
Outer Gas Flow Rate:	15 L min^{-1}
ICP Torch (97):	Ames Lab construction, outer tube extended to 35 mm from tip of aerosol injection tube, torch used for gaseous introduction was extended to 32 mm, (relative to normal extension of 20 mm)
Direct Injection Probe:	Dimensions shown in text and corresponding figures
Monochromator:	Model VM-502-V, Acton Research Corp.
Focal Length:	0.2 m
Grating:	1200 grooves mm^{-1}, MgF_2 coated
Slit Widths:	10 μm
Slit Heights:	5 mm (exit), 3 mm (entrance)
Photomultiplier for Analytical Studies:	Model G-26H314LF Solar Blind, EMI
Bias Voltage:	-1600 V
Photomultiplier Tube for Diagnostic Studies:	Model DA-781, Acton Research Corp. with Model 9635 QB/5 PMT, EMI
Bias Voltage:	-800 V
He Purge Gas Flow Rate:	~1 - 2 L min^{-1} for Mode 1 cone (3 mm dia. orifice)
Position of Sampling Orifice:	22 mm from load coil, on center
Detection Facilities:	
Amplifier:	Model 417, Keithley Instruments
Active Filter:	Model 1021A, Spectrum
Printer:	Model 200XY, Houston Recorders
Computer Facility:	
Computer:	Apple IIe computer
Data Acquisition System:	ISAAC Model 42A, Cyborg
Printer:	Apple Dot Matrix Printer
Ultrasonic Nebulizer:	Ames Lab construction (98)
Nebulizer Ar Flow Rate:	0.8 L min^{-1}
Auxiliary Ar Flow Rate:	0.3 L min^{-1}
Desolvation Temperature:	110 - 120°C
ICP Power:	1.3 kW
Nebulizer Power:	~40 W
Transducer Frequency:	1.33-1.36 MHz
Uptake Rate:	2 mL min^{-1}
Injection Volume (FIA):	500 μL

Table II. (Continued)

Cross-Flow Pneumatic Nebulizer:	Ames Lab construction (99)
Spray Chamber:	Ames Lab construction, Scott-type (97)
Nebulizer Ar Flow Rate:	0.8 L min^{-1}
ICP Power:	1.3 or 1.5 kW dependent on nebulizer used[a]
Uptake Rate:	1 mL min^{-1}
Injection Volume (FIA):	200 μL
Ar Lateral Profile Studies:	
Position of Sampling Orifice:	19 mm from load coil
Slit Widths:	50 μm wide for both slits
He Purge Gas Flow Rate:	~0.4 L min^{-1} for Mode 1 cone (0.34 mm dia. orifice)
Digital Voltmeter:	Model 403, Janus Control Corp.
Printer:	Model 511A, Monsanto Electronics

[a]Two pneumatic nebulizers were used. One nebulizer produced mist more efficiently, therefore, power was increased to maintain a stable plasma. The more efficient nebulizer was employed for the interference effect, precision, and the B, Bi, Ge, and Si LOD studies, and for the wavelength scans.

Ar ICP and vacuum monochromator assembly

As shown in Figures 4 and 5, the ICP (A) was operated horizontally with the torch protruding through a hole in the grounded copper shielding box (B). An optical filter at the viewing aperture on the box protected observers from the intense ultraviolet (UV) radiation. The functions of the shielding box and the reverse orientation of the copper leads to the load coil to reduce radiofrequency interference (RFI) will be discussed in a later section. The RF generator supplied power to the impedance matching network. The impedance matching network (not shown), ICP, and shielding box were mounted on three orthogonal translation stages so that spatially-resolved observations could be made by moving the plasma relative to the monchromator. An unique clamp and motion assembly, devised by the Machine Shop at the Ames Laboratory, was used for the "towards-away" horizontal movement of the ICP with respect to the cone assembly. A lab jack was used to raise and lower the plasma. A 4 RPM AC synchronous motor (Hurst Mfg. Corp. of Princeton, IN) was used to assemble a translator that provided an uniform "left-right" horizontal movement of the plasma with respect to the cone assembly. The translator assembly was constructed in the Machine Shop and was attached to the bottom of the existing ICP translator assembly. The 4 RPM motor had less than 0.1% error in its rotational speed and could translate the plasma assembly easily at the rate of 5.12 mm min^{-1} (equivalent to 1.28 mm of travel per revolution). This translational speed allowed for the acquisition of a spatial profile of the plasma in about 5 minutes.

The gas supply of the flow control system for the ICP consisted of three argon gas cylinders in series, from which the outer, aerosol, and auxiliary gas flows originated. Dekoron tubing was used for the gas

lines. The aerosol gas proceeded from the cylinders (regulator set at 75 psi) to the pressure regulator (set at 20 to 40 psi, dependent upon the flow rate desired), to the rotameter, then to a diaphragm flow controller (fully opened) backed by a toggle valve. A pressure gauge was inserted between the diaphragm flow controller and toggle valve. The aerosol gas flow rate was adjusted by the pressure regulator. The outer and auxiliary gases proceeded from the argon gas cylinders (regulator set at 75 psi) to their respective flow regulator valves and rotameters. The outer and auxiliary gas flow rates were adjusted by their respective flow regulator valves.

The 0.2 m vacuum monochromator was fitted with a phosphor-sensitized photomultiplier tube and interchangable gratings. The monochromator had an aperture ratio of a nominal f/4.5, and short (0.2 m) optical pathlength with only one reflecting surface. The monochromator was used in the V-configuration, as shown in Figure 4. Two aberration-corrected, concave holographic gratings, one coated with Os and the other with Al and MgF_2 were utilized. The reflectance curves from 50.0 to 400.00 nm of these two gratings are shown in Figure 6. The reflectance of the MgF_2 grating was superior (150 to 200%) to that of the Os grating for the 120 to 400 nm wavelength region, but was somewhat inferior (30 to 100%) for the 50 to 110 nm wavelength region (100). Therefore, the MgF_2 grating was mainly used for analytical work above 110 nm, while the Os grating was used for wavelengths below 110 nm.

The monochromator was evacuated via a dual-stage, rotary vane vacuum pump (TRIVAC Model D 30A, Leybold-Heraeus Inc., Export, PA 15632) through a pumping port adapter that was mounted at the side of the monochromator. Insertion of a foreline trap with copper sieve (Model CT-4-1501-C-NW, Nor-

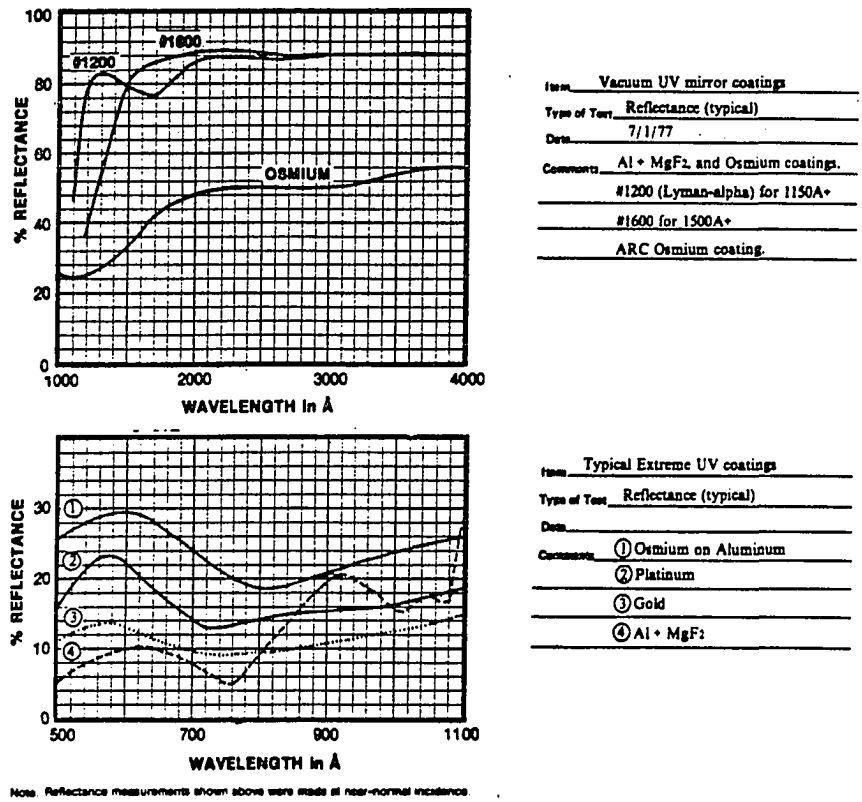

Figure 6. Reflectance curves demonstrating the efficiency of various Acton Research Corp. coatings for use in the vacuum UV region (Figure reprinted from Reference 100)

Cal Products, Inc., Yreka, CA 96097) in the pipeline prevented pump oil vapors from contaminating the interior surfaces of the monochromator. A bellows valve was incorporated into the pipeline to allow closure of the pipe, so that initially, low pressure could be maintained, and so that secondly, an inert gas could be added. A thermocouple vacuum gauge was inserted in the pipeline to measure the pressure inside the monochromator. An oil trap (SE Smoke Eliminator, Leybold-Heraeus Inc.) was used at the exhaust port of the pump to prevent loss of pump fluid and contamination of the monochromator.

An inlet valve installed at the side of the monochromator was used as the inlet for the purge gas. The purge gas proceeded from a gas cylinder (regulator set at 15 to 20 psi) to two needle valves in parallel. The two needle valves, coarse and fine, were used for adjustment of the He gas flow rate. Purging of the monochromator with He provided an optically transparent path without the necessity of providing differential pumping. Although a vacuum path would allow the monochromator to transmit the entire range of VUV radiation with respect to using an inert gas, a considerable amount of pump capacity would be needed to adequately evacuate the system with the entrance slit open to the atmosphere. Also, contamination of the grating of the monochromator from atmospheric pollutants could occur.

Direct optical probe sampling

The theory of illumination of a grating through an entrance slit without any condensing lenses is discussed in Appendix B. The rationale used in Appendix B was utilized for the design and construction of an optimum cone assembly with the desired requirements of optical sampling efficiency and spectral and spatial resolution. The determinations of the

optical field of view of the monochromator with various cone assemblies are presented below.

Plasma-cone interfaces The operation of a horizontal ICP impinging upon a circular orifice, rectangular orifice, or an orifice situated on the Rowland circle have been referred to as Mode 1, 2, or 3 operations, respectively. No matter which orifice was used, the plasma impinged upon and flowed around a water-cooled, copper cone that served as the optical sampler, as shown in Figure 5 with a Mode 1 cone. The functions of the gasket [H], nylon screws, and detachable copper strap [M] for the reduction of RFI will be mentioned in a later section. The Viton gasket (1/16" thick) provided a vacuum seal between the cone assembly and the monochromator. The copper strap was detachable from the shielding box in order to facilitate movement of the plasma when the plasma was not in operation. An optical mask [D] was employed to limit the effective height of the entrance slit because the slit baffles originally supplied with the monochromator could not be adapted to the entrance slit chamber when the cone assembly was attached. The mask consisted either of a non-reflective black foil, sandwiched between the cone flange and gasket, or of a non-reflective black tape aperture affixed to the back surface of the cone flange. The latter method was used for most of the studies. Optical radiation from the plasma passed through the sampling orifice, and entrance slit, into the monochromator for Modes 1 and 2, whereas, for Mode 3, the sampling orifice itself served as the "virtual" source of plasma optical radiation. Helium purge gas flowed through the monochromator and sampling orifice into the plasma to form a plume. The plume cooled the sampling orifice, deflected the plasma stream around the cone tip, and prevented solid deposition near the orifice. The depth of penetration of

this plume into the plasma could be adjusted by varying the He pressure supplied to the monochromator. Helium was chosen as purge gas because it was transparent in the wavelength region of interest (> 58 nm). The plume and sampler did not disturb the electrical operation of the ICP if they were inside the luminous white tip of the plasma, i.e., if the sampler tip was located within 45 mm from the load coil. A mild electrical discharge formed between the plasma and sampler if the two were separated by 50 to 150 mm.

A flange supported the cone in the plasma. The dimensions of this flange are shown in Figure 7. The cone was attached to the flange by four screws. An o-ring groove in the flange provided a seal between the flange and cone and eliminated the need for an o-ring groove on every cone that was constructed. The cooling coil prevented meltdown of the flange and cone. This copper flange was employed for the Mode 1 and 2 cones. An entirely different entrance slit chamber was constructed for Mode 3 cones.

Mode 1 cones The Mode 1 cone consisted of a "pre-entrance slit" cone with a circular orifice and was attached to the flange situated upon the entrance slit chamber of the monochromator, as shown in Figure 5. The specifications of the Mode 1 cone with a 0.34 mm diameter orifice are shown in Figure 8. The tap holes in the cone were used as a holder that supported a Viton plug over the cone orifice so that the monochromator could be sealed from the atmosphere. The clearance holes were used to screw the cone onto the flange.

Two orifice sizes, 0.34 and 3 mm diameter, were used for the bulk of in the work done for this dissertation. The smaller orifice was used for spatially sampling a very narrow volume element of the plasma, usually for diagnostic studies of the ICP. The larger orifice was employed for

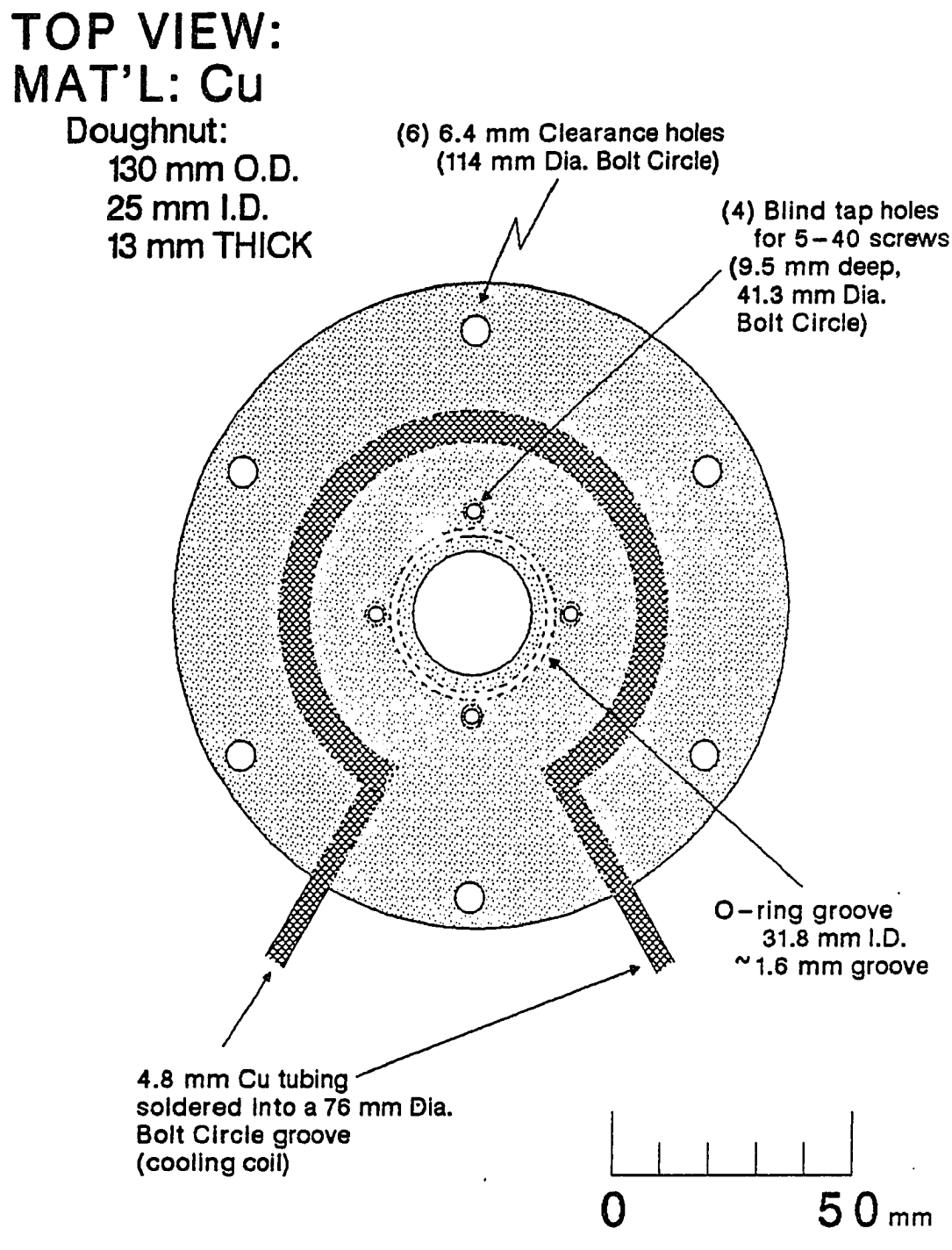

Figure 7. Dimensions of the copper flange that was employed for the attachment of Mode 1 and 2 cones

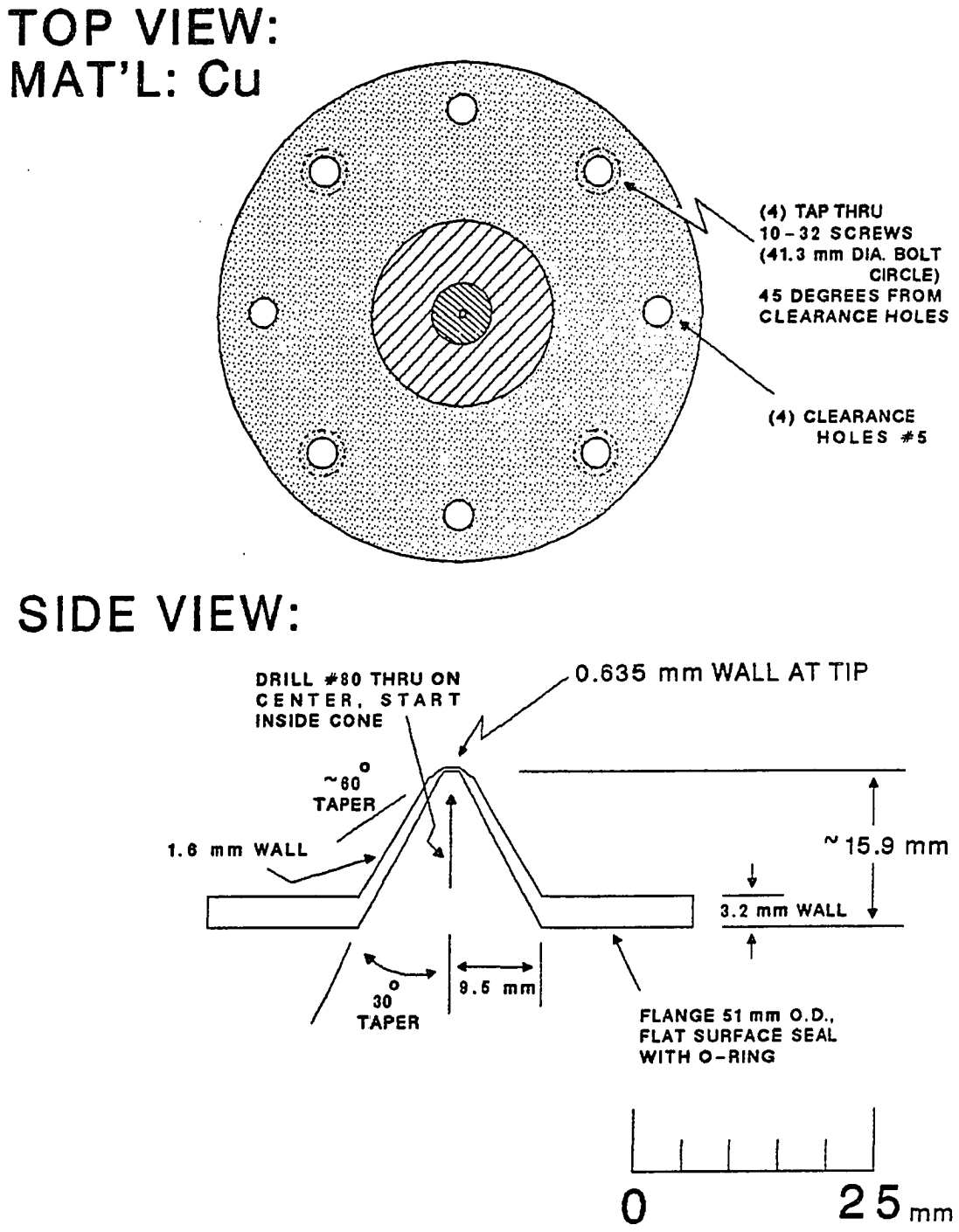

Figure 8. Dimensions of the Mode 1 cone with a 0.34 mm diameter orifice

sampling a large volume element of the plasma, especially the emission from the axial channel of the ICP. Another Mode 1 cone with a 0.34 mm diameter orifice was made with a height from its base to its top of ~25 mm, instead of the ~16 mm stated in Figure 8. This extended Mode 1 cone, called the Mode 1E cone, was employed for probing deep within the ICP torch near the top of the load coil.

Mode 2 cones The Mode 2 cone, in the form of a "pre-entrance slit" cone with a rectangular orifice, was designed so that a larger volume element of the plasma could be observed by the monochromator. The dimensions of the wedges and additional flange for the Mode 2 cone assembly can be found in Figure 9, which illustrates a schematic diagram of the cone attached to a monochromator and inserted into a horizontally oriented Ar plasma. With the use of the main copper flange and a smaller (63.5 mm O.D.) flange attached to it, two copper wedges [C] were held onto the smaller flange to create a slit. A known width of sheet metal was inserted in the middle of the flange while the two copper wedges were pressed together (against the sheet metal) and screwed onto the flange. The sheet metal was removed so that the slit had a known width at the interface. An orifice of any desired dimension could be created from the Mode 2 cone.

Mode 3 cones An ideal illumination system should place the orifice (as a slit) of the sampling cone on the Rowland circle so that the orifice served as the entrance slit of the monochromator. To accomplish this goal a slit chamber was fabricated that allowed the "entrance slit" orifice to be mounted on the Rowland circle. This cone assembly was designated as the Mode 3 cone. Details of the construction of this Mode 3 cone assembly are described elsewhere (101). The Mode 3 cone assembly was

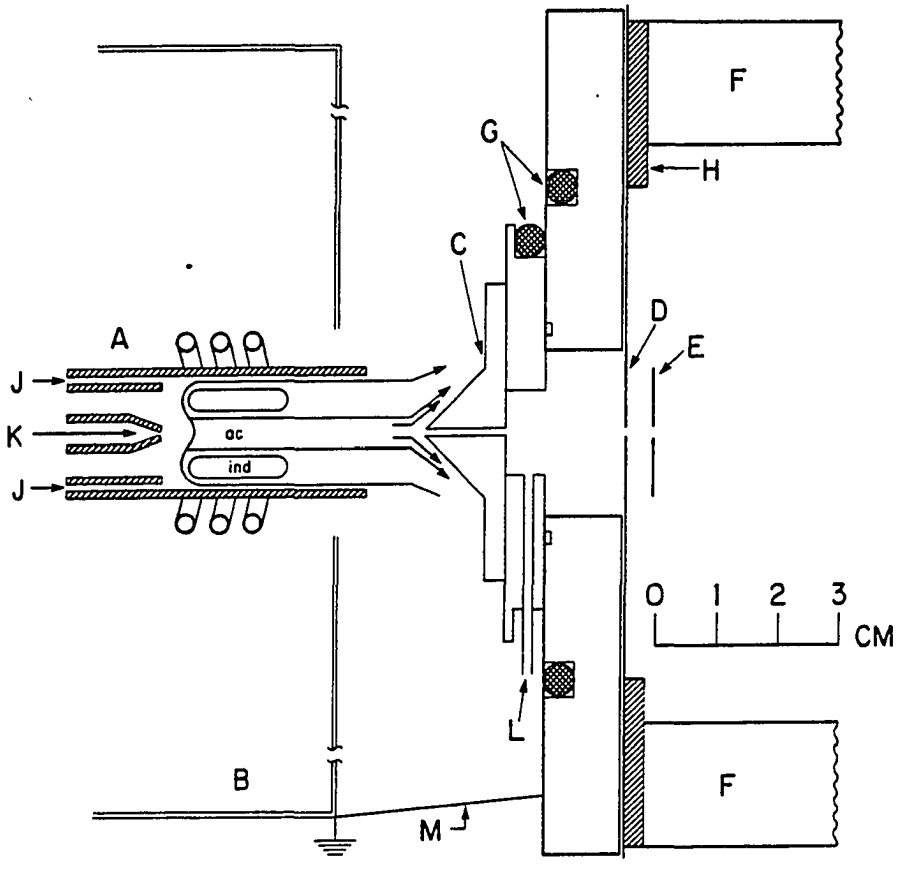

Figure 9. Side view of ICP and Mode 2 cone assembly
[A-F,M] same legend as Figure 4, [G] cooling coils, [H] Viton gasket, [J] plasma gas, [K] nebulizer gas, [L] piping for He purge gas, [ac] axial channel, [ind] induction region

anodized at Colors Inc. of Indianapolis, Indiana to reduce the reflection of light.

Operation of Mode 3 increased the collection of light and the field of view with respect to Modes 1 and 2. Regardless of the dimensions of the cone orifice, the entire surface of the grating could be illuminated with a Mode 3 cone, whereas, optimum use of the grating did not necessarily occur when Mode 1 and 2 cones were used. Theoretically, Mode 3 should produce higher resolution than Modes 1 and 2. However, because emission from the intense argon annulus was "seen" by the grating, problems from higher spectral background may arise.

The following theory presents the crucial requirements of an orifice contained in a Mode 3 cone. Every point of light at the entrance slit, located on the Rowland circle, was imaged as a vertical line at the exit slit. Many points of light contained within a line parallel to the rulings of the grating, i.e., points of light that have the same angle of incidence on the grating, were imaged as a single vertical line at the exit slit. When the points of light were contained in a line not parallel to the rulings of the grating, i.e., points of light that have different angles of incidence on the grating (large circular orifice), a broad peak resulted at the exit slit. Each point of light along the length of the circular orifice imaged a vertical line at a different position relative to the exit slit. As the monochromator scanned the wavelength region, the accumulation of all the vertical lines imaged from each point of light is seen as a broad peak. To maintain the best spectral resolution, a slit-type orifice, parallel to the rulings of the grating, must be utilized.

Only a circular orifice (0.34 mm diameter) could be constructed as the "entrance slit" for the Mode 3 cone with present technology. Spectral

resolution could be improved for the circular orifice of the Mode 3 cone by decreasing its diameter, but light collection will also decrease dramatically. Use of a slit-type orifice would be ideal for resolution and light collection due to its small width and large height with respect to the circular orifice. Unfortunately, the construction of a slit-type orifice (on the order of 10 to 100 μm wide) that is heat-resistant and sharp-edged has been an impossible task. Therefore, a Mode 3 cone assembly was not employed in the plasma studies discussed in this dissertation. If a slit-type orifice can be constructed along with appropriate baffles in the cone assembly, it would be interesting to observe the benefits of the employment of a Mode 3 cone for direct optical probe sampling.

Optical field of view of the monochromator Appendix C shows a listing and a description of the computer programs; ADVFOV.BAS, FVADD1.BAS, FVADD2.BAS, and FVADD3.BAS; which were used in the calculations of the fields of view employed in these optical probe sampling experiments.

Cones used for diagnostic studies For the lateral profile studies it was desirable to restrict the field of view "seen" by the monochromator to provide an acceptable degree of spatial resolution. The viewing field was determined by a computer program that projected lines from the edges of the mask (or entrance slit) through the sampling orifice into the plasma. With a Mode 1 cone and a 0.34 mm diameter orifice, mathematical analysis of this ray diagram revealed that the geometric viewing field had the dimensions of a 0.34 mm diam. circle at the plane of the sampling orifice, 0.6 mm wide x 2.9 mm high oval at the top of the load coil and 0.8 mm wide x 5.1 mm high oval at the base of the plasma, as

shown in Figure 10. A cross-section of the viewing field at the base of the plasma is shown superimposed with an end-on view of the ICP in Figure 11. The width of this observed volume was essentially determined by the diameter of the sampling orifice, whereas the height was a function of the mask height as well as the diameter of the sampling orifice. Some vignetting (102-104) undoubtedly occurred along the edges of the field of view. However, the dimensions listed include the vignetted portions; they thus represent the total cross sections from which light could strike the grating. With the sampling orifice centered on the ICP, the upper and lower edges of the viewing field at the plasma base (Figure 11) fell near the outer edge of the axial channel. Therefore, intensities detected with the sampling orifice centered on the ICP were taken to be representative of the axial channel. It should be emphasized that this end-on viewing method provided no vertical spatial resolution, and that the relative intensities observed represented a summation of emission viewed down the plasma length within the volume element depicted in Figure 10.

The optical arrangement shown in Figure 10 resulted in the illumination of the grating that was only 2 mm wide (neglecting diffraction by the entrance slit) by 2.7 cm high. If the effect of the diffraction of light was calculated, the area of incident radiation on the grating increased in width by 0.8 mm under the conditions of a 50 μm entrance slit and radiation of 100 nm. Diffraction did not appear to be a major factor in the illumination of the grating. The ruled area of the grating was much larger (4 cm wide x 3.5 cm high) so that most of the rulings were not illuminated. Obviously, the ideal spectral resolution and optical conductance of the monochromator were not achieved with this arrangement. Both of these qualities could be enhanced by enlarging the

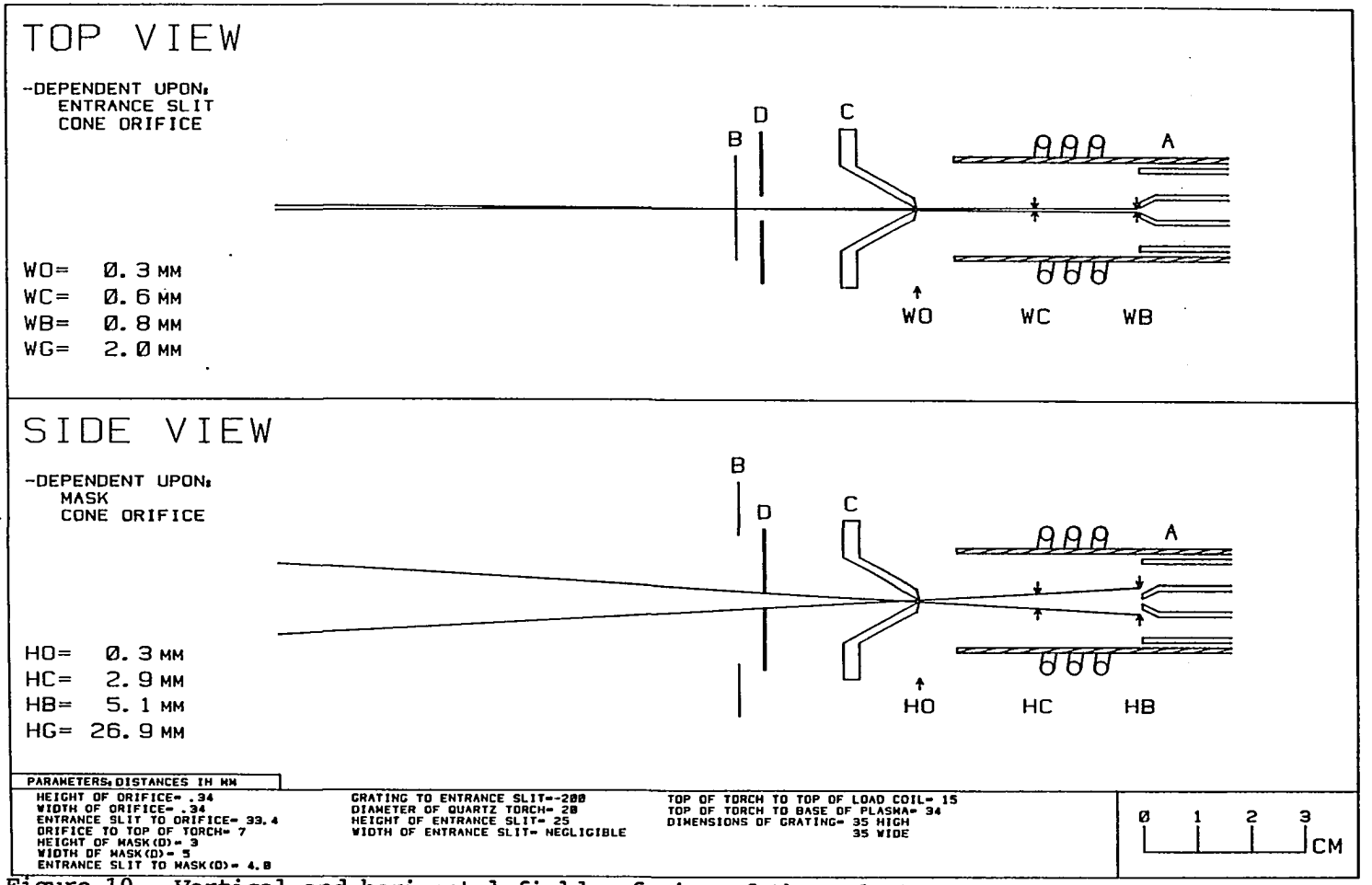

Figure 10. Vertical and horizontal fields of view of the Mode 1 cone assembly (0.34 mm diameter orifice). The letters; A, B, C, and D; designate the ICP torch, entrance slit, cone assembly, and mask, respectively. The terms; WO and HO, WC and HC, WB and HB, and WG and HG; are the widths and heights for the fields of view at the planes of the cone orifice, top of the load coil, base of the plasma, and grating, respectively

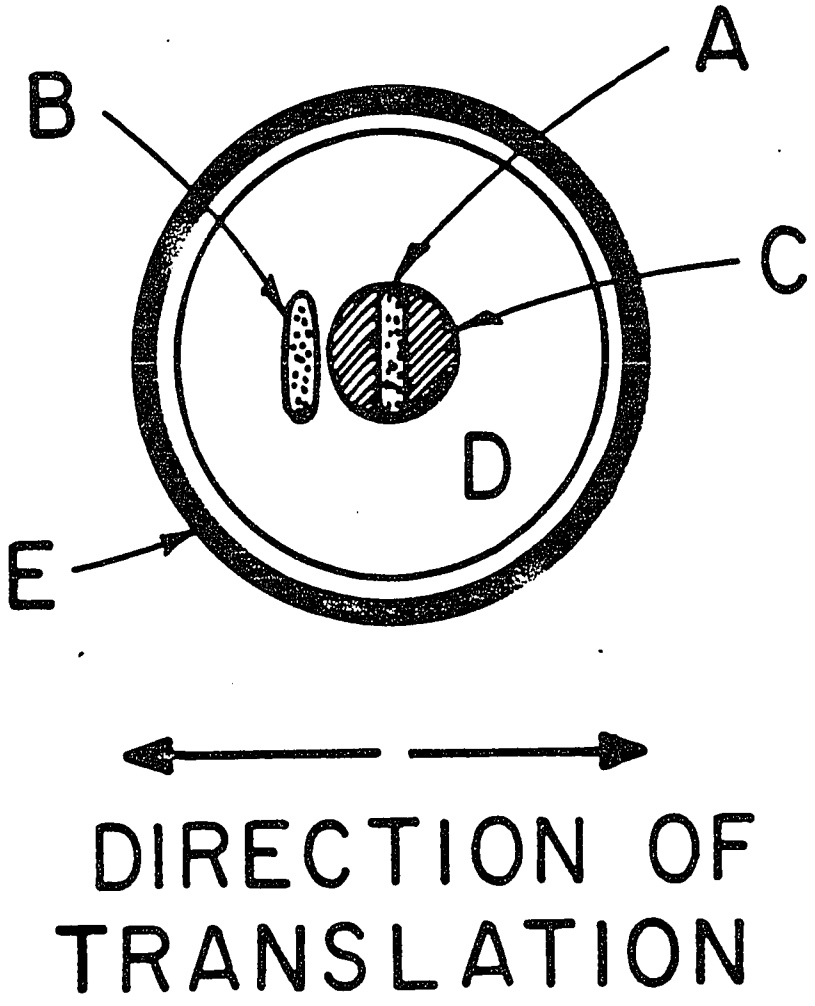

Figure 11. End-on view of ICP showing plasma regions and cross-sectional area of viewing volume at base of plasma:
A. Viewed area with sampler centered on plasma (lateral position = 0)
B. Viewed area with sampler off center at lateral position = 3.5 mm
C. Axial channel
D. Induction region
E. Outer tube of torch

sampling orifice, by moving the orifice closer to the entrance slit, or by replacing the circular orifice with a rectangular, slit-like aperture. All of these measures did increase spectral intensities but at the expense of spatial resolution.

The Mode 1E cone was employed for an even more limited field of view down the length of the axial channel. With the placement of the orifice of this extended cone at a position of 2 mm above the load coil, an example of the field of view of the monochromator is shown in Figure 12. This cone assembly was utilized for the selective observation of Ar and H_2 emission that occurred low in the plasma.

A slit-like sampling orifice (Mode 2, aperture 1 mm wide x 10 mm high) was employed for observing the relatively weak spectral features near the ionization limit of Ar. Thus, these data represented intensities that were spatially integrated over a rectangular plasma volume much larger than that indicated in Figures 10 and 12, although a Mode 1 cone (3 mm diameter orifice) was mainly used for observation of weak spectral line features in most of the spectra scanned in the VUV.

Cones used for analytical studies Operation of an ICP with a Mode 1 cone (large circular orifice) or Mode 2 cone (rectangular orifice) of the appropriate dimensions could yield optimum detection of VUV radiation from the axial channel of the ICP. An advantage in the use of the Mode 2 cone was that the size of the rectangular orifice can be altered quite easily by the wedges to yield the desired dimensions, whereas, the dimensions of the circular orifice that was drilled into a Mode 1 cone were fixed for that particular cone design. However, a Mode 1 cone of the desired dimensions of viewing possessed an easier-to-mount and more symmetrical orifice than the "slit-type" (Mode 2) cone and should

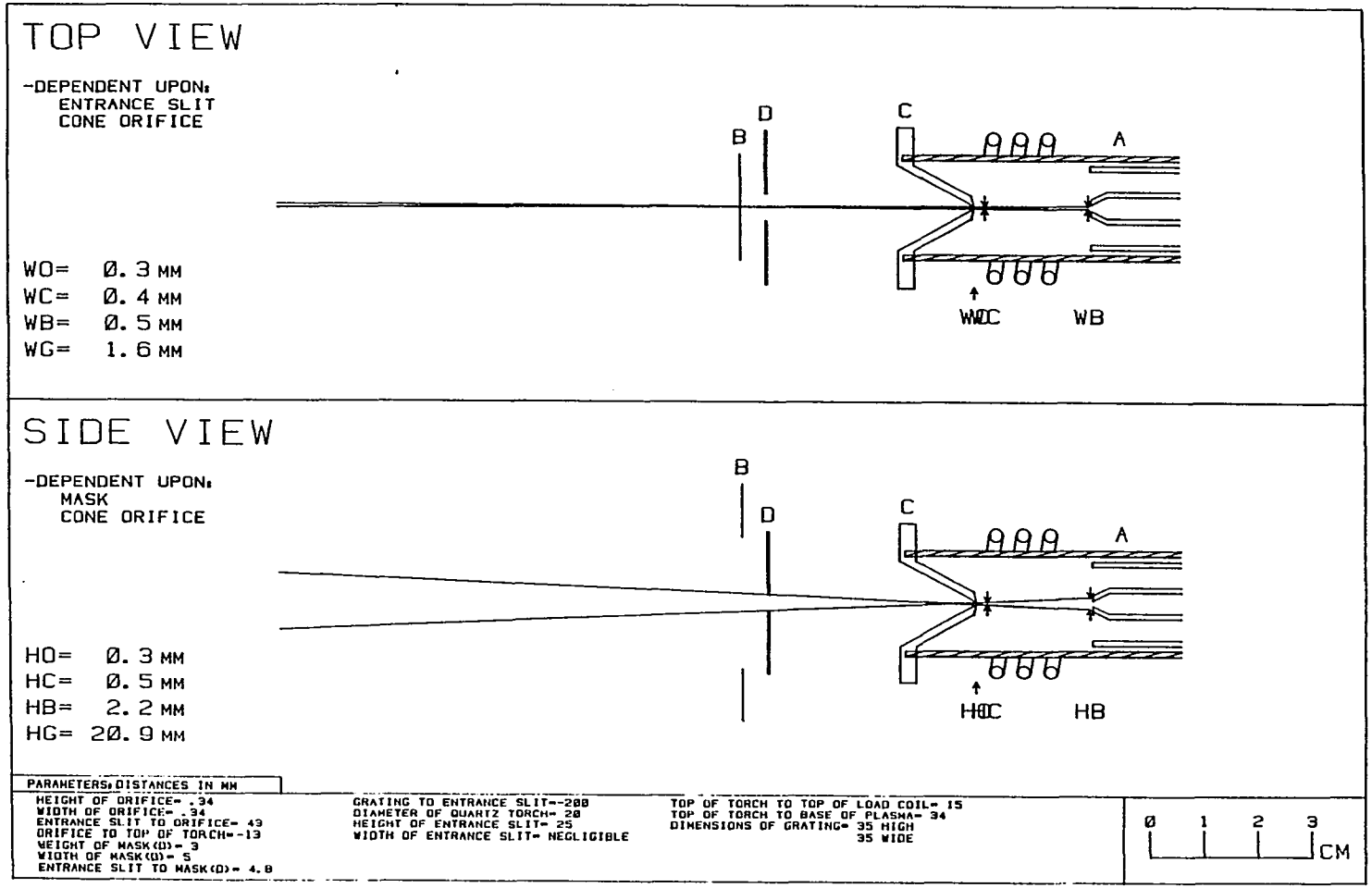

Figure 12. Vertical and horizontal fields of view of the Mode 1E cone assembly (0.34 mm diameter orifice). The symbols in this figure are previously described in Figure 10

result in a more defined field of view because the wedges of the Mode 2 cones could not be shaped into a fully enclosed opening. After experimentation with a Mode 2 cone with various orifice shapes, a Mode 1 cone, similar to the one described in the diagnostic section, was modified to incorporate the optimum orifice size found with the Mode 2 cone for maximum analyte emission from the plasma. A 3 mm hole(rather than 340 μm) was drilled as the cone orifice. This relatively large orifice facilitated analytical studies with the Ar ICP. The field of view of this cone assembly had the approximate dimensions of 10 mm high and 7 mm wide at the base of the plasma, as listed in Figure 13.

For the limits of detection (LOD) and interelement effect studies, the orifice, monochromator, and plasma were aligned so that the field of view of the spectrometer was as shown in Figure 13. The entrance slit and cone orifice limited the horizontal field of view, whereas the grating and cone orifice limited the vertical field of view. The height of the grating was fully illuminated whereas only half its width was illuminated. With a 3 mm diameter cone orifice, the field of view encompassed most of the axial channel where analyte emission occurred.

Methods of sample introduction

Aqueous sample introduction A Kniseley-type, pneumatic cross-flow nebulizer (99), combined with a Scott-type spray chamber (97), as shown in Figure 14, was used. Sample solution was drawn into the nebulizer with a peristaltic pump. With a cross-flow pneumatic nebulizer, nebulizer gas flowed across the capillary that transported the sample solution. The impact of the gas upon the solution created aerosol droplets that were carried by the nebulizer gas through the central tube of the torch into the axial channel of the ICP.

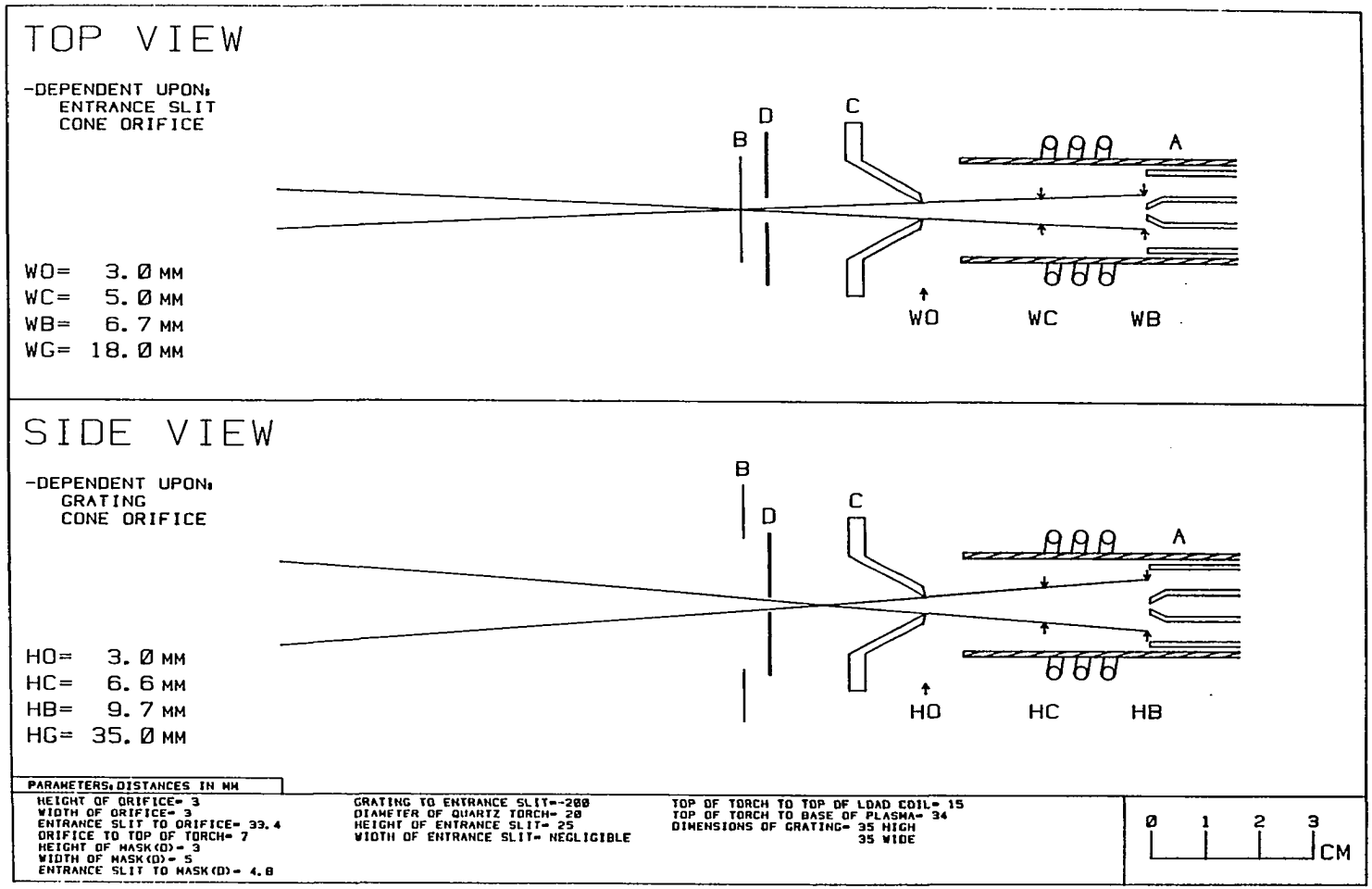

Figure 13. Vertical and horizontal fields of view of the Mode 1 cone assembly (3 mm diameter orifice). The symbols in this figure are previously described in Figure 10

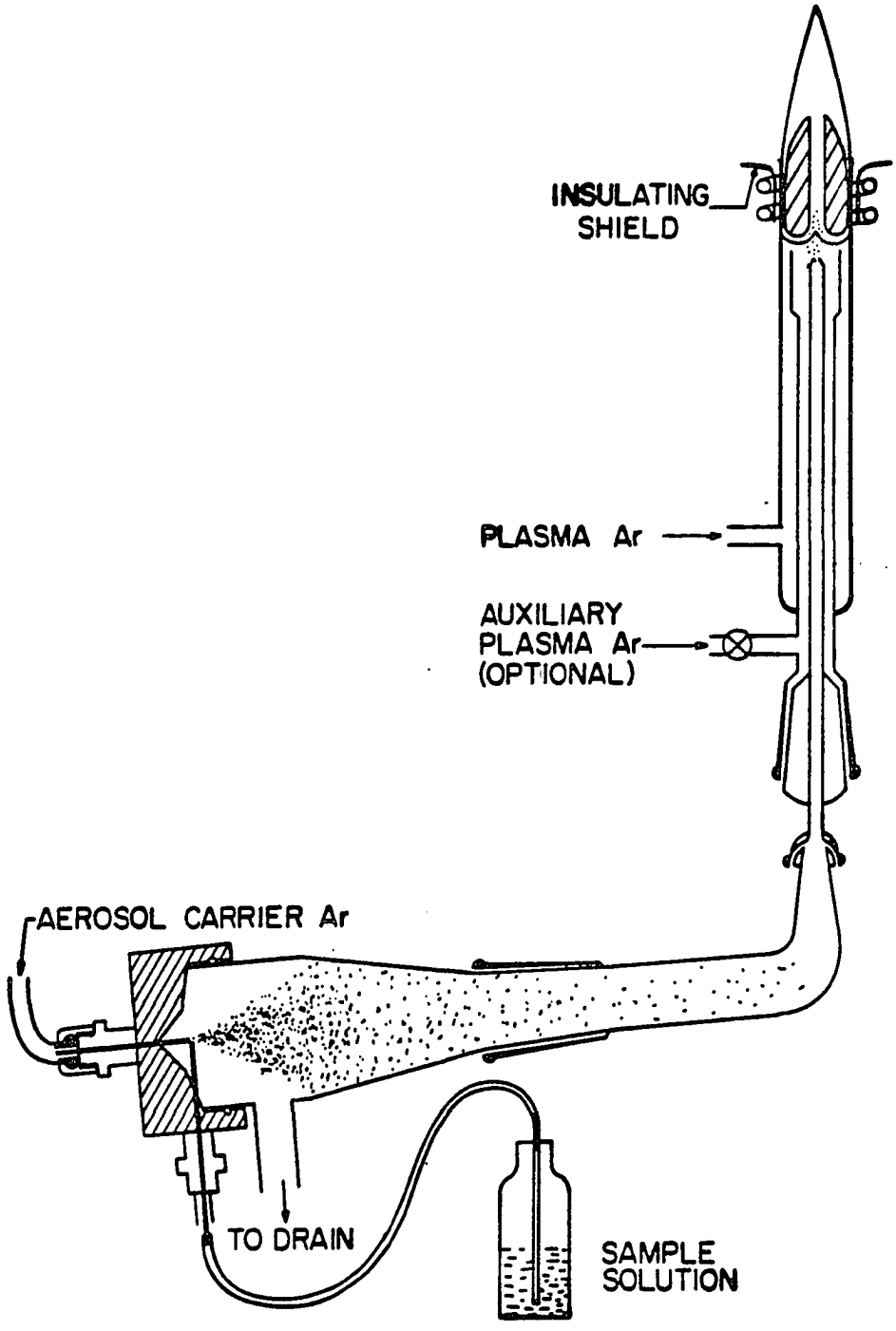

Figure 14. Ames Laboratory adjustable crossflow pneumatic nebulizer, conical spray chamber, and torch assembly

The ultrasonic nebulization system that was used has been described previously (98). Figure 15 illustrates the USN sampling system with aerosol desolvation. The analyte aerosol was swept through a conical spray chamber containing a Teflon baffle and into a heated desolvation tube. The analyte particles proceeded through a condenser to the injector tube of the ICP torch. The aluminum and Teflon transducer holder used for this study was similar in construction to the all Teflon mount used earlier (98), except that aluminum was incorporated in the top portion of the transducer holder design to provide a better seal for the cooling water lines. The width of the transducer holder was reduced from 41 to 35.5 mm, and the width of the spray chamber tube from 45 mm to 40 mm (36 mm i.d.). The assembly of the transducer holder and the operation of the USN system were analogous to earlier reports (98), except that the quartz plate was slightly smaller in diameter. Eccobond 55 and Catalyst 11 from Emerson and Cummings, Inc., were used to bond the USN transducer to the quartz plates, instead of the normal epoxy supplied in the storeroom. About 17 parts of Catalyst 11 and 100 parts of Eccobond 55 by weight were mixed together to form the adhesive. After application, the bonded parts were cured at 250°F (121°C) for 2 hours.

A new USN power supply was designed, constructed, and tested at Instrumentation Services by G. Holland and H. Skank. Earlier forms of the power supplies for the USN employed conventional vacuum tubes and RF technology, and were either built at the Ames Laboratory or obtained from Plasma-Therm. The new power supply is an all solid-state unit. A potentiostat was used to select the voltage output. A thumbwheel switch was used to obtain the desired frequency output. It was assumed that the bandwidth of the transducer was broader than the smallest change in the

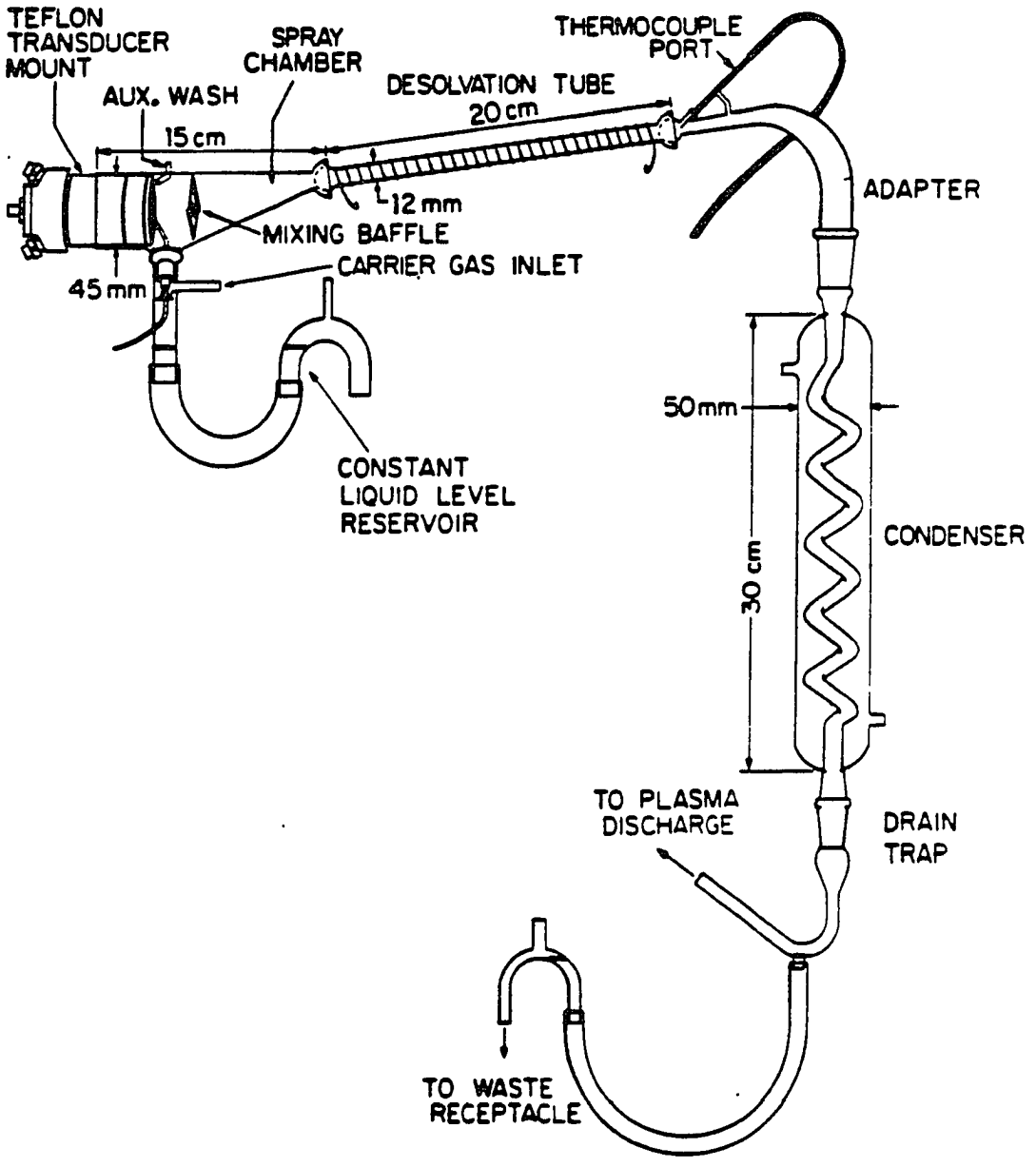

Figure 15. Schematic diagram of the Ames Laboratory ultrasonic nebulization sample introductory system and desolvation train

digital frequency thumbwheel switch (100 Hz). The range of the frequency output was from 1.0 to 1.6 MHz. Power meters (forward and reflected) were incorporated in a separate box that could be connected by a coaxial cable to the power supply. Relative power readings could be taken in this manner. The power supply delivered up to 50 watts to a 50 ohm resistive load.

The analyte solutions and carrier streams were continually drawn from a reservoir by a peristaltic pump and were introduced into either a cross-flow pneumatic nebulizer and Scott-type spray chamber or an ultrasonic nebulizer. Flow injection analysis (FIA) provided a rapid, precise means of changing samples without the background disturbance associated with air inclusion into the nebulizer and plasma. FIA was accomplished by employing a syringe loaded, sample loop injector (Model 7125, Rheodyne, Inc., Cotati, CA 94928) in line between the peristaltic pump and the nebulizer. The dead volume from the sample loop injector to the respective nebulizers was kept to a minimum (~20 to 30 μL) by the use of a short length of 0.3 mm i.d. Teflon tubing. The sample loop injector was switched manually to introduce a discrete sample volume to the nebulizers.

Gaseous sample introduction A schematic drawing of the direct injection probe (DIP) and ICP torch is shown in Figure 16. The ICP torch was an extended Fassel type (97) with a side injector gas inlet near the bottom. Also, the outer tube was extended to 32 mm from the top of the inner tube to prevent air entrainment. The basic construction principles of the DIP were derived from the direct injection nebulizer (DIN) for liquids (105-107). The DIP was incorporated directly within the ICP torch so that the tip of the quartz capillary was located just below the end of the injector gas tube. The quartz capillary (SpecTran Corporation,

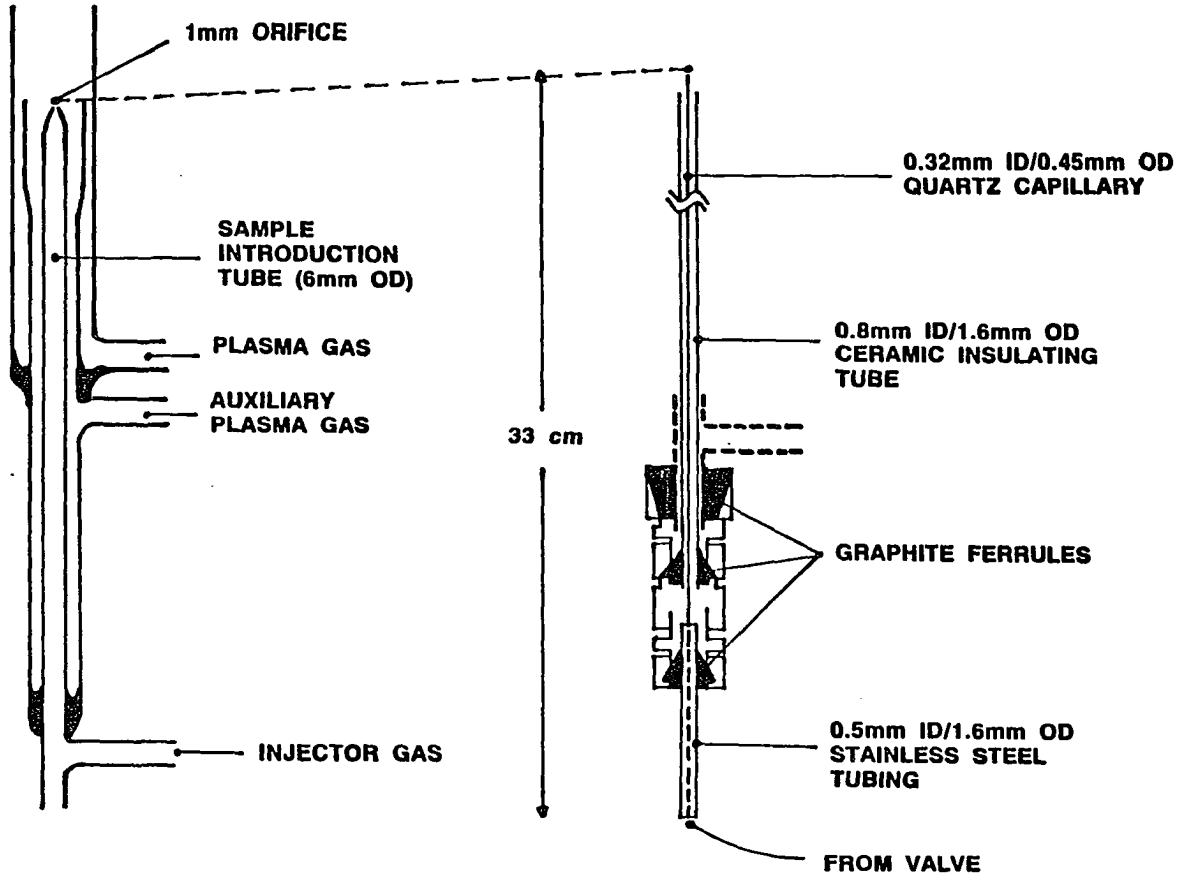

Figure 16. ICP torch (left) and DIP (right)

Sturbridge, MA 01566) was glued to a piece of stainless steel tubing for support in the Swagelok fitting. A low dead volume union connected the capillary to a short length of Teflon tubing (0.3 mm ID, 1.6 mm OD) that led to a 10-port Valco injection valve (1/16" ports, Alltech Associates, Inc., Deerfield, IL 60015). The dead volume between the injection valve and the tip of the quartz capillary was about 30 to 40 μL.

A detailed view of the tip of the DIP is shown in Figure 17. Sample carrier gas [A, Figure 17] flowed through the quartz capillary [B] to the base of the plasma. A ceramic insulating tube [C] (Omegatite 450, Omega Engineering, Inc., Stamford, CT 06907) positioned and supported the capillary. Argon injector gas [D], at a flow rate of 0.8 L min^{-1}, flowed between the injector gas tube [E] and insulating tube [C] and swept the sample from the capillary into the axial channel of the ICP. The alignment of the quartz capillary [B] relative to the ceramic tube [C] and the injector gas tube [E] was not critical because the injector gas flow rate was more than 100-fold greater than the sample carrier gas flow rate. Also, the samples were already gaseous, i.e., the DIP did not need to also serve as a nebulizer (105).

Flow injection analysis (FIA) of gaseous samples was accomplished by the employment of a 10-port injection valve in line between the DIP and the gas handling assembly; the schematic of the valve is shown in Figure 18. In position A, the sample gas filled the left sample loop while the sample carrier gas swept the contents of the right sample loop to the DIP assembly. With a sample gas flow rate of ~10 mL min^{-1}, the loops were adequately flushed prior to the transportation of the contents of the loops by the sample carrier gas at a rate of 2 - 3 mL min^{-1}. When the valve was switched to position B, the sample carrier gas transported

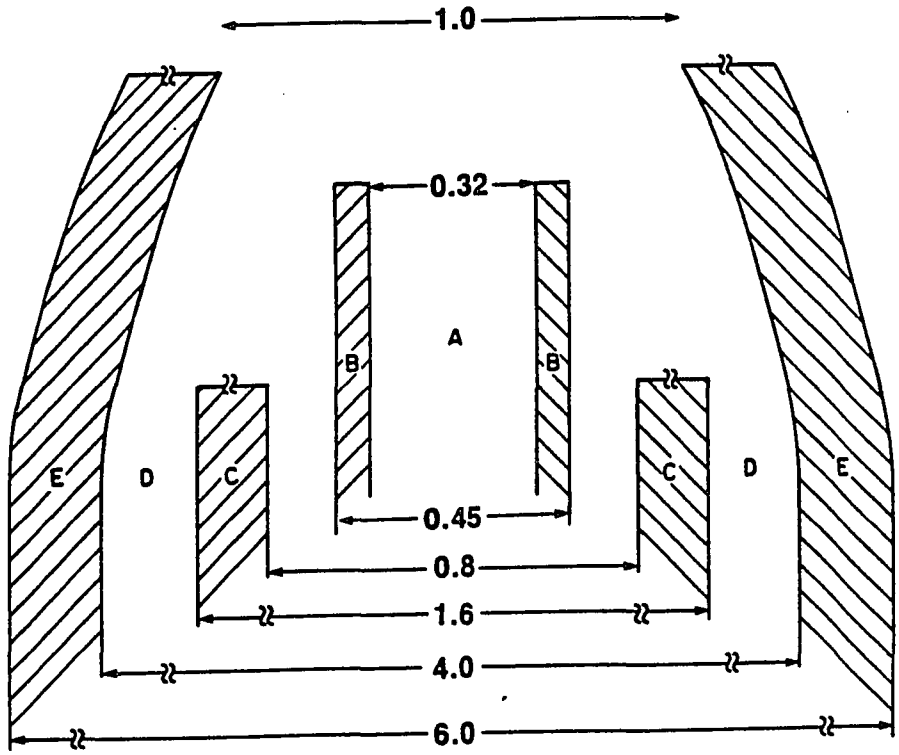

Figure 17. Closeup diagram of the tip of the DIP. Dimensions are in mm. See text for description of lettering system

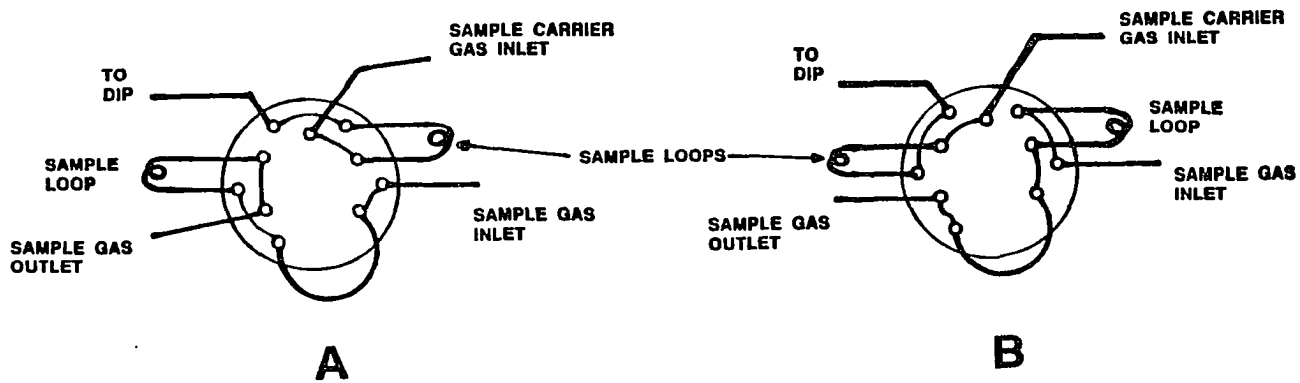

Figure 18. Schematic diagram of the two positions of the 10-port injection valve used for the FIA of gaseous samples into the DIP assembly

the contents in the left sample loop, which was previously filled, to the DIP while the other sample loop was filled with sample gas. This process was repeated for alternate injections of 2 sample loop volumes filled from the same gas source. The injection valve was switched by manual or electrical actuation. A Valco two position electric valve actuator was used for electrical actuation. The gas sampling valve that was utilized was similar to that described by Miller and Seliskar (108). Our gas handling and sampling assembly employed a 10-port injection valve and directional valves for the continuous or FIA introduction of gaseous samples into the ICP, which differed from the assembly in the work of Fry et al. (5) that utilized pneumatic actuators for slider injection valves.

The entire gas handling and sampling assembly including the injection valve and DIP is shown in Figure 19. Argon gas [A] was supplied to the plasma, auxiliary, and injector gas inlet of the ICP torch [J]. The Ar sample carrier gas [A] flowed to a directional valve [C] and was diverted to either a flowmeter [B] or directional valve [D]. From valve [D], the sample carrier gas entered the 10-port injection valve [G] and swept the contents of a sample loop into the DIP [I]. Sample gas [F] was piped into directional valve [E] where the gas proceeded to the injection valve [G]. After the sample gas filled a sample loop, the gas exited the injection valve [G] and advanced to a flowmeter [H]. During wavelength selection, sample gas [F] was directed continuously into the ICP by valve [E] to valve [D], which redirected the sample gas to the injection valve [G] and then on to the DIP [I].

Detection facilities

Photomultiplier tube (PMT) detectors A scintillator PMT was employed for the detection of VUV radiation below 110 nm. Sodium

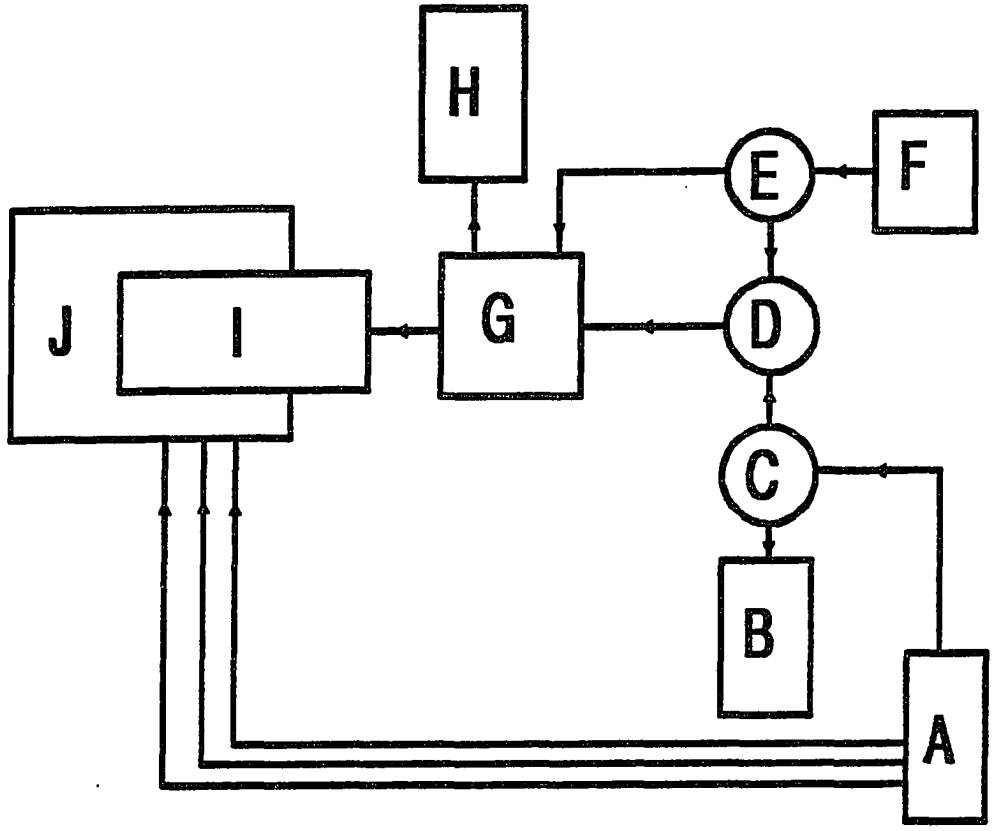

Figure 19. Schematic diagram of the entire gas handling and sampling assembly for gaseous sample introduction into the ICP by DIP-ICP-VUV-AES
[A] Ar gas cylinder and corresponding flowmeters and metering valves, [B,H] flowmeters, [C,D,E] 3-way directional valves, [F] sample gas cylinder and corresponding metering valve, [G] 10-port injection valve, [I] direct injection probe, and [J] ICP torch

salicylate was used as the fluorescent medium on the scintillator plate. A maximum voltage of 1200 V could be applied to the PMT, although 800 V was normally used. Although some windowless detectors do work well, it was decided to proceed with a scintillator/PMT combination. This scintillator/PMT combination provided a natural barrier to the pressure differential between the monochromator and PMT.

A solar blind PMT was utilized during most studies especially when signal detection below 110 nm was not required. The solar blind PMT had the following characteristics: MgF_2 window, linear focused tube type, and a spectral range of 110 to 360 nm. A PMT adapter flange was used to mount the solar blind PMT and its housing onto the exit slit chamber. When the monochromator was evacuated, the voltage to the solar blind PMT was turned off in order to avoid damage to the PMT. An arc discharge from the photocathode surface can occur under certain low pressure conditions (109). Voltages up to 2000 V (normally 1600 V) were applied to the PMT only after the monochromator had been purged with gas and pressurized to one atmosphere.

Recording electronics and data acquisition The output signal from the PMT was proportional to the amount of emission at a particular wavelength that the monochromator "saw" in the plasma. The output signal (current) was amplified by a Keithley picoammeter and converted to a voltage that was displayed by a Houston X-Y recorder. The Houston recorder had a patented capacitance position transducer that provided removal of electrical noise associated with potentiometers or slide-wire devices (110), although some problems still existed with RF interference with the recorder. The components mentioned above comprised the normal mode of acquiring spectra.

Various components were added to the recording electronics to enhance the quality of the recorded spectra and capabilities of spectra manipulation. An Apple IIe computer coupled with an ISAAC chromatography software module by Cyborg Corporation was incorporated in the detection system. The operating procedures for the ISAAC-Apple IIe system will be summarized in a later section.

A Spectrum 1021A active filter was employed between the picoammeter and the ISAAC-Apple IIe system to reduce the amount of noise encountered at the high sensitivity attenuation settings of the picoammeter. The picoammeter output was filtered electronically with a low pass filter that allowed signals whose frequencies were below a certain threshold to pass through undistorted (111). The threshold value was varied between 0.02 and 5 Hz. Because the active filter could only reject high frequency noises for input signals up to 1 V, and provided effective filtering without attenuation only for signals below 0.2 V, a 10-turn potentiometer with 1 kΩ resistance was used to convert the 0 to 3 V full scale signal of the picoammeter into a 0 to 0.1 V full scale signal. The gain of the active filter was switched to 10 so that a 0 to 1 V full scale signal was received at the X-Y recorder and ISAAC chromatography module.

Discussion of Radio Frequency Interference (RFI) Problems

Signal detection and recording were susceptible to electronic noise caused by radiofrequency interference. The problems of RFI and the modifications that were incorporated in the system to reduce the contributions to electrical noise are summarized in this section.

Theory

All RFIs are caused by radiative, inductive, conductive, and/or capacitive coupling (112). Radiative coupling occurs when the measuring circuits of the instrument are exposed to electrical fields. The fields indirectly produce false signals in the measuring circuit. Inductive coupling exists when the measuring circuit is in close proximity to a changing magnetic field of a motor, transformer, or circuit. Conductive coupling is associated with multiple ground connections that are not at the same potential. Leakage paths from the circuits to ground exist because total isolation from ground is not feasible. These multiple ground connections and leakage paths create potential differences that result in current flow between the separate ground points, producing fluctuations in current in the measuring circuit. Capacitive coupling occurs when leakage paths to ground exist. Unlike conductive coupling, these paths are capacitive in nature instead of conductive.

All forms of electrical coupling to the measuring circuits of the instrument result in some degree of perturbation and/or inaccuracy in the measurement. Random and intermittent occurrences of noise in the measuring circuit usually result because sources of RFI do not efficiently couple to measuring circuits, in most cases.

Instrumental modifications to reduce RFI

Several experimental modifications greatly reduced the magnitude of the RFI problem. A copper shielding box with overlapping seams and a screen mesh for the viewing aperture was used to enclose the plasma. Only two other apertures existed in the box, one for the top of the torch and the other for the bottom of the torch and gas lines. This copper shielding box, which was attached to ground, helped to confine the

radiofrequency radiation that originated from the plasma and load coil and allowed no current to flow through the box because the box possessed low impedance and was a good reflector of RF radiation.

The copper leads to the load coil were reversed from their normal orientation, i.e., the tubing leading to the leftmost turn (closest to the shielding box) of the load coil was connected to ground, while the righthand turn (farthest from the shielding box) led to the RF terminal of the impedance matching network. This arrangement is clearly shown in Figure 20. This reversed orientation greatly alleviated arcing from the load coil to the shielding box or sampler.

As shown in Figure 20, a Teflon or Viton gasket [H] was used to electrically isolate the cone assembly from the monochromator [F]. Nylon screws affixed the cone flange [G] to the monochromator and the gasket was sandwiched between them to provide the electrical isolation. When the plasma impinged upon the cone, RF waves radiated to the cone. A flexible copper strap [M], attached from the cone assembly to ground at the shielding box, prevented RF radiation from conductive and /or capacitive coupling through the gasket to the monochromator. This arrangement isolated the cone assembly from the monochromator and "diverted" RF radiation back to ground by a low impedance ground path. The copper strap, folded as an accordion, was 0.003 in. thick and had a very low impedance, which is important for grounding applications. Braided straps have an impedance ten times that of solid straps and wire has an even higher impedance (113).

The magnitude of the RFI problems was also reduced by magnetic/electrostatic shielding of the PMT. The solar blind PMT housing also was provided with RFI shielding. The preamplifier of the picoammeter

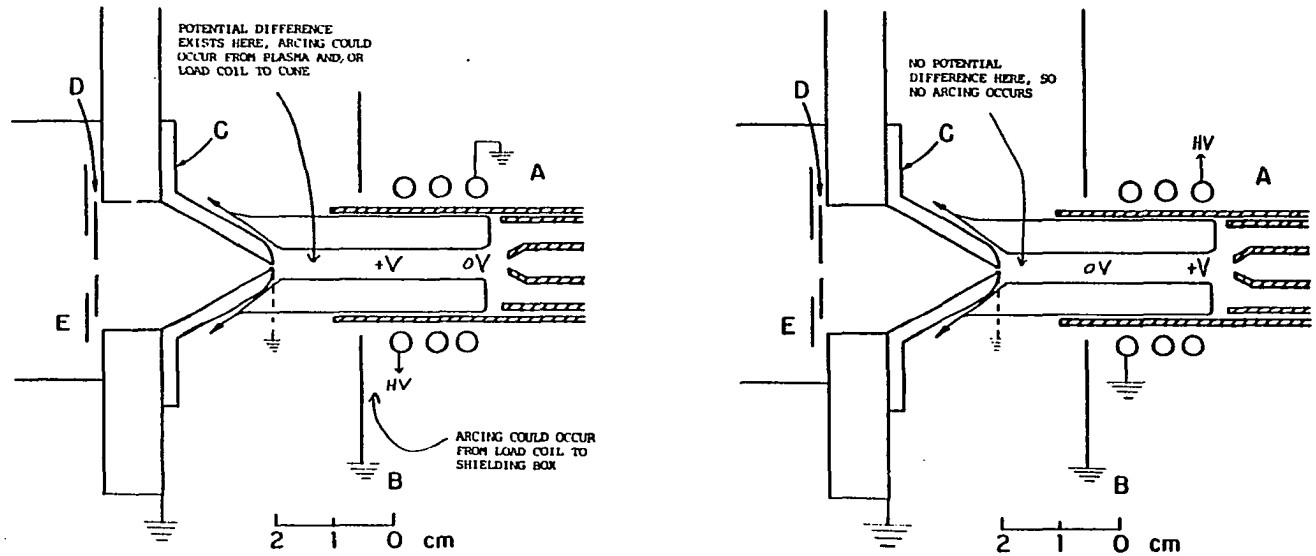

Figure 20. Comparison of the orientation of the copper leads to the load coil for
(A) conventional ICP-AES and
(B) the present work (reverse orientation with respect to conventional ICP-AES).
Symbols A through E are the same as shown in Figure 4

was connected with a 6 in. BNC coaxial cable to the signal output of the PMT. The proximity of the preamplifier with respect to the PMT reduced amplification of RF signals that could be picked up by the coaxial cable. With changing magnetic field, the voltage, resulting from inductive coupling, is directly proportional to the net area enclosed by the loops of the measuring circuit (112). In a coaxial cable, the signal leads were twisted to provide adjacent areas, enclosed by the circuit loops, of equivalent magnitude, but opposite in sign. Therefore, equal but opposed induced voltages lead to the absence of any net inductive RF coupling. Physical separation of high power leads from low power signal leads also reduced inductive RF coupling.

A spectrum 1021A active filter for detector noise was employed between the picoammeter and the ISAAC-Apple IIe system as described earlier. The ISAAC-Apple IIe system was more receptive to noise than the recorder. The computer screen displayed peak cycles throughout the background. The peak cycles were observable when the attenuator setting on the picoammeter was at 10^{-10} amps. At this high sensitivity setting, an oscilloscope was employed to detect these peak cycles. When all plasma instrumentation was off with the exception of the picoammeter, the oscilloscope detected 15 ms cycles (60 Hz) originating from the picoammeter. Although the recorder with its long time constant (up to 1 s) detected these cycles as random noise, the computer, sampling from 10 to 100 times s^{-1}, could detect this noise as a cyclic phenomenon. This 60 Hz noise was the major contributor to the dark current. The active filter slightly reduced the peak signal intensity but drastically reduced the background noise, thereby improving the LOD of the analyte.

Operating Procedures

Extensive references to Figures 3 and 4 will be made in the following discussion of the operating procedures. Letters that are underlined with brackets refer to components in Figure 4 and bold letters in brackets refer to components in Figure 3.

Setup and initiation of plasma

The following actions were performed before ignition of the ICP was attempted. If the scintillator PMT was in use, voltage was applied to the PMT before evacuation of the monochromator. If the solar blind PMT was in use, voltage was not applied to the PMT during evacuation because of the damage that may occur to the PMT. Voltage was applied to the PMT only when the pressure in the monochromator was stabilized at one atmosphere. The cone assembly [C] was attached to the entrance slit chamber before the initial evacuation of the monochromator, and the sampling orifice was sealed vacuum tight by a Viton plug. The mechanical pump [H] was turned on and its bellows valve slowly opened to allow the pump to evacuate the monochromator [G] through the pumping port [I]. When a pressure of a few mtorr was reached, the bellows valve was closed, and He purge gas was then released through the inlet valve [L] into the monochromator. The inlet valve was then closed, and the bellows valve was again opened. Repetition of the above cycle reduced the air content of the monochromator and gas line to an acceptable level. Pressure in the monochromator during the purging did not exceed one atmosphere. When a pressure of a few mtorr was reached after performing the procedure discussed above, the bellows valve was closed and the purge gas, helium [J], was released through the inlet valve into the monochromator. The vacuum between the bellows valve and pump was released by opening a relief valve to the atmosphere. After the

vacuum was released, the relief valve was closed. When a pressure slightly greater than atmospheric pressure was attained in the monochromator, the Viton plug was removed from the sampling orifice and helium gas escaped out of that orifice. The positive pressure inside the monochromator prevented air from entering the monochromator during the removal of the Viton plug. Care was taken to insure that the monochromator was vacuum tight so that air could not leak into the system during evacuation or purging. All vacuum seals were periodically checked. Pressure in the monochromator was never allowed to greatly exceed one atmosphere because of the possibility of breaking vacuum seals.

After the evacuation/purging cycle was completed and helium gas flowed through the cone assembly, the ICP was ignited by the following procedure. The cone was grounded via a short detachable copper strap [M] to the copper shielding box [B]. The cone itself was initially positioned and centered 1 cm from the top of the outer quartz tube of the torch [A]. If the plasma was initiated at distances greater than approximately 10 cm, arcing invariably occurred from the plasma tail flame to the cone. The outer, auxiliary, and aerosol gas flow rates were set at 15, 0.45, and 0.0 L min^{-1}, respectfully. The pressure regulator on the aerosol gas line was set at the appropriate pressure that delivered the desired gas flow rate. The diaphragm flow controller was closed. The RF generator [D] was turned on and its potentiometer was positioned at 680, which corresponded to 1.3 kW of forward power delivered to the impedance matching network [C]. A Tesla coil was turned on until the spark initiated the plasma as power from the generator was increased to the desired level. After the plasma was ignited, the aerosol gas flow was slowly initiated by a diaphragm flow controller, and the auxiliary gas line was then closed by a flow regulator

valve. Care was taken to increase the aerosol gas flow rate slowly, while continuously adjusting the capacitors in the coupling box to maintain minimum reflected power and plasma stability. When the aerosol gas flow rate reached about 0.4 L min^{-1}, the peristaltic pump was turned on (1.0 mL min^{-1}), and aerosol was created by the cross-flow nebulizer [B] and transported into the plasma. The diaphragm flow controller was slowly rotated to a wide open setting, allowing the plasma to stabilize between adjustments. A completely open setting of the diaphragm flow controller resulted in an aerosol gas flow of 0.8 L min^{-1} when the pressure regulator was set at 21 or 40 psi, dependent upon the particular pneumatic nebulizer that was used. The procedure outlined above consistently led to a stable plasma that impinged upon the cone assembly.

The He purge gas flow prevented any contamination of the monochromator by the plasma, but during plasma operation, solids were deposited as a film on the outer surface of the cone. The deposited film was wiped from the cone with a damp tissue after plasma operation. Removal of the cone for intensive cleaning (e.g., with steel wool) was necessary only once a month. No deterioration in the shape of the cone orifice was evident after several hundred hours of exposure to the plasma.

Air must be prevented from entering the atmosphere of the monochromator during ICP-VUV-AES operation. A quick method to determine if air had entered the monochromator was to scan the background N I lines. If the intensity ratio of N I 174.27 and 174.52 nm/N I 149.26 and 149.47 nm was unusually high (>5) then nitrogen (air) had leaked into the system. The intensity of the N I 174.27, 174.52 nm and N I 149.26,149.47 nm lines were usually of the same magnitude when evacuation and purging of the monochromator was performed adequately. When air entered the

monochromator, the N I 149.26, 149.47 nm lines were more susceptible to absorption than the N I 174.27, 174.52 nm lines.

Data acquisition

The operating procedure for the ISAAC-Apple IIe system [N] is documented in the Cyborg ISAAC instruction manual (114). The input wires of the ISAAC module were connected to the input of the recorder. After the initial insertion of the ISAAC chromatography disks (version #1.1.0) into the disk drives, the Apple IIe computer screen displayed appropriate instructions for the operation of data collection and manipulation. When the monochromator was scanned over the desired wavelength region and the computer was in the data collection mode, data acquisition started when any key was depressed. The recorder was simultaneously started. When the instruction menu shown on the computer screen followed, it was possible to collect data, display data, detect peaks in a spectrum, produce the desired baseline, filter the baseline and peak data from the noise, calculate the adjusted peak heights and areas, and print out the above results with the ISAAC-Apple IIe system. The following are instructions for the ISAAC-Apple IIe system that have not been previously documented. The offset on the ISAAC module should be set at 502. For a 0 to 3 V range, the range on the ISAAC module should be set at 620 and for a 0 to 1 V range, the setting should be at 208.

Experimental studies

Preparation of reference solutions

Aqueous solutions For the LOD determinations, stock solutions of the various elements at 100 to 10,000 μg mL^{-1} were prepared. Appropriate dilutions of the stock solutions served as the reference solutions for LOD determinations. For the interelement effect studies,

individual 50 μmole mL^{-1} solutions of Br, Cl, and Al were prepared by dissolving either NaBr, NaCl, or $Al(NO_3)_3 \cdot 9H_2O$ in water and diluting to volume. A Na concomitant stock solution was prepared from $NaNO_3$. Aliquots of these stock solutions were combined and diluted with deionized distilled water to obtain the necessary concentrations for the Na interference studies. For the Al - Ca interelement effect studies, aliquots from a stock solution of Ca and Al were introduced into volumetric flasks to obtain concentrations of 0.5 μmole mL^{-1} of Ca and Al, respectively. Aliquots from the interferent stock solutions, prepared from $Al(NO_3)_3 \cdot 9H_2O$ and $CaCO_3$, were added to the corresponding solutions to obtain the necessary concentrations for the interference studies. To compensate for any shift in the background underlying the Br, Cl, Al, and Ca lines, reference blank solutions containing 0, 3, 10, 30, 100, and 300 μmole mL^{-1} Na, Al, or Ca, corresponding to the same total Na, Al, or Ca concentrations in the Br, Cl, Al, and Ca solutions, were used for background correction.

Gaseous samples Welding grade argon gas was used as the outer, auxiliary, injector and sample carrier gas flows. A single gas mixture was utilized for the limits of detection of various nonmetals and FIA experiments; this mixture contained 99 ppm (v/v) SF_6, 99 ppm Freon 12 (CF_2Cl_2), and 98 ppm Freon 13B1 (CF_3Br) with the balance as argon (Matheson Gas Products, Joliet, Illinois 60434). In the FIA mode, sample loop volumes from 50 to 250 μL provided the capability of injecting analyte in amounts of approximately 7 to 34 ng S, 15 to 75 ng Cl, 17 to 83 ng Br, and 5 to 25 ng C.

Caution was taken when gases containing F were introduced into the ICP because of the chemical reactivity of F atoms with the quartz torch

and the metal sampling cone. These observations confirmed those of Fry et al. (5) who found that low sample gas flow rates could result in severe erosion of the torch unless proper experimental procedures were implemented. At an injector gas flow rate of ~0.3 L min^{-1}, the sample gas was diluted by the injector gas so that the erosion rate of the torch was minimized. Any discoloration of the torch due to erosion by atomic fluorine did not hinder observation of analyte emission from the plasma because end-on viewing was employed in the present study. During introduction of other elements into the plasma, the surface of the copper sampling cone was only slightly discolored after a day of plasma operation. During two to four hours of operation with SF_6 being introduced into the plasma at low injector gas flow rates, the rate of discoloration was accelerated but this mild erosion of the cone did not affect the size of the sampling orifice, and the cone could be easily cleaned. The same cone was used throughout these studies and nebulization experiments for a total operating time of several hundred hours.

Analytical figures of merit studies A solar blind PMT was used because the signal-to-noise ratios were superior to those obtained from the scintillator PMT described previously. Although the signal intensity of the lines from 100 to 160 nm decreased 10 to 20-fold (5-fold for lines near 200 nm) for the solar blind with respect to the scintillator PMT, the noise fluctuations (at 171.7 nm) decreased roughly 30 to 60-fold. Thus, the signal to noise ratio increased roughly 3 to 12-fold for the solar blind with respect to the scintillator PMT. The solar blind PMT did not detect second order spectra of the lines with wavelengths below 113 nm so the background from 160 to 225 nm with the solar blind PMT was cleaner from emission lines with respect to the scintillator PMT. Use of a

grating coated with MgF_2 (instead of an Os) increased the intensity of all lines from 100 to 200 nm by 100 to 200% (150 to 175% near 200 nm), while background noise fluctuations (at 171.7 nm) were similar for the two gratings.

For aqueous sample introduction into the ICP, LODs were determined as the concentration of analyte that produced a net peak height that was three times the standard deviation of the background as measured by the following procedure. Intensities were measured 5 times per second and the standard deviation was calculated for a 20 s background blank. This process was repeated for 5 to 10 different 20 s background blanks; the standard deviations used to estimate the detection limits were the average of these 5 to 10 determinations. A setting of 0.02 Hz for the active filter was used during most of the figures of merit and interelement effect studies.

The computer program (LODS), listed in Appendix C, was used for the calculation of LODs based upon the data acquired from the ISAAC-Apple IIe system. The data files were kept on floppy discs for future reference.

For the detection limit studies with DIP introduction of the gaseous mixture described in the Gaseous samples section, sample loop volumes from 50 to 250 μL were injected into the axial channel of the plasma. The monochromator was set for the wavelength of interest and the LODs were calculated in the same manner as reported for aqueous samples. These LOD values were extrapolated from injections of the reference mixtures that contained concentrations considerably above (100X) the detection limits because of the unavailability of inexpensive commercial standards and the difficulty to readily make more dilute standards. This extrapolation was valid because a) calibration curves in ICP-AES were typically linear at

concentrations near the detection limit (115), and b) previous studies employing aqueous nebulization yielded linear calibration curves for various VUV lines including the same lines of Br and Cl used in this work. A low pass electronic filter was used to allow signals whose frequencies were below a certain threshold to pass through undistorted. A threshold value of 0.02 Hz was used for the LOD studies with the 250 μL loop. Similar absolute LODs were obtained with 50 μL sample loops and a threshold value of 0.1 Hz for the filter. The threshold value that was used for the flow injection profiles will be noted in the figures.

Fluorine atomic emission Sulfur hexafluoride (99.8%, Matheson) was introduced into the DIP at ~2 to 3 mL min^{-1} and was then swept into the axial channel of the ICP with the injector gas flow (0.3 L min^{-1}). For the blank spectrum, Ar was introduced into the DIP at ~10 mL min^{-1}. The fluorine spectra were detected with a scintillator-PMT detector and Os-coated grating by viewing the axial channel off center (by 3mm) with the sampling orifice about 10 mm from the load coil (versus the normal 22 mm for observation of lines from other nonmetals). Also, the auxiliary gas flow rate was increased to 0.45 L min^{-1}. These variations in the operating parameters led to greater signal/noise ratios of the F I emission lines than the employment of the normal operating conditions.

Diagnostic studies A scintillator PMT was used to observe spectra below 100 nm due to the inability of the window (MgF_2) of the solar blind PMT to transmit radiation below 115 nm. The response of the sodium salicylate scintillator was relatively constant from 30 to 100 nm (116).

For the initial spatial studies of the Ar resonance lines, the photomultiplier response was measured by a conventional electrometer and

recorded on an X-Y recorder. Integrated intensity data were measured using a digital voltmeter and printer to record the electrometer output. The background intensity for these integration experiments was measured at 110 nm. For the spatially resolved results reported in the Ar resonance line studies, the ICP was translated laterally in 1 mm increments.

CHAPTER III. AQUEOUS SAMPLE INTRODUCTION

General Features of VUV Region

Common background features

The only intense Ar lines in the VUV were at 104.82 and 106.67 nm, which are only observable with a scintillator PMT. Relatively intense background emission lines from H, C, N, and O occurred in the VUV region (Figure 21). The low background emission was a benefical characteristic that is inherent in the VUV region. The spectral lines observed were quite similar to those previously reported by Carr and Blades (77), who viewed the plasma from its side. The continuum background level in the VUV region was one to two orders of magnitude less intense than the visible region. The low background level should, theoretically, improve the signal to noise ratio with respect to the near infrared (NIR) lines. The continuum background level was mainly due to scattered light and emission from molecular band systems with no measurable contributions from radiofrequency interference. The addition of nebulized water to the axial channel led to the emission of weak lines in the 160 nm region, which were similar to the line-like band spectrum previously reported for molecular H_2 (117,118). The origin and diagnostic significance of these lines will be addressed in Chapter V. Also, spectral features in the wavelength range below 100 nm with and without the addition of nebulized water into the plasma will be described in Chapter V.

Common analyte lines

Prominent lines emitted by various Group IIIB-VIIB elements in the wavelength range of the solar blind photomultiplier are tentatively assigned in Table III. Only emission lines whose intensities were greater

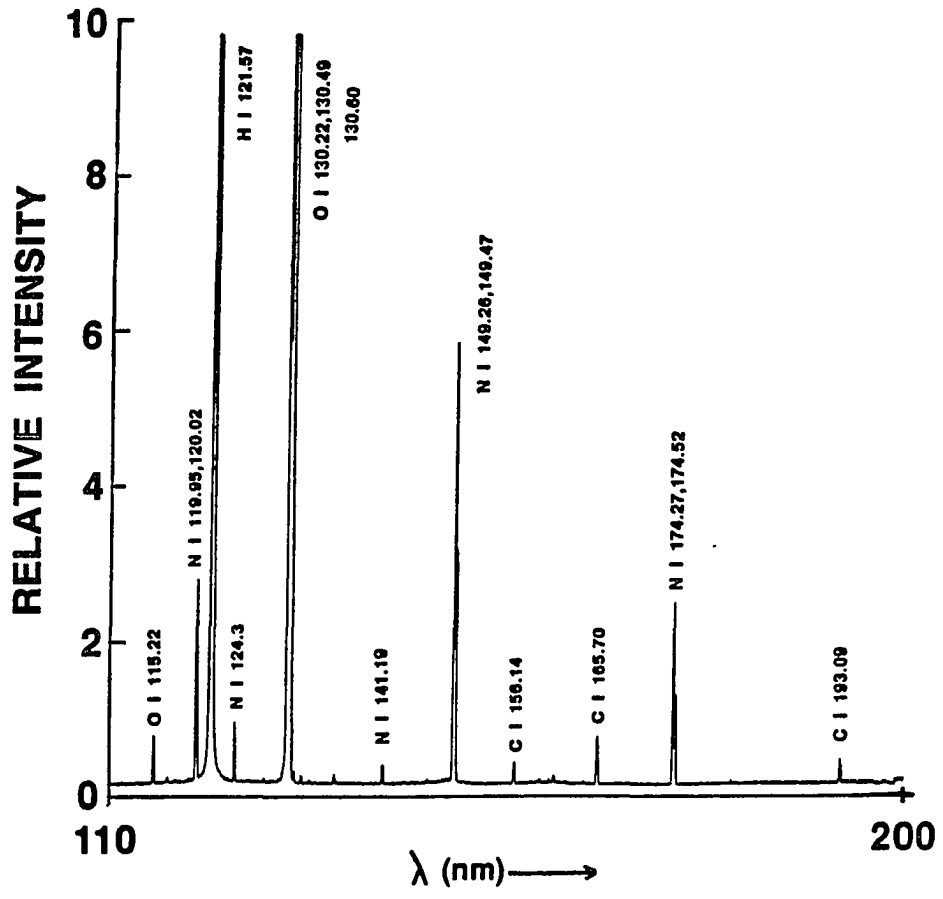

Figure 21. Wavelength scan from 110 to 200 nm of the background spectrum from an ICP using the Mode #1 cone (3 mm diameter orifice) assembly and the solar blind PMT for detection

Table III. Prominent lines emitted in the region 115 - 295 nm by various Group IIIB–VIIB elements excited in an ICP. Pneumatic nebulization was the mode of sample introduction. Only spectral lines whose intensities are greater or equal to 5 percent of the most intense line of that particular element are listed.

Element	Wavelength (nm)	Relative Intensity[a]
Al II	167.08	100
As I	157.39,157.47, 157.59	9
As I	159.36	15
As I	175.86	11
As I	180.62	9
As I	189.04	100
As I	193.76	81
As I	197.26	47
As I	199.04,199.11	21
As I	200.33	30
As I	228.81	64
As I	234.98	45
As I	278.02	7
B II	136.25	12
B I	166.69,166.73	8
B I	182.59,182.64	42
B I	208.89,208.96	34
B I	249.68,249.77	100
Bi II	124.11	10
Bi II	143.68	21
Bi II	145.51	14
Bi II	153.32	21
Bi II	161.14	6
Bi II	177.71	24
Bi II	179.19	45
Bi II	190.24	80
Bi I	195.39	8
Bi I	206.17	25
Bi I	213.36,213.43	10
Bi I	222.83	40
Bi I	223.06	100
Bi I	227.66	8
Bi I	289.80	8
Bi I	293.83	6
Br I	121.08	6
Br I	131.77	26
Br I	138.46	14
Br I	144.99	19
Br I	148.85	60
Br I	153.17	34
Br I	154.07	100
Br I	157.48	17
Br I	157.64	9
Br I	158.23	5
Br I	163.34	15
Cl I	118.88	12
Cl I	133.57	26
Cl I	134.72	100
Cl I	135.17	39
Cl I	136.34	24
Ga II	141.44	100
Ga I	229.42	9
Ga I	250.02	8
Ga I	287.42	21
Ga I	294.36,294.42	32

[a]All intensities are relative to the most intense line (normalized to 100) of that particular element.

Table III. (Continued)

Element	Wavelength (nm)	Relative Intensity[a]
Ge II	123.71	11
Ge II	126.19	18
Ge II	160.26	40
Ge II	164.93	70
Ge I	199.89	13
Ge I	201.91	7
Ge I	204.17	17
Ge I	204.38	15
Ge I	206.52	8
Ge I	206.87	25
Ge I	209.43	37
Ge I	219.87	29
Ge I	241.74	9
Ge I	259.25	31
Ge I	265.12,265.16	100
Ge I	269.13	16
Ge I	270.96	26
Ge I	275.46	25
I I	142.55	14
I I	145.74,145.88, 145.80,145.91	8
I I	158.26	12
I I	161.76	20
I I	164.08,164.21	6
I I	178.28	100
I I	179.91	12
I I	183.04	15
In II	158.64	100
In II	230.61	15
P I	138.15,138.17	7
P I	168.60	9
P I	169.41,169.45	8
P I	177.50	100
P I	178.29	69
P I	178.77	36
P I	185.89,185.94	42
P I	213.55,213.62	70
P I	214.91	40
P I	215.29,215.41	5
P I	253.57,253.40	15
P I	255.33,255.49	?

Element	Wavelength (nm)	Relative Intensity[a]
Pb II	120.36	5
Pb II	143.39	22
Pb II	167.15	33
Pb II	168.22	64
Pb II	172.68	10
Pb II	179.67	10
Pb II	182.20	34
Pb I	217.00	21
Pb II	220.35	100
Pb I	261.42	21
Pb I	266.32	6
Pb I	280.20	15
Pb I	283.31	15
S I	142.51	14
S I	143.33	9
S I	147.30,147.40, 147.44,147.45	12
S I	148.17,148.31, 148.32	8
S I	166.67	22
S I	180.73	100
S I	182.04	57
S I	182.63	19
Sb II	138.48	7
Sb I	138.89,138.96	5
Sb II	143.66	14
Sb II	143.83	10
Sb II	150.43,150.58	8
Sb II	151.33	15
Sb II	156.55	25
Sb II	158.46	14
Sb I	160.00	10
Sb I	171.69,171.75	7
Sb I	176.27,176.37	10
Sb I	178.09	8
Sb I	180.02	6
Sb I	181.05	7
Sb I	181.42	8
Sb I	187.12	32
Sb I	188.26	7
Sb I	192.71	5
Sb I	195.04	21

Table III. (Continued)

Element	Wavelength (nm)	Relative Intensity[a]
Sb I	204.96	11
Sb I	206.83	100
Sb I	209.84	7
Sb I	213.71	8
Sb I	213.97	14
Sb I	214.18	5
Sb I	214.49	12
Sb I	217.58	86
Sb I	217.92	24
Sb I	220.85	7
Sb I	231.15	62
Sb I	252.85	50
Sb I	259.81	45
Sb I	287.79	5
Se I	153.04	17
Se I	157.95,158.00	12
Se I	160.65	14
Se I	161.74	8
Se I	167.12	6
Se I	185.52	24
Se I	196.09	100
Se I	203.99	45
Se I	206.28	16
Si ?	125.95	9
Si ?	126.38	15
Si II	152.67	14
Si II	153.34	26
Si I	169.62	5
Si I	169.79	7
Si I	184.61	8
Si I	184.75	17
Si I	185.07	26
Si I	190.13	6
Si I	198.90	8
Si I	212.41	37
Si I	220.80	5
Si I	221.09	14
Si I	221.67	22
Si I	243.52	10
Si I	250.69	34
Si I	251.43	52
Si I	251.61	100
Si I	251.92	20
Si I	252.41	27
Si I	252.85	35
Si I	288.16	35
Sn II	129.09	6
Sn II	131.66	10
Sn II	140.05	40
Sn II	147.50	55
Sn II	175.79	49
Sn II	181.12	22
Sn II	183.18	7
Sn II	189.99	100
Sn I	215.08,215.14	6
Sn I	220.97	7
Sn I	224.61	12
Sn I	226.89	11
Sn I	231.72	6
Sn I	235.48	18
Sn II	242.17	10
Sn I	284.00	17
Sn I	286.33	7
Te I	170.00	33
Te I	175.10	9
Te I	175.94	8
Te I	179.57,179.63	6
Te I	182.24	23
Te I	185.06	9
Te I	185.21	6
Te I	185.72	10
Te I	200.20	10
Te I	208.12	9
Te I	214.28	100
Te I	214.73	13
Te I	225.90	15
Te I	238.33	16
Te I	238.58	26
Tl II	132.17	26
Tl II	190.86	100
Tl I	276.79	21

than 5% of the most intense line of that element in the 113 to 295 nm region are shown. The relative intensities for the various lines shown in Table III were typical and depended on experimental factors such as the pressure attained when the monochromator was first evacuated, the purity of the He purge gas and Ar gas, the spectral response of the grating and detector, and plasma conditions. The values of the wavelengths were derived from previous tabulations by Kelly et al. (119,120) for wavelengths less than 200 nm (vacuum values), and Winge et al. (12) and Wohlers (121) for those greater than 200 nm (air values).

Many possible emission lines for analysis exist in the UV and VUV regions. For the wavelength region observed, most of the elements in Table III have their most intense emission line in the VUV region. Even for some elements that possess their strongest line in the UV, the signal/noise ratios of some VUV lines were superior to the UV lines due to the lower background noise in the VUV region. Extensive research on the VUV emission lines of metals has not been accomplished. Spectral interferences of very weak neighboring lines could complicate the determination of nonmetals, metalloids, and selected metals in real world samples. Care must be taken to prepare background blanks and matrix matched analytical standards to insure that emission is obtained from the desired analyte and not an unwanted concomitant.

The most intense lines of Br and Cl are shown in Figure 22. From these spectra, it was apparent that Br and Cl were detectable at trace levels. An example of the peaks observed when an aqueous solution containing 100 ng mL^{-1} Br was repetitively injected via flow injection into an ultrasonic nebulizer is shown in Figure 23. Flow injection analysis allowed for the observation of a continuous background blank

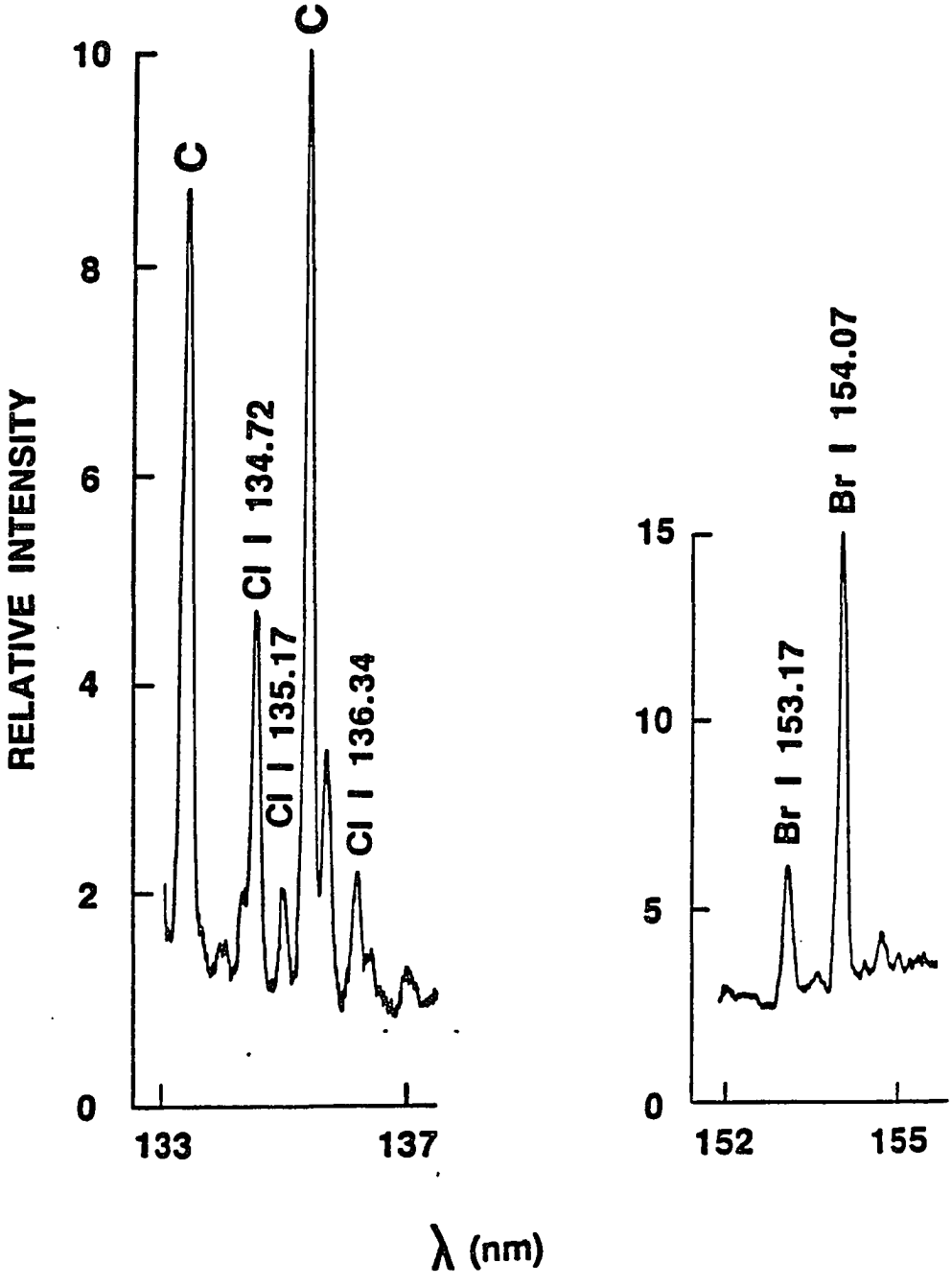

Figure 22. Wavelength scans of the Cl and Br resonance emission lines during continuous introduction of NaCl (18 μg mL^{-1} Cl) and NaBr (40 μg mL^{-1} Br) solutions by pneumatic nebulization. The same arbitrary units are used for the vertical scales in the two spectra. The two strongest lines in the first spectrum (marked C) are believed to be from carbon

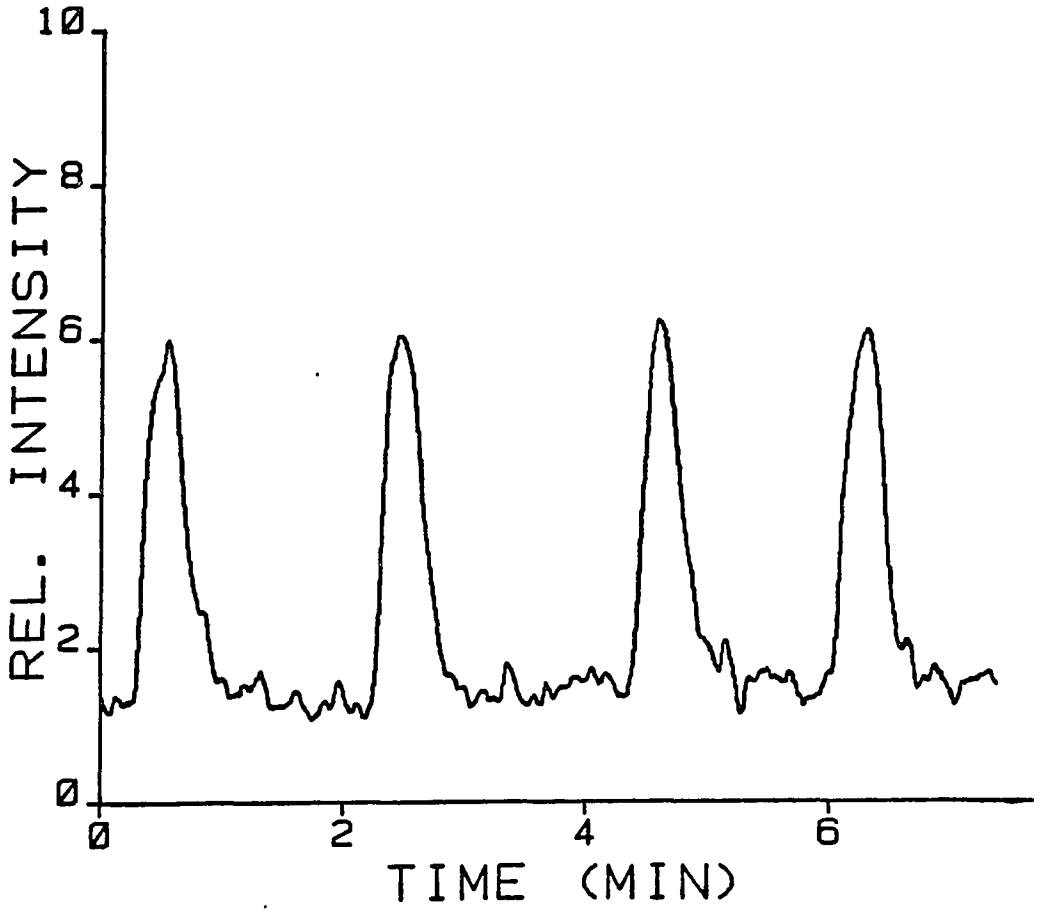

Figure 23. Peaks observed when 500 μL volumes of a solution containing 100 ng mL^{-1} of Br were introduced by flow injection into an ultrasonic nebulizer. The Br I 154.07 nm line was measured

without the introduction of air bubbles into the plasma. Whenever air did enter the plasma, a deviation in the background level resulted.

Atlas of emission lines

A serial listing of emission lines in the 113 - 295 nm region of the Group IIIB - VIIB elements (except Po and At, but including H) excited in an ICP, in order of wavelength, is shown in Table IV. Similar procedures to the prominent line study (Table III) were used for the determination of wavelength values and intensity readings, which were within two to three orders of magnitude of the most intense line of that particular element in the given wavelength region. The intensity readings should be taken as the average values obtained under the conditions of that particular day's run. The listing of the prominent lines of the Group IIIB-VIIB elements serve as a helpful guide to the relative intensities of the VUV lines as compared to the near UV lines and to the detection and assignment of intense emission lines in the 113 to 295 nm region, but caution should be exercised in that interferences could result from weak lines not listed in Table IV.

Emission lines of the halogens were detectable down to 118.88 nm (Cl I). The second order spectrum of intense background lines could cause some spectral interference in the 230 to 295 nm region.

Analytical Figures of Merit

Limits of detection

The monochromator was positioned on the line of interest for these studies. For the sample volumes and filter settings used, the FIA emission signal attained a peak height of 75 to 100% of the steady state signal. The measured LOD in the VUV and near UV regions for various Group

Table IV. Emission lines in the 113 to 295 nm region by the Group IIIB-VIIB elements excited in an ICP. Serial listing in order of wavelength.

Element	Wavelength (nm)	Relative Intensity[a]
N I	113.42,113.44, 113.50	—[b]
N I	115.21,115.28	—[b]
O I	115.21	—[b]
N I	116.39,116.43	—[b]
N I	116.75,116.85	—[b]
N I	117.65,117.77	—[b]
Cl I	118.88	12
N I	118.90	—[b]
Si II	119.04,119.33 119.45,119.74	2
C I	119.45	—[b]
N I	119.96,120.02, 120.07	—[b]
Pb II	120.36	5
Br I	121.08	6
H I	121.57	—[b]
Br I	122.11	3
Br I	122.33,122.44, 122.69	—[c]
N I	122.50,122.54	—[b]
Br I	122.81	4
N I	122.88	—[b]
Br I	123.24	1
Ge II	123.71	11
Bi II	124.11	10
N I	124.32,124.33	—[b]
Br I	125.17	2
I I	125.92,125.95	<1
C I	125.95	—[b]
Si ?[d]	125.95	9
C I	126.10,126.11, 126.14,126.16	—[b]
Ge II	126.19	18
Si ?[d]	126.38	15
Ge II	126.47	3
As II	126.64	3
C I	127.76,127.77	—[b]
C I	127.99,128.01, 128.09	—[b]
Br I	128.03	—[c]
Sn II	129.09	6
S I	129.56,129.62	5
O I	130.22	—[b]
O I	130.49	—[b]
O I	130.60	—[b]
N I	131.05,131.10	—[b]
C I	131.14	—[b]
S I	131.66	2
Sn II	131.66	10
I I	131.75	<1
Br I	131.77	26
N I	131.90,131.97	—[b]
Tl II	132.17	26
S I	132.35	1
N I	132.66,132.79	—[b]
S I	132.66	<1
C I	132.91,132.96	—[b]
C II	133.45,133.57	—[b]
Cl I	133.57	26

[a]Not corrected for changing plasma and monochromator conditions and nonlinearity of the detection system, all intensities are relative to the most intense line (normalized to 100) of that particular element.

[b]Contaminant background emission line.

[c]Intensity reading too difficult to measure due to the presence of background lines, etc.

[d]Ion or atom designation unknown.

Table IV. (Continued)

Element	Wavelength (nm)	Relative Intensity[a]
As II	134.15	<1
Cl I	134.72	100
Bi II	134.79	3
Cl I	135.17	39
C I	135.58	—[b]
N I	135.59	—[b]
C I	135.71	—[b]
O I	135.85	—[b]
B II	136.25	12
Cl I	136.34	24
As II	137.51	2
P I	137.71,137.79	2
B I	137.84,137.87, 137.90	3
P I	137.94	4
Cl I	137.95	5
P I	138.15,138.17	7
I I	138.32	2
Br I	138.46	14
Sb II	138.48	7
Sb I	138.89,138.96	5
Cl I	138.97,139.00	<1
I I	139.08	<1
Bi II	139.39	2
Se I	139.54,139.59	3
Cl I	139.65	<1
Sn II	140.05	40
S I	140.15	1
Se I	140.54,140.64, 140.66	2
S I	140.93	<1
N I	141.19	—[b]
Ga II	141.44	100
I I	142.14	4
As I	142.30	1
S I	142.51	14
I I	142.55	14
P I	143.0	<1
S I	143.33	9
Pb II	143.39	22
As I	143.47,143.48	2
Se I	143.53,143.58	3
Sb II	143.66	14
Bi II	143.68	21
S I	143.69	3
Sb II	143.83	10
Se I	144.68,144.70	2
P I	144.75	<1
S I	144.82	2
Se I	144.92	1
Br I	144.99	19
P I	145.30	<1
Bi II	145.51	14
Se I	145.63	2
I I	145.74,145.75, 145.80,145.88, 145.91	8
C I	145.90	—[b]
Ga II	146.37	—[c]
C I	146.38	—[b]
Te ?[d]	146.53	1
C I	146.74	—[b]
Sb I	146.88	3
S I	147.30,147.40, 147.44,147.45	12
Sn II	147.50	55
S I	148.17,148.31, 148.32	8
C I	148.18	—[b]
Bi II	148.69	2
S I	148.71	2
Br I	148.85	60
Sn II	148.91	5
N I	149.26,149.28	—[b]
N I	149.47	—[b]
Se I	150.09	2
Sb II	150.43,150.58	8
I I	150.70	<1
Te ?[d]	151.03	4
Pb II	151.24	1
Sb II	151.33	15
I I	151.43,151.47	2
I I	151.80	<1
Si II	152.67	14
Se I	153.04	17
Se I	153.13	4
Br I	153.17	34
Sb I	153.27	3
Bi II	153.32	21
Si II	153.34	26

Table IV. (Continued)

Element	Wavelength (nm)	Relative Intensity[a]
Bi II	153.81	3
Te ?[d]	154.02	2
Br I	154.07	100
P I	154.33	1
B I	154.64,154.69	<1
Te I	155.53	2
B I	155.87,155.91	<1
As I	155.62,155.72	1
C I	156.07,156.14	—[b]
Sb II	156.55	25
B I	156.63,156.67	<1
B I	157.33,157.37	2
As I	157.39,157.47, 157.59	9
Br I	157.48	17
Br I	157.64	9
Ge II	157.69	4
Se I	157.95,158.00	12
Br I	158.23	5
I I	158.26	12
Sb II	158.46	14
In II	158.64	100
As I	158.80	2
As I	159.36	15
I I	159.36	4
Si I	159.45	1
Sb I	160.00	10
B I	160.04,160.08	3
C I	160.26	—[b]
Ge II	160.26	40
Se I	160.65	14
Bi II	161.14	6
Se I	161.74	8
I I	161.76	20
Si I	162.29	1
B II	162.36,162.38, 162.40,162.42, 162.44	<1
Si I	162.94,162.99	3
Br I	163.34	15
Si I	163.40	1
In II	164.01	4
I I	164.08,164.21	6
Bi I	164.43	3
As I	164.43	1
Te I	164.50	2
Ge II	164.93	70
C I	165.63,165.70	—[b]
Te I	166.31	1
B I	166.26-166.48	1
Ge I	166.35	<1
S I	166.67	22
B I	166.69,166.73	8
Si I	166.76,166.85	<1
Al II	167.08	100
Ge I	167.10	2
P I	167.11,167.17, 167.25	3
Se I	167.12	6
Te ?[d]	167.14	3
Pb II	167.15	33
In II	167.19	<1
Si I	167.26	2
In II	167.40	<1
P I	167.46	2
Si I	167.52	2
Se I	167.53	4
Te I	167.81,167.94	3
P I	167.97	3
Ge I	168.13	2
Pb II	168.22	64
P I	168.60	9
Te I	168.85	2
P I	168.93,169.02	<1
Se I	169.07	3
Ge I	169.11	1
Si I	169.33	2
P I	169.41,169.45	8
Si I	169.62	5
Si I	169.79	7
Sn II	169.94	5
Te I	170.00	33
In II	170.00	<1
Si I	170.06	2
As I	170.12	1
I I	170.21	1

Table IV. (Continued)

Element	Wavelength (nm)	Relative Intensity[a]	Element	Wavelength (nm)	Relative Intensity[a]
Si	170.46[e],170.50[f]	1	P I	178.29	69
Te I	170.67,170.80	3	Bi II	178.75	3
In I	171.15	<1	P I	178.77	36
Ge I	171.68	2	Sb I	178.82	2
Sb I	171.69,171.75	7	As I	178.99	1
P I	171.86,171.90, 171.93	2	As I	179.18	<1
			Bi II	179.19	45
Al II	172.13	<1	Se I	179.53	<1
Sb I	172.34	4	Te I	179.57,179.63	6
Al II	172.50	1	Pb II	179.67	10
Pb II	172.68	10	I I	179.91	12
As I	172.98	<1	Sb I	180.02	6
Te I	173.06	<1	As I	180.62	9
As I	173.24,173.29	1	S I	180.73	100
Te I	173.30	1	Si I	180.90	3
Sb I	173.62	5	Sb I	181.05	7
As I	173.95	3	Sn II	181.12	22
N I	174.27	—[b]	Si I	181.41	2
N I	174.52	—[b]	Sb I	181.42	8
Te I	175.10	9	Si II	181.69,181.74	4
C I	175.19	—[b]	B I	181.78,181.84	4
Bi I	175.21	—[c]	S I	182.04	57
Sn II	175.79	49	Pb II	182.20	34
As I	175.86	11	Te I	182.24	23
Te I	175.94	8	Sn I	182.30	1
Sb I	176.27,176.37	10	Bi II	182.38	3
Al II	176.38,176.40	<1	Te I	182.55	<1
Si I	176.50,176.55, 176.56,176.58	<1	B I	182.59,182.64	42
			S I	182.63	19
Sb I	176.58	2	Te I	182.89	<1
Al II	176.76	2	Sb I	182.95	3
Bi I	176.78	4	I I	183.04	15
In II	177.08	<1	As I	183.13,183.17	2
Si I	177.09	1	Sn II	183.18	7
P I	177.50	100	P I	183.48	<1
Bi II	177.71	24	Si I	183.65	1
As I	178.05,178.15	2	Si I	184.14	3
Sb I	178.09	8	As I	184.44,184.46	2
S I	178.23	<1	I I	184.45	2
I I	178.28	100	Si I	184.61	8

[e]Spectral line originates from neutral atom state.

[f]Spectral line originates from singly ionized state.

Table IV. (Continued)

Element	Wavelength (nm)	Relative Intensity[a]
P I	184.72	5
As I	184.73	1
Si I	184.75	17
As I	185.02	2
Te I	185.06	9
Si I	185.07	26
P I	185.12,185.21	3
Te I	185.21	6
Si I	185.25	5
Bi I	185.26	2
Te I	185.37	3
Se I	185.52	24
Te I	185.72	10
Se I	185.88	4
P I	185.89,185.94	42
Sn I	186.03	1
As I	186.04,186.05	3
Te I	186.05	2
Ge I	186.11	2
Sn I	186.55,186.59	1
Sb I	186.82	3
Sb I	187.12	32
Si I	187.48	<1
Ge I	187.60	1
I I	187.64	<1
Sb I	188.26	7
Bi I	188.87	1
As I	189.04	100
Sb I	189.13	1
Si I	189.32	<1
Pb I	189.89	<1
Sn II	189.99	100
Si I	190.13	6
Bi II	190.24	80
Ge I	190.47	3
Pb I	190.48	3
Tl II	190.86	100
Se I	191.38	<1
Ge I	191.76	2
Se I	191.92	<1
Sn I	192.53	1
Sb I	192.71	5
C I	193.09	--[b]
In II	193.63	<1
As I	193.76	81
Ge	193.83[e],193.89[f]	2
Ge I	194.41,194.47	3
Sb I	195.04	21
Sn I	195.21	<1
Bi I	195.39	8
Ge I	195.51	3
Bi I	195.95	2
Se I	196.09	100
Ge I	196.20	3
Ge I	197.09	2
As I	197.26	47
In II	197.75	<1
Si I	197.76	3
Sb I	197.82,197.92	2
Si I	197.92	3
Si I	198.06	2
Si I	198.32	3
Sn I	198.42	<1
Sb I	198.61	3
Si I	198.64	3
Ge I	198.83	3
Si I	198.90	8
As I	199.04,199.11	21
Te I	199.48	3
Se I	199.51	<1
As I	199.54	3
Ge I	199.89	13
Te I	200.20	10
As I	200.33	30
As I	200.92	4
As I	201.33	2
Ge I	201.91	7
Bi I	202.12	1
P I	202.35	2
Sb I	202.40	3
Sb I	202.95	2
P I	203.35	4
Sb I	203.98	4
Se I	203.99	45
Sn I	204.07	1
Ge I	204.17	17
Ge I	204.38	15
Sb I	204.96	11
Pb I	205.33	<1
Ge I	205.45	2
Ge I	205.72	2
Si I	205.81	3

Table IV. (Continued)

Element	Wavelength (nm)	Relative Intensity[a]
Bi I	206.17	25
I I	206.2	4
Se I	206.28	16
Ge I	206.52	8
B I	206.64,206.67, 206.69,206.72	1
Sb I	206.83	100
Ge I	206.87	25
Sn III	207.00	1
Sn I	207.31	2
Se I	207.48	3
In II	207.93	<1
Te I	208.12	9
Ge I	208.60	3
Pb I	208.84	<1
B I	208.89,208.96	34
Ga II	209.13	4
Sn I	209.16	2
Ge I	209.43	37
Sn I	209.64	2
Sb I	209.84	7
Sn I	210.09	<1
Ge I	210.58	3
Bi I	211.03	5
As I	211.30	1
Sn I	211.39	3
Pb I	211.50	<1
Sb I	211.85	3
Si I	212.41	37
Ge I	212.47	4
Sb I	212.74	3
Bi I	213.36,213.43	10
P I	213.55,213.62	70
Sb I	213.71	8
Sb I	213.97	14
Sb I	214.18	5
Te I	214.28	100
As I	214.41	2
Sb I	214.49	12
Te I	214.73	13
P I	214.91	40
Sn I	215.08,215.14	6
P I	215.29,215.41	5
Bi I	215.56	2
As I	216.55	3
Pb I	217.00	21
Sb ?[d]	217.02	3
Sb I	217.58	86
Sb I	217.92	24
Bi I	218.96	1
Sn I	219.45	3
Ge I	219.87	29
Sn I	219.93	4
Sb I	220.13	4
Bi I	220.33	2
Pb II	220.35	100
Si I	220.80	5
Sb I	220.85	7
Sn I	220.97	7
Si I	221.09	14
Si I	221.67	22
Sb I	222.07	4
Sb I	222.49	3
Bi I	222.83	40
Bi I	223.06	100
Tl I	223.79	1
Sn I	224.61	12
Pb I	224.69	4
Te I	225.55	2
Te I	225.90	15
Sb I	226.25	4
Al I	226.3-226.9	<1
Te I	226.56	2
Sn I	226.89	11
Bi I	227.66	8
Sn I	228.67	2
As I	228.81	64
Ga I	229.42	9
N,O I	230.5	--[g]
In II	230.61	15
Sb I	230.65	4
Sb I	231.15	62
Ge I	231.42	2
Sn I	231.72	6

[g]Second order background emission line.

Table IV. (Continued)

Element	Wavelength (nm)	Relative Intensity[a]
Ge I	232.79	3
Sn I	233.48	—[c]
N I	233.6	—[g]
Ga I	233.83	2
As I	234.40	2
As I	234.98	45
Sn I	235.48	18
Sn II	236.83	2
As I	236.97,237.08	5
Ge I	237.91	2
Tl I	237.97	4
As I	238.12	2
Te I	238.33	16
Te I	238.58	26
P I	238.6	1
Pb I	239.38	3
N I	240.0	—[g]
Ge I	241.74	9
Sn II	242.17	10
N I	243.1	—[g]
Si I	243.52	10
Pb I	244.38	1
Pb I	244.62	1
Ga I	245.01	4
As I	245.65	3
Pb I	247.64	3
C I	247.86	—[b]
Sn	248.34[e],248.35[f]	3
N I	248.6	—[g]
As I	249.29	2
Sn I	249.57	3
B I	249.68,249.77	100
Ge I	249.80	4
Ga I	250.02	8
Si I	250.69	34
Si I	251.43	52
Si I	251.61	100
Si I	251.92	20
Si I	252.41	27
Sb I	252.85	50
Si I	252.85	35
Te I	253.07	2
Si I	253.24	<1
Ge I	253.32	3
P I	253.40,253.57	15
Sn I	254.66	3
P I	255.33,255.49	—[c]
In I	256.02	<1
Sn I	257.16	2
Pb I	257.73	2
Tl I	258.01	2
Ge I	259.25	31
Sb I	259.81	45
O I	260.4	—[g]
O I	261.0	—[g]
O I	261.2	—[g]
Pb I	261.42	21
N I	262.2	—[g]
Bi I	262.79	5
Si I	263.13	4
N I	263.9	—[g]
Ge I	265.12,265.16	100
Pb I	266.32	6
Ge I	269.13	16
Sn I	270.65	—[c]
Tl I	270.92	1
Ge I	270.96	26
In I	271.03	1
Ga I	271.97	3
Ge I	274.04	2
As I	274.5	2
In I	275.39	<1
Ge I	275.46	25
Tl I	276.79	21
Sb I	277.00	5
As I	278.02	7
Bi I	278.05	1
Pb I	280.20	15
Pb I	282.32	3
Pb I	283.31	15
Sn I	284.00	17
As I	286.04	3
Sn I	286.33	7
Pb I	287.33	3
Ga I	287.42	21
Sb I	287.79	5
Si I	288.16	35
Bi I	289.80	8
Tl I	291.83	2
Bi I	293.83	6
Ga I	294.36,294.42	32

IIIB-VIB elements for either pneumatic or ultrasonic nebulization for the present system and for other optical ICP systems are listed in Table V. The detection limits shown in Table V for the Group IIIB-VIB elements were comparable to the best reported values in the ICP-AES literature for pneumatic nebulization. The detection limits with ultrasonic nebulization in the present work were superior by about 4- to 12-fold over the pneumatic nebulization values. Most of the VUV lines were more sensitive than the UV lines conventionally employed. The elements Al, Ga, and In each emitted one strong VUV line that yielded LODs that were superior to the conventional UV lines utilized in a typical optical system (12). For ultrasonic nebulization, the limits of detection of the Group IIIB elements were even more improved.

As shown in Table VI, detection limits obtained in the present work for Br and Cl were far superior to the best reported values in the ICP-AES literature. Comparisons of the limits of detection observed for Br, Cl, and I with the present apparatus, with conventional optical systems, with microwave-induced plasma (MIP) emission, and with He ICP emission are presented in Table VI. The limits of detection obtained for Br and Cl for pneumatic nebulization and direct observation of the VUV lines via the sampling orifice were from 16- to 1200-fold superior to those observed for the other plasmas with pneumatic nebulization. The limits of detection for Br and Cl obtained by ultrasonic nebulization and ICP-VUV-AES were from 25- to 800-fold better than for MIP and He ICP emission with ultrasonic nebulization (50,51,53,54).

Fluorine is not represented in Tables III to VI, because the presence of F I resonance lines (95.2 and 95.5 nm or upper energy levels of 13.02 and 12.98 eV, respectively) could not be verified, even when a

Table V. Estimated limits of detection for the prominent lines of various element with different ICP-AES systems

Element and Line (nm)	Limit of Detection (ng mL^{-1}) with ICP-AES							
	FIA-ICP-VUV-AES Present Work		Winge et al. Work[a]		Other Work			
	Pneum. Neb.	Ultras. Neb.	Wave-length	Pneum. Neb.	Wave-length	Pneum. Neb.	Wave-length	Ultras. Neb.
Al II 167.08	0.4	0.04	I 309.27	23	II 167.08	1[b], 0.6[c]	I 308.22	0.4[d]
As I 189.04	25	3	- -	-	I 189.04	13[b], 110[e], 13[g], 15[h], 70[i]	I 189.04	15[f]
As I 193.76	40	-	I 193.70	53	I 193.76	25[b], 160[e]	I 193.76	5[f], 2[d]
B I 182.6	15	0.8[j]	I 249.77	4.8	I 182.64	3[b], 6[g]	I 208.95	16[f]
Bi II 143.68	200	10	I 223.06	34	- -	-	- -	-
Bi II 190.24	90	20	- -	-	II 190.24	60[b]	- -	-
Ga II 141.44	9	0.8	I 294.36	46	- -	-	- -	-
Ge II 160.26	60	4	I 209.43	40	- -	-	- -	-
Ge II 164.93	40	2	- -	-	II 164.92	50[b], 10[k]	- -	-
In II 158.64	4	0.5	II 230.61	63	II 158.7	3[k]	- -	-
P I 177.50	15	3.[l]	I 213.62	76	I 177.50 I 214.9 I 178.3	15[b], 60[e], 8[g] 60[h] 53[i]	I 213.62	6[f]
Pb II 168.22	25	2	- -	-	II 168.22 II 182.2	15[k] 50[b]	- -	-
Pb II 220.35	60	6	II 220.35	42	II 220.35	50[i]	II 220.35	1[d]
S I 180.73	10	2	- -	-	I 180.73	15[b], 50[e,m], 24[g], 60[h], 4[i]	I 182.04	3000[f]
Sb II 156.55	100	10	- -	-	- -	-	- -	-
Sb I 206.83	50	14	I 206.83	32	- -	-	- -	-
Se I 153.04	60	9	- -	-	- -	-	- -	-
Se I 196.09	40	7	I 196.03	75	I 196.09	30[b], 200[e]	I 196.09	40[f,d]

Si	II	153.34	30	2.5	- -	-	- -	-	- -	-
Si	I	185.07	60	5	- -	-	I 185.07	30[b]	- -	-
Si	I	251.61	60	6	I 251.61	12	- -	-	- -	-
Sn	II	147.50	30	3	- -	-	II 175.8	25[k]	- -	-
Sn	II	189.99	20	4	II 189.99	25	II 189.99	15[b],18[g]	II 189.99	6[f]
Te	I	170.00	30	5	- -	-	- -	-	- -	-
Te	I	214.28	60	5	I 214.28	41	- -	-	- -	-
Tl	II	190.86	30	5	II 190.86	40	II 190.86	35[b]	II 190.86	10[f]

[a]Reference 12.

[b]Reference 15.

[c]Reference 122. Note: S/N = 2.

[d]Reference 16.

[e]Reference 17.

[f]Reference 14.

[g]Reference 20. Note: LOD is for I^-, LOD for I_2 is 0.5 ng mL^{-1}.

[h]Reference 13.

[i]Reference 21. Note: S/N = 2.

[j]Loss of linear response for low concentration samples due to a desolvation effect (98).

[k]Reference 23.

[l]Ultrasonic nebulizer desolvation temperature = 80°C.

[m]Reference 24.

Table VI. Comparison of limits of detection for various AES techniques for the detection of Br, Cl, and I in aqueous solutions

Technique	Nebulization	Limits of Detection (ng mL^{-1})		
		Br	Cl	I
FIA-ICP-VUV-AES[a] (present work)	pneumatic	50	50	20
	ultrasonic	8	15	6
ICP-VUV-AES	pneumatic	3000[b] 800[d]	10000[c] 6000[d]	50[b] 200[d] 16[e]
MIP[f]	pneumatic	60000	2000	7000
	ultrasonic	3000	400	800
He ICP[g]	ultrasonic	5000	13000	—

[a]Solutions containing aqueous Br, Cl, and I salts nebulized. Lines used: Br I 154.07, Cl I 134.72, I I 178.28 nm.

[b]Reference 15. Lines used: Br I 163.34, I I 178.28 nm.

[c]Reference 8. Line used: Cl 133.57 nm.

[d]Reference 17. Lines used: Br I 154.07 nm, Cl I 134.72 nm, I I 178.28 nm.

[e]Reference 20. Line used: I I 178.28 nm. Note: LOD is for I^-, LOD for I_2 is 0.5 ng mL^{-1}.

[f]References 50,51. Lines used: Br II 478.55, Cl II 479.45, I I 206.16 nm.

[g]Reference 53,54. Lines used: Br I 827.24, Cl I 725.67 nm.

scintillator-PMT detector and an Os-coated grating were used. During introduction of aqueous aerosols with a solution of NH_4FHF, this wavelength region is obscured by a strong H I and a weak N I line in the background spectrum. Introduction of the sample as SF_6 in dry Ar, i.e., with no aqueous aerosol present, reduced the H I line interference; under these conditions, weak F I emission could be observed, as noted in the next chapter.

Nygaard and coworkers (8) reported a LOD for F I 685.60 nm line of 2000 $\mu g\ mL^{-1}$ by pneumatic nebulization of an aqueous solution of the halide into the ICP. The details surrounding the concentration and nature of the F solution used for the LOD could not be accurately extracted from their manuscript. This analysis has been the only reported occurrence of F I lines emitted by an Ar ICP with nebulization of aqueous solutions.

Linearity and Precision

As shown in Figure 24, the ranges of linear response of the prominent lines of Br, Cl, I, S, and P were about 3.5 to four orders of magnitude. Deviation from linearity occurred in the 300 to 1000 $\mu g\ mL^{-1}$ concentration range. No plateau in the emission signal was evident even at concentrations of 1000 $\mu g\ mL^{-1}$ S and P, and of 10,000 $\mu g\ mL^{-1}$ Br, Cl, and I.

The precision of the emission signals for Al, Br, Ge, and Pb was calculated by measuring the relative standard deviation of net peak intensities obtained from repeated flow injections into either a pneumatic or an ultrasonic nebulizer; these results are shown in Table VII. The ultrasonic nebulizer used in this study yielded somewhat less precise emission signals than the pneumatic nebulizer. For either nebulizer, the

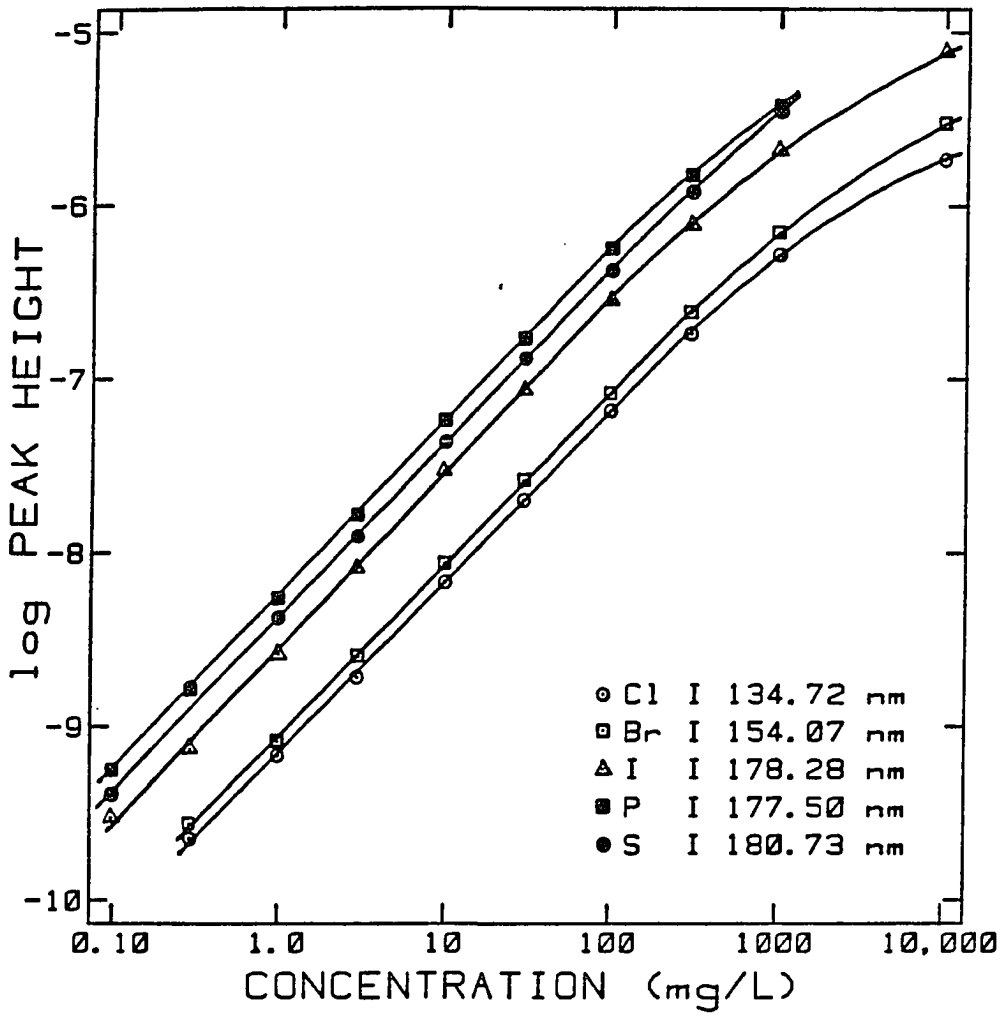

Figure 24. Calibration curves for Cl, Br, I, P, and S at their prominent VUV resonance lines obtained by pneumatic nebulization

Table VII. Precision of peak emission intensities obtained by FIA-ICP-VUV-AES with pneumatic nebulization and ultrasonic nebulization with aerosol desolvation

Element and Line (nm)	Concentration ($\mu g\ mL^{-1}$)	Relative Standard Deviation (%)[a] Pneumatic Nebulization	Ultrasonic Nebulization
Al II 167.08	1	1.0	2.0
	0.01	3.9	- -
	0.001	- -	6.5
Br I 154.07	100	0.9	1.9
	1	5.4	2.2
Ge II 164.93	10	0.9	2.8
	1	1.7	- -
	0.1	- -	2.5
Pb II 168.22	10	1.3	2.6
	1	4.5	- -
	0.1	- -	4.1

[a]Derived from 8 - 12 injections.

precision of the emission intensities should improve if automatic rather than manual injections are employed (123).

Interelement effect studies

The effect of increasing Na concentration, as $NaNO_3$, on the emission intensity of Br, Cl, and Al was examined with both nebulizers. Ammonium salts of Cl and Br were avoided during ultrasonic nebulization because they yielded lower emission signals than the corresponding Na salts. We attribute this observation to partial loss of the ammonium salts in the desolvation device, as described previously for B and Hg (98). The Cl, Al, and Br signals in the presence of added $NaNO_3$ were normalized to those obtained without added $NaNO_3$.

The effects of Na concomitant on the intensities of the Br I, Cl I, and Al II lines during pneumatic and ultrasonic nebulization are shown in Figure 25. The effect of Na on the line intensities was small, i.e., the relative change in analyte signal was 10% or less over the range of Na concentration used. Thus, the present system shows considerable tolerance to interference effects induced by easily ionized concomitants such as Na.

It has been shown that the vertical spatial emission profiles of analyte lines change as the Na concentration in the sample is increased. In general, addition of sufficient Na enhances the emission intensity of analyte lines at low observation positions, whereas analyte signal is depressed high in the axial channel (124). With conventional optical systems for viewing an ICP from its side, the observation height can be selected to straddle the "cross-over" position where the enhancement turns into a suppression, thus minimizing the overall effect of concomitants on analyte signal (125). In the present system, the emission intensity observed for a particular analyte is optically integrated down the axial

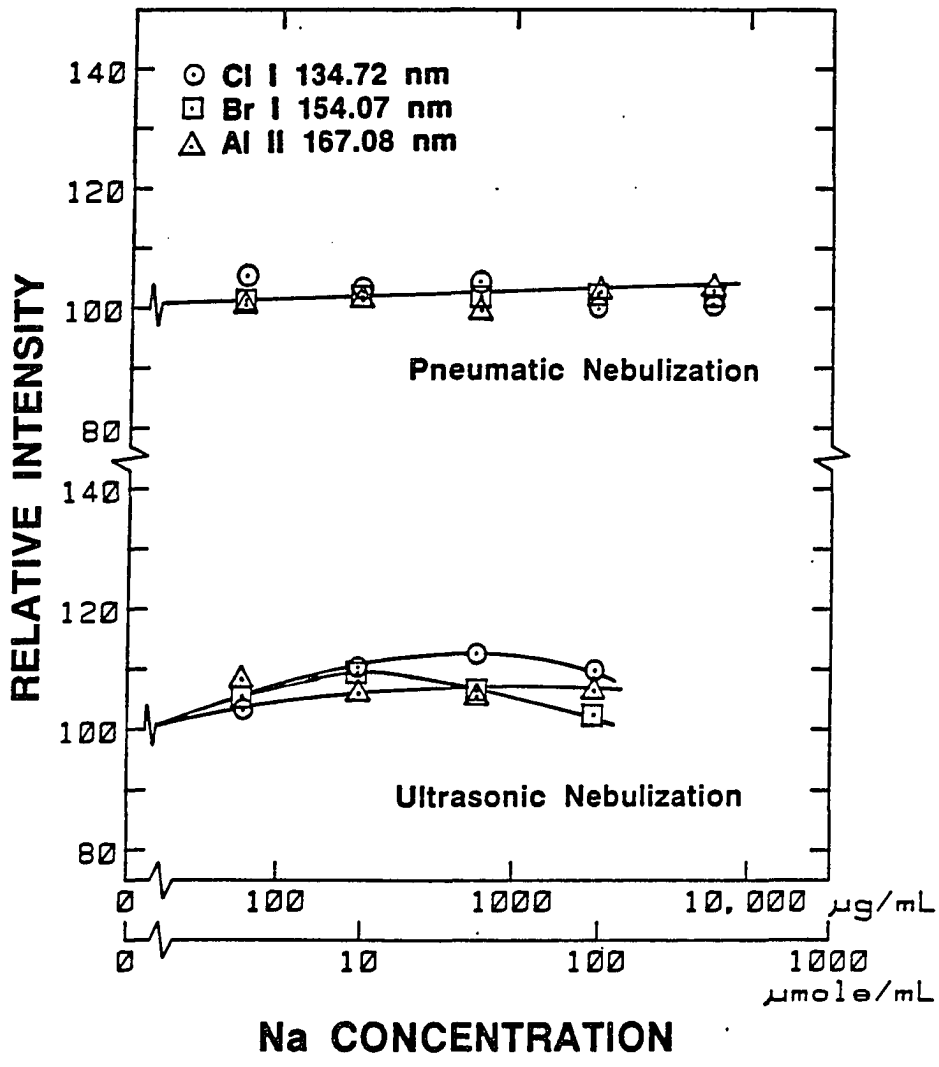

Figure 25. Effect of Na on Br, Cl, and Al emission intensities with pneumatic nebulization and ultrasonic nebulization with desolvation
(0.5 μmole mL^{-1} Br, 0.5 μmole mL^{-1} Cl, and 0.5 μmole mL^{-1} Al)

channel as shown in Figure 13. It is likely that a similar juxtaposition of enhancement and suppression effects occurs for the "end-on" viewing mode used in the present work. This conclusion is consistent with the results of Demers, who measured the interference induced by Na on the conventional UV lines of Ca, Cd, Cr, and Mo while viewing the ICP down the axial channel (115). Use of a smaller sampling orifice would permit a detailed, spatially-resolved study of the interference behavior of Br I and Cl I. This study could provide interesting fundamental information about excitation in an ICP; Br and Cl are unique in that their neutral atoms possess high excitation energies (ca. 8 and 9 eV, respectively), and they are less efficiently ionized than other analyte elements typically used for these studies. It is interesting that insertion of a sampling orifice into an ICP for optical detection did not yield the more extensive and complex interference effects reported for ICP mass spectrometry (126-129), i.e., the mere presence of a metal cone in the ICP cannot be responsible for such interference effects in ICP-MS (130).

The effects of Ca concomitant on the normalized intensity of the Al II 167.08 nm line are shown in Figure 26. With pneumatic nebulization, Ca concomitant induced only moderate depression of Al II intensity for moderate Ca concentrations ($\leq$1000 μg mL^{-1}). At high Ca concentrations (e.g., 12000 μg mL^{-1}), the Al II line was suppressed by 20%. The dependence of the normalized Al II intensity on Ca concentration became more severe (-40% at 4000 μg Ca mL^{-1}) when ultrasonic nebulization was utilized. Similar interference trends also occurred for the effects of Al concomitant on the intensity of the Ca II 184 nm line. The Ca II line was depressed by 15% in the presence of 8100 μg Al mL^{-1} during pneumatic nebulization and 50% during ultrasonic nebulization of 2700 μg Al mL^{-1}.

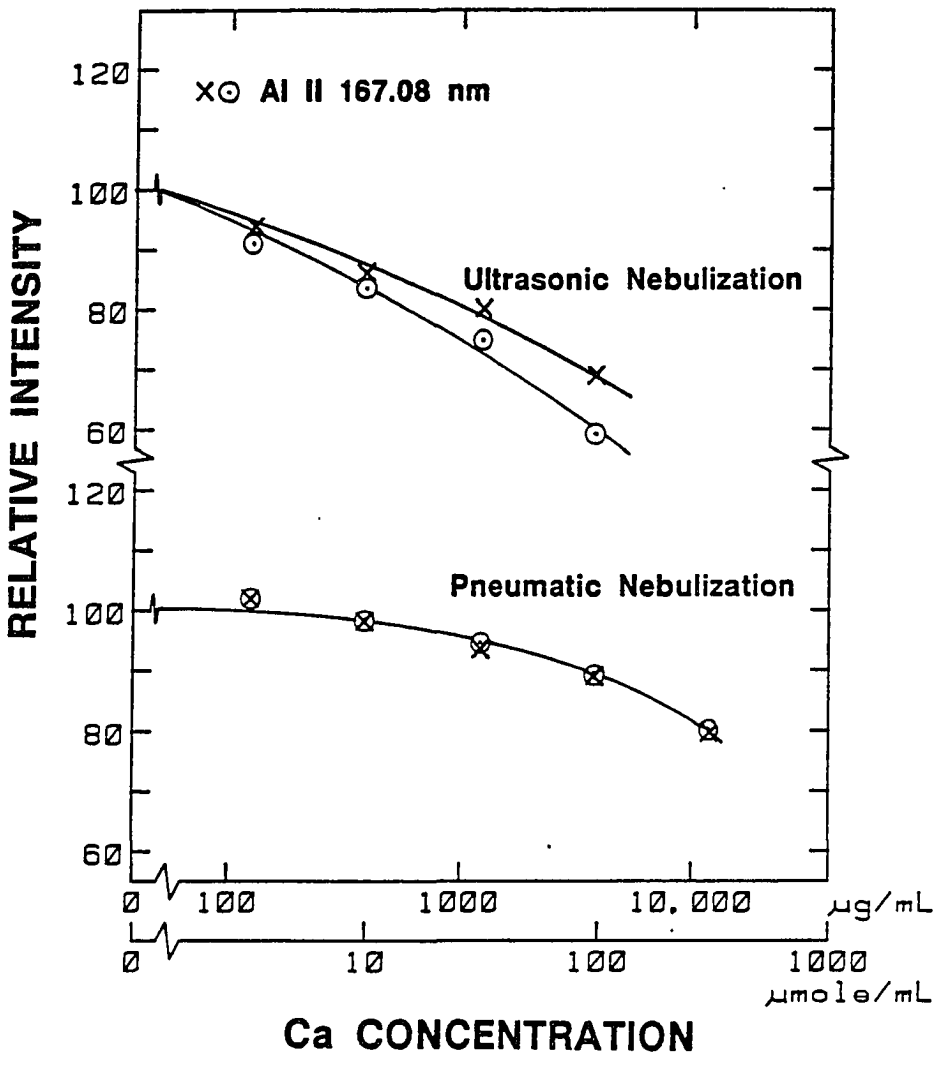

Figure 26. Effect of Ca on Al emission intensity with pneumatic nebulization and ultrasonic nebulization with desolvation. The different plotting symbols represent duplicate runs performed on different days with different sets of solutions (0.5 μmole mL^{-1} Al)

The results of the Ca - Al interference studies for pneumatic nebulization were analogous to the data for Al on Ca II 393.4 nm emission for conventional (i.e., side-on) viewing of observation heights in the 15 to 20 mm range (98,125,115) and for end-on viewing (115). For ultrasonic nebulization, the Ca II line at 184 nm was depressed more severely in the presence of Al than the conventional Ca II line (393.4 nm) was in earlier studies (98). Finally, dilution of the sample by a factor of 10 would attenuate the Ca-Al interference effects observed for ultrasonic nebulization to the levels observed for pneumatic nebulization and would yield comparable powers of detection for the two nebulizers.

Background interferences

An organic solvent, CH_3OH at 1% concentration, was introduced into the ICP and the resulting VUV spectrum is shown in Figure 27A. That spectrum exhibited strong C lines and the CO 4th positive molecular band system. The wavelengths of the CO band heads coincided with those tabulated in Headrick and Fox (131). The CO molecular bands severely hampered the detection of many analytical lines in the VUV region. The region near the Br I 154.07 nm line was overlapped with a CO molecular band. This molecular band system was also emitted from the He discharge-afterglow (132,133) and intensified when CO_2 gas was introduced.

Figure 28 illustrates the interference of the CO 4th positive band system with the S I 180.7, 182.0, and 182.6 nm lines. At 1% acetonitrile in water (Figure 28E), the intensity of the 179.2 nm band front was about twice the magnitude of the peak intensity from S I 180.73 nm. It is clear that when organic solvents are used, alternative emission lines may have to be selected.

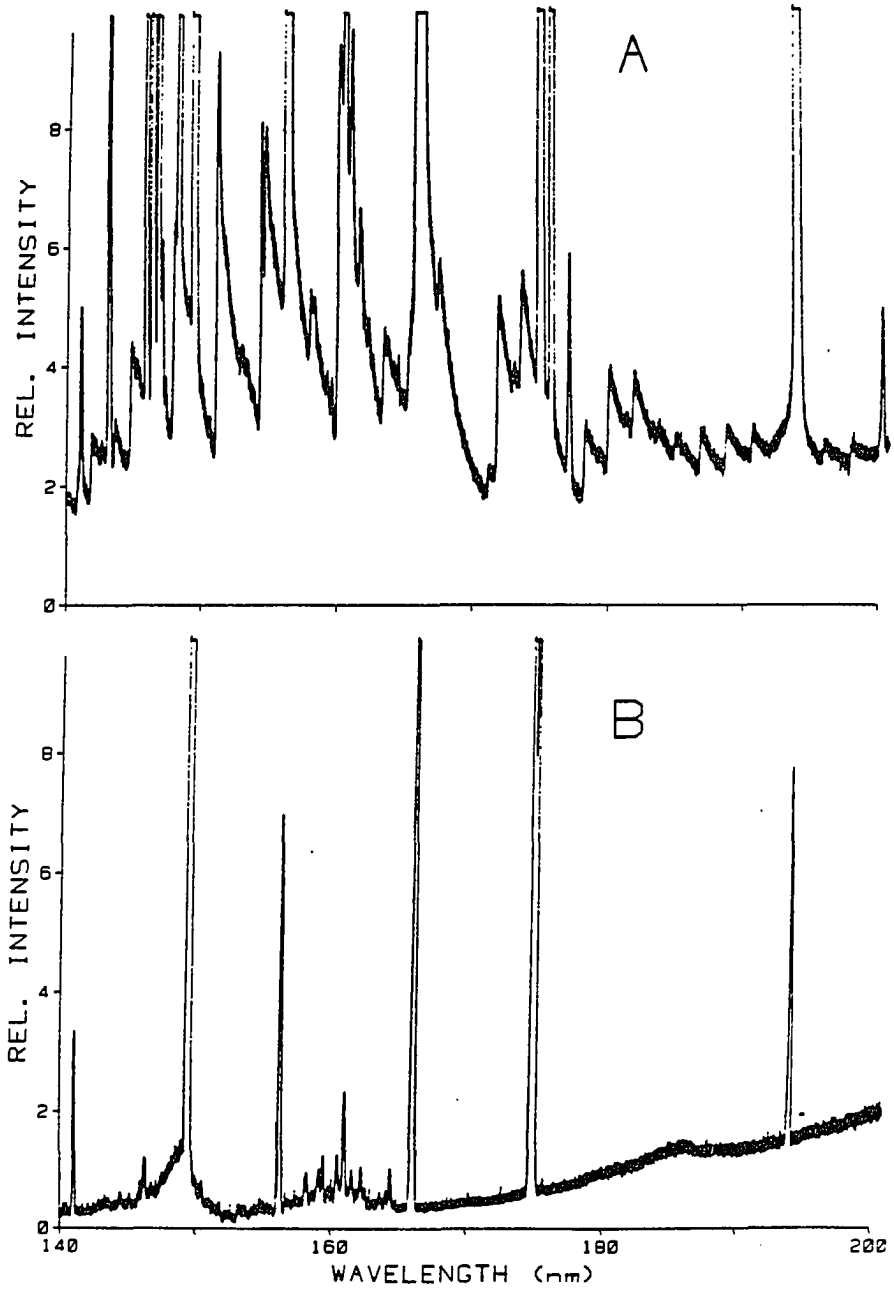

Figure 27. Emission spectra from 140 to 200 nm of
(A) pneumatic nebulization of 1% CH_3OH and
(B) distilled deionized water into the axial channel of the ICP

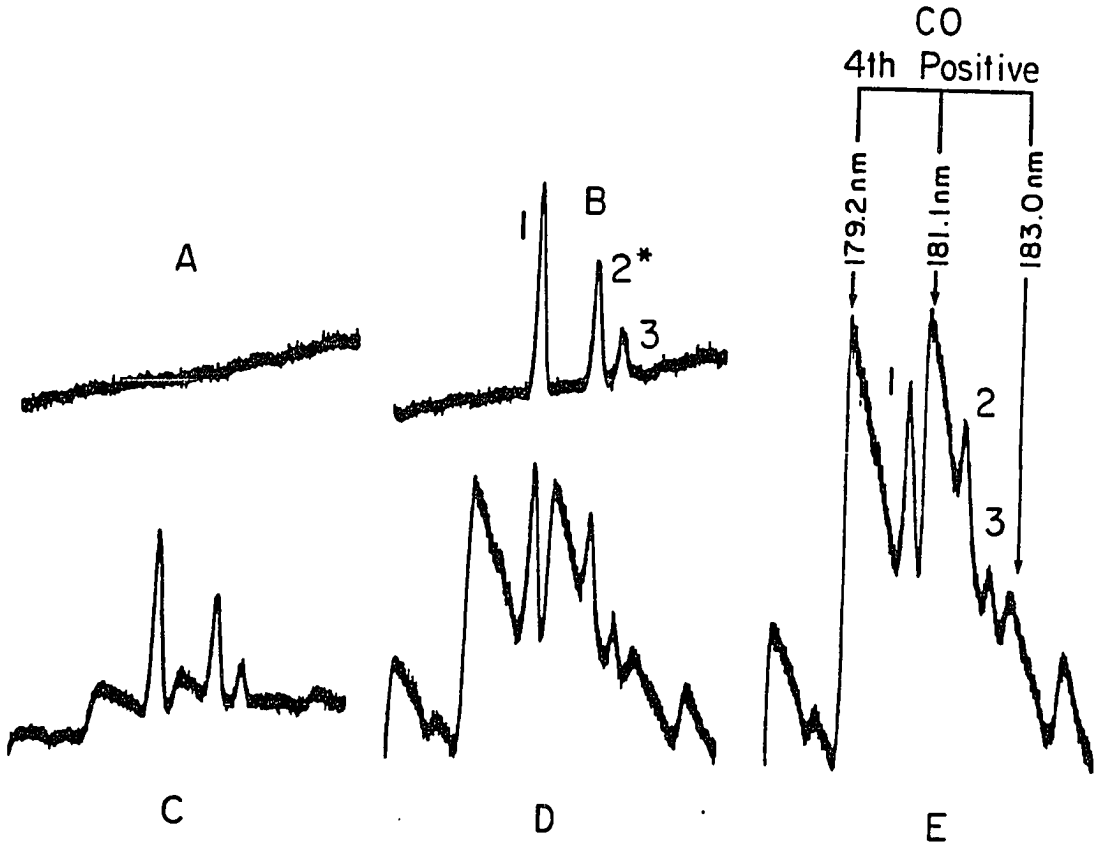

Figure 28. Spectral interference of the CO fourth positive molecular band system on the (1) 180.7 nm, (2) 182.0 nm, and (3) 182.6 nm wavelengths of sulfur in the presence of

(A) distilled deionized water;

(B) 1 μg mL^{-1} as S of SO_4^{2-} in distilled deionized water;

(C) 1 μg mL^{-1} as S of SO_4^{2-} in 0.1% acetonitrile;

(D) 1 μg mL^{-1} as S of SO_4^{2-} in 0.5% acetonitrile; and

(E) 1 μg mL^{-1} as S of SO_4^{2-} in 1.0% acetonitrile

Other background interferences from H I lines around 90 to 100 nm, the H_2 molecular band system from 120 to 170 nm, and the Ar_2 molecular emission continuum from 110 to 150 nm are described in detail in Chapter V (Diagnostic studies).

CHAPTER IV. GASEOUS SAMPLE INTRODUCTION

General Features of VUV Region

The background and analyte spectral lines in the VUV region were identical to those observed with pneumatic nebulization, although the O I and H I lines were less intense when dry Ar was introduced into the plasma. The absence of nebulized water with the DIP resulted in the disappearance of molecular band emission by hydrogen around 160 nm (117,118), and a lower background level at wavelengths above 130 nm. A detailed study of the H_2 molecular band system and the omission of certain spectral features in the VUV region resulting from the absence of nebulized water are discussed in Chapter V.

Analytical Figures of Merit

Limits of detection

The absolute LODs for Br, Cl, S, and C were in the sub-ng range, as indicated in Table VIII. These values surpassed by two to three orders of magnitude those reported by Hughes and Fry (6,7) when the near IR lines were observed. This improvement was mainly attributed to the employment of the more sensitive VUV lines and to the small dispersion of the sample plug provided by the low dead volume interface. The C I 165.7 nm line was chosen for carbon detection because it was more sensitive than the conventional C I 193 nm by a factor of 2 to 3. The relative LODs (ng mL^{-1} of Ar) for Br, Cl, S, and C (Table IX) were on the order of 1 ng mL^{-1}. Compared to Hughes and Fry (6,7), these relative LODs were superior by 3 to 4 orders of magnitude. In the present work, a much larger sample loop

Table VIII. Comparison of the absolute limits of detection for Br, Cl, S, and C for gaseous sample introduction into the ICP

Element and Line (nm)	Absolute Limits of Detection(ng)	
	DIP-ICP-VUV-AES	near IR lines[a]
Br I 154.07	0.1	50
Cl I 134.72	0.3	50
S I 180.73	0.05	6
C I 165.7	1	130

[a]References 6 and 7.

Table IX. Comparison of the relative limits of detection for Br, Cl, S, and C for gaseous sample introduction into the ICP

Element and Line (nm)	Relative Limits of Detection(ng/mL) DIP-ICP-VUV-AES (250 μL loop)	near IR lines[a] (8 μL loop)
Br I 154.07	0.4	6200
Cl I 134.72	1.2	6200
S I 180.73	0.2	750
C I 165.7	4	16000

[a]References 6 and 7.

(250 μL volume) was used than in the work of Hughes and Fry (8 μL volume), which accounted for the additional improvement in relative LODs.

It is also instructive to compare the LODs obtained in the present work with those obtained for gaseous sample introduction into other plasmas. First, consider other plasmas sustained in Ar, e.g., microwave induced plasmas (MIPs) (27,29) and afterglows (56). The absolute LODs obtained while monitoring VUV lines from the Ar ICP were superior to those obtained from these other Ar plasmas with various lines by factors of 2 to 1000 (27,29,56). The use of He instead of Ar gas for the MIP or afterglow allowed more efficient excitation of higher energy levels of the nonmetals, which were not efficiently populated in an Ar plasma. For these He plasmas, the best detection limits were in the range of tens of pg s^{-1} for some nonmetals, including Br and Cl (31-34,36,37,39,46,47,57). These LODs were comparable to or up to an order of magnitude better than our values (Table VIII). Thus, in terms of LODs, DIP-ICP-VUV-AES is competitive with He emission sources and superior to other Ar emission sources for elemental analysis of gaseous samples. Of course, our instrumentation has the additional advantage that it can be readily converted for the analysis of nebulized aqueous solutions with LODs better than those obtained presently with other He or Ar plasmas.

Spectral scans of fluorine atomic emission

It was reported in Chapter III that the F I resonance lines at about 95 nm were not observed during introduction of aqueous aerosol. With the conditions reported in the Fluorine atomic emission section, the F I resonance lines at 95.2 and 95.5 nm were observable during introduction of SF_6 through the DIP into the axial channel, as shown in Figure 29. Also, S II lines were evident in the 98 to 102 nm region. On center viewing and

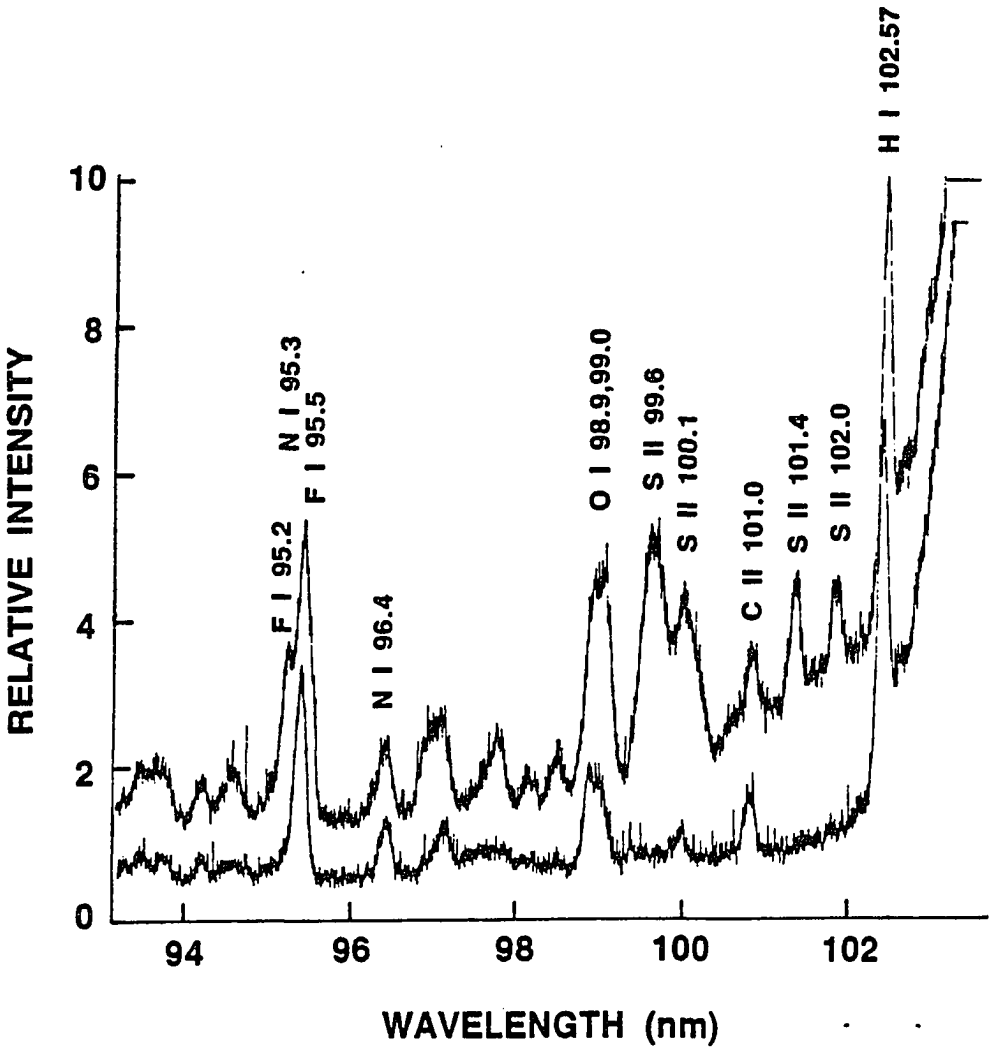

Figure 29. Wavelength scans from 93 to 103.5 nm while SF_6 in Ar was introduced into the ICP. In the DIP, this flow of SF_6 was diluted by Ar gas (Figure 17) to a total injector gas flow rate of 0.3 L min^{-1} (top scan). For the blank spectrum, Ar was substituted for the SF_6 (bottom scan). The top spectrum has been offset above the bottom spectrum

normal injector gas flow rates (0.8 L min^{-1}) resulted in weak F I lines that could not be distinguished from the N I line at 95.3 nm. Employment of a low injector gas flow rate, which gave optimum emission of the F I IR lines in the work of Fry et al. (5), and off center viewing of the axial channel allowed us to distinguished the F I resonance lines from the noisy background and the N I 95.3 nm line. Other F I lines corresponding to transitions that terminated in the upper levels of these VUV lines have been observed from an Ar ICP (1,5,72). The present work is the first report of F I resonance lines, although, at present, these lines are too weak to have much analytical utility. Gaseous sample introduction greatly attenuated the H I line at 95.0 nm, which obscured the wavelength region for F I detection during introduction of aqueous aerosol. The same F I lines (95.2 and 95.5 nm) have also been observed during introduction of SF_6 into a He discharge-afterglow with the monochromator system used in this study (133), which substantiated the conclusion that these lines were indeed from atomic fluorine. The reasons for the relative weakness of the F I lines in the VUV region from an Ar ICP are not clear and merit further study.

Typical flow injection analysis (FIA) profiles

The Br I emission signals achieved after alternate injections of 250 and 100 μL sample volumes are shown in Figure 30. Similar results were obtained for the other elements studied. The Br concentration injected was approximately 200 $\mu g\ g^{-1}$ of argon. The 250 μL injections, which contained 83 ng Br, yielded the broad peaks that reached an obvious steady state level. The narrow peaks, which briefly reached the steady state level, resulted from 100 μL injections containing only 33 ng Br. This observation of peak heights near the steady state level for 100 μL

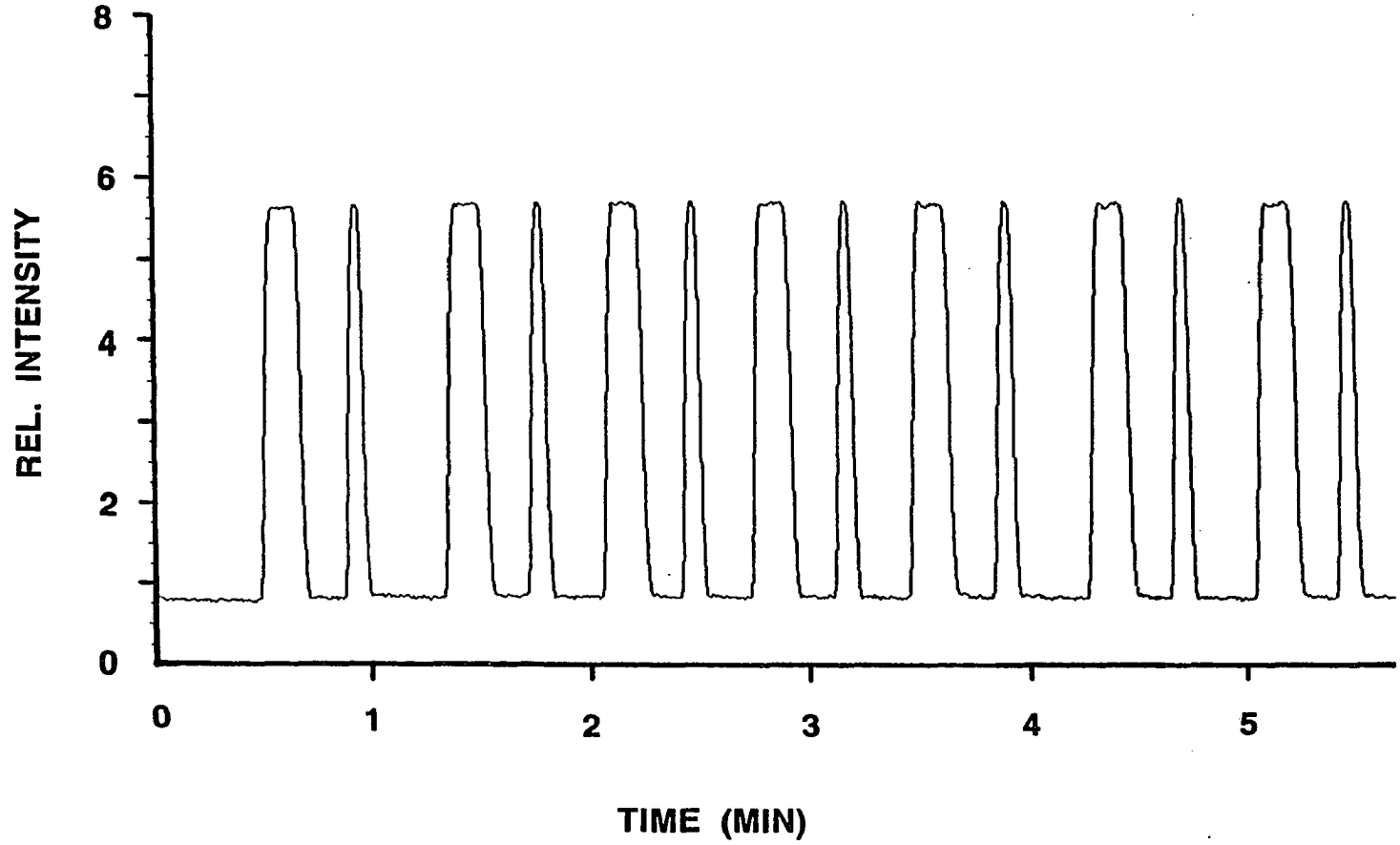

Figure 30. Alternate flow injections of 250 and 100 μL sample volumes of 98 ppm (v/v) Freon 13B1 in argon while monitoring Br I 154.07 nm emission. The threshold value for the low pass filter was set at 0.05 Hz in this flow injection profile. The injection valve was actuated electrically here and for Figure 31

injections indicated that the dead volume of the DIP was substantially less than 100 μL, in agreement with the 30 to 40 μL estimate described in the Instrumentation section. The relative standard deviation of the Br I 154.07 nm peak heights for the 7 FIA injections of 250 and 100 μL sample volumes, as shown in Figure 30, were 0.4 and 0.9%, respectively.

Repeated injections of 16 ng of Br in 50 μL of Ar are shown in Figure 31. Within a three minute span, 34 injections were performed. This figure illustrates how rapidly our system can detect low ng quantities of Br. The two slightly different peak heights resulted from alternating between two different sample loops that were not quite identical in volume. The relative standard deviations of the peak emission signals for each loop were 1.4 and 0.8%, i.e., slightly worse than for the larger loops in Figure 30.

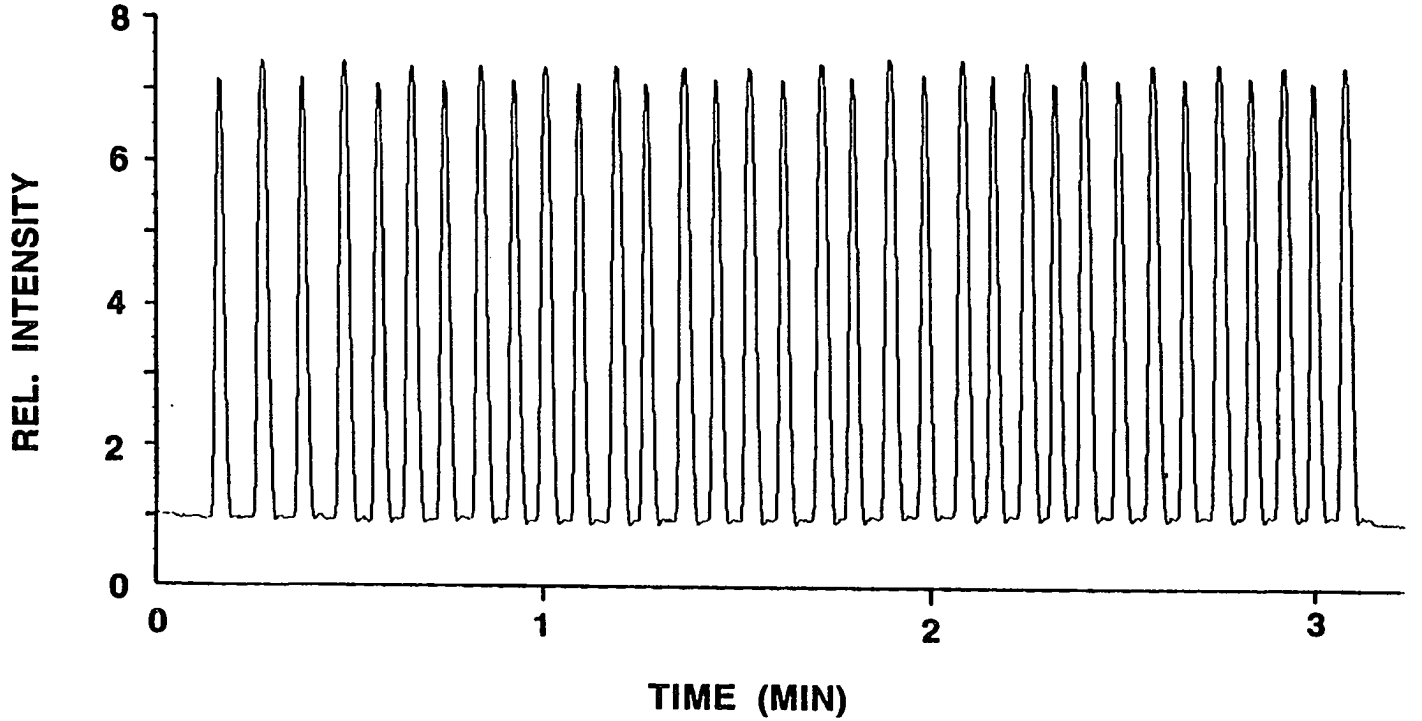

Figure 31. Br I 154.07 nm emission was observed by DIP-ICP-VUV-AES with rapid alternate flow injections of 2 different 50 μL sample volumes of 98 ppm (v/v) Freon 13B1 in argon. The threshold value for the low pass filter was set at 0.1 Hz in this flow injection profile

CHAPTER V. DIAGNOSTIC STUDIES OF THE ICP

General Discussion

The orifice based optical sampler was employed for the acquisition of diagnostic data of various VUV emission lines and molecular bands. Spectra were obtained on a laterally resolved basis through the length of the plasma. Particular emphasis was focused on the spatial distribution of the Ar resonance line emission at 104.82 and 106.67 nm. Our observations are correlated with the recently reported results of Carr and Blades (77) and with the radiation trapping model for energy transfer in ICPs (134-138).

A typical spectrum of the background of an argon ICP from 100 to 200 nm and the tentative peak assignments are presented in Figure 32. This spectrum was obtained by a scintillator PMT whereas the spectrum in Figure 21 was obtained with a solar-blind PMT. Other than the presence of the two Ar lines at 104.82 and 106.67 nm and the H I 102.57 nm, the two spectra are understandably quite similar.

Ar Resonance Lines

A recording of a portion of the VUV emission spectrum observed with the viewing field centered on the axial channel of an Ar ICP is shown in Figure 33 (lower left-side spectrum). The argon resonance lines at 104.82 and 106.67 nm arising from the lower energy transitions (139)depicted in Figure 34 are clearly evident. The relative intensities of the two lines are in general agreement with those reported by Carr and Blades (77) as well as those listed in the Kelly wavelength table (120) and the original papers that reported the initial observation of these lines from an

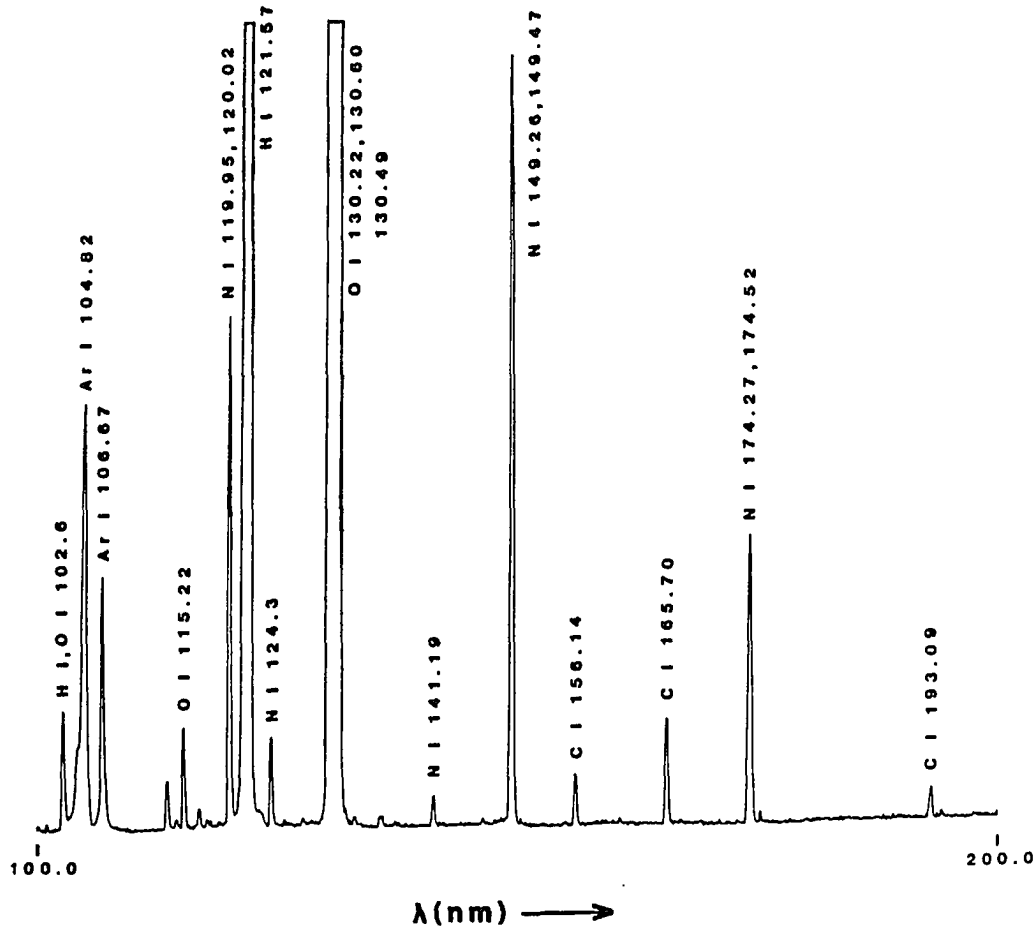

Figure 32. Wavelength scan from 100 to 200 nm of the background spectrum from an ICP using the Mode #1 cone (0.34 mm diameter orifice) assembly and the scintillator PMT for detection

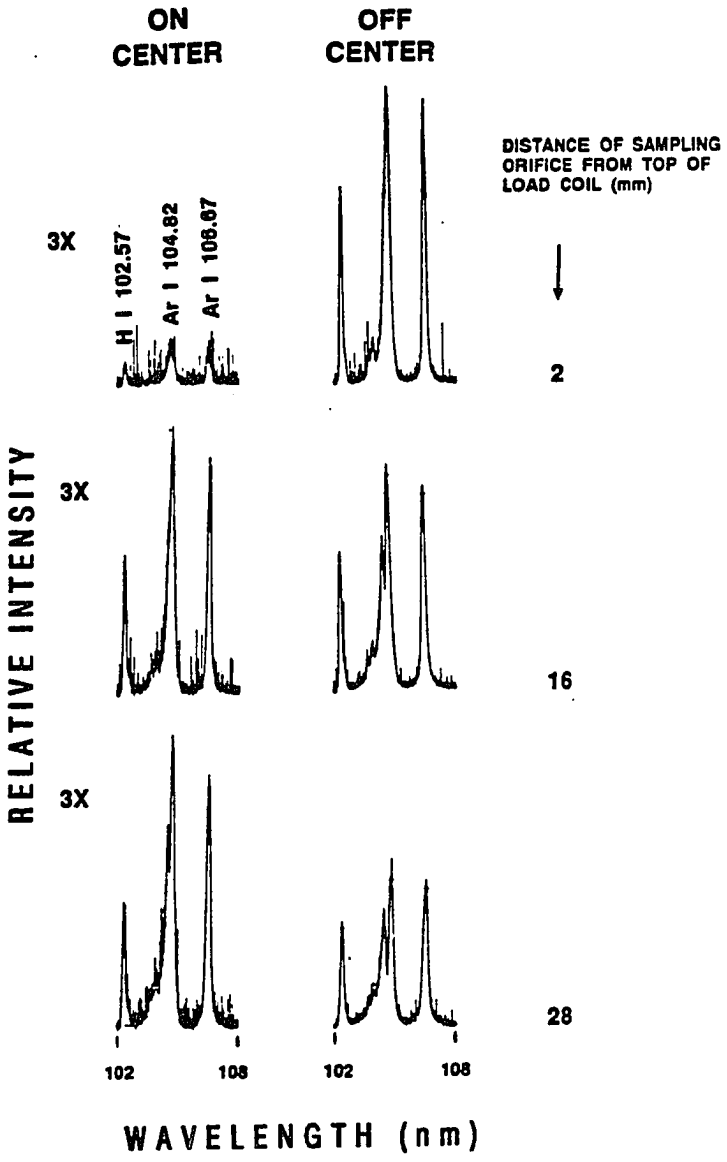

Figure 33. Emission spectra from 102 to 108 nm with the sampler placed on center and also displaced off center (3.2 mm) for various vertical displacements. The on center data were enhanced 3.33-fold for this figure

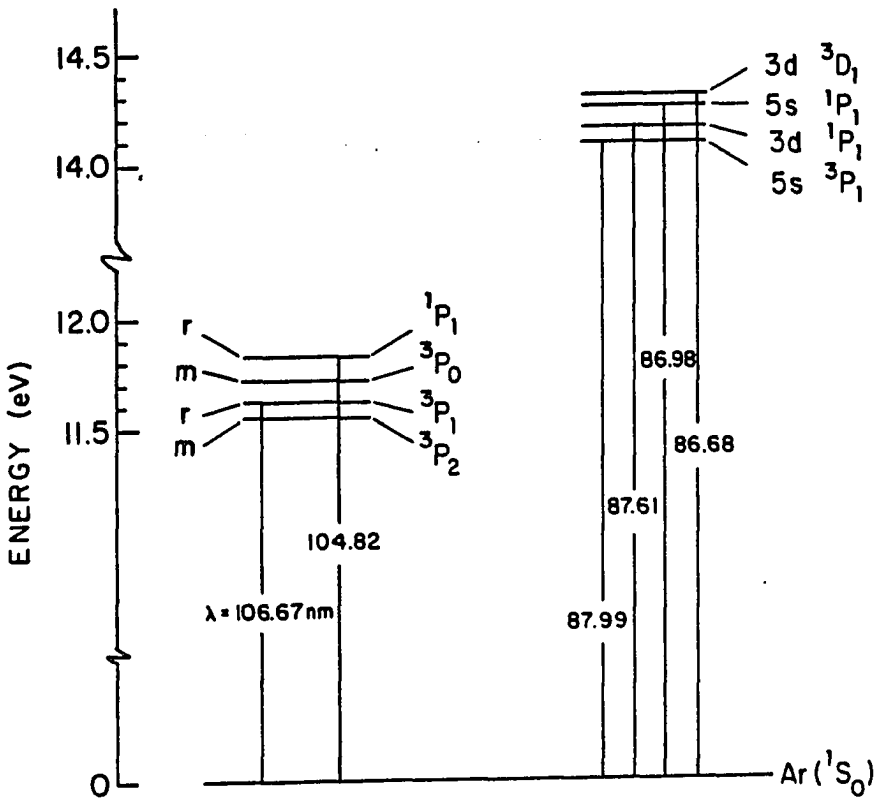

Figure 34. Partial energy level diagram for neutral Ar. Term symbols taken from Reference 139. All wavelengths are in nm

evacuated arc (140-143). The humps on the low wavelength side of the Ar I 104.82 nm line, which have appeared in all the spectra observed by us with pneumatic nebulization, have been attributed to O I emission at 103.92, 104.09, and 104.17 nm (77,120). The 104.82 nm line is slightly split at the top in agreement with Carr and Blades (77). This splitting is due to self-absorption and will be described in a subsequent section of this dissertation. The following results are based on measurements of the other Ar I line at 106.67 nm; the intensities of both Ar I lines behaved in a similar fashion with respect to plasma operating parameters.

Influence of operating parameters upon resonance lines

As shown in Figure 35 an increase in forward power from 1.0 to 1.5 kW caused a linear increase in the net intensity ($I_{Ar,\ 106}$) for Ar I 106.67 nm. Presumably, the number density $n(^3P_1)$ of Ar atoms in the $^3P_1$ state also increased with forward power to the same extent in the volume element through the axial channel seen by the spectrometer. These observations agree with data of Uchida et al. for the $^3P_2$ metastable level, the number density of which can be probed by atomic absorption (144). It should also be noted that if the line plotted in Figure 35 is extrapolated to lower powers it does not pass through the origin.

As with the Uchida et al. data, the extrapolation of the plot to lower power does not produce a zero intensity intercept. This is not surprising because substantial reductions in forward power lead to marked changes in plasma dimensions and eventual instability of the discharge. For the relatively high excitation energy of the Ar I 106.67 nm line (11.6 ev), only a small increase in excitation temperature (T_{exc}) with forward power is necessary to cause the threefold intensity increase shown in Figure 35. For T_{exc} in the 5000 - 6000 K range, a T_{exc} increase of only

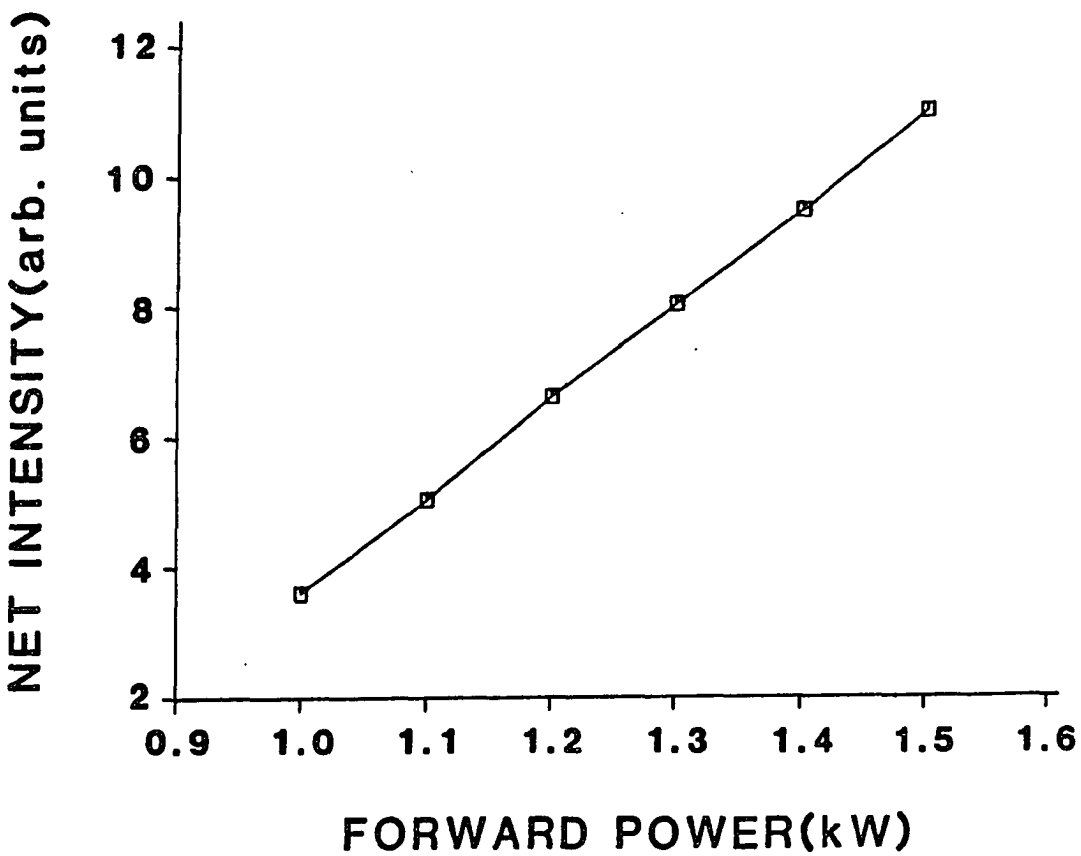

Figure 35. Intensity of Ar I 106.67 nm as function of forward power when axial channel is viewed.
Aerosol gas flow rate = 0.8 L min^{-1}

200 to 400 K can readily account for the observed dependence of $I_{Ar,\ 106}$ on forward power. In an ancillary experiment, $I_{Ar,\ 106}$ increased by approximately 40% when there was no nebulized water in the aerosol gas flow, which indicated that the axial channel was slightly "hotter" in the absence of nebulized water. This behavior is in contrast to that reported by Alder et al., who measured a tendency for temperature and electron density to decrease as the water content of the aerosol carrier gas decreased (134).

Lateral studies

The lateral spatial profiles of $I_{Ar,\ 106}$ shown in Figure 36 are very similar to radial profiles obtained by fluorescence for Ar metastable atoms by Hieftje and Carr (145) but show a more pronounced central valley than the data of Uchida et al. (146) and Nojiri et al. (147). The "cooling" effect of increasing aerosol carrier gas flow rate is also evident, particularly in the axial channel. This observation is consistent with earlier reported data (134,148-150). Because of the high excitation energy of this line, only a slight asymmetry in the lateral T_{exc} profile will cause a noticeable asymmetry in the observed intensity profile (151).

Self-absorption and self-reversal of the Ar resonance lines The spectra shown in Figures 33 and 37 were observed with the viewing field off centered 3.2 and 3.5 mm from the plasma axis, respectively (B, Figure 11). In this position the spectrometer observed the induction region and the toroidal Ar flow moving downstream toward the torch end. With the spectrometer viewing this region, the Ar I 104.82 nm line was extensively self-reversed, to a much greater extent than when the volume element viewed was centered on the axial channel. It may seem surprising that

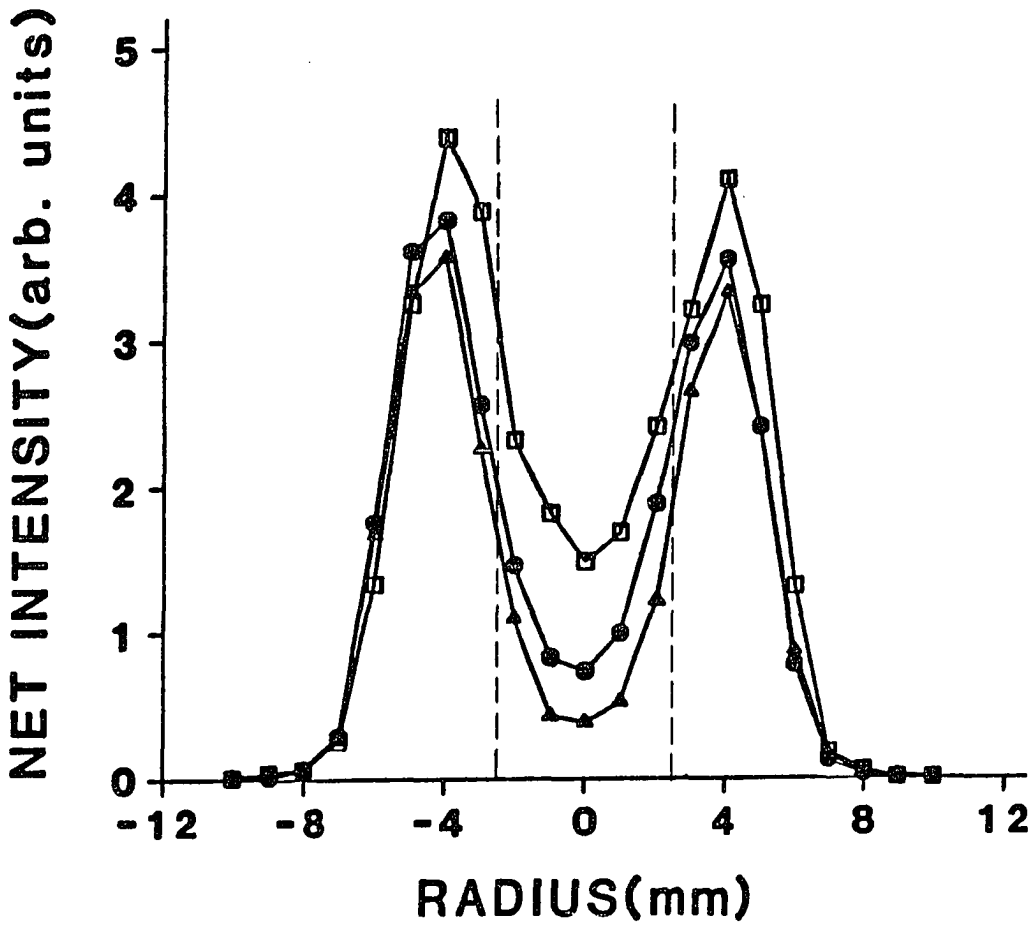

Figure 36. Lateral intensity profiles for Ar I 106.67 nm for various aerosol carrier gas flow rates:
□ 0.5 L min^{-1}
● 0.8 L min^{-1}
▲ 1.2 L min^{-1}.
Dashed lines indicate the approximate diameter of the axial channel. Forward power = 1.3 kW, observation height = 19 mm from load coil

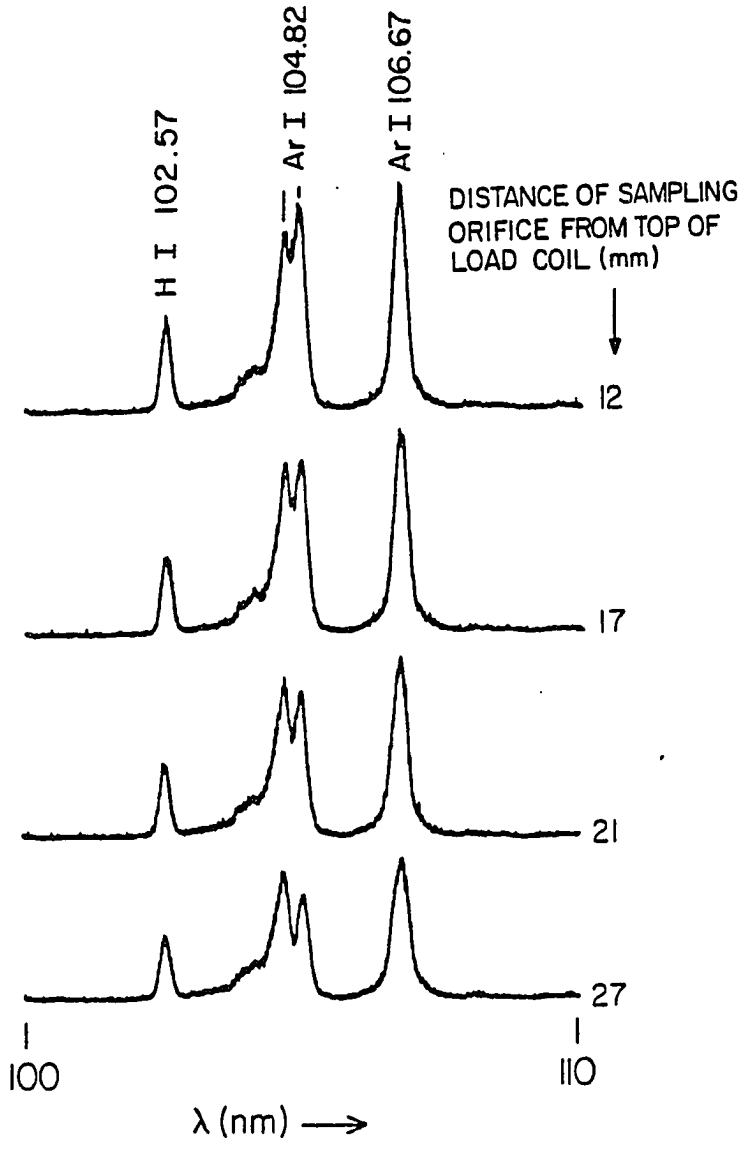

Figure 37. Emission spectra with the sampler displaced 3.5 mm laterally (B, Figure 11) for various vertical displacements. Entrance and exit slits were 25 μm wide for this recording. Forward power = 1.3 kW, aerosol gas flow = 0.8 L min^{-1}

self-absorption should be extensive enough to cause self reversal when viewing the induction region and its downstream flow. In actuality this behavior is precisely as expected. At a lateral position of 3.5 mm the spectrometer is observing radiation that travels from a high temperature region (i.e., the induction region inside the load coil) through a lower temperature zone. Thus Ar atoms in the downstream flow between the hot induction region and the sampling orifice have ample opportunity to absorb Ar resonance radiation before it can be detected by the spectrometer. The spectra in Figure 37 obtained at different observation positions show that the extent of self reversal of the 104.82 nm line increases with distance from the load coil, which corroborates the above explanation as the source of self-reversal. In contrast, when the axial channel is viewed (Figure 33, lower left-side), T_{exc} is highest at approximately 20 mm from the load coil (148,152,153), which is just in front of the sampling orifice. Thus self-absorption and self-reversal are much less evident when viewing the axial channel. Further observations of the behavior of the Ar resonance lines, on and off centered, are discussed in the depth profile section.

It is also interesting that self-absorption of the 104.82 nm line is much more extensive than for the 106.67 nm line. Presumably this is because the 104.82 nm line arises from an electric dipole allowed transition ($^1P_1 - {}^1S_0$) with a transition probability for emission listed as 5.1×10^8 s^{-1} (154). The other resonance line involves a less probable transition ($^3P_1 - {}^1S_0$) with a smaller transition probability for emission (1.2×10^8 s^{-1}). Therefore, reabsorption of the 106.67 nm line is less likely than for the 104.82 nm line. Even so, some self-absorption of the 106.67 nm line is evident because its intensity actually decreases as the separation between load coil and sampling orifice increases. The

observation of self-absorption for these lines has definite implications for the radiation trapping hypothesis for energy transfer in ICPs; these implications will be described in detail in a subsequent section.

Estimation of number density of Ar atoms in the $^3P_1$ level If self-absorption effects are neglected for the moment, the spatially resolved data of Figure 36 indicate that $n(^3P_1)$, when the induction region and its downstream flow are viewed, exceeds $n(^3P_1)$ in the axial channel by a factor of two to eight depending on aerosol carrier gas flow rate. This observation may be used to estimate the approximate magnitude of $n(^3P_1)$ in the axial channel, referred to hereafter as $n(^3P_1)_{ac}$. If the assumption is made that the population of $^3P_1$, within the volume element viewed in the induction region, corresponds to some weighted average excitation temperature, then the observed intensity ratio for Ar I 106.67 nm in the axial channel $(I_{Ar,106})_{ac}$ to that in the induction region $(I_{Ar,106})_{ind}$ may be expressed as follows:

$$\frac{n(^3P_1)_{ac}}{n(^3P_1)_{ind}} = \frac{(I_{Ar,106})_{ac}}{(I_{Ar,106})_{ind}}$$

$$n(^3P_1)_{ac} = \frac{(I_{Ar,106})_{ac}\,[n(^3P_1)_{ind}]}{(I_{Ar,106})_{ind}}$$

$$= \frac{(I_{Ar,106})_{ac}\,[n_{Ar,ind}\; e^{-E^*/kT_{exc,ind}}]}{(I_{Ar,106})_{ind}}$$

$$= \frac{(I_{Ar,106})_{ac}}{(I_{Ar,106})_{ind}} \quad \frac{(N_o P)}{RT_{g,ind}} e^{-E^*/kT_{exc,ind}} \qquad [1]$$

In these equations $n_{Ar,ind}$ = total Ar number density in the induction region, P = pressure (1 atm), R = ideal gas constant, $T_{g,ind}$ and $T_{exc,ind}$ = gas and excitation temperature in the induction region, respectively (149), k = Boltzmann constant, N_0 = Avogadro's number, and E^* = energy of excited Ar level. The partition function of the neutral Ar atom is not included because it essentially equals unity at ICP temperatures (155).

Estimated values for $n(^3P_1)$ in the axial channel are listed in Table X for a range of intensity ratios and several possible maximum temperatures for the induction region. A T_{exc} value for the induction region of 9000 to 10,000 K yields a value for $n(^3P_1)$ of the order of 10^{11} cm^{-3} in the axial channel, which is in approximate agreement with previous number density measurements for the metastable Ar levels (147,156). This assumed T_{exc} range is consistent with experimental measurements in the induction region just above the load coil (152) but is considerably higher than excitation temperatures measured at any radial location 20 mm above the load coil where the sampling cone is positioned. This conclusion is consistent with the concept that the spectrometer is actually viewing a long section of the ICP as shown in Figures 10 and 11. When the induction region is viewed, some self-absorption of the 106.67 nm line does occur (Figures 33 and 37). If a correction factor for self-absorption is deduced from Figure 37 and included in Equation [1], the calculated number densities of $^3P_1$ are only approximately 30% lower than those shown in Table II, thus verifying the validity of these $n(^3P_1)$ estimations for the axial channel. We caution the reader that these tentative calculations are only meant to indicate the order of magnitude of $n(^3P_1)$ so that this quantity may be compared with previous measurements for the metastable levels. Self-reversal of the 104.82 nm line makes it difficult to

Table X. Calculated values for number density of $^3P_1$ Ar atoms in axial channel

$\frac{(I_{Ar,\ 106})_{ac}}{(I_{Ar,\ 106})_{ind}}$	$T_{exc,ind}$(K)	$n(^3P_1)_{ac}$ in cm^{-3} for $T_{g,ind}$ = 6000–8000
0.50	8000	$2 - 3 \times 10^{10}$
	9000	$1 - 2 \times 10^{11}$
	10000	$6 - 8 \times 10^{11}$
0.25	8000	$1 - 2 \times 10^{10}$
	9000	$7 - 10 \times 10^{10}$
	10000	$3 - 4 \times 10^{11}$
0.12	8000	$5 - 7 \times 10^{9}$
	9000	$4 - 5 \times 10^{10}$
	10000	$1 - 2 \times 10^{11}$

estimate the number density for the other resonant state ($^1P_1$) by this approach.

Relation to radiation trapping model for energy transfer in the ICP

Alder et al. (134) initially noted that Ar resonant radiation should be strongly self-absorbed in the ICP. Subsequently, Blades and Hieftje (135) suggested that Ar resonant photons formed in the induction region may transfer energy to the axial channel via repetitive absorption and re-emission events, and that the populations of the Ar metastable levels (Figure 34) become equilibrated with (i.e., approximately equal in number density to) those of the nearby resonance levels. Blades (136) later described calculated results to further suggest that such processes could "assist" ionization in the axial channel. Mills and Hieftje (137) recently reported detailed calculations of the extent and duration of Ar resonance radiation trapping in the ICP.

The first step toward determining the importance of any ICP mechanism should be experimental verification of the presence of the proposed energetic species. Along with the report by Carr and Blades (77), the present work proves conclusively that Ar resonant photons exist in the type of ICP used for analytical spectroscopy. In addition, we show that Ar resonant photons generated in the induction region can be absorbed by downstream Ar atoms. It is therefore certain that a similar process occurs for Ar resonant photons that are radiated into the axial channel from the induction region. Other experimental evidence presented in this paper supports the radiation trapping model. Thus, the spatial intensity distribution and determined dependence of Ar resonant line intensity on power and aerosol carrier gas flow rate in the presence or absence of water are consistent with the radiation trapping hypothesis and with

analogous measurements for the Ar metastable level populations (144-147,156). Also, the approximate estimate of $n(^3P_1)$ in the axial channel revealed number density values that could be similar to previous measurements for the metastable levels, thereby providing tentative evidence that the populations of the resonance and metastable levels could be equilibrated. The four higher energy resonance lines (86.68, 86.98, 87.61, and 87.99 nm, easily seen in Figure 38B) detected in this study with excitation energies of ~14 eV (Figure 34) have also been proposed to contribute to radiation trapping (135). In spite of the above consistencies, we caution the reader to recognize that the present study does not determine the extent to which radiation trapping contributes to excitation, ionization, and energy transfer in ICPs. Evaluation of the relative contributions of the numerous proposed mechanisms to ICP composition and properties remains a challenging objective.

Depth profiles

Spatial scans of the Ar resonance lines were taken at various radial positions within the plasma from 0 to 28 mm above the load coil in increments of 2 mm, on and off center of the axial channel. A Mode 1E cone with a 0.34 mm diameter orifice was used to constrict the field of view. Several scans of Ar lines have been discussed and shown earlier in Figure 33. From these spectral scans, simulated depth profiles of the relative intensities of Ar I 106.67 nm for on and off center viewing at different observation heights above the load coil were plotted in Figure 39. The intensity of the Ar I 106.67 nm line at 2 mm above the load coil with off center viewing was 30-fold more than observed while viewing on center, although the enhancement decreased to only 2.5-fold when an observation height of 22 mm was used. Figure 39 shows that the intensity

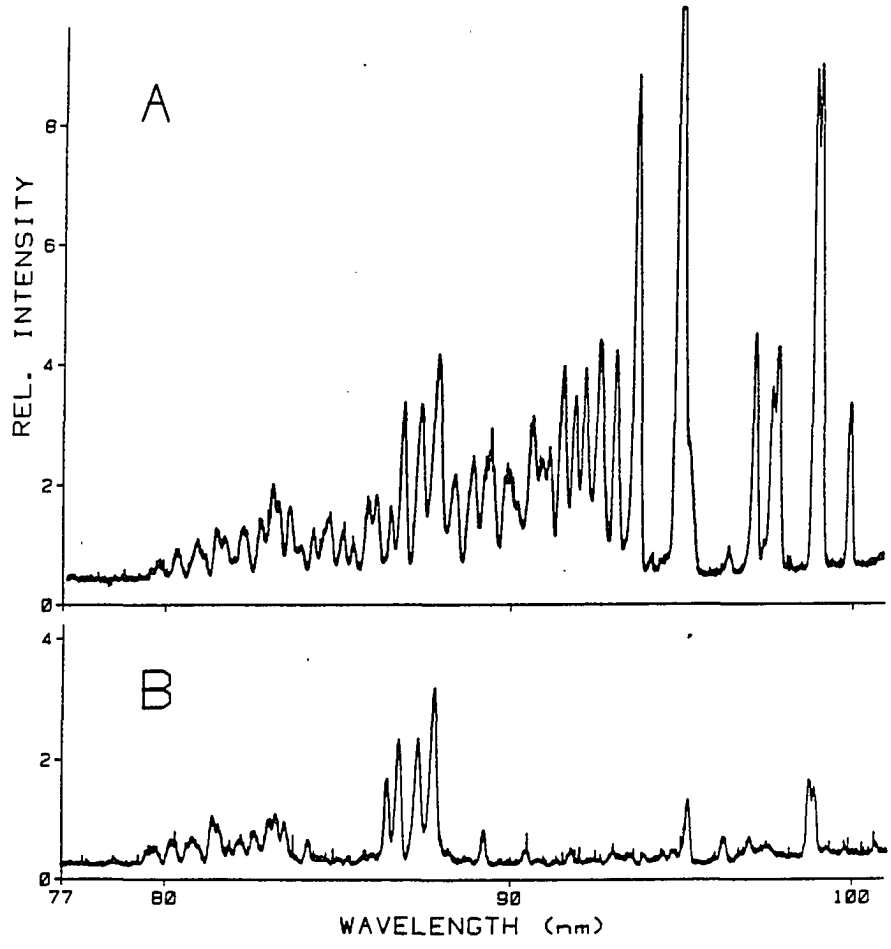

Figure 38. Emission spectra from 77 to 102 nm of
(A) pneumatic nebulization of distilled deionized water and
(B) dry Ar introduced into the plasma

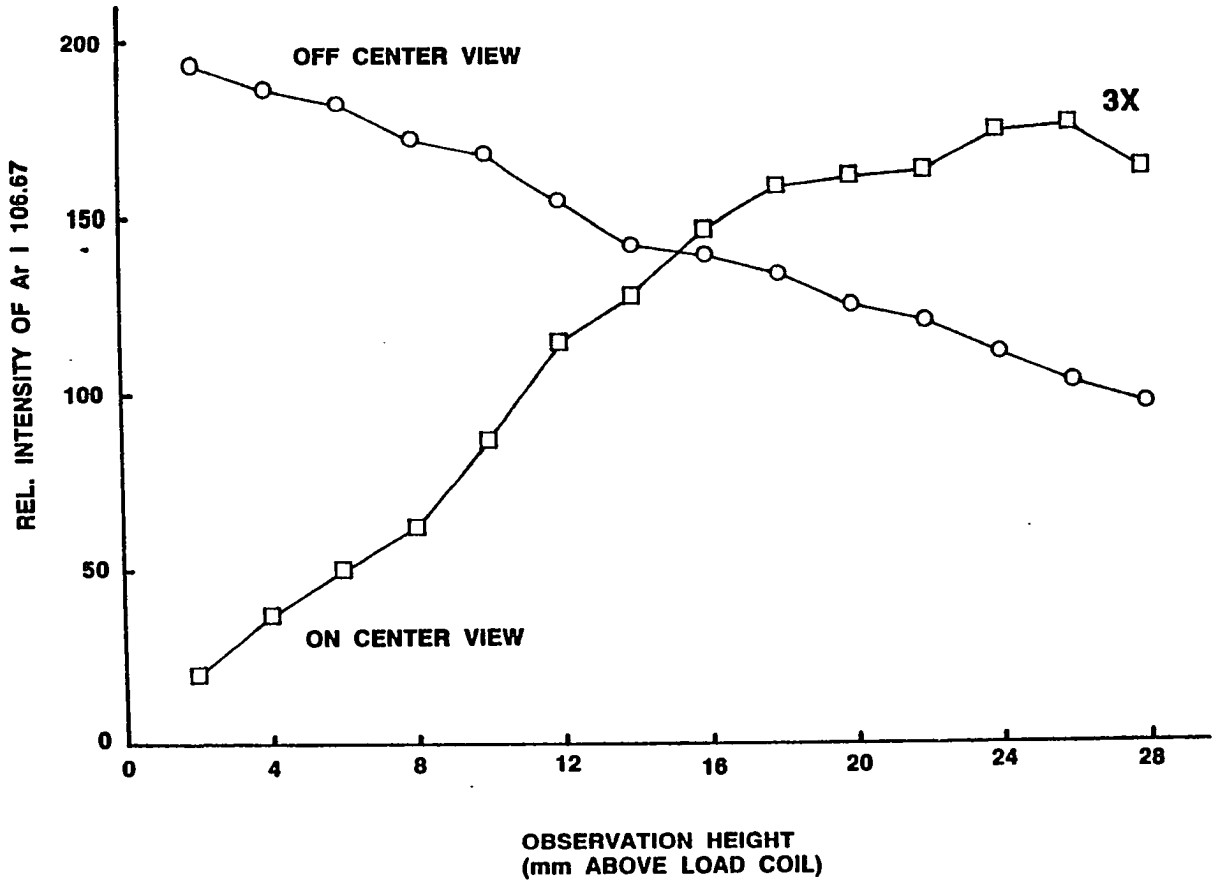

Figure 39. Emission intensity of Ar I 106.67 nm observed on and off center of the axial channel at different observation heights above the load coil through a Mode 1E cone (0.34 mm dia. orifice). The on center data were enhanced 3.33-fold

of the Ar resonance radiation at 106.67 nm was maximum at a position low (<2 mm above the load coil) in the induction region. Also, within the axial channel, the rate of increase of the intensity of the Ar I 106.67 nm line was maximum at 8 to 16 mm above the load coil. With the construction of a crude derivative plot from the data in Figure 39, the previous statements concerning the location of maximum Ar emission were verified, as shown in Figure 40. The site of maximum Ar resonance emission within the axial channel coincided with the volume of the plasma where analyte would be excited within an ICP. It must be noted that the intensity difference between emission observed from two observation heights does not represent the emission only between these two heights, but also from the slightly larger field of view along the plasma length for the higher observation height with respect to the lower height. As an exploratory study, the present procedure was adequate for the general location of maximum Ar resonance emission in the axial channel. In the future, the origin of maximum Ar emission could be more accurately determined with a cone assembly that will minimize the divergence of the field of view (cylindrical rather than conical dimensions).

A similar experiment was performed for the Zn II 202.55 and 206.20 nm and Zn I 213.86 nm lines, as shown in Figure 41. More Zn I intensity occurred very low in the plasma with respect to the Zn II intensity although that was not particularly the case higher in the plasma. The location of the maximum increase in intensity of Zn I and II lines originated in the 4 to 14 mm region above the load coil, which corresponded to the region of maximum emission from the Ar resonance line at 106 nm. If emission from other analytes could be associated with the region of maximum Ar emission especially for upper energy states of

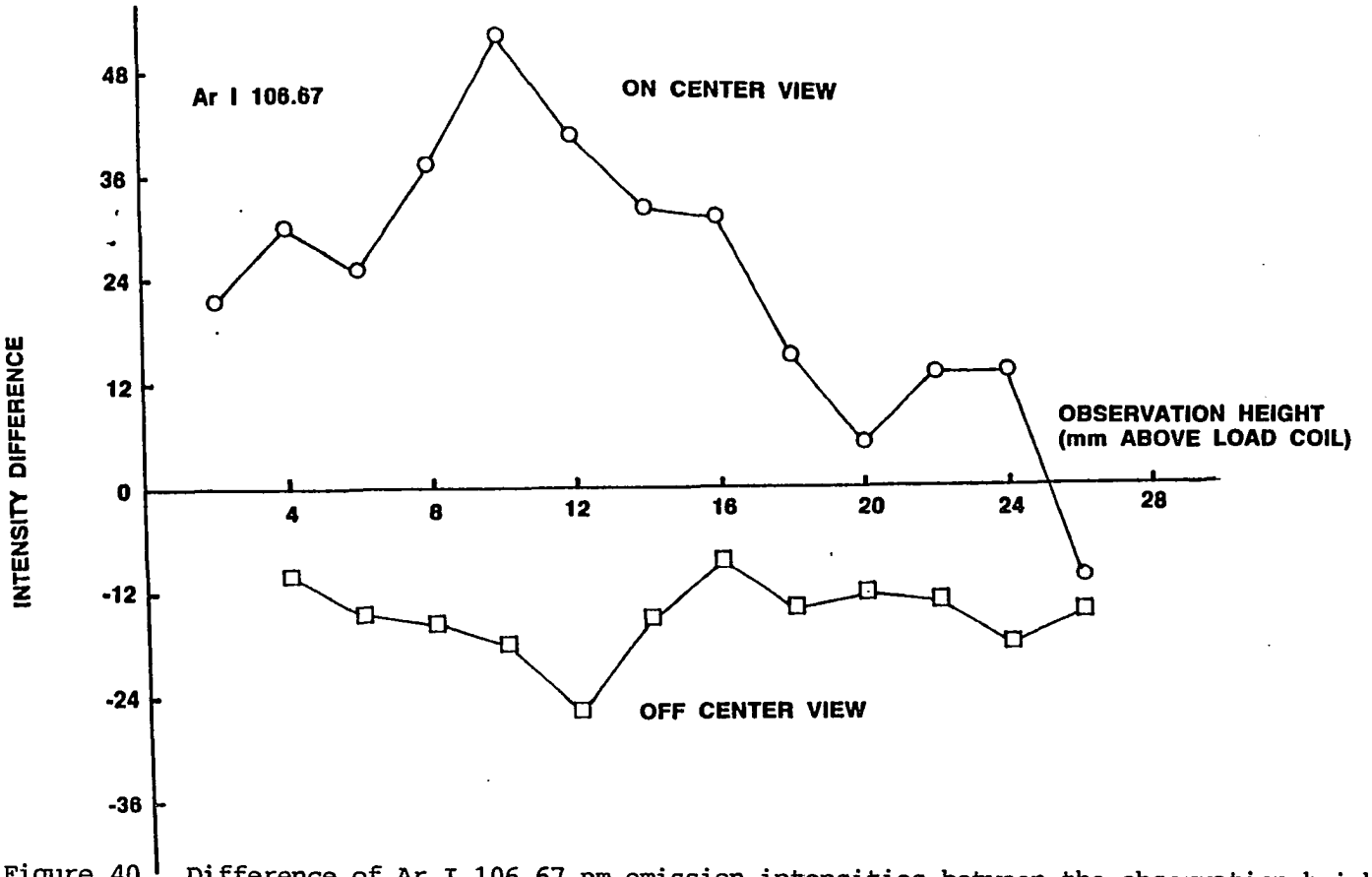

Figure 40. Difference of Ar I 106.67 nm emission intensities between the observation heights of (x+2) mm and (x-2) mm above the load coil was plotted at x mm on the X-axis. This graph was a crude representation of the derivative of the plot in Figure 39. The on center data were enhanced 3.33-fold

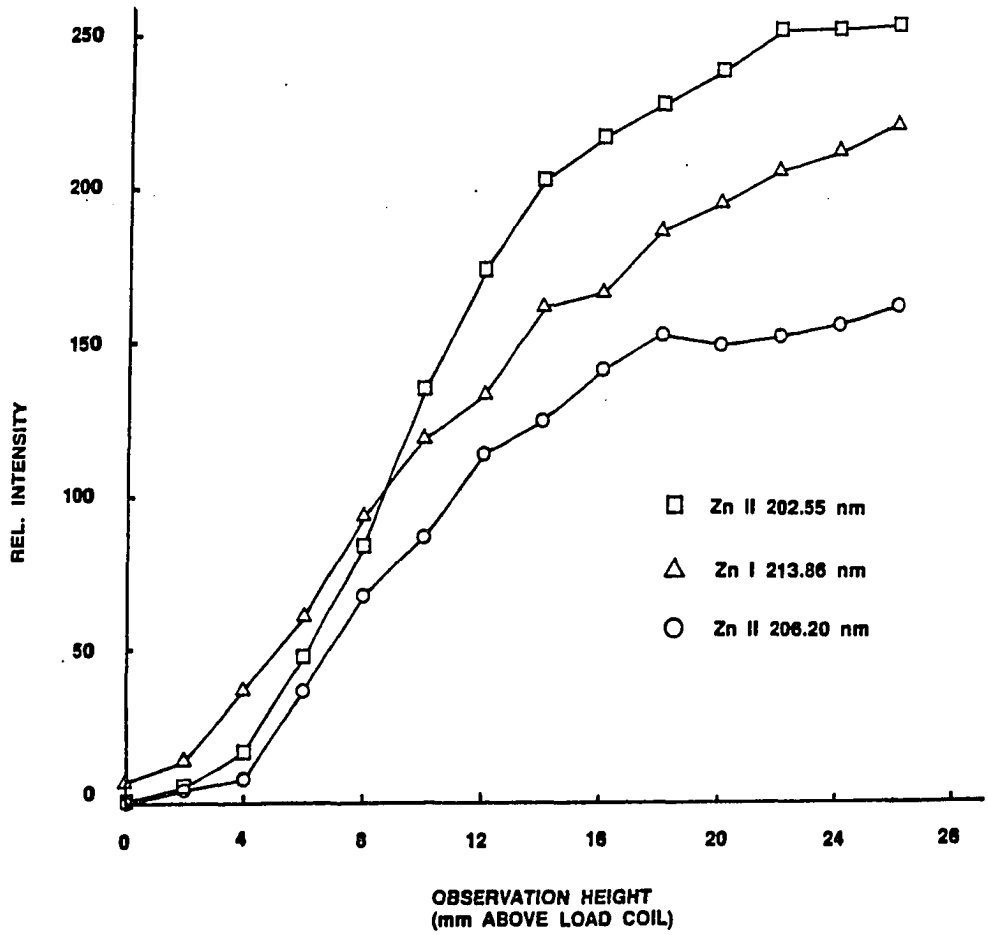

Figure 41. Emission intensities of some Zn I and II lines observed at different observation heights above the load coil with on center viewing through a Mode 1E cone (0.34 mm dia. orifice)

analytes that coincide with the resonance states of Ar, radiation trapping could gain further support as an important excitation mechanism in the ICP.

Miscellaneous Ar resonance line studies

Ar lines below 100 nm The spectrum observed in the region 93 - 100 nm (Figure 38) corresponds closely with that reported previously by Carr and Blades (77). Some interesting features are discernable below 93 nm. The Ar resonance lines at 86.68, 86.98, 87.61 and 87.99 nm have been discussed earlier. The progression of partly resolved lines below 86 nm corresponds to Ar resonance transitions from excited states at even higher energies (120). As shown in Figures 38 and 42, the spectrum exhibits an abrupt low-wavelength threshold at 78.8 $\pm$0.2 nm, which agrees closely with the ionization energy of Ar (15.76 eV, 78.67 nm). Emission of photons of lower wavelengths would not be expected from the ICP; photoionization of neutral Ar would deplete such photons even if excitation were sufficiently energetic to populate the appropriate energy levels (157). The background below 78.7 nm corresponds primarily to scattered light in the spectrometer with small contributions from photomultiplier dark current and occasional RF noise spikes.

Addition of easily ionizable element When an aerosol created by pneumatic nebulization of a solution containing about 0.5% Na, an easily ionizable element, was introduced into the axial channel, no effect upon the Ar I 104.82 and 106.67 nm resonance lines was observed, confirming the results reported by Carr and Blades (77).

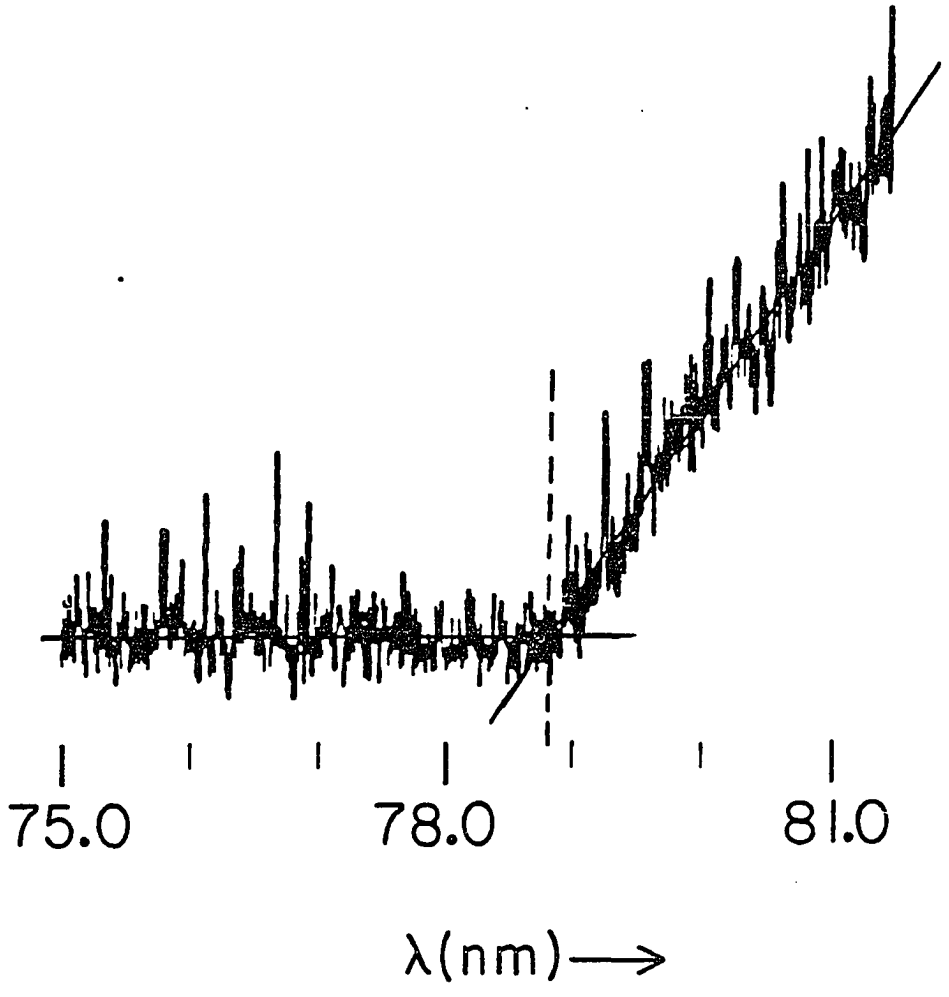

Figure 42. Emission spectrum with sampler centered in axial channel. Slit widths of 250 μm were used to obtain sufficient intensity for this recording. The background at 75.0 nm corresponds to approximately 8 x 10^{-10} amps

Ar as Purge Gas

When the monochromator was purged with Ar instead of He, a small but noticeable difference in the baseline from about 110 to 140 nm was evident, as shown in Figure 43A. The perturbation in the baseline was from Ar_2, which emits a band in the 110 to 140 nm region (158-160). Possibly, Ar purge gas that exited the cone orifice interacted with the Ar plasma at the cone orifice. At this interface between the plasma and cone, excited Ar_2 was formed and its emission continuum was observed. It can also be seen in Figure 43 that the Ar resonance lines at 104.82 and 106.67 nm disappeared when Ar was used as the purge gas (note that the H I 102.57 nm line "survives"). In order to detect emission from the Ar resonance lines, this emission must enter the monochromator through the sampling orifice and transverse a long optical path of Ar to the PMT. The Ar purge gas within the monochromator absorbed the line emission, thus indicating that the emission arised from Ar resonance transitions. Also, emission below 94 nm was suppressed when Ar gas was used as the purge gas, as shown in Figure 44. This suppression could be due to the absorption of radiation below 94 nm by the Ar gas that resides within the monochromator. Many Ar lines originate at energy levels with transitions below 94 nm.

With Ar as the purge gas, the relative intensities of the background and analyte lines from 100 to 160 nm decreased from 40 to 90% of those observed when He was used as the purge gas. The background noise fluctuations (at 171.7 nm) and analyte lines near 200 nm were not suppressed with the use of Ar as the purge gas. Therefore, an Ar purge could be used for analytical and diagnostic studies but He would be the preferred gas due to its higher transparency to VUV radiation.

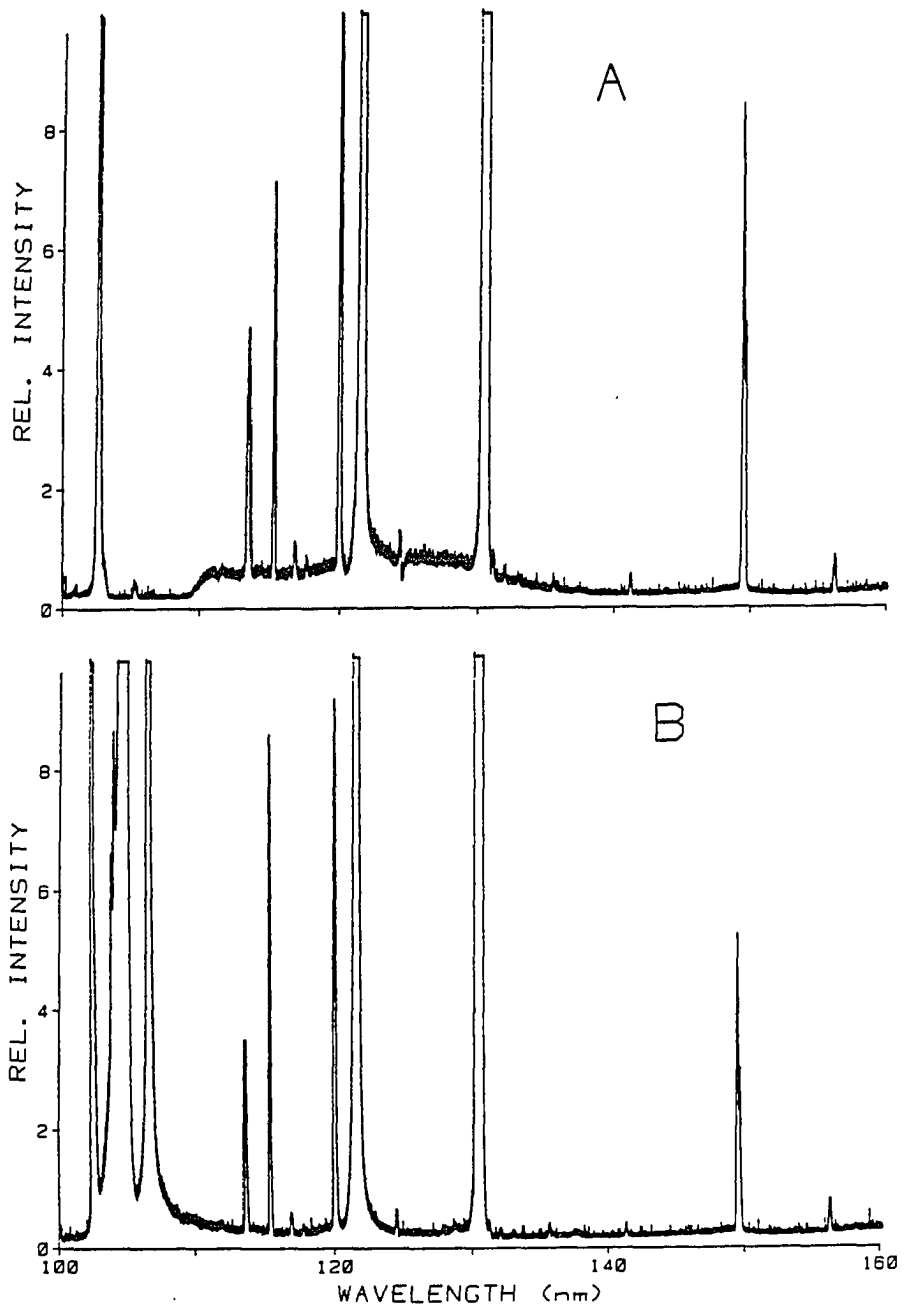

Figure 43. Emission spectra from 100 to 160 nm during pneumatic nebulization of distilled deionized water into the plasma with (A) Ar purge gas flow and (B) He purge gas flow exiting the orifice of the cone attached to the monochromator

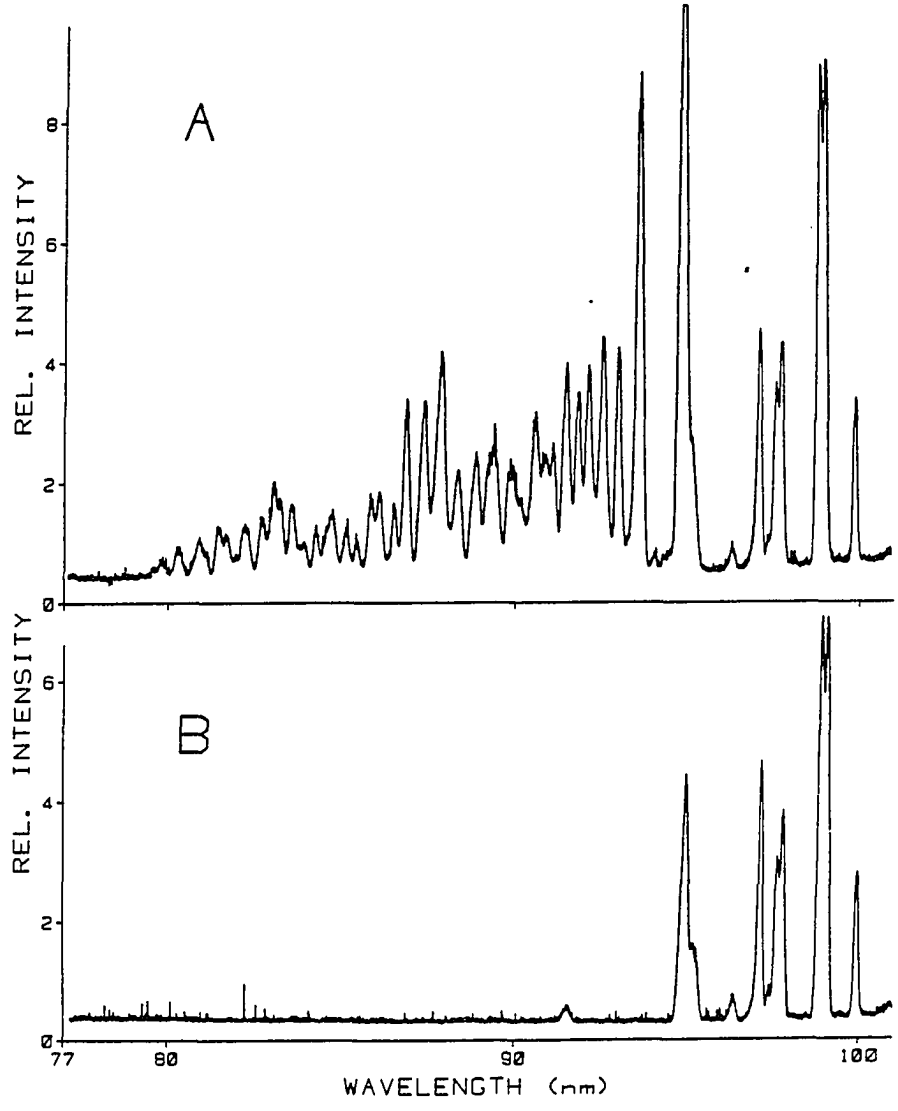

Figure 44. Emission spectra from 77 to 102 nm during pneumatic nebulization of distilled deionized water into the plasma with
(A) He purge gas flow and
(B) Ar purge gas flow exiting the orifice of the cone attached to the monochromator

H_2 Molecular Band System

A group of weak lines around 160 nm was detected and the background level between 130 and >175 nm was elevated when H_2O was nebulized versus the introduction of dry Ar gas into the axial channel (Figure 45). The lines around 160 nm could not be identified with atomic or ionic emission of any elements that have been studied, rather they coincided with the "many-lined molecular hydrogen spectrum" (116,117). Usually the H_2 band system consisted of a conglomeration of lines that extended from 85 to 167 nm (116,117,161,162) and had been observed at the Ames Laboratory from a He discharge-afterglow source (133). The band system observed with the ICP-VUV-AES apparatus was from the Lyman bands of H_2 with transitions from $B^1\Sigma_u^+$-$X^1\Sigma_g^+$, some of which were not observable with our system. A partial energy level diagram of H_2 (163) is illustrated in Figure 46. Another H_2 band system (the Werner bands) resides at wavelengths below 130 nm and have a higher excited state level ($C^1\Pi_u$) than the Lyman bands (161). The Werner bands were not apparent above the background noise in our spectra. Lack of Werner bands and some Lyman bands indicated that the observable excited states of H_2 were populated by selective energy transfer processes rather than simple thermal excitation.

Other experimental studies of H_2 in the presence of excess Ar (164) indicated that near-resonant electronic energy transfer from Ar to H_2 by collisions between excited Ar atoms and H_2 yielded excitation from only particular vibrational-rotational levels of the $B^1\Sigma_u^+$ state of H_2. Argon resonance states of $4s^1P_1$ and $^3P_1$ (104.82 and 106.67 nm transitions to the ground state, respectively) selectively excited certain vibrational-rotational levels of H_2 of similar energy to the Ar I states as stated in Equation [2] (164).

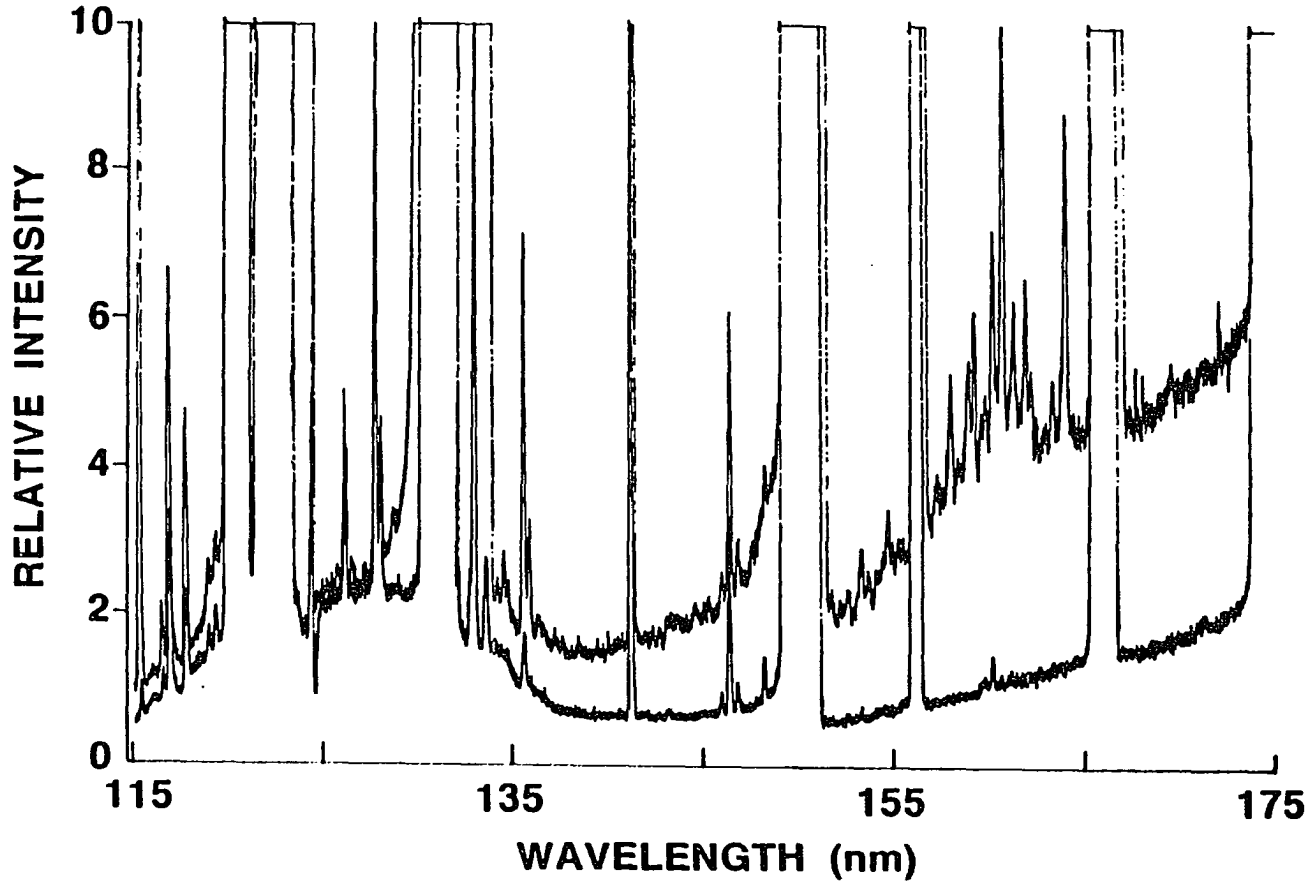

Figure 45. Wavelength scans from 115 to 175 nm of distilled deionized water nebulized by a pneumatic nebulizer (upper scan) and Ar gas directly introduced (lower scan) into the axial channel of the ICP. Full scale sensitivity of $1X10^{-8}$ A, Mode 1 cone with a 3 mm dia. orifice, 0.8 L min^{-1} nebulizer gas flow rate, power of 1.55 kW, and 22 mm observation height were employed. The upper spectrum was not offset in the Y-axis from the lower spectrum

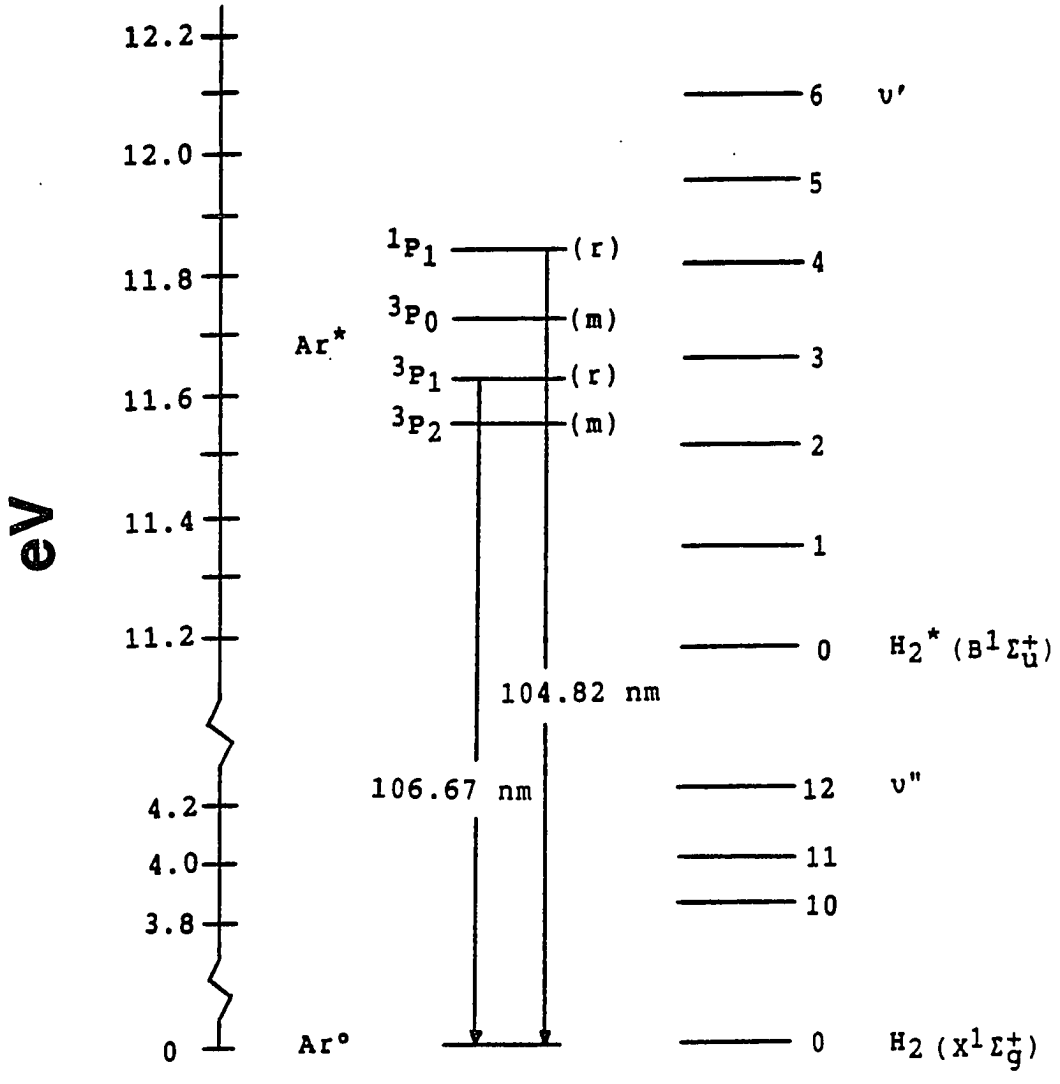

Figure 46. Partial energy level diagram for neutral Ar and molecular hydrogen. Term symbols taken from References 117 and 139. All wavelengths are in nm

$$H_2(X^1\Sigma_g^+,\ v''=0,J) + Ar^* \longrightarrow H_2(B^1\Sigma_u^+,\ v',J') + Ar + \Delta E \qquad [2]$$

The term, ΔE, was the energy released to translation. Alternatively, absorption of an Ar resonance photon by H_2 accompanied by fluorescence could also explain the selective excitation of the $B^1\Sigma_u^+$ state of H_2 followed by emission of the simplified H_2 band system in the presence of Ar (118,165). Argon resonance radiation from 104.82 and 106.67 nm selectively excited H_2 from the ground state to the $v'=4,5$ and $v'=3$ levels, respectively, of the $B^1\Sigma_u^+$ state (164). Fluorescence from different vibrational levels in the $B^1\Sigma_u^+$ state of H_2 could occur after excitation from energy levels other than the $v''=0$ ground state of H_2 (118).

Experiments were run to confirm the identity of the species responsible for the H_2 band system. The band system observed during nebulization of H_2O into the plasma (Figure 47B) is compared with that observed during introduction of H_2 gas via the DIP (Figure 47A). The same features were observed in the two spectra, which illustrated that the band emission occurred from H_2. In the case of the nebulization of H_2O, a possible mechanism in the development of the H_2 band system was that water, when nebulized and introduced into the axial channel, dissociated into H and O atoms. These H atoms recombined to form H_2 (166). Although the initial ground state of H_2 was unknown, the following H_2 $B^1\Sigma_u^+$-$X^1\Sigma_g^+$ transitions could tentatively be assigned in the wavelength region shown in Figure 47. The group of lines, associated with the excited vibrational state v' to ground vibrational state v" transitions -denoted as [v',v"]- between 157 and 165 nm, were [3,10] from 158.8 to 161.1 nm, [3,11] from

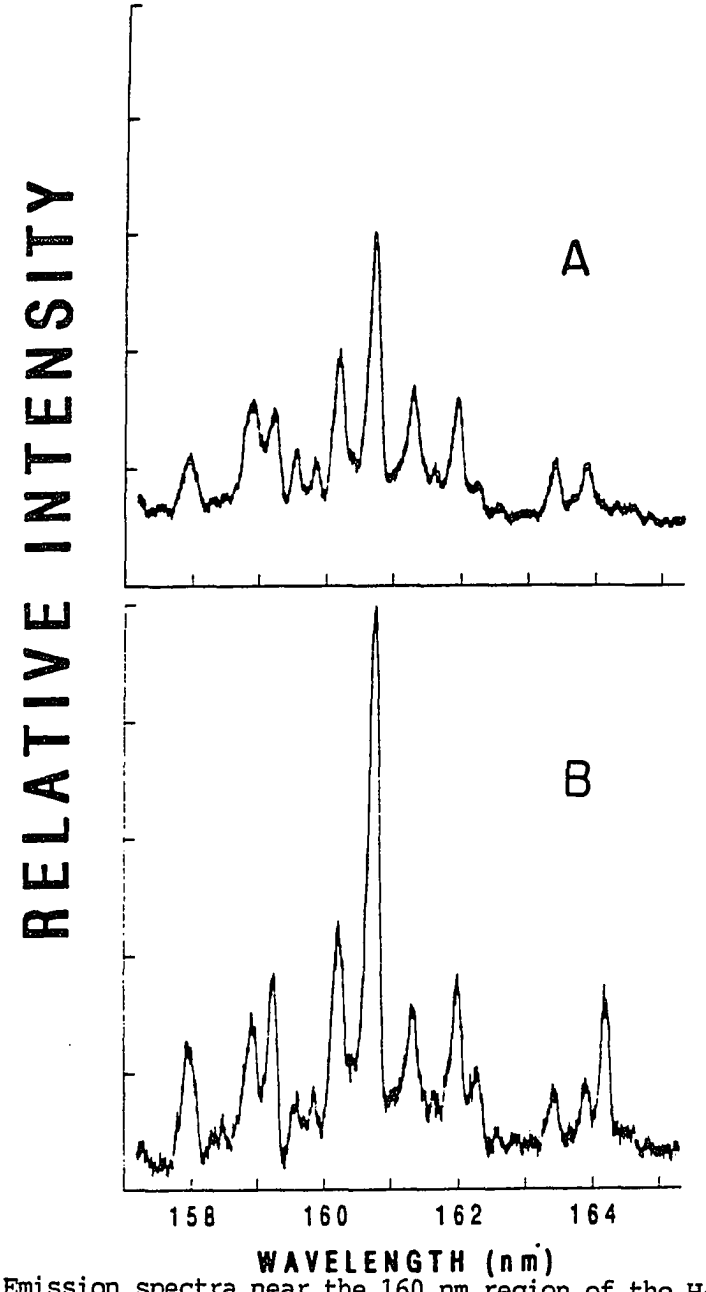

Figure 47. Emission spectra near the 160 nm region of the H_2 molecular band system obtained by the
(A) introduction of 5% H_2 in Ar by the DIP at a rate of 133 mL min^{-1} and
(B) pneumatic nebulization of H_2O into the axial channel.
An observation height of 22 mm above the load coil and a Mode 1 cone with a 3 mm dia. orifice were used. Both intensity scales were $1X10^{-8}$ A full scale except that current suppression ($4.5X10^{-9}$ A) was employed on the lower spectrum

163 to 164 nm, [4,11] from 160 to 162 nm, [5,11] from 157.2 to 158.7 nm, and [5,12] from 160.7 to 162 nm. The origin of the emission line at 164.1 nm in Figure 47B had not been confirmed, but that line had not been observed during introduction of dry Ar into the ICP.

Work has been done on the observation of the D_2 band system (167) and the D_2 bands in the presence of Ar (164,165). The upper scan in Figure 48 shows the D_2 band system from 157 to 165 nm emitted when D_2O was nebulized. A comparison to the analogous H_2 band system is shown in the lower scan. The band systems were quite different due to the different energy levels associated with H_2 and D_2. Dependent upon the initial state of D_2 prior to resonant energy transfer from or collisional excitation with excited Ar atoms, various vibrational levels in the B electronic state of D_2 have been known to be excited (v'= 4, 6, 7, or 9 in References 164,165). The band systems obtained with nebulization of D_2O and introduction of D_2 gas into the axial channel of the ICP were quite similar, which confirmed that the band emission occurred from D_2.

Because nebulization of H_2O into the ICP produced this band system, spatially resolved experiments were performed to determine the origin of this radiation. A Mode 1E cone with a 0.34 mm diameter orifice was used to sample radiation within the axial channel and from the induction region of the plasma. The H_2 band system was observable in the axial channel (Figure 49A) but was absent from the induction region (Figure 49B). All other background emission lines, from C, H, N, and O, increased in intensity, off scale in Figure 49B, when the induction region was viewed. The intensities of the C, H, N, and O emission lines (off scaled lines in Figure 50B) also increased for on center viewing when the observation height of the cone assembly was increased from 2 to 22 mm above the load

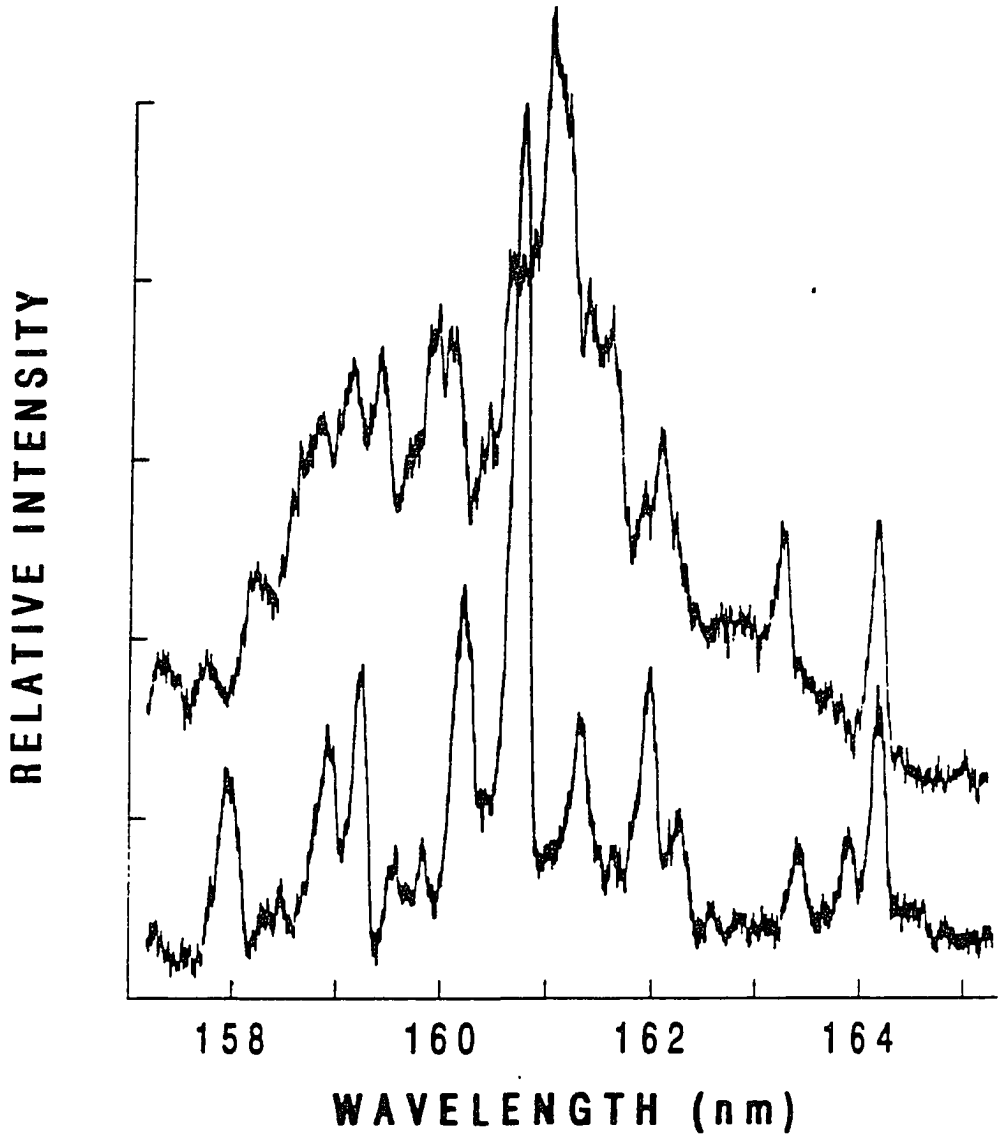

Figure 48. Emission spectra near the 160 nm region of the H_2 (lower scan) and D_2 (upper scan) molecular band system obtained by the pneumatic nebulization of H_2O and D_2O, respectively. A Mode 1 cone with a 3 mm dia. orifice and an observation height of 22 mm were used. Both spectra were collected with $1X10^{-8}$ A full scale and current suppression of $4.5X10^{-9}$ A. The upper spectrum was offset one-fifth of full scale in the Y-axis so the features of the two band systems can be easily compared

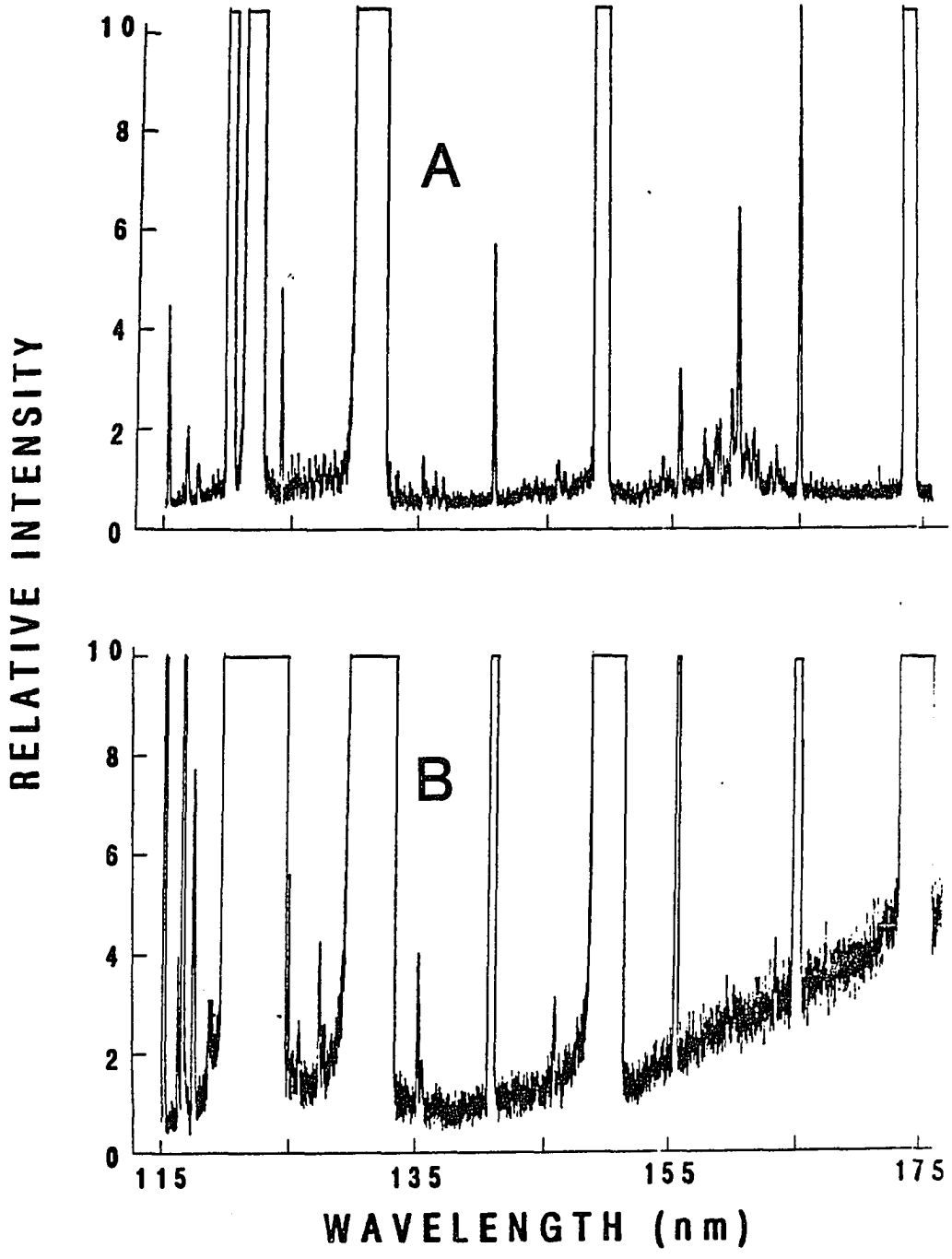

Figure 49. Emission spectra from 115 to 175 nm of the (A) On center and (B) Off center (3.9 mm) view of the ICP through a Mode 1E cone (0.34 mm dia. orifice) at observation heights of 6 and 10 mm above the load coil, respectively. Full scale deviation is equivalent to $1X10^{-9}$amps

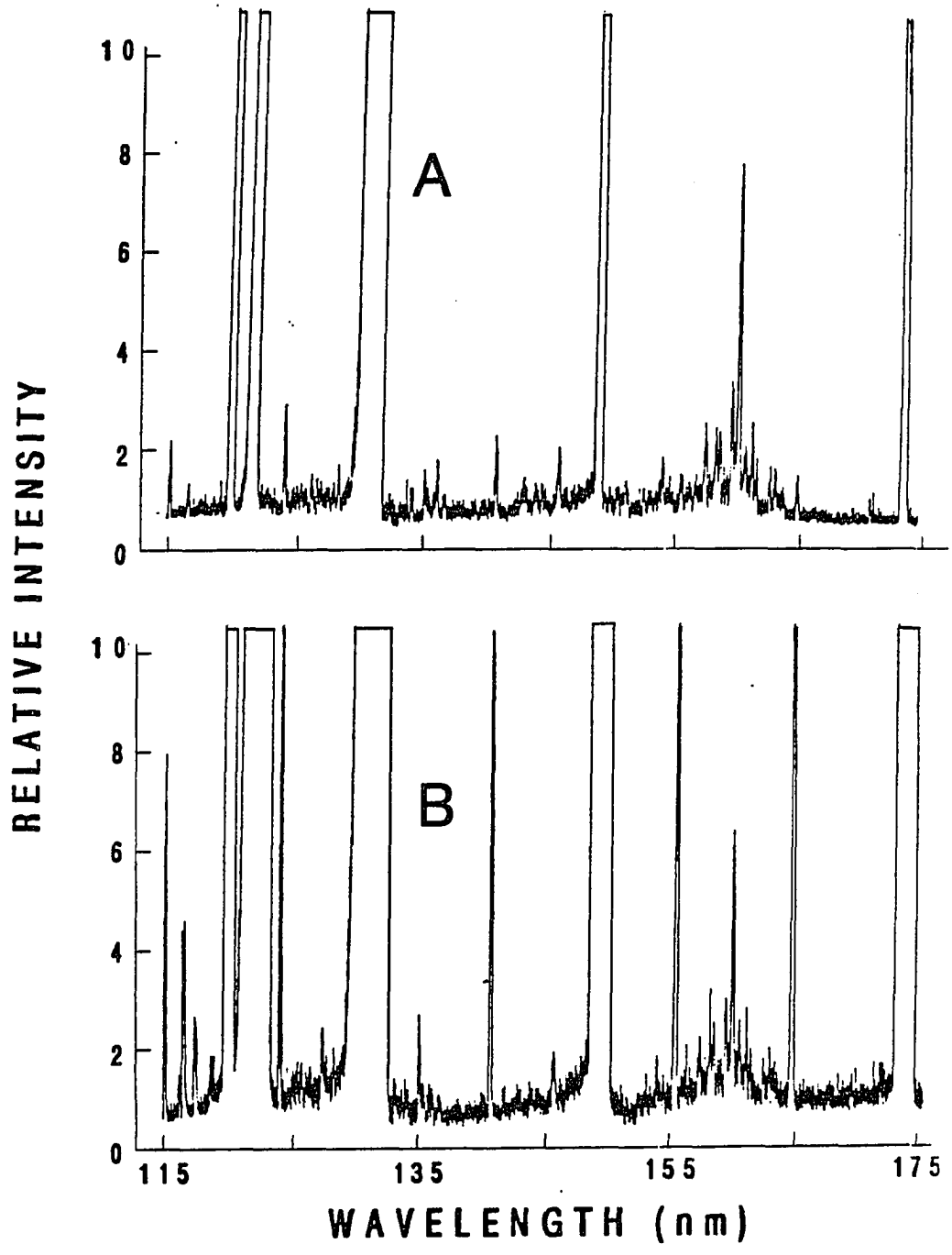

Figure 50. Emission spectra from 115 to 175 nm of the on center view of the ICP through a Mode 1E cone (0.34 mm dia. orifice) at observation heights of
(A) 2 mm and (B) 22 mm above the load coil. Full scale deviation is equivalent to $1X10^{-9}$amps

coil. The enhanced emission showed that most of the intensity of the C, H, N, and O lines occurred near the analytical zone (as shown earlier, the Ar and Zn analyte line emission reached a maximum at around 10 to 12 mm above the load coil). This observation was in sharp contrast to the behavior of the H_2 band system. Assuming that emission from the H_2 band system extended uniformly across the entire cross section of the small field of view of the cone assembly (Figure 12), the magnitude of emission perceived by the monochromator detection system should not change as the distance between the emission and the cone assembly increased. This conclusion was supported by the spectra shown in Figure 49 and was proven in Appendix B with a light source of uniform brightness and sufficient area. Because the emission intensity of the H_2 band system was unchanged as the observation height of the cone assembly increased, very little or no molecular emission originated at sampling heights greater than 2 mm above the load coil in the axial channel of the ICP. Although the cone was unable to probe below the top turn of the load coil, the H_2 emission may have occurred as low as just above the inner tube of the torch.

The low resolution of the monochromator and the uncertainty of the initial state of H_2 has made it difficult to definitely assign the emission lines to specific molecular transitions. The simplification of the molecular band system in an Ar ICP versus a He discharge-afterglow, verification of similar emission from H_2 and H_2O introduction into the plasma, and additional spatial studies indicated that emission from the H_2 band system existed low in the axial channel of the ICP. The interaction of excited Ar atoms by collision or resonant energy transfer with H_2 lends support to the radiation trapping mechanism proposed for analyte excitation within an Ar ICP. This H_2 study shows the first experimental

evidence of a molecule or atom other than Ar being excited within an Ar ICP by resonant energy transfer from excited Ar atoms (i.e., Penning excitation). If energy transfer from Ar atoms can occur to hydrogen molecules, then it would be logical to conclude that excited Ar atoms could transfer energy to analytes that have resonant states as they pass through the axial channel of the ICP.

Spectral Features at Low Wavelengths

An experiment was performed to attempt to observe neon emission (73.59 and 74.37 nm). When Ne flow rates from zero to 0.17 L min^{-1} were bled into the aerosol Ar gas (0.8 L min^{-1}), no significant Ne signal could be detected. The absence of Ne emission indicated that either some Ar atoms in the ICP were being photoionized by neon emission or the Ar ICP did not possessed enough energy to excite Ne atoms. Therefore, it was possible that any radiation emitted from an ICP with wavelengths below 78.6 nm (corresponding to the ionization potential for Ar) was absorbed by Ar within the plasma.

The presence of the H I lines at 91.4 to 92.1, 92.32, 92.62, 93.07, 93.78, 94.97, and 97.25 nm; and the O I lines at 97.17, 97.3, 97.64, 97.80, 98.9, 99.0, 99.95 nm could be seen in Figure 38A, whereas these lines were absent or dramatically reduced in intensity (for the O I lines) with the introduction of dry Ar into the plasma (Figure 38B). The origin of the molecular band system in the 85 to 92 nm region (Figure 38A) could not be determined at this time, but this band system was also observable when N_2 was introduced through the DIP and then into the ICP. Only the Ar I lines in the wavelength regions of 79 to 84 nm and 86 to 89 nm; N I lines at 90.7, 95.2 to 95.4, 96.4, and 96.5; and some weak lines from O I

were present in Figure 38B that obviously resulted from impurities or contaminates in the Ar gas or the plasma environment.

CHAPTER VI. SUMMARY AND CONCLUSIONS

The optical sampling probe has been employed for sampling VUV photons for diagnostic studies (168) and for the detection of the resonance lines of nonmetals, metalloids, and selected metals with pneumatic and ultrasonic nebulization of aqueous solutions (169), and of nonmetals in gaseous samples by the employment of the direct injection probe (DIP) (170). With solar-blind PMT detection, detection limits were 50 ng mL^{-1} for the resonance lines of Br and Cl during injection into the plasma of aerosols of aqueous solutions generated by pneumatic nebulization. With ultrasonic nebulization, the detection limits improved to 8 ng mL^{-1} for Br and 15 ng mL^{-1} for Cl. Detection limits for Br and Cl in the form of an aqueous sample were far superior to the best reported values in the Ar and He ICP, and microwave-induced plasma (MIP)-AES literature. Detection limits for most of the Group IIIB-VIB elements were comparable or superior to the best reported values in the ICP-AES literature. Analytical calibration curves were linear over a range of 3.5 to four orders of magnitude in concentration. Each of the Group IIIB elements (Al, Ga, and In) possessed at least one intense line in the VUV region that yielded better limits of detection than the conventional ultraviolet lines typically observed. Emission signals from Br, Cl, and Al were not strongly affected by high concentrations of Na. The interference induced by Ca on Al emission (and vice versa) in the VUV region was similar under this mode of observation to that described in the literature for observation of the normal UV lines either axially or conventionally (i.e., from the side).

Another significant breakthrough in the present work included the determination of nonmetals in gases by their direct injection into the ICP by a device called a direct injection probe (DIP). This unique interface with low dead volume (<40 μL) was used for introduction of gaseous samples directly into the axial channel of the ICP. Injection of a gaseous mixture of compounds containing the elements Br, Cl, S, and C resulted in detection limits of 0.1, 0.3, 0.05, and 1 ng, respectively. These detection limits were by far the best obtained for these elements in a gaseous form by ICP-AES and are comparable to or an order of magnitude worse than those obtained by AES with He plasmas. Precision of the analyte emission intensities was 1% relative standard deviation or better. The low dead volume interface resulted in low sample dispersion that allowed for fast sampling times and virtually no memory effects without sacrificing signal peak height, even for sample volumes as low as 50 μL. The extension of ICP-AES analysis to the determination of nonmetals, metalloids, and/or selected metals in aqueous and gaseous samples illustrated the value of this optical sampling approach in the VUV.

Because this optical viewing system does not use any lenses, mirrors, or windows with a scintillator-PMT combination detector, VUV radiation can be detected down to 78.7 nm, the wavelength corresponding to the ionization energy of Ar. Therefore, this ICP-VUV-AES system was also applied as a diagnostic tool in the examination of excitation mechanisms in the ICP, especially with the observation of the Ar resonance lines at 104.8 and 106.7 nm. The intensity of Ar I 106.67 nm was studied for various plasma operating parameters and observation positions. The number density for the upper state for this line ($^3P_1$) was estimated to be of the order of 10^{11} cm^{-3} in the axial channel, which was similar in magnitude to

the populations of the nearby metastable Ar levels measured previously. The Ar I line at 104.82 nm was self reversed indicating that Ar resonant radiation can definitely be trapped in the inductively coupled plasma. These results and the observations of the H_2 band system are consistent with the radiation trapping hypothesis but did not quantitatively determine the magnitude of energy transfer from the induction region to the axial channel by this mechanism.

CHAPTER VII. FUTURE PROSPECTS

The potential of the direct optical radiation sampling technique has been demonstrated. This technique is a successful step towards the ultimate goal of the determination of all elements by ICP-AES. Interference effects in complex matrices, impurities contained in the plasma gases, and contamination problems with samples have restricted progress towards an universal detector. The methods employed in this research project demonstrated the utility of using optical probes for the detection of VUV radiation. Dan Wiederin, a graduate student in Dr. Houk's group, will inherit the instrumentation used in this research. Analyses on real-world samples will contribute to the understanding of possible interference effects in the VUV. More experimental diagnostic studies of the Ar resonance lines, H_2 band system, and analyte intensity profiles will assist in the support of existing plasma theories as well as substantiate new excitation mechanisms.

A logical extension of the DIP work would be to develop a similar interface with appropriate heating elements that could be adapted for introduction of capillary gas chromatographic effluents into the ICP for atomic emission detection. Work is being done on the design of heating elements for this interface that will be compatible with the environment within an ICP torch during plasma operation. Employment of the direct injection nebulizer (DIN), which originated at the Ames Laboratory (105-107), with the ICP-VUV-AES system would yield an element-specific liquid chromatographic detector for nonmetals.

When Akbar Montaser comes to Ames this summer for a return visit, either Dan Wiederin and/or I will perform more extensive VUV studies of

the He ICP. Detection limits in the range of 100 to 2000 pg s^{-1} for Br, Cl, and S were achieved in preliminary studies. Unfortunately due to the short time previously devoted to this work, improvements in the system could not be completed during his first visit. Grounding techniques that reduced the pinch from an Ar ICP-MS cone interface might solve the inherent problem of the He ICP discharging to the cone. Also, if the impedance matching network under development by Montaser is operational, it may be possible to ignite our older model plasma (the plasma employed in the present VUV work) with He gas.

Other than the capacity to optically observe VUV radiation, another utility of a cone orifice in the field of atomic emission is the generation of a supplementary electrical discharge by extracting the axial channel of an argon ICP into a small vacuum chamber (171). The discharge enhances the intensities of ion lines by factors of up to 13 relative to intensities observed from the ICP alone. Neutral atom lines from elements with high ionization energies (>= 9 eV) are also enhanced but by less than ion lines; neutral atom lines from easily ionized elements are suppressed by the discharge. These effects are attributed to more efficient atomization, excitation, and ionization in the discharge and to the tendency of analyte species to be constricted or concentrated closer to the central axis of the ICP as they flow into the discharge.

LITERATURE CITED

(1) Windsor, D. L.; Denton, M. B. J. Chromatogr. Sci. 1979 17, 492-496.

(2) Hughes, S. K.; Brown, R. M.; Fry, R. C. Appl. Spectrosc. 1980 34, 338-348.

(3) Northway, S. J.; Fry, R. C. Appl. Spectrosc. 1980 34, 332-338.

(4) Brown, R. M. Jr.; Fry, R. C. Anal. Chem. 1981 53, 532-538.

(5) Fry, R. C.; Northway, S. J.; Brown, R. M.; Hughes, S. K. Anal. Chem. 1980 52, 1716-1722.

(6) Hughes, S. K.; Fry, R. C. Anal. Chem. 1981 53, 1111-1117.

(7) Hughes, S. K.; Fry, R. C. Appl. Spectrosc. 1981 35, 493-497.

(8) Nygaard, D. D.; Schleicher, R. G.; Leighty, D. A. Am. Lab. 1985 17(6), 59-60,62.

(9) Stubley, E. A.; Horlick, G. Appl. Spectrosc. 1984 38, 162-168.

(10) Windsor, D. L.; Denton, M. B. Appl. Spectrosc. 1978 32, 366-371.

(11) Nygaard, D. D.; Chase, D. S.; Leighty, D. A. Res. Dev. 1984 FEB, 172-175.

(12) Winge, R. K.; Peterson, V. J.; Fassel, V. A. Appl. Spectrosc. 1979 33, 206-219.

(13) Irgolic, K. J.; Stockton, R. A.; Chakraborti, D; Beyer, W. Spectrochim. Acta, Part B 1983 38B, 437-445.

(14) Bear, B. Ames Laboratory Quarterly Report, 3/28/78-6/28/78.

(15) Nygaard, D. D.; Leighty, D. A. Appl. Spectrosc. 1985 39, 968-976.

(16) Olson, K. W.; Haas, Jr., W. J.; Fassel, V. A. Anal. Chem. 1977 49, 632-637.

(17) Wohlers, C.; Fassel, V. A.; Bear, B.; Layton, E. Ames Laboratory/U.S. DOE-Iowa State University (Unpublished data).

(18) Kirkbright, G. F.; Ward, A. F.; West, T. S. Anal. Chim. Acta 1972 62, 241-251.

(19) Kirkbright, G. F.; Ward, A. F.; West, T. S. Anal. Chim. Acta 1973 64, 353-362.

(20) Hayakawa, T.; Kikui, F.; Ikeda, S. Spectrochim. Acta, Part B 1982 37B, 1069-1073.

(21) Landsberger, S.; Jervis, R. E.; Balicki, A. Intern. J. Environ. Anal. Chem. 1985 19, 219-225.

(22) Ellebracht, S. (Paper #99 presented at the 1982 Winter Conference on Plasma Spectrochemistry, Orlando, FL).

(23) Uehiro, T.; Morita, M.; Fuwa, K. Anal. Chem. 1985 57, 1709-1713.

(24) Wallace, G. F. At. Spectrosc. 1980 1, 38.

(25) Morita, M.; Uehiro, T.; Fuwa, K. Anal. Chim. Acta 1984 166, 283-288.

(26) Pyen, G. S.; Long, S.; Browner, R. F. Appl. Spectrosc. 1986 40, 246-251.

(27) Dagnall, R. M.; West, T. S.; Whitehead, P. Anal. Chim. Acta 1972 60, 25-35.

(28) Beenakker, C. I. M.; Bosman, B.; Boumans, P. W. J. M. Spectrochim. Acta, Part B 1978 33B, 373-381.

(29) Abdillahi, M. M.; Tschanen, W.; Snook, R. D. Anal. Chim. Acta 1985 172, 139-145.

(30) Bache, C. A.; Lisk, D. J. Anal. Chem. 1967 39, 786-789.

(31) McLean, W. R.; Stanton, D. L.; Penketh, G. E. Analyst 1973 98, 432-442.

(32) Beenakker, C. I. M. Spectrochim. Acta, Part B 1977 32B, 173-187.

(33) Dingjan, H. A.; DeJong, H. J. Spectrochim. Acta, Part B 1983 38B, 777-781.

(34) Bruce, M. L.; Workman, J. M.; Caruso, J. A.; Lahti, D. J. Appl. Spectrosc. 1985 39, 935-942.

(35) Abdillahi, M. M.; Snook, R. D. Analyst 1986 111, 265-267.

(36) Estes, S. A.; Uden, P. C.; Barnes, R. M. Anal. Chem. 1981 53, 1829-1837.

(37) Tanabe, K.; Haraguchi, H.; Fuwa. K. Spectrochim. Acta, Part B 1981 36B, 633-639.

(38) Uden, P. C.; Slatkavitz, K. J.; Barnes, R. M.; Deming, R. L. Anal. Chim. Acta 1986 180, 401-416.

(39) Chiba, K.; Haraguchi, H. Anal. Chem. 1983 55, 1504-1508.

(40) Chiba, K.; Yoshida, K.; Tanabe, K.; Ozaki, M.; Haraguchi, H.; Winefordner, J. D.; Fuwa, K. Anal. Chem. 1982 54, 761-764.

(41) Zerezghi, M.; Mulligan, K. J.; Caruso, J. A. J. Chromatogr. Sci. 1984 22, 348-352.

(42) Goode, S. R.; Chambers, B.; Buddin, N. P. Appl. Spectrosc. 1983 37, 439-443.

(43) Qing-Yu, O.; Guo-Chuen, W.; Ke-Wei, Z.; Wei-Lu, Y. Spectrochim. Acta, Part B 1983 38B, 419-425.

(44) Haas, D. L.; Caruso, J. A. Anal. Chem. 1985 57, 846-851.

(45) Goode, S. R.; Chambers, B.; Buddin, N. P. Spectrochim. Acta, Part B 1985, 40B, 329-333.

(46) Bruce, M. L.; Caruso, J. A. Appl. Spectrosc. 1985 39, 942-949.

(47) Cerbus, C. S.; Gluck, S. J. Spectrochim. Acta, Part B 1983 38B, 387-397.

(48) Jansen, G. W.; Huf, F. A.; DeJong, H. J. Spectrochim. Acta, Part B 1985 40B, 307-316.

(49) Michlewicz, K. G.; Carnahan, J. W. Anal. Chim. Acta 1986 183, 275-280.

(50) Michlewicz, K. G.; Carnahan, J. W. Anal. Chem. 1985 57, 1092-1095.

(51) Michlewicz, K. G.; Carnahan; J. W. Anal. Chem. 1986 58, 3122-3125.

(52) Seliskar, C. J.; Warner, D. K. Appl. Spectrosc. 1985 39, 181-183.

(53) Chan, S.; Montaser, A. Spectrochim. Acta, Part B 1985 40B, 1467-1472.

(54) Chan, S.; Van Hoven, R. L.; Montaser, A. Anal. Chem. 1986 58, 2342-2343.

(55) Rice, G. W.; D'Silva, A. P.; Fassel, V. A. Appl. Spectrosc. 1984 38, 149-154.

(56) Rice, G. W.; D'Silva, A. P.; Fassel, V. A. Anal. Chim. Acta 1984 166, 27-38.

(57) Rice, G. W.; D'Silva, A. P.; Fassel, V. A. Spectrochim. Acta, Part B 1985 40B, 1573-1584.

(58) Ellebracht, S. R.; Fairless, C. M.; Manahan, S. E. Anal. Chem. 1978 50, 1649-1651.

(59) Ellebracht, S. R.; Fairless, C. M. In "Developments in Atomic Plasma Spectrochemical Analysis", Barnes, R. M., Ed., Heyden and Sons Ltd.: Philadelphia, 1981; pp. 392-395.

(60) Ellebracht, S. R.; Swain, P. D. Anal. Chem. 1979 51, 1605-1609.

(61) Ellebracht, S. R.; Swain, P. D.; Treybig, D. S. In "Developments in Atomic Plasma Spectrochemical Analysis", Barnes, R. M., Ed., Heyden and Sons Ltd.: Philadelphia, 1981; pp. 351-360.

(62) Ellebracht, S. R.; Treybig, D. S. Anal. Chem. 1980 52, 1633-1636.

(63) Wendt, R. H.; Fassel, V. A. Anal. Chem. 1965 37, 920-922.

(64) Greenfield, S.; Jones, I. L.; Berry, C. T. Analyst 1964 89, 713-720.

(65) Carnahan, J. W.; Mulligan, K. J.; Caruso, J. A. Anal. Chim. Acta 1981 130, 227-241.

(66) Fassel, V. A. Science 1978 202, 183-191.

(67) Keane, J. M.; Brown, D. C.; Fry, R. C. Anal. Chem. 1985 57, 2526-2533.

(68) Hughes, S. K.; Brown, R. M.; Fry, R. C. Appl. Spectrosc. 1981 35, 396-400.

(69) Keane, J. M.; Fry, R. C. Anal. Chem. 1986 58, 790-797.

(70) Schleisman, A. J. J.; Fateley, W. G.; Fry, R. C. J. Phys. Chem. 1984 88, 398-401.

(71) Schleisman, A. J. J.; Pivonka, D. E.; Fateley, W. G.; Fry, R. C. Appl. Spectrosc. 1986 40, 464-473.

(72) Mautz, K. E.; Parsons, M. L.; Moore, C. B. Appl. Spectrosc. 1987 41, 219-226.

(73) Garton, W. R. S. Adv. Atom. Molec. Phys. 1966 2, 93-176.

(74) Lincke, R. In "Plasma-Diagnostics", Lochte-Holtgreven, W., Ed., North Holland Pub. Co.: Amsterdam, 1968; pp. 375-382.

(75) Kumar, V.; Datta, A. K. Appl. Opt. 1979 18, 1414-1417.

(76) Denton, M. B.; Heine, D. R.; Babis, J. S. Appl. Spectrosc. 1980 34, 595-598.

(77) Carr, J. W.; Blades, M. W. Spectrochim. Acta, Part B 1984 39B, 567-574.

(78) Carnahan, J. W. Am. Lab. 1983 15(8), 31-36.

(79) Beenakker, C. I. M. Spectrochim. Acta, Part B 1976 31B, 483-486.

(80) Bauer, C. F.; Skogerboe, R. K. Spectrochim. Acta, Part B 1983 38B, 1125-1134.

(81) Michlewicz, K. G.; Urh, J. J.; Carnahan, J. W. Spectrochim. Acta, Part B 1985 40B, 493-499.

(82) Tanabe, K.; Haraguchi, H.; Fuwa, K. Spectrochim. Acta, Part B 1981 36B, 119-127.

(83) Freeman, J. E.; Hieftje, G. M. Spectrochim. Acta, Part B 1985 40B, 475-492.

(84) Freeman, J. E.; Hieftje, G. M. Appl. Spectrosc. 1985 39, 211-214.

(85) Pivonka, D. E.; Fateley, W. G.; Fry, R. C. Appl. Spectrosc. 1986 40, 291-297.

(86) Pivonka, D. E.; Schleisman, A. J. J.; Fateley, W. G.; Fry, R. C. Appl. Spectrosc. 1986 40, 766-772.

(87) Hubert, J.; Van Tra, H.; Chi Tran, K.; Baudais, F. L. Appl. Spectrosc. 1986 40, 759-766.

(88) Wolnik, K. A.; Miller, D. C.; Seliskar, C. J.; Fricke, F. L. Appl. Spectrosc. 1985 39, 930-934.

(89) Carr, J. W.; Blades, M. W. Spectrochim. Acta, Part B 1984 39B, 667-675.

(90) Houk, R. S.; Fassel, V. A.; Flesch, G. D.; Svec, H. J.; Gray, A. L.; Taylor, C. E. Anal. Chem. 1980 52, 2283-2289.

(91) Douglas, D. J.; Houk, R. S. Prog. Anal. Atomic Spectrosc. (In press).

(92) Gray, A. L.; Date, A. R. Analyst 1983 108, 1033.

(93) Muller, D.; Vadla, C.; Vujnovic, V. Space Sci. Rev. 1972 13, 563-564.

(94) Rogoff, G. L. Appl. Opt. 1985 24, 1733-1735.

(95) Apel, C. T.; Duchane, D. V.; Palmer, B. A.; Bieniewski, T. M.; Pena, H. V.; Cox, L. E.; Gallimore, D. L.; Vincent, K.; Lopez, M.; Kline, J. V.; Steinhaus, D. W. In "Developments in Atomic Plasma Spectrochemical Analysis", Barnes, R. M., Ed., Heyden and Sons Ltd.: Philadelphia, 1981; pp. 383-391.

(96) Apel, C. T.; Faires, L. M.; Bieniewski, T. M.; Lopez, M. F.; Niemczyk, T. M. (Paper #150 presented at the 1982 Pittsburgh Conference, Altantic City, NJ).

(97) Scott, R. H.; Fassel, V. A.; Kniseley, R. N.; Nixon, D. E. Anal. Chem. 1974 46, 75-80.

(98) Fassel, V. A.; Bear, B. R. Spectrochim. Acta, Part B 1986 41B, 1089-1113.

(99) Kniseley, R. N.; Amenson, H.; Butler, C. C.; Fassel, V. A. Appl. Spectrosc. 1974 28, 285-286.

(100) Literature from Acton Research Corporation, Acton, MA; Product 210 Data Sheet.

(101) LaFreniere, B. R. Ames Laboratory Quarterly Report, 11/17/83-5/17/84.

(102) Strong, J. "Concepts of Classical Optics", W. H. Freeman and Company, San Francisco, 1958.

(103) Jenkins, F. A.; White, H. E. "Fundamentals of Optics", 2nd ed., McGraw-Hill Book Co., Inc.: New York, 1950.

(104) Sawyer, R. A. "Experimental Spectroscopy", 3rd ed., Dover Publications, Inc.: New York, 1963.

(105) Lawrence, K. E.; Rice, G. W.; Fassel, V. A. Anal. Chem. 1984 56, 289-292.

(106) LaFreniere, K. E.; Rice, G. W.; Fassel, V. A. Spectrochim. Acta, Part B 1985 40B, 1495-1504.

(107) LaFreniere, K. E.; Fassel, V. A.; Eckels, D. E. Anal. Chem. 1987 59, 879-887.

(108) Miller, D. C.; Seliskar, C. J. Appl. Spectrosc. 1986 40, 566-567.

(109) Literature from EMI GENCOM Inc., Plainview, NY; Ultraviolet and solar-blind photomultipliers.

(110) Literature from Houston Instruments, Austin, TX; Series 200 XY recorders.

(111) Nester, P. Spectrum Corporation, Newark, DE; personal discussion.

(112) McAdam, W.; Van Deventer, D. ISA J. 1960 7(4), 48-52.

(113) Sitter, R. P. Instrum. Technol. 1978 25, 59-65.

(114) ISSAC Chromatext Reference Library by Cyborg Corporation, Newton, MA.

(115) Demers, D. R. Appl. Spectrosc. 1979 33, 584-591.

(116) Samson, J. A. R. "Techniques of Vacuum Ultraviolet Spectroscopy", John Wiley and Sons Inc.: New York, 1967.

(117) Herzberg, G.; Howe, L. L. Can. J. Phys. 1959 37, 636-659.

(118) Takezawa, S.; Innes, F. R.; Tanaka, Y. J. Chem. Phys. 1966 45, 2000-2010.

(119) Kelly, R. L. "A Table of Emission Lines in the Vacuum Ultraviolet for All Elements" (University of California Lawrence Radiation Laboratory Report 5612) 1959.

(120) Kelly, R. L.; Palumbo, L. J. "Atomic and Ionic Emission Lines Below 2000 Angstroms: Hydrogen through Krypton" U. S. Government Printing Office: Washington, D.C., 1973; Naval Research Laboratory Report 7599.

(121) Wohlers, C. C. ICP Inf. Newsl. 1985 10, 593-688.

(122) Uehiro, T.; Morita, M.; Fuwa, K. Anal. Chem. 1984 56, 2020-2024.

(123) FIAtron Systems, Inc., Oconomococ, WI; SHS-300 Automated ICP/DCP Solution Handling System brochure.

(124) Blades, M. W.; Horlick, G. Spectrochim. Acta, Part B 1981 36B, 881-900.

(125) Larson, G. F.; Fassel, V. A.; Scott, R. H.; Kniseley, R. N. Anal. Chem. 1975 47, 238-243.

(126) Olivares, J. A.; Houk, R. S. Anal. Chem. 1986 58, 20-25.

(127) Beauchemin, D.; McLaren, J. W.; Berman, S. S. Spectrochim. Acta, Part B 1987 42B, (Accepted).

(128) Gregoire, D. C. Appl. Spectrosc. 1987 41, (Accepted).

(129) Crain, J. S.; Houk, R. S. (In preparation).

(130) Houk, R. S.; Lim, H. B. Anal. Chem. 1986 58, 3244-3248.

(131) Headrick, L. B.; Fox, G. W. Phys. Rev. 1930 35, 1033-1037.

(132) LaFreniere, B. R. Ames Laboratory Quarterly Report, 11/17/84-2/17/85.

(133) D' Silva, A. P.; LaFreniere, K. E.; LaFreniere, B. R.; Weidner, J.; Fassel, V. A. Ames Laboratory/U.S. DOE-Iowa State University (In preparation).

(134) Alder, J. F.; Bombelka, R. M.; Kirkbright, G. F. Spectrochim. Acta, Part B 1980 35B, 163-175.

(135) Blades, M. W.; Hieftje, G. M. Spectrochim. Acta, Part B 1982 37B, 191-197.

(136) Blades, M. W. Spectrochim. Acta, Part B 1982 37B, 869-879.

(137) Mills, J. W.; Hieftje, G. M. Spectrochim. Acta, Part B 1984 39B, 859-866.

(138) Miller, M. H.; Eastwood, D.; Hendrick, M. S. Spectrochim. Acta, Part B 1984 39B, 13-56.

(139) Moore, C. E. "Atomic Energy Levels," NBS Circular 467, (U. S. Government Printing Office, Washington, DC, 1949), Vol. 1, p. 211.

(140) Lyman, T.; Saunders, F. A. Nature 1925 116, 358.

(141) Saunders, F. A. Proc. Nat. Acad. Sci. 1926 12, 556-560.

(142) Hertz, G. Naturwissenschaften 1926 14, 648.

(143) Boyce, J. C. Phys. Rev. 1935 48, 396-402.

(144) Uchida, H.; Tanabe, K.; Nojiri, Y.; Haraguchi, H.; Fuwa, K. Spectrochim. Acta, Part B 1980 35B, 881-883.

(145) Hieftje, G. M.; Carr, J. W. Am. Lab. 1983 15(5), 66-74.

(146) Uchida, H.; Tanabe, K.; Nojiri, Y.; Haraguchi, H.; Fuwa, K. Spectrochim. Acta, Part B 1981 36B, 711-718.

(147) Nojiri, Y.; Tanabe, K.; Uchida, H.; Haraguchi, H.; Fuwa, K.; Winefordner, J. D. Spectrochim. Acta, Part B 1983 38B, 61-74.

(148) Kalnicky, D. J.; Fassel, V. A.; Kniseley, R. N. Appl. Spectrosc. 1977 31, 137-150.

(149) Kornblum, G. R.; de Galan, L. Spectrochim. Acta, Part B 1977 32B, 71-96.

(150) Gunter, W. H.; Visser, K.; Zeeman, P. B. Spectrochim. Acta, Part B 1983 38B, 949-958.

(151) Blades, M. W. Appl. Spectrosc. 1983 37, 371-375.

(152) Furuta N.; Horlick, G. Spectrochim. Acta, Part B 1982 37B, 53-64.

(153) Houk R. S.; Olivares, J. A. Spectrochim. Acta, Part B 1984 39B, 575-587.

(154) Wiese, W. L.; Smith, M. W.; Miles, B. M. "Atomic Transition Probabilities," NSRDS-NBS 22, U. S. Government Printing Office: Washington, DC, 1969; Vol. 2, p. 192.

(155) Drawin, H. W.; Felenbok, P. "Data for Plasmas in Local Thermodynamic Equilibrium," Gauthier-Villars: Paris, 1965.

(156) Mermet, J. M.; Trassy, C. Rev. Phys. Appl. 1977 12, 1219.

(157) Ng, C. Y. "Molecular Beam Photoionization Studies of Molecules and Clusters," In "Advances in Chemical Physics", Prigogine, I. and Rice, S. A., Eds., Wiley: New York, 1983; Vol. 52, p. 263.

(158) Tanaka, Y.; Jursa, A. S.; LeBlanc, F. J. J. Opt. Soc. Am. 1958 48, 304-308.

(159) Wilkinson, P. G. Can. J. Phys. 1967 45, 1715-1727.

(160) Huffman, R. E.; Larrabee, J. C.; Tanaka, Y. Appl. Opt. 1965 4, 1581-1588.

(161) Richardson, O. W. "Molecular Hydrogen and Its Spectrum", Yale Univ. Press: London, 1934; Chapter IV.

(162) Zaidel, A. N.; Shreider, E. Ya "Vacuum Ultraviolet Spectroscopy", Translated by Z. Lerman, Ann Arbor-Humphrey Science Publishers: Ann Arbor, MI, 1970.

(163) Dieke, G. H.; Hopfield, J. J. Phys. Rev. 1927 30, 400-417.

(164) Fink, E. H.; Wallach, D.; Moore, C. B. J. Chem. Phys. 1972 56, 3608-3618.

(165) Takezawa, S.; Innes, F. R.; Tanaka, Y. J. Chem. Phys. 1967 46, 4555-4561.

(166) Wood, R. Phil. Mag. 1921 42, 729-745.

(167) Bredohl, H.; Herzberg, G. Can. J. Phys. 1973 51, 867-887.

(168) Houk, R. S.; Fassel, V. A.; LaFreniere, B. R. Appl. Spectrosc. 1986 40, 94-100.

(169) LaFreniere, B. R.; Houk, R. S.; Fassel, V. A. Anal. Chem. 1987 59, (Accepted).

(170) LaFreniere, B. R.; Houk, R. S.; Fassel, V. A. Ames Laboratory/U.S. DOE-Iowa State University (In preparation).

(171) Houk, R. S.; LaFreniere, B. R.; Lim, H. B.; Fassel, V. A. Appl. Spectrosc. 1987 41, 391-395.

(172) Harrison, G. R.; Lord, R. C.; Loofbourow, J. R. "Practical Spectroscopy", Prentice-Hall Inc.: New York, 1948; pp. 92-93.

(173) Nielsen, J. R. J. Opt. Soc. Am. 1930 20, 701-718.

(174) Eckels, D. Ames Laboratory/U.S. DOE-Iowa State University.

ACKNOWLEDGEMENTS

I would like to gratefully acknowledge the helpful support, guidance, and encouragement extended by Dr. Velmer A. Fassel and Dr. R. Sam Houk during the course of this study. Their critical review of my work is greatly appreciated.

I would like to thank: Barry, Bill, Bob, Brian, Bruce, Carmen, Clark, Dan, Dave, Dean, Deanna, Deb, Denny, Dick, Doug, Ed, Erik, Gary, Glenn, Harry, Ivy, Jack, Jackie, Jean, Jim, Joe, Joel, John, "Johnnnnny", Kim, Lance, Larry, Laura, Linda, Marc, Margo, Marilyn, Mark, Martha, Martin, Marty, Mary, Mike, Moi, Nancy, Pete, Rob, Ross, Roy, Royce, Sam, Sheryl, Stephan, Steve, Tammy, Tim, Tina, Tom, Tonya, Wayne, and all others that I regretfully missed and/or intentionally left out for their help and the wonderful memories during my years at Iowa State University, which I'll always cherish. Also, I would like to acknowledge the many other people at the Ames Laboratory and Iowa State University that contributed towards my research, compilation of my dissertation, and friendship during the course of my study.

My financial support throughout graduate school by the Ames Laboratory/DOE and the Standard Oil of Ohio Graduate Fellowship has been greatly appreciated.

I would like to express my appreciation to my parents, Robert and Lorraine LaFreniere, for their support and encouragement throughout my entire "career" as a student, even through they still ask me, "Now, what area of chemistry are you studying?" and "What is analytical chemistry?".

Finally, I could never express the importance of my wife, Kimberly LaFreniere, through this laborious interval in my life. Her support,

friendship, love, and cooking have helped sustain my emotional and physical self throughout graduate school. Although graduate school is a rough time for marriages, our marriage has grown stronger. I hope that I can appreciate her talents and friendship even more after graduate school. Thank you.

APPENDIX A. COMPILATION OF ACRONYMS AND ABBREVIATIONS

AES	atomic emission spectrometry
APAG	atmospheric pressure afterglow
APAN	atmospheric pressure active nitrogen
cm	centimeter
conc.	concentration
DCP	direct current plasma
DIN	direct injection nebulizer
DIP	direct injection probe
DOE	Department of Energy
FIA	flow injection analysis
FID	flame ionization detector
FTS	Fourier transform spectroscopy
GC	gas chromatography
HPLC	high performance liquid chromatography
Hz	hertz
ICP	inductively coupled plasma
ICP-AES	inductively coupled plasma-atomic emission spectrometry
ICP-MS	inductively coupled plasma-mass spectrometry
IR	infrared
kW	kilowatt
L	liter
LOD	limit of detection
MED	microwave-excited emissive detector
MHz	megahertz
min	minute

MIP	microwave induced plasma
mL	milliliter
mm	millimeter
MS	mass spectroscopy
ng	nanogram
NIR	near infrared
nm	nanometer
pg	picogram
ppb	part per billion
ppm	part per million
PMT	photomultiplier tube
RF	radio-frequency
RFI	radio-frequency interference
RPM	revolutions per minute
s	second
TLC	thin layer chromatography
USN	ultrasonic nebulizer
UV	ultraviolet
VIS	visible
VUV	vacuum ultraviolet
W	watt
μg	microgram
μL	microliter
μm	micrometer (micron)

APPENDIX B. ILLUMINATION OF A GRATING THROUGH AN ENTRANCE SLIT

Purpose of Exercise

If a plasma-VUV monochromator system without any condensing lenses is considered, then there are two strategies for maximum illumination of the grating. First, the distance between the plasma and the entrance slit should be decreased so that the solid angle for collection of emission from the plasma by the grating is increased. Second, the field of view of the monochromator should be defined by the construction of an optical ray diagram of the plasma-monochromator system so that the physical dimensions of an ICP-VUV interface can be determined. A number of modes of illuminating optical spectrometers with such a sampling probe can readily be visualized.

General Theory

An optical ray diagram of the specific monochromator system used was drawn to determine the field of view of the monochromator. Figure B-1 illustrates the illumination of a grating through a rectangular slit of relatively narrow width (172). Light diffraction by the slit is assumed to be negligible. In Figure B-1, vertical planes A and A′ are defined by the slit edges and the ruled width of the grating. In Figure B-1, planes C and C′ are defined, respectively, by the bottom of the slit edge and the ruled height of the grating and by the top of the slit and the ruled height of the grating. Planes B and B′ are defined, respectfully, by the top of the slit edge and the bottom of the ruled height of the grating and by the bottom of the slit edge and top of the rule height of the grating. The volume bounded by vertical planes A and A′ and planes B and B′ will be abbreviated as the volume element AA′-BB′ and similar abbreviations for

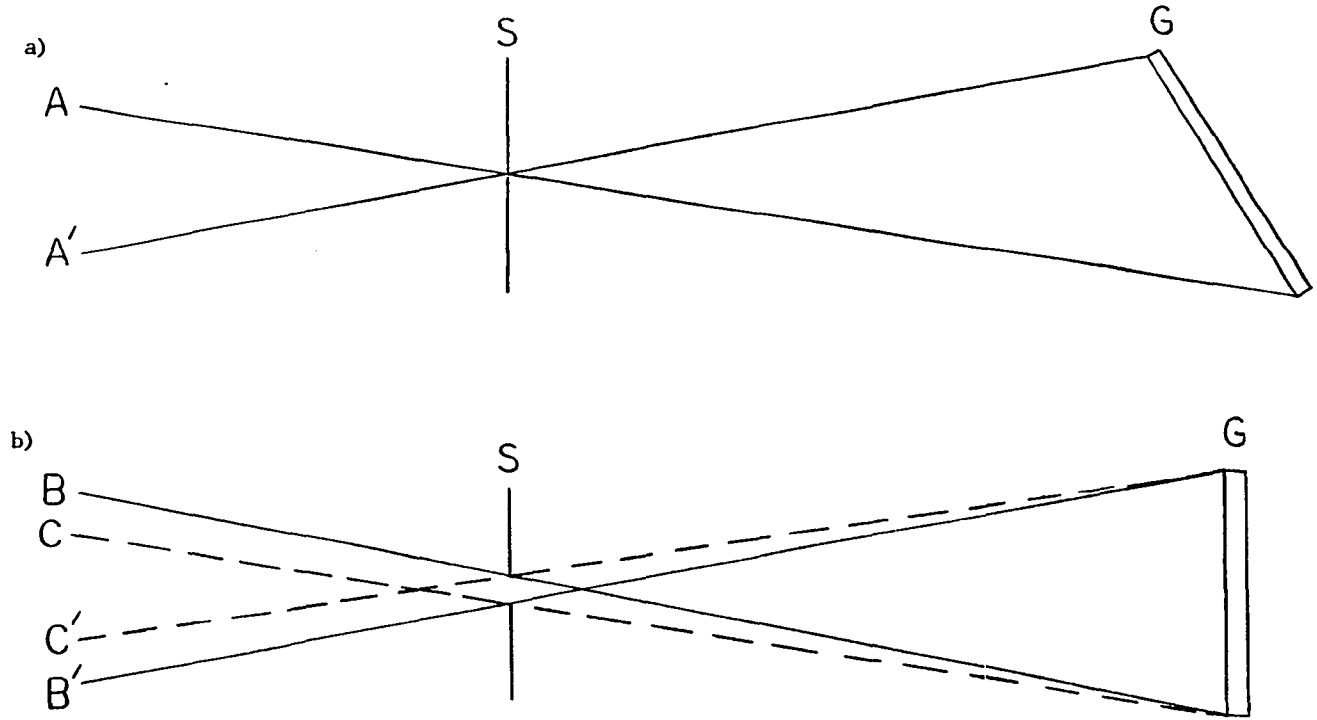

Figure B-1. Illumination of a grating through a rectangular slit
(a) top view, and (b) side view;
S, slit; G, grating; A,A′,B,B′,C,C′, boundaries of the field of view

other volume elements will be used. Radiation that originates within the volume element AA'-CC' and passes through the entrance slit does illuminate the grating. Radiation that passes through the entrance slit and originates within the volume element AA'-BB', and not within the previously mentioned volume element AA'-CC', does not necessarily illuminate the grating. In this vignetted region (AA'-BB' minus AA'-CC'), radiation can either hit or miss the grating dependent upon the angle of entry into the slit and the location of the original source. Radiation originating outside the volume element AA'-BB' will not illuminate the grating and may cause scattered light effects in the monochromator. In essence, the volume bounded by planes AA' and BB' represents the viewing field of the monochromator.

Let us assume a light source of uniform brightness and sufficient area (not a point source). Figure B-1 can be used to determine the maximum illumination of the grating with this light source in a specified monochromator arrangement without any condensing lenses. For maximum illumination, the light source can be placed in any vertical plane parallel to the entrance slit as long as the area of the light source extends across an entire cross section of the volume element AA'-BB' (104). If the light source fulfills the above condition, the distance between the source and the slit is not related to the degree of illumination and illumination of the grating can not be enhanced by the use of a condensing lens. If the light has an area that is smaller than the cross section defined by planes AA'-BB', then as the light source approaches the slit, the solid angle from the light source to the slit increases. For the conditions discussed above, the use of a condensing lens can be beneficial to increase illumination of the grating. The

mathematical rigor required to prove the statements made in this paragraph can be found in Nielsen (173).

Figures that illustrate the fields of view of the three modes of analysis for our ICP-VUV-AES system are presented in Chapter II. Vertical planes A and A′ and planes B and B′ constitute the boundaries of these fields of view.

APPENDIX C. COMPUTER PROGRAMS

Optical Field of View of the Monochromator

Computer programs; named ADVFOV.BAS, FVADD1.BAS, FVADD2.BAS, and FVADD3.BAS and listed in Table C-I, were written in BASIC-11/RT-11 language for the calculation of the field of view of a given cone and monochromator assembly. The assumptions for these programs were as follows. The distance from the grating to the entrance slit, the dimensions of the grating, the maximum height of the entrance slit, the diameter of the quartz torch, and the distances from the top of the load coil and base of the plasma to the top of the torch have been assigned their values in the beginning of the main program, ADVFOV.BAS. These values could only be changed if their corresponding variables were assigned new values within the main program, ADVFOV.BAS. The width of the entrance slit was assumed to be negligible and light diffraction was not taken into account. The masks, plasma, and orifice were assumed to be positioned symmetrically with respect to the optical path.

The variable parameters during the execution of the program were as follows: (a) dimensions of the cone orifice, mask, and a second mask; (b) the distances from the entrance slit to the cone orifice, mask, and a second mask; (c) the distance from the cone orifice to the top of the torch; and (d) the observation height above the load coil in which a field of view was requested. Once these parameters were chosen with program, ADVFOV.BAS, the top and side fields of view were calculated with programs, ADVFOV.BAS and FVADD1.BAS, respectively. The top and side fields of view of the cone and monochromator assembly at the planes of the base of the plasma, top of the load coil, cone orifice, mask, second mask, grating,

Table C-I. BASIC computer programs; named ADVFOV.BAS, FVADD1.BAS, FVADD2.BAS, and FVADD3.BAS; used for the calculation of the field of view of a given cone and monochromator assembly

FILENAME: ADVFOV.BAS PAGE 001

```
10 REM WRITTEN BY BRYANT LAFRENIERE ,BEGINNING 2/26/85 ,FINISHED 7/17/85
20 REM THIS PROGRAM WILL ACCEPT VARIOUS PARAMETERS THAT DESCRIBE AN ICP-VUV-AES
30 REM APPARATUS, AND WILL CALCULATE
40 REM THE FIELD OF VIEW INTO A PLASMA FROM THE MONOCHROMATOR.
50 REM THE FOLLOWING STATEMENTS WILL BE HELPFUL FOR MANIPULATION OF THE FIXED
60 REM PARAMETERS IN THE PROGRAM.
70 REM
80 REM
90 REM ALL MEASUREMENTS ARE IN MM.
100 REM FIXED PARAMETERS THAT CAN BE CHANGED ONLY WITHIN THIS PROGRAM
110 REM
120 REM CHANGE DISTANCE FROM GRATING TO ENTRANCE SLIT-G1-AT LINE 240
130 REM CHANGE EFFECTIVE DIMENSIONS OF GRATING-W1,H1-AT LINE 250
140 REM CHANGE DISTANCE FROM TOP OF THE TORCH TO THE TOP OF THE LOAD COIL(T1)
150 REM AT LINE 260
160 REM CHANGE DISTANCE FROM THE TOP OF THE TORCH TO THE BASE OF THE PLASMA(T2)
170 REM -TOP OF THE INNER TORCH-AT LINE 270
180 REM CHANGE THE MAXIMUM HEIGHT OF THE ENTRANCE SLIT-S1-AT LINE 280
190 REM CHANGE THE QUARTZ TORCH DIAMETER-D1-AT LINE 340
200 REM A8=DISTANCE FROM THE ENTRANCE SLIT TO THE TOP OF THE TORCH
210 DIM N$(2),M$(2),P$(2),Q$(2),M(2),F(2)
220 DIM G(2),V1(2),V2(2),V3(2),V4(2),V5(2)
230 DIM K(2),V6(2),V7(2),V8(2),H1(2)
240 G1=-200
250 W1=35 \ H1=35
260 T1=12
270 T2=31
280 S1=25
290 A1=1 \ A2=1 \ A3=1 \ A4=100
300 A5=100 \ A6=5.20000E-03 \ A7=1
310 C1=1 \ C2=1 \ C3=1.202 \ E$="N"
320 D$="N" \ X=1
330 R$="N" \ Z=0
340 D1=20
350 DEF FNA(F1,F2,F3)=ABS(F1)*F2/ABS(F3)
360 DEF FNB(F4,F5,F6,F7)=F4+SGN(F5-F4)*ABS(F4-F5)/(F7/F6+1)
370 DEF FNC(F4,F5,F6,F7,F8)=ABS(F8-FNB(F4,F5,F6,F7))*F6/ABS(FNB(F4,F5,F6,F7)-F4)
380 DEF FND(E1,E2)=(E1-G1)/((E2/H1)+1)+G1
390 DEF FNE(E1,E2,E3)=ABS(E3-FND(E1,E2))*H1/(FND(E1,E2)-G1)
400 DEF FNF(F4,F6,Z8,F8)=ABS(F8-Z8)*F6/ABS(Z8-F4)
410 DEF FNG(F4)=X6*(F4-Z6)/(Z6-X4)
420 DEF FNH(F4)=H1*(F4-Z6)/(Z6-G1)
430 DEF FNX(F9)=(W+Z6+F9*((D-Z6)/9))*R
440 DEF FNY(F9)=(Y+F9*((B4/2)/9))*R
500 PRINT  \ PRINT  \ PRINT "PARAMETERS FOR THE ICP-VUV FIELD OF VIEW ";
510 PRINT "CALCULATIONS."
520 PRINT  \ PRINT "ALL PARAMETERS SHOULD BE INPUTTED IN MM."
530 PRINT  \ PRINT "THE FOLLOWING PARAMETERS CAN ONLY BE CHANGED WITHIN THE ";
540 PRINT "PROGRAM."
550 PRINT "ASSUMED:"
560 PRINT "     A)DISTANCE FROM GRATING TO ENTRANCE SLIT= ";G1;" MM."
570 PRINT "     B)EFFECTIVE AREA OF THE GRATING= ";W1;" MM WIDE AND ";H1;
580 PRINT " MM HIGH."
590 PRINT "     C)ENTRANCE SLIT WIDTH IS NEGLIGIBLE."
600 PRINT "     D)DISTANCE FROM THE TOP OF THE TORCH TO THE TOP OF THE LOAD"
610 PRINT "       COIL= ";T1;" MM AND THE TOP OF THE TORCH TO THE BASE OF"
620 PRINT "       THE PLASMA= ";T2;" MM."
```

Table C-I. (Continued)

```
FILENAME:   ADVFOV.BAS                                    PAGE  2

630 PRINT "     E)QUARTZ TORCH DIAMETER= ";D1;" MM."
640 PRINT "     F)THE MASK,PLASMA,AND ORIFICE ARE POSITIONED SYMMETRICALLY"
650 PRINT "       WITH RESPECT TO THE OPTICAL PATH."
655 PRINT "     G)LIGHT DIFFRACTION IS NEGLECTED."
660 PRINT  \ PRINT "AFTER READING THE ABOVE INFORMATION, TYPE A LETTER";
670 PRINT " THEN A CARRIAGE RETURN TO SEE TABLE OF CHANGEABLE PARAMETERS."
680 INPUT I$
690 PRINT  \ PRINT  \ PRINT "INPUT ALL PARAMETER VALUES IN MM."
700 PRINT "  1)HEIGHT OF THE ORIFICE? ";A1
710 PRINT "  2)WIDTH OF THE ORIFICE? ";A2
720 PRINT "  3)DISTANCE FROM THE ENTRANCE SLIT TO THE ORIFICE? ";A3
730 PRINT "  4)MASK USED(Y/N)? ";R$
740 IF R$="N" THEN 780
750 PRINT "    HEIGHT OF THE MASK? ";A4
760 PRINT "    WIDTH OF THE MASK? ";A5
770 PRINT "    DISTANCE FROM THE ENTRANCE SLIT TO THE MASK? ";A6
780 PRINT "  5)A 2ND MASK USED(Y/N)? ";E$
790 IF E$="N" THEN 830
800 PRINT "    HEIGHT OF THE 2ND MASK? ";C1
810 PRINT "    WIDTH OF THE 2ND MASK? ";C2
820 PRINT "    DISTANCE FROM THE ENTRANCE SLIT TO THE 2ND MASK? ";C3
830 PRINT "  6)DISTANCE FROM THE ORIFICE TO THE TOP OF THE TORCH? ";A7
840 PRINT "  7)DO YOU WISH TO CALCULATE A FIELD OF VIEW FOR A CERTAIN"
850 PRINT "    OBSERVATION HEIGHT ABOVE THE LOAD COIL(Y/N)? ";D$
860 PRINT "     HEIGHT ABOVE LOAD COIL? ";X
870 PRINT "  8)FIELD OF VIEW WILL BE CALCULATED.(NOTE: MAKE SURE THAT THE";
880 PRINT "    7 PARAMETER VALUES ABOVE ARE CORRECT.)"
890 PRINT "  9)LIST OF THE PARAMETERS WILL BE REPRINTED."
900 PRINT  \ PRINT "SELECT ONE (1-9,9=REPRINT LIST):";
910 INPUT S2
920 ON S2 GO TO 15000,15040,15080,15130,15300,15460,15510,1000,690
1000 PRINT
1010 PRINT "DO YOU WANT TO STORE THE FIELD OF VIEW DATA INTO A FILE(Y/N)";
1020 INPUT C$
1030 P1=0 \ IF C$="N" THEN 1110
1040 PRINT "TYPE THE FILENAME THAT THE FIELD OF VIEW DATA WILL BE STORED IN."
1050 PRINT "(TYPE NAME.DAT WITH NAME HAVING NO MORE THAN 6 LETTERS.)"
1060 LINPUT B$
1070 PRINT "TYPE A FILE #(1-9).";
1080 INPUT P1
1090 IF P1<1 THEN 1070
1100 IF P1>9 THEN 1070
1110 GOSUB 20090
1120 IF Z=3 THEN OVERLAY "FVADD2" LINE 3000
1500 REM CALCULATIONS OF THE FIELDS OF VIEW
1510 A8=A3+A7
1520 REM THIS SECTION INVOLVES THE CALCULATION OF THE TOP FIELD OF VIEW.
1530 REM FNA IS A FUNCTION THAT USES SIMILIAR TRIANGLES TO CALCULATE THE
1540 REM FIELD OF VIEW AT LOCATION F1 THAT IS DEPENDENT UPON THE ENTRANCE
1550 REM SLIT AND F3
1560 H$="CONE ORIFICE"
1570 IF A3=0 THEN 1660
1580 H$="ENTRANCE SLIT"
1590 IF FNA(A6,A2,A3))A5 THEN 1660
1600 IF FNA(G1,A2,A3))W1 THEN 1720
1610 IF E$="N" THEN 1630
1620 IF FNA(C3,A2,A3))C2 THEN 1770
```

Table C-I. (Continued)

```
FILENAME:   ADVFOV.BAS                                    PAGE   3


1630 G$="CONE ORIFICE"
1640 T8=A2 \ T9=A3
1650 GO TO 1790
1660 IF FNA(G1,A5,A6))W1 THEN 1720
1670 IF E$="N" THEN 1690
1680 IF FNA(C3,A5,A6))C2 THEN 1770
1690 G$="MASK"
1700 T8=A5 \ T9=A6
1710 GO TO 1790
1720 IF E$="N" THEN 1740
1730 IF FNA(C3,W1,G1))C2 THEN 1770
1740 G$="GRATING"
1750 T8=W1 \ T9=G1
1760 GO TO 1790
1770 G$="2ND MASK"
1780 T8=C2 \ T9=C3
1790 B5=FNA(A8+T2,T8,T9) \ L5=FNA(A8+T1,T8,T9) \ R5=FNA(A3,T8,T9)
1800 M5=FNA(A6,T8,T9) \ G5=FNA(G1,T8,T9) \ S5=FNA(C3,T8,T9)
1810 E5=FNA(A8+T1-X,T8,T9) \ P5=FNA(-85,T8,T9)
1820 OVERLAY "FVADD1" LINE 3000
1830 REM
1840 REM
7980 REM
7990 REM
8000 PRINT  \ PRINT "SELECT     1-SEE PARAMETERS"
8010 PRINT TAB(11);"2-SEE PARAMETERS AND INTRODUCTORY INFORMATION"
8020 PRINT TAB(11);"3-REPRINT FIELD OF VIEW DATA"
8025 PRINT TAB(11);"4-STORE FIELD OF VIEW DATA FOR PLOTTING"
8030 PRINT TAB(11);"5-END PROGRAM"
8040 INPUT Z
8045 IF Z<1 THEN 8000
8046 IF Z>5 THEN 8000
8050 ON Z GO TO 690,500,1000,8500,30000
8500 PRINT
8510 PRINT "DO YOU WANT TO STORE THE FIELD OF VIEW DATA INTO A FILE FOR"
8515 PRINT "PLOTTING RAY DIAGRAMS(Y/N)";
8520 INPUT I$
8530 PRINT  \ IF I$="N" THEN 8000
8550 PRINT "TYPE THE FILENAME THAT THE FIELD OF VIEW DATA (FOR PLOTTING)"
8555 PRINT "WILL BE STORED INTO."
8560 PRINT "(TYPE  NAME.FOV  WITH NAME HAVING NO MORE THAN 6 LETTERS.)"
8570 LINPUT T$
8580 PRINT  \ PRINT "TYPE A FILE #(1-9).";
8590 INPUT P
8600 PRINT  \ PRINT "DO YOU WANT THE INNER BOUNDARY(IF ANY) OF THE VIGNETTED";
8601 PRINT " REGION"
8610 PRINT "PLOTTED ON YOUR RAY DIAGRAMS(Y/N)";
8620 INPUT S$
8630 PRINT  \ PRINT "DO YOU WANT THE CONDITIONS (DISTANCES AND DIMENSIONS OF"
8640 PRINT "THE CONE ASSEMBLY,ETC.) OF THE FIELD OF VIEW WRITTEN ON YOUR"
8645 PRINT "RAY DIAGRAM(Y/N)";
8650 INPUT L$
8660 PRINT  \ PRINT "DO YOU WANT TO OFFCENTER THE PLASMA(CENTER OF THE AXIAL"
8661 PRINT "CHANNEL) FROM THE CONE ORIFICE,I.E. OPTICAL PATH(Y/N)";
8690 INPUT A$
8695 M1(1)=0 \ M1(2)=0
8780 IF A$="N" THEN 8760
```

Table C-I. (Continued)

```
FILENAME:   ADVFOV.BAS                                    PAGE   4

8710 PRINT "TYPE THE NUMBER OF MILLIMETERS THAT THE PLASMA IS OFFCENTERED.";
8720 INPUT M1(1)
8760 GOSUB 20090
8762 OVERLAY "FVADD3" LINE 3000
8763 REM
8764 REM
15000 PRINT  \ GOSUB 20000 \ PRINT "WHAT IS THE HEIGHT OF THE ORIFICE";
15010 INPUT A1
15020 IF A1<=0 THEN 15000
15030 GO TO 900
15040 PRINT  \ GOSUB 20000 \ PRINT "WHAT IS THE WIDTH OF THE ORIFICE";
15050 INPUT A2
15060 IF A2<=0 THEN 15040
15070 GO TO 900
15080 PRINT  \ GOSUB 20020
15090 PRINT "WHAT IS THE DISTANCE FROM THE ENTRANCE SLIT TO THE ORIFICE";
15100 INPUT A3
15110 IF A3<0 THEN 15080
15120 GO TO 900
15130 PRINT  \ PRINT "WILL A MASK BE USED(Y/N)";
15140 INPUT R$
15150 A4=100 \ A5=100 \ A6=5.20000E-03
15160 IF R$="N" THEN 900
15170 PRINT  \ GOSUB 20000
15180 PRINT "WHAT IS THE HEIGHT OF THE MASK";
15190 INPUT A4
15200 IF A4<=0 THEN 15170
15210 PRINT "WHAT IS THE WIDTH OF THE MASK";
15220 INPUT A5
15230 IF A5<=0 THEN 15210
15240 PRINT  \ GOSUB 20020
15250 PRINT "YOU CAN NOT ENTER ZERO(TRY 0.01)."
15260 PRINT "WHAT IS THE DISTANCE FROM THE ENTRANCE SLIT TO THE MASK";
15270 INPUT A6
15280 IF A6=0 THEN 15240
15290 GO TO 900
15300 PRINT  \ PRINT "WILL A 2ND MASK BE USED(Y/N)";
15310 INPUT E$
15320 C1=1 \ C2=1 \ C3=1.202
15330 IF E$="N" THEN 900
15340 GOSUB 20000 \ PRINT "WHAT IS THE HEIGHT OF THE 2ND MASK";
15350 INPUT C1
15360 IF C1<=0 THEN 15340
15370 PRINT "WHAT IS THE WIDTH OF THE 2ND MASK";
15380 INPUT C2
15390 IF C2<=0 THEN 15370
15400 GOSUB 20020
15410 PRINT "DO NOT ENTER ZERO FOR DISTANCE."
15420 PRINT "WHAT IS THE DISTANCE FROM THE ENTRANCE SLIT TO THE 2ND MASK";
15430 INPUT C3
15440 IF C3=0 THEN 15410
15450 GO TO 900
15460 PRINT  \ PRINT "IF THE ORIFICE IS WITHIN THE TORCH,SPECIFY DISTANCE";
15470 PRINT " AS NEGATIVE."
15480 PRINT "WHAT IS THE DISTANCE FROM THE ORIFICE TO THE TOP OF THE TORCH";
15490 INPUT A7
15500 GO TO 900
```

Table C-I. (Continued)

FILENAME: ADVFOV.BAS PAGE 5

```
15510 PRINT  \ PRINT "DO YOU WISH TO CALCULATE A FIELD OF VIEW FOR A CERTAIN"
15520 PRINT "OBSERVATION HEIGHT ABOVE THE LOAD COIL(Y/N)";
15530 INPUT D$
15540 IF D$="N" THEN 900
15550 PRINT "BE SURE THAT THE HEIGHT ABOVE THE LOAD COIL DOES NOT EXCEED"
15560 PRINT "THE DISTANCE BETWEEN THE LOAD COIL AND THE CONE ORIFICE."
15570 PRINT "AT WHAT HEIGHT ABOVE THE LOAD COIL,DO YOU WISH TO CALCULATE"
15580 PRINT "A FIELD OF VIEW";
15590 INPUT X
15600 IF X)T1+A7 THEN 15550
15610 GO TO 900
17000 PRINT #P,"MACRO BEGIN"
17010 PRINT #P," CLIN (";S1#R;",0),(0,0),(0,";1#R;"),(";S1#R;",";1#R;")"
17020 PRINT #P," LIN (0,0),(";3#R;",";1#R;");(";4#R;",0),(";7#R;",";
17021 PRINT #P,1#R;")"
17025 PRINT #P," LIN (";8#R;",0),(";11#R;",";1#R;")"
17030 PRINT #P," LIN (";12#R;",0),(";15#R;",";1#R;");(";16#R;",0),(";
17031 PRINT #P,19#R;",";1#R;")"
17035 PRINT #P," LIN (";20#R;",0),(";23#R;",";1#R;")"
17040 PRINT #P," LIN (";24#R;",0),(";27#R;",";1#R;");(";28#R;",0),(";
17041 PRINT #P,31#R;",";1#R;")"
17045 PRINT #P," LIN (";32#R;",0),(";35#R;",";1#R;")"
17050 PRINT #P," LIN (";36#R;",0),(";39#R;",";1#R;");(";40#R;",0),(";
17051 PRINT #P,43#R;",";1#R;")"
17060 PRINT #P," LIN (";44#R;",0),(";47#R;",";1#R;");(";48#R;",0),(";
17061 PRINT #P,51#R;",";1#R;")"
17070 PRINT #P,"MACRO END"
17080 PRINT #P,"MACRO EXECUTE (";(W+A8)#R;",";(Y+M1(I)+(D1/2-1))#R;")"
17090 PRINT #P,"MACRO EXECUTE (";(W+A8)#R;",";(Y+M1(I)-(D1/2))#R;")"
17100 PRINT #P,"MACRO BEGIN"
17110 PRINT #P," CLIN (";(S1-T2)#R;",0),(";X1#R;",0),(";X1#R;",";
17111 PRINT #P,1#R;"),(";(S1-T2)#R;",";1#R;")"
17120 PRINT #P,"MACRO END"
17130 PRINT #P,"MACRO EXECUTE (";(W+D)#R;",";(Y+M1(I)+(D1/2-3))#R;")"
17140 PRINT #P,"MACRO EXECUTE (";(W+D)#R;",";(Y+M1(I)-(D1/2-2))#R;")"
17150 PRINT #P,"MACRO BEGIN"
17160 PRINT #P," CIR ";.25#L;" (0,";(D1/2+3)#R;")"
17170 PRINT #P," LIN (";-1.75#R;",";D1/2#R;"),(";-1.25#R;",";(D1/2+3)#R;")"
17180 PRINT #P," LIN (";.75#R;",";D1/2#R;"),(";1.25#R;",";(D1/2+3)#R;")"
17190 PRINT #P,"MACRO END"
17200 FOR I1=1.25 TO 11.25 STEP 5
17210 PRINT #P,"MACRO EXECUTE (";(W+C+X1+I1)#R;",";(Y+M1(I))#R;")"
17220 PRINT #P,"MACRO EXECUTE (";(W+C+X1+I1)#R;",";(Y+M1(I))#R;"),180"
17230 NEXT I1
17240 RETURN
17300 U1=R#(D+X1+3) \ U2=(D+X1)#R \ U3=S#3#R
17310 PRINT #P,"CLIN (";(A8+S1)#R;",";U3;"),(";U1;",";U3;"),(";U2;",";U3/2;")"
17320 PRINT #P,"CLIN (";U2;",";U3/2;"),(";U2;",";U3/6;"),(";U1;",";S#2#R;")"
17330 PRINT #P,"CLIN (";U1;",";S#2#R;"),(";(A8+S1)#R;",";S#2#R;")"
17340 RETURN
17400 PRINT #P,"MACRO BEGIN"
17410 PRINT #P," CLIN (";-.5#R;",";2#S#R;"),(";-11#R;",";8#S#R;"),(";
17411 PRINT #P,-11#R;",";15#S#R;")"
17420 PRINT #P," CLIN (";-11#R;",";15#S#R;"),(";-14#R;",";15#R#S;")"
17430 PRINT #P," CLIN (";-14#R;",";15#S#R;"),(";-14#R;",";8#S#R;")";
17440 PRINT #P,",(0,0),(";-.5#R;",";2#S#R;")"
17450 PRINT #P,"MACRO END"
```

Table C-I. (Continued)

FILENAME: ADVFOV.BAS PAGE 6

```
17460 PRINT #P,"MACRO EXECUTE (";(W+A3)*R;",";(Y+S*F(I))*R;")"
17470 RETURN
17500 PRINT #P,"MACRO EXECUTE (";(W+A6)*R;",";(Y+M(I))*R;")"
17510 PRINT #P,"MACRO EXECUTE (";(W+A6)*R;",";(Y-M(I))*R;"),180"
17520 RETURN
17600 PRINT #P,"MACRO EXECUTE (";(W+C3)*R;",";(Y+K(I))*R;")"
17610 PRINT #P,"MACRO EXECUTE (";(W+C3)*R;",";(Y-K(I))*R;"),180"
17620 RETURN
17700 PRINT #P,"LIN (0,";.1*R;"),(0,";10*R;")"
17705 PRINT #P,"LIN (0,";-.1*R;"),(0,";-10*R;")"
17710 RETURN
17750 PRINT #P,"LIN (0,";S1/2*R;"),(0,";(S1/2+10)*R;");(0,";
17760 PRINT #P,-S1/2*R;"),(0,";(-S1/2-10)*R;")"
17770 RETURN
17800 PRINT #P,"CLET 0.4 (";A3*R;",";(-P3*R)-.4;")WO"
17810 PRINT #P,"CLET 0.4 (";C*R;",";(-P3*R)-.4;")WC"
17820 PRINT #P,"CLET 0.4 (";D*R;",";(-P3*R)-.4;")WB"
17825 IF A3=0 THEN 17850
17830 PRINT #P,"CLET 0.4 (0,";12*R;")B"
17850 RETURN
17900 PRINT #P,"CLET 0.4 (";A3*R;",";(-P3*R)-.4;")HO"
17910 PRINT #P,"CLET 0.4 (";C*R;",";(-P3*R)-.4;")HC"
17920 PRINT #P,"CLET 0.4 (";D*R;",";(-P3*R)-.4;")HB"
17925 IF A3=0 THEN 17950
17930 PRINT #P,"CLET 0.4 (0,";(S1/2+12)*R;")B"
17950 RETURN
18000 PRINT #P,"LET 0.7 (.2,9.50)TOP VIEW"
18010 PRINT #P,"LET 0.3 (.2,9.0)-DEPENDENT UPON:"
18020 PRINT #P,"LET 0.3 (.2,8.8)   ";H$
18030 PRINT #P,"LET 0.3 (.2,8.6)   ";G$
18040 PRINT #P,USING W$,6.9,"WO=",R5
18050 PRINT #P,USING W$,6.6,"WC=",L5
18060 PRINT #P,USING W$,6.3,"WB=",B5
18070 PRINT #P,USING W$,6,"WG=",G5
18080 RETURN
18200 PRINT #P,"LET 0.7 (.2,5.00)SIDE VIEW"
18210 PRINT #P,"LET 0.3 (.2,4.5)-DEPENDENT UPON:"
18220 PRINT #P,"LET 0.3 (.2,4.3)   ";J$
18230 PRINT #P,"LET 0.3 (.2,4.1)   ";K$
18240 PRINT #P,USING W$,2.5,"HO=",R6
18250 PRINT #P,USING W$,2.2,"HC=",L6
18260 PRINT #P,USING W$,1.9,"HB=",B6
18270 PRINT #P,USING W$,1.6,"HG=",G6
18280 IF S$="N" THEN 18500
18290 IF V$="N" THEN 18460
18300 PRINT #P,"LET 0.2 (.2,3.45)-INNER BOUNDARY(- - -) OF"
18310 PRINT #P,"LET 0.2 (.2,3.30) VIGNETTED REGION:"
18320 PRINT #P,USING Y$,3.15,"VB=",B4
18330 IF L4>0 THEN PRINT #P,USING Y$,3,"VC=",L4
18340 IF R4>0 THEN PRINT #P,USING Y$,2.85,"VO=",R4
18350 REM VIGNETTED INNER BOUNDARY DRAWING
18370 FOR I4=0 TO 8 STEP 2
18380 PRINT #P,"LIN (";FNX(I4);",";FNY(I4);"),(";FNX(I4+1);",";FNY(I4+1);")"
18390 PRINT #P,"LIN (";FNX(I4);",";FNY(-I4);"),(";FNX(I4+1);",";FNY(-I4-1);
18391 PRINT #P,")"
18400 NEXT I4
18450 GO TO 18500
```

Table C-I. (Continued)

FILENAME: ADVFOV.BAS PAGE 7

```
18460 PRINT #P,"LET 0.2 (.2,3.45)-THE ENTIRE SIDE FIELD OF VIEW"
18470 PRINT #P,"LET 0.2 (.2,3.30) TO THE BASE OF THE PLASMA"
18480 PRINT #P,"LET 0.2 (.2,3.15) IS A VIGNETTED REGION."
18500 RETURN
19000 PRINT #P,"LET 0.2 (.2,1.05)PARAMETERS:DISTANCES IN MM"
19010 PRINT #P,"CLIN (0,1.18),(3,1.18),(3,1.00)"
19020 PRINT #P,"LIN (0,1.00),(";15-(30*R+.9);",1.00)"
19030 PRINT #P,"LET 0.2 (.3,0.87)HEIGHT OF ORIFICE=";A1
19040 PRINT #P,"LET 0.2 (.3,0.74)WIDTH OF ORIFICE=";A2
19050 PRINT #P,"LET 0.2 (.3,0.61)ENTRANCE SLIT TO ORIFICE=";A3
19060 PRINT #P,"LET 0.2 (.3,0.48)ORIFICE TO TOP OF TORCH=";A7
19070 IF R$="N" THEN 19110
19080 PRINT #P,"LET 0.2 (.3,0.35)HEIGHT OF MASK(D)=";A4
19090 PRINT #P,"LET 0.2 (.3,0.22)WIDTH OF MASK(D)=";A5
19100 PRINT #P,"LET 0.2 (.3,0.09)ENTRANCE SLIT TO MASK(D)=";A6
19110 PRINT #P,"LET 0.2 (3.8,0.87)GRATING TO ENTRANCE SLIT=";G1
19120 PRINT #P,"LET 0.2 (3.8,0.74)DIAMETER OF QUARTZ TORCH=";D1
19130 IF A3=0 THEN 19150
19135 PRINT #P,"LET 0.2 (3.8,0.61)HEIGHT OF ENTRANCE SLIT=";S1
19140 PRINT #P,"LET 0.2 (3.8,0.48)WIDTH OF ENTRANCE SLIT= NEGLIGIBLE"
19150 IF E$="N" THEN 19190
19160 PRINT #P,"LET 0.2 (3.8,0.35)HEIGHT OF 2ND MASK(E)=";C1
19170 PRINT #P,"LET 0.2 (3.8,0.22)WIDTH OF 2ND MASK(E)=";C2
19180 PRINT #P,"LET 0.2 (3.8,0.09)ENTRANCE SLIT TO 2ND MASK(E)=";C3
19190 PRINT #P,"LET 0.2 (7.3,0.87)TOP OF TORCH TO TOP OF LOAD COIL=";T1
19200 PRINT #P,"LET 0.2 (7.3,0.74)TOP OF TORCH TO BASE OF PLASMA=",T2
19210 PRINT #P,"LET 0.2 (7.3,0.61)DIMENSIONS OF GRATING=";H1;"HIGH"
19220 PRINT #P,"LET 0.2 (7.3,0.48)                    ";W1;"WIDE"
19230 IF A$="N" THEN 19300
19240 PRINT #P,"LET 0.2 (7.3,0.35)PLASMA OFFCENTERED BY ";M1(1);"MM"
19300 RETURN
20000 PRINT "REMEMBER,YOU CAN NOT ENTER A NEGATIVE NUMBER OR ZERO(TRY 0.01)."
20010 RETURN
20020 PRINT "REMEMBER,THE ENTRANCE SLIT WILL BE DESIGNATED AS DISTANCE ZERO"
20030 PRINT "WITH POINTS TOWARD THE ORIFICE AS POSITIVE AND POINTS TOWARD"
20040 PRINT "THE GRATING AS NEGATIVE."
20050 RETURN
20060 L4=0 \ R4=0 \ M4=0
20070 S4=0 \ E4=0
20080 RETURN
20090 PRINT  \ PRINT "PLEASE WAIT, SCIENCE TAKES TIME!"
20100 RETURN
30000 CLOSE
31000 END
```

Table C-I. (Continued)

FILENAME: FVADD1.BAS PAGE 001

```
3000 REM THIS SECTION INVOLVES THE CALCULATION OF THE SIDE FIELD OF VIEW
3010 REM THAT IS INDEPENDENT OF THE DIMENSIONS OF THE GRATING. IF NOT,
3020 REM IT WILL PROCEED TO ANOTHER SECTION.
3030 REM FNB IS A FUNCTION THAT USES SIMILIAR TRIANGLES TO FIND THE INTERSECTION
3040 REM POINT OF THE TWO LINES FROM THE FIELD OF VIEW THAT IS DEPENDENT
3050 REM UPON THE F5,F7 AND F4,F6.
3060 REM FNC IS A FUNCTION THAT USES SIMILIAR TRIANGLES AND FUNCTION FNB TO
3070 REM FIND THE FIELD OF VIEW AT LOCATION F8 THAT IS DEPENDENT UPON
3080 REM THE F5,F7 AND F4,F6.
3090 IF A3=0 THEN 3260
3100 IF FNC(0,A6,S1,A4,A3))A1 THEN 3180
3110 IF E$="N" THEN 3130
3120 IF FNC(0,A6,S1,A4,C3))C1 THEN 3330
3130 IF FNC(0,A6,S1,A4,G1))H1 THEN 3720
3140 J$="ENTRANCE SLIT" \ K$="MASK"
3150 X4=0 \ X6=S1
3160 X5=A6 \ X7=A4
3170 GO TO 3500
3180 IF FNC(0,A3,S1,A1,A6))A4 THEN 3260
3190 IF E$="N" THEN 3210
3200 IF FNC(0,A3,S1,A1,C3))C1 THEN 3400
3210 IF FNC(0,A3,S1,A1,G1))H1 THEN 3720
3220 J$="ENTRANCE SLIT" \ K$="CONE ORIFICE"
3230 X4=0 \ X6=S1
3240 X5=A3 \ X7=A1
3250 GO TO 3500
3260 IF E$="N" THEN 3280
3270 IF FNC(A6,A3,A4,A1,C3))C1 THEN 3340
3280 IF FNC(A6,A3,A4,A1,G1))H1 THEN 3720
3290 J$="MASK" \ K$="CONE ORIFICE"
3300 X4=A6 \ X6=A4
3310 X5=A3 \ X7=A1
3320 GO TO 3500
3330 IF FNC(C3,A6,C1,A4,0))S1 THEN 3460
3340 IF FNC(C3,A6,C1,A4,A3))A1 THEN 3410
3350 IF FNC(C3,A6,C1,A4,G1))H1 THEN 3720
3360 J$="2ND MASK" \ K$="MASK"
3370 X4=C3 \ X6=C1
3380 X5=A6 \ X7=A4
3390 GO TO 3500
3400 IF FNC(C3,A3,C1,A1,0))S1 THEN 3460
3410 IF FNC(C3,A3,C1,A1,G1))H1 THEN 3720
3420 J$="2ND MASK" \ K$="CONE ORIFICE"
3430 X4=C3 \ X6=C1
3440 X5=A3 \ X7=A1
3450 GO TO 3500
3460 IF FNC(C3,0,C1,S1,G1))H1 THEN 3720
3470 J$="2ND MASK" \ K$="ENTRANCE SLIT"
3480 X4=C3 \ X6=C1
3490 X5=0 \ X7=S1
3500 Z8=FNB(X4,X5,X6,X7)
3510 REM FNF IS A SHORTENED FUNCTION FNC
3520 B6=FNF(X4,X6,Z8,A8+T2) \ L6=FNF(X4,X6,Z8,A8+T1) \ R6=FNF(X4,X6,Z8,A3)
3530 M6=FNF(X4,X6,Z8,A6) \ G6=FNF(X4,X6,Z8,G1) \ S6=FNF(X4,X6,Z8,C3)
3540 E6=FNF(X4,X6,Z8,A8+T1-X) \ P6=FNF(X4,X6,Z8,-85)
3550 REM THIS SECTION DETERMINES,TO WHAT DEGREE,VIGNETTING OCCURS WITHIN THE
3560 REM SIDE FIELD OF VIEW TO THE BASE OF THE PLASMA.
```

Table C-I. (Continued)

FILENAME: FVADD1.BAS PAGE 2

```
3570 IF X5)X4 THEN 3590
3580 X3=X4 \ X4=X5 \ X5=X3 \ X3=X6 \ X6=X7 \ X7=X3
3590 V$="N" \ IF X7)=X6 THEN 4250
3600 Z6=(X5-X4)/((X6/X7)-1)+X5
3610 IF Z6)=A8+T2 THEN 4250
3620 V$="Y" \ GOSUB 20060
3630 REM FUNCTION FNG CALCULATES THE INNER BOUNDARY OF THE VIGNETTED FIELD
3640 REM OF VIEW BY USE OF SIMILIAR TRIANGLES.
3650 B4=FNG(A8+T2)
3660 IF Z6(A8+T1 THEN L4=FNG(A8+T1)
3670 IF Z6(A3 THEN R4=FNG(A3)
3680 IF R$="Y" THEN IF Z6(A6 THEN M4=FNG(A6)
3690 IF E$="Y" THEN IF Z6(C3 THEN S4=FNG(C3)
3700 IF D$="Y" THEN IF Z6(A8+T1-X THEN E4=FNG(A8+T1-X)
3710 GO TO 4250
3720 REM THIS SECTION INVOLVES THE CALCULATION OF THE SIDE FIELD OF VIEW
3730 REM THAT IS GRATING DEPENDENT.
3740 J$="GRATING"
3750 REM FND IS A FUNCTION THAT USES SIMILIAR TRIANGLES TO FIND THE
3760 REM INTERSECTION POINT OF TWO LINES FROM THE FIELD OF VIEW THAT IS
3770 REM DEPENDENT UPON THE GRATING AND E1,E2.
3780 REM FNE IS A FUNCTION THAT USES SIMILIAR TRIANGLES AND FND TO FIND
3790 REM THE FIELD OF VIEW AT LOCATION E3 THAT IS DEPENDENT UPON THE
3800 REM GRATING AND E1,E2.
3810 IF A3=0 THEN 3920
3820 IF A6(=FND(0,S1) THEN 3840
3830 IF FNE(0,S1,A6))A4 THEN 3920
3840 IF A3(=FND(0,S1) THEN 3860
3850 IF FNE(0,S1,A3))A1 THEN 4000
3860 IF E$="N" THEN 3890
3870 IF C3(=FND(0,S1) THEN 3890
3880 IF FNE(0,S1,C3))C1 THEN 4060
3890 K$="ENTRANCE SLIT"
3900 S7=0 \ S8=S1
3910 GO TO 4080
3920 IF A3(=FND(A6,A4) THEN 3940
3930 IF FNE(A6,A4,A3))A1 THEN 4000
3940 IF E$="N" THEN 3970
3950 IF C3(=FND(A6,A4) THEN 3970
3960 IF FNE(A6,A4,C3))C1 THEN 4060
3970 K$="MASK"
3980 S7=A6 \ S8=A4
3990 GO TO 4080
4000 IF E$="N" THEN 4030
4010 IF C3(=FND(A3,A1) THEN 4030
4020 IF FNE(A3,A1,C3))C1 THEN 4060
4030 K$="CONE ORIFICE"
4040 S7=A3 \ S8=A1
4050 GO TO 4080
4060 K$="2ND MASK"
4070 S7=C3 \ S8=C1
4080 Z8=FND(S7,S8) \ B6=FNE(S7,S8,A8+T2) \ L6=FNE(S7,S8,A8+T1)
4090 R6=FNE(S7,S8,A3) \ M6=FNE(S7,S8,A6) \ G6=FNE(S7,S8,G1)
4100 S6=FNE(S7,S8,C3) \ E6=FNE(S7,S8,A8+T1-X) \ P6=FNE(S7,S8,-85)
4110 REM THIS SECTION DETERMINES,TO WHAT DEGREE,VIGNETTING OCCURS WITHIN THE
4120 REM SIDE FIELD OF VIEW TO THE BASE OF THE PLASMA.
4130 V$="N" \ IF S8)=H1 THEN 4250
```

Table C-I. (Continued)

FILENAME: FVADD1.BAS PAGE 3

```
4140 Z6=(S7-G1)/((H1/S8)-1)+S7
4150 IF Z6)=A8+T2 THEN 4250
4160 V$="Y" \ GOSUB 20060
4170 REM FUNCTION FNH CALCULATES THE INNER BOUNDARY OF THE VIGNETTED FIELD
4180 REM OF VIEW BY USE OF SIMILIAR TRIANGLES.
4190 B4=FNH(A8+T2)
4200 IF Z6(A8+T1 THEN L4=FNH(A8+T1)
4210 IF Z6(A3 THEN R4=FNH(A3)
4220 IF R$="Y" THEN IF Z6(A6 THEN M4=FNH(A6)
4230 IF E$="Y" THEN IF Z6(C3 THEN S4=FNH(C3)
4240 IF D$="Y" THEN IF Z6(A8+T1-X THEN E4=FNH(A8+T1-X)
4250 OVERLAY "FVADD2" LINE 3000
4260 REM
4270 REM
```

Table C-I. (Continued)

```
FILENAME:   FVADD2.BAS                                    PAGE 001


3000 REM THE FOLLOWING ARE DEFINITIONS TO FACILITATE A SHORTER PRINTOUT. X(1)S
3010 REM RELATE TO THE TOP FIELD OF VIEW AND X(2)S
3020 REM RELATE TO THE SIDE VIEW. OTHER DEFINITIONS CAN BE DETERMINED FROM
3030 REM THE PART OF THE PROGRAM THAT PRINTS OUT THE FIELD OF VIEW DATA.
3040 N$(1)=" TOP " \ N$(2)=" SIDE "
3050 M$(1)=" SIDE " \ M$(2)=" TOP "
3060 P$(1)=" OTHER SIDE " \ P$(2)=" BOTTOM "
3070 Q$(1)=" WIDTH " \ Q$(2)=" HEIGHT "
3080 K(1)=C2/2 \ K(2)=C1/2
3090 M(1)=A5/2 \ M(2)=A4/2 \ F(1)=A2/2 \ F(2)=A1/2
3100 G(1)=W1/2 \ G(2)=H1/2 \ V1(1)=B5/2*SGN(A8+T2) \ V1(2)=B6/2*SGN(A8+T2-Z8)
3110 V2(1)=L5/2*SGN(A8+T1) \ V2(2)=L6/2*SGN(A8+T1-Z8) \ V3(1)=R5/2*SGN(A3)
3120 V3(2)=R6/2*SGN(A3-Z8) \ V4(1)=M5/2*SGN(A6) \ V4(2)=M6/2*SGN(A6-Z8)
3130 V5(1)=G5/2*SGN(G1) \ V5(2)=G6/2*SGN(G1-Z8)
3140 V6(1)=S5/2*SGN(C3) \ V6(2)=S6/2*SGN(C3-Z8)
3150 V7(1)=E5/2*SGN(A8+T1-X) \ V7(2)=E6/2*SGN(A8+T1-X-Z8)
3160 V8(1)=P5/2*SGN(-85) \ V8(2)=P6/2*SGN(-85-Z8)
3170 REM
3180 IF C$="N" THEN 3200
3190 OPEN B$ FOR OUTPUT AS FILE #P1
3200 FOR N1=1 TO 2
3210 IF N1=1 THEN P=P1
3220 PRINT #P, \ PRINT #P,"  PARAMETERS OF THE FIELD OF VIEW CALCULATIONS"
3230 PRINT #P,"============================================================"
3240 PRINT #P, \ PRINT #P,"  DISTANCES IN MM"
3250 PRINT #P,"--------------------"
3260 PRINT #P,"HEIGHT OF THE ORIFICE= ";A1
3270 PRINT #P,"WIDTH OF THE ORIFICE= ";A2
3280 PRINT #P,"FROM ENTRANCE SLIT TO THE ORIFICE= ";A3
3290 IF R$="N" THEN 3330
3300 PRINT #P,"HEIGHT OF THE MASK= ";A4
3310 PRINT #P,"WIDTH OF THE MASK= ";A5
3320 PRINT #P,"FROM ENTRANCE SLIT TO THE MASK= ";A6
3330 IF E$="N" THEN 3370
3340 PRINT #P,"HEIGHT OF THE 2ND MASK= ";C1
3350 PRINT #P,"WIDTH OF THE 2ND MASK= ";C2
3360 PRINT #P,"FROM THE ENTRANCE SLIT TO THE 2ND MASK= ",C3
3370 PRINT #P,"FROM THE ORIFICE TO THE TOP OF THE TORCH= ";A7
3380 PRINT #P,"FROM THE GRATING TO THE ENTRANCE SLIT= ",G1
3390 PRINT #P,"FROM THE TOP OF THE TORCH TO THE TOP OF THE LOAD COIL= ";T1
3400 PRINT #P,"FROM THE TOP OF THE TORCH TO THE BASE OF THE PLASMA= ";T2
3410 IF A3=0 THEN 3440
3420 PRINT #P,"HEIGHT OF THE ENTRANCE SLIT= ";S1
3430 PRINT #P,"WIDTH OF THE ENTRANCE SLIT= NEGLIGIBLE."
3440 PRINT #P,"DIMENSIONS OF THE GRATING= ";H1;" HIGH, ";W1;" WIDE."
3450 PRINT #P,"DIAMETER OF THE QUARTZ TORCH= ";D1
3460 PRINT #P, \ PRINT #P, \ PRINT #P,"     FIELD OF VIEW"
3470 PRINT #P,"=========================" \ PRINT #P,
3480 PRINT #P,"THE FIELD OF VIEW HAS THE DIMENSIONS OF ";R6;" MM HIGH AND "
3490 PRINT #P,R5;" MM WIDE AT THE PLANE OF THE SAMPLING ORIFICE, ";L6;" MM"
3500 PRINT #P,"HIGH AND ";L5;" MM WIDE AT THE TOP OF THE LOAD COIL, AND "
3510 PRINT #P,B6;" MM HIGH AND ";B5;" MM WIDE AT THE BASE OF THE PLASMA,"
3520 PRINT #P,"WHEN VIEWING END-ON,THROUGH THE PLASMA AXIAL CHANNEL."
3530 IF R$="N" THEN 3570
3540 PRINT #P,
3550 PRINT #P,"THE FIELD OF VIEW HAS THE DIMENSIONS OF ";M6;" MM HIGH"
3560 PRINT #P,"AND ";M5;" MM WIDE AT THE PLANE OF THE MASK"
```

Table C-I. (Continued)

FILENAME: FVADD2.BAS PAGE 2

```
3570 IF E$="N" THEN 3600
3580 PRINT #P,"AND ";S6;" MM HIGH AND ";S5;" MM WIDE AT THE PLANE OF "
3590 PRINT #P,"THE 2ND MASK."
3600 PRINT #P,
3610 IF G$="GRATING" THEN PRINT #P,"THE GRATING WIDTH IS FULLY ILLUMINATED."
3620 IF J$="GRATING" THEN PRINT #P,"THE GRATING HEIGHT IS FULLY ILLUMINATED."
3630 PRINT #P,"THE ILLUMINATED AREA AT THE PLANE OF THE GRATING IS ";G6;" MM";
3640 PRINT #P," HIGH"
3650 PRINT #P,"AND ";G5;" MM WIDE,WHEN LIGHT DIFFRACTION IS NEGLECTED."
3660 PRINT #P,
3670 IF D$="N" THEN 3710
3680 PRINT #P,"THE FIELD OF VIEW HAS THE DIMENSIONS OF ";E6;" MM HIGH AND"
3690 PRINT #P,E5;" MM WIDE AT A HEIGHT OF ";X;" MM ABOVE THE LOAD COIL."
3700 PRINT #P,
3710 PRINT #P,"THE TOP FIELD OF VIEW IS DEPENDENT UPON THE DIMENSIONS";
3720 PRINT #P,"(WIDTHS) OF THE "
3730 PRINT #P,G$;" AND ";H$;"(WHICH HAS NEGLIGIBLE WIDTH)."
3740 PRINT #P,"THE SIDE FIELD OF VIEW IS DEPENDENT UPON THE DIMENSIONS",
3750 PRINT #P,"(HEIGHTS) OF THE"
3760 PRINT #P,J$;" AND ";K$;" ."
3770 IF V$="Y" THEN 3810
3780 PRINT #P," THE ENTIRE SIDE FIELD OF VIEW TO THE BASE OF THE PLASMA IS"
3790 PRINT #P," A VIGNETTED REGION."
3800 GO TO 3910
3810 PRINT #P," DIMENSIONS OF THE INNER BOUNDARY OF THE VIGNETTED REGION";
3820 PRINT #P,"(SIDE VIEW):"
3830 PRINT #P,"  AT BASE OF PLASMA= ";B4;" MM HIGH."
3840 IF L4>0 THEN PRINT #P,"  AT TOP OF LOAD COIL= ";L4;" MM HIGH."
3850 IF R4>0 THEN PRINT #P,"  AT SAMPLING ORIFICE= ";R4;" MM HIGH."
3860 IF M4>0 THEN PRINT #P,"  AT MASK= ";M4;" MM HIGH."
3870 IF S4>0 THEN PRINT #P,"  AT 2ND MASK= ",S4;" MM HIGH."
3880 IF E4>0 THEN PRINT #P,"  AT";X;" MM ABOVE TOP OF LOAD COIL=";E4;" MM HIGH"
3890 PRINT #P,"  AND ORIGINATES AT ";Z6-A3;" MM IN FRONT OF THE SAMPLING"
3900 PRINT #P,"  ORIFICE."
3910 PRINT #P,
3920 REM
3930 IF P1=0 THEN 8000
3940 PRINT #P,
3950 PRINT #P,
3960 PRINT #P,"THE FIELD OF VIEW DATA ARE STORED IN FILE ",B$
3970 REM
3980 IF N1=2 THEN 4050
3990 P=0
4000 CLOSE #P1
4010 PRINT "PLEASE PRESS THE RETURN KEY TO PRINTOUT THE FIELD OF VIEW DATA "
4020 PRINT "ON THE TERMINAL.";
4030 INPUT I$
4040 NEXT N1
4050 PRINT  \ PRINT "-------------------------------------------------------"
4060 PRINT  \ PRINT "IN ORDER TO PRINT A HARD COPY OF THE PARAMETERS AND THE"
4070 PRINT "DIMENSIONS OF THE FIELD OF VIEW,FOLLOW THE INSTRUCTIONS GIVEN";
4080 PRINT " BELOW."
4090 PRINT  \ PRINT "  1)ATTACH THE CABLE FROM THE TERMINAL TO THE PRINTER."
4100 PRINT "    TURN ON THE PRINTER,AND PRESS THE ON LINE BUTTON."
4110 PRINT "  2)TYPE  'R PRINT'"
4120 PRINT "  3)PRESS  (RETURN)"
4130 PRINT "  4)TYPE  'Y' IF YOU WANT A COMPRESSED PRINTOUT"
```

Table C-I. (Continued)

```
FILENAME:  FVADD2.BAS                                    PAGE  3


4140 PRINT "    PRESS  (RETURN) IF YOU WANT A NORMAL SPACED PRINTOUT"
4150 PRINT "  5)TYPE YOUR FILENAME  '";B$;"'"
4160 PRINT "  6)TYPE AN OTHER FILENAMES TO BE PRINTED,THEN PRESS (RETURN)"
4170 PRINT "    TO START THE PRINTER."
4180 PRINT  \ PRINT "-------------------------------------------------------"
4190 GO TO 8000
4200 REM
4210 REM
```

Table C-I. (Continued)

FILENAME: FVADD3.BAS PAGE 001

```
3000 OPEN T$ FOR OUTPUT AS FILE #P
3010 REM W AND Y ARE USED TO SET THE ORIGIN.
3020 REM R IS USED AS THE MAGNIFICATION FACTOR.
3030 REM S IS USED FOR VALUES +1 AND -1
3040 W=0 \ Y=0
3050 R=.06
3060 C=A8+T1 \ D=A8+T2 \ L=R*25
3070 S=1 \ X1=.5
3080 REM START LOADING INFO INTO FILE #P FOR EDRAW PROGRAM
3090 REM  I=1 FOR TOP VIEW    , I=2 FOR SIDE VIEW
3100 FOR I=1 TO 2
3110 W=135
3120 IF I=1 THEN Y=128.5
3130 IF I=2 THEN Y=53.5
3140 PRINT #P,"ORG (";W*R;",";(Y+M1(I))*R;")"
3150 GOSUB 17000
3160 S=1
3170 GOSUB 17300
3180 S=-1
3190 GOSUB 17300
3200 PRINT #P,"ORG (";W*R;",";Y*R;")"
3210 S=1
3220 GOSUB 17400
3230 S=-1
3240 GOSUB 17400
3250 IF R$="N" THEN IF E$="N" THEN 3320
3260 PRINT #P,"MACRO BEGIN"
3270 PRINT #P," CLIN (";.15*R;",";12*R;"),(";.15*R;",0),(";-.15*R;",0)"
3280 PRINT #P," CLIN (";-.15*R;",0),(";-.15*R;",";12*R;")"
3290 PRINT #P,"MACRO END"
3300 IF R$="Y" THEN IF A6)-85 THEN  GOSUB 17500
3310 IF E$="Y" THEN IF C3)-85 THEN  GOSUB 17600
3320 IF A3=0 THEN 3340
3330 ON I GOSUB 17700,17750
3340 PRINT #P,"LIN (";D*R;",";V1(I)*R;"),(";-85*R;",";V8(I)*R;")"
3350 PRINT #P,"LIN (";D*R;",";-V1(I)*R;"),(";-85*R;",";-V8(I)*R;")"
3360 PRINT #P,"MACRO BEGIN"
3370 PRINT #P," ARR 0.18,0 (0,0)"
3380 PRINT #P," LIN (0,0),(-0.12,0)"
3390 PRINT #P,"MACRO END"
3400 PRINT #P,"MACRO EXECUTE (";(W+D)*R;",";(Y+ABS(V1(I)))*R;"),-90"
3410 PRINT #P,"MACRO EXECUTE (";(W+D)*R;",";(Y-ABS(V1(I)))*R;"),90"
3420 PRINT #P,"MACRO EXECUTE (";(W+C)*R;",";(Y+ABS(V2(I)))*R;"),-90"
3430 PRINT #P,"MACRO EXECUTE (";(W+C)*R;",";(Y-ABS(V2(I)))*R;"),90"
3440 P3=ABS(V1(I))
3450 IF ABS(V1(I)))D1/2+5-M1(I) THEN 3480
3460 P3=D1/2+5-M1(I)
3470 IF D1/2+5-M1(I))F(I)+9 THEN 3500
3480 IF ABS(V1(I)))F(I)+9 THEN 3500
3490 P3=F(I)+9
3500 PRINT #P,"MACRO EXECUTE (";(W+A3)*R;",";(Y-P3)*R;"),90"
3510 REM
3520 ON I GOSUB 17800,17900
3530 PRINT #P,"CLET 0.4 (";(A8+40)*R;",";((D1/2)+M1(I)+2)*R;")A"
3540 PRINT #P,"CLET 0.4 (";(A3-12.5)*R;",";(F(I)+17)*R;")C"
3550 IF R$="N" THEN 3580
3560 IF A6(=-85 THEN 3580
```

Table C-I. (Continued)

```
FILENAME:   FVADD3.BAS                                          PAGE  2


3570 PRINT #P,"CLET 0.4 (";A6$R;",";(M(I)+14)*R;")D"
3580 IF E$="N" THEN 3610
3590 IF C3<=-85 THEN 3610
3600 PRINT #P,"CLET 0.4 (";C3*R;",";(K(I)+14)*R;")E"
3610 PRINT #P,"ORG (0,0)"
3620 W$="LET 0.4 (.2,#.##)'LL###.#"
3630 Y$="LET 0.2 (.2,#.##)  'LL###.# MM"
3640 ON I GOSUB 18000,18200
3650 I2=0
3660 IF I=2 THEN I2=4.4
3670 FOR I3=60 TO 69 STEP 3
3680 PRINT #P,"LET 0.3 (1.7,";I3/10-I2;")MM"
3690 NEXT I3
3700 NEXT I
3710 IF L$="N" THEN 3740
3720 REM
3730 GOSUB 19000
3740 PRINT #P,"MACRO BEGIN"
3750 PRINT #P," CLIN (0,.3),(0,0),(";30*R;",0),(";30*R;",.3)"
3760 PRINT #P," LIN (";10*R;",0),(";10*R;",.3);(";20*R;",0),(";20*R;",.3)"
3770 PRINT #P," CLET 0.3 (0,.36)0"
3780 PRINT #P," CLET 0.3 (";10*R;",.36)1"
3790 PRINT #P," CLET 0.3 (";20*R;",.36)2"
3800 PRINT #P," CLET 0.3 (";30*R;",.36)3"
3810 PRINT #P," LET 0.4 (";30*R+.1;",0)CM"
3820 PRINT #P,"MACRO END"
3830 PRINT #P,"MACRO EXECUTE (";15-(30*R+.6);",0.3)"
3840 PRINT #P,"CLIN (15,1.00),(";15-(30*R+.9);",1.00),(";15-(30*R+.9);",0)"
3850 PRINT #P,"REC (0,0),(15,10)"
3860 PRINT #P,"LIN (0,5.50),(15,5.50)"
3870 PRINT  \ PRINT "-------------------------------------------------"
3880 PRINT  \ PRINT "IN ORDER TO PLOT YOUR RAY DIAGRAMS ON THE PLOTTER WITH THE"
3890 PRINT "EDRAW PROGRAM,FOLLOW THE INSTRUCTIONS BELOW."
3900 PRINT  \ PRINT "  1)TURN THE PLOTTER ON,SET A PEN IN HOLDER#1, AND SET THE"
3910 PRINT "    PLOT LIMITS TO SLIGHTLY GREATER THAN A 10 INCH HIGH AND 15 INCH"
3920 PRINT "    WIDE RECTANGLE."
3930 PRINT "  2)TYPE  'LOAD IB'"
3940 PRINT "  3)TYPE  'R EDRAW'"
3950 PRINT "  4)TYPE  'PLT'"
3960 PRINT "  5)TYPE YOUR FILENAME  '";T$;"'"
3970 PRINT "  6)TYPE  '1.0015'"
3980 PRINT "  7)PRESS  (RETURN)"
3990 PRINT "  8)PRESS  (RETURN)"
4000 PRINT "  9)PRESS  (RETURN) IF A NEW PEN IS BEING USED."
4010 PRINT "    TYPE  '6' IF IT IS AN OLD PEN."
4020 PRINT " 10)WAIT! WHEN PLOTTER IS READY,PRESS  (RETURN) IF PLOT LIMITS"
4030 PRINT "    WERE SET."
4040 PRINT  \ PRINT "-------------------------------------------------"
4050 CLOSE #P
4060 GO TO 8000
4070 REM
4080 REM
```

and the specified observation height above the load coil were determined. If the side field of view was not entirely vignetted, the inner boundary of the vignetted region was also calculated. The programs were able to find the two limiting apertures of the cone and monochromator assembly (orifice, mask, etc.) that determined the fields of view. Overlay program, FVADD2.BAS, outputted the values of the parameters of the fields of view calculations and the dimensions of the top and side fields of view into a file that could be printed at a later time. Overlay program, FVADD3.BAS, along with the main program, ADVFOV.BAS, manipulated the data of the fields of view into a file that can be used with EDRAW (a graphics program written at the Ames Laboratory (174)) for the construction of the field of view ray diagrams. The accuracy of the fields of view data should be taken, at least to several tenths of a mm, but normally to 1 mm. Computer printouts of the final resulting data from the programs can be seen in the optical field of view section in Chapter II.

Limits of Detection (LODs)

The computer program; LODS, listed in Table C-II; utilized the data obtained from the ISAAC-Apple IIe computer system during analyte introduction into the Ar ICP in order to calculate the LODs of the analyte. The information that was required for the LODS program was the name of the data file of the disk, the point number of the first background point, the total number of background points wanted for calculation of background noise, the number of peaks in which LOD calculations were needed, an identifying characteristic of each peak (name, retention time, or wavelength), the concentration of the element in the solution for each peak, and the background corrected height for each

Table C-II. BASIC computer program, named LODS, used with the ISAAC-Apple IIe computer system for the calculations of limits of detection of elements determined by ICP-AES or any other technique that measures signal and background values

```
1  REM  NOT REALLY COPYRIGHTED BY
     BRYANT LAFRENIERE -- 2/7/84

2  REM  PROGRAM OF CALCULATIONS O
     F LIMITS OF DETECTIONS FOR D
     ATA OBTAINED BY ISAAC
3  REM  F$=DATA FILE NAME, FI=FIR
     ST BCKGD PT
4  REM  NU=# OF BCKGD PTS(FINAL J
      VALUE), FP=MEMORY SPACE COR
     RESPONDING TO FIRST PT, X()=
     BCKGD PTS, MN=MEAN OF BCKGD,
      SU=SUM, SS=SUM OF SQUARES,
     SD=STD DEVIATION
5  REM     NI=# OF PEAKS, P$()=PEA
     K NAME, CN()=CONC OF PEAK, H
     T()=HEIGHT OF PEAK, FL=FINAL
      BCKGD PT, NS=NOISE, LD=LOD
6  REM  REVISED BY BRYANT LAFRENI
     ERE ---6/18/84
10 D$ =  CHR$ (4): REM  CONTROL D

15  DIM X(250),HT(20),CN(20),P$(2
     0)
18  PRINT "INSERT DATA DISK IN DR
     IVE 2.": PRINT
20  INPUT "TYPE YOUR TOTAL DATA F
     ILE NAME EXACTLY. ";F$: PRINT

30  PRINT D$"BLOAD ";F$;",A8200,D
     2,S6"
45  IF  LEFT$ (K$,1) = "Y" GOTO 9
     0
50  INPUT "TYPE THE POINT # OF YO
     UR FIRST BACKGROUND POINT. "
     ;FI: PRINT
55  IF FI < 0 GOTO 50
60  INPUT "TYPE THE # OF POINTS(I
     NCLUDING AND AFTER THE FIRST
      BACKGROUND POINT) ONE WANTS
      TO USE FOR THE BASELINE NOI
     SE(DO NOT ENTER A # >250). "
     ;NU: PRINT
70  IF NU > 250 OR NU < 1 GOTO 60

90  IF  LEFT$ (Z$,1) = "Y" GOTO 1
     50
100  INPUT "TYPE THE # OF PEAKS(2
     0 PEAKS MAXIMUM) IN WHICH LO
     D CALCULATIONS ARE NEEDED. "
     ;NI: PRINT
103  IF NI > 20 OR NI < 1 GOTO 10
     0
105  PRINT "TYPE 'EACH' PEAK DATA
      SEPARATELY. ": PRINT
110  FOR L = 1 TO NI
120  PRINT "TYPE #";L;" PEAK'S NA
     ME,RET TIME,OR WAVELENGTH(MA
     XIMUM 10 CHARACTERS),A COMMA
     ,CONC IN PPB,A COMMA,AND THE
      BCKGD CORRECTED HEIGHT. "
125  INPUT " ";P$(L),CN(L),HT(L)
130 P$(L) = P$(L) + "          "
135  PRINT
140  NEXT L
150  PRINT : PRINT "PLEASE WAIT,S
     CIENCE TAKES TIME! ": PRINT

180  GOSUB 1000: REM   DETERMINE
     THE MEAN OF THE NOISE

190  GOSUB 1500: REM  DETERMINE T
     HE STD OF THE NOISE
199  PRINT : PRINT
200  PRINT "TURN ON THE PRINTER N
     OW,THEN PRESS A LETTER KEY."
201  GET A$
202  PR# 1
203  PRINT : PRINT : PRINT : PRINT

205 FL = FI + NU - 1
210  PRINT "FOR THE FILE ";F$;" ,
     THE BACKGROUND POINTS FROM P
     OINT#";FI;" TO POINT#";FL;"
     ARE AS FOLLOWS."
220  FOR LL = 1 TO NU
230  PRINT X(LL);" ";
240  NEXT LL
250  PRINT : PRINT
255 RD = SD / MN * 100
260  PRINT "FOR THE BACKGROUND PO
     INTS, MEAN= ";MN;" ,STD DEV=
      ";SD;" ,AND REL STD DEV= ";
     RD;"% RSD"
270  PRINT
280 NS = 3 * SD
290  FOR KK = 1 TO NI
300 LD = CN(KK) * NS / HT(KK)
310  PRINT "FOR THE PEAK "; LEFT$
     (P$(KK),10);" AT A CONCENTRA
     TION OF ";CN(KK);" PPB,WITH
     A HEIGHT OF ";HT(KK);" ,ONE
     CALCULATES A LOD OF ";LD;" P
     PB."
320  PRINT
330  NEXT KK
400  PR# 0: PRINT : PRINT
405 S$ = "N"
410  INPUT "DO YOU WANT TO CALCUL
     ATE MORE LODS?(Y/N) ";S$: PRINT
     : PRINT
420  IF  LEFT$ (S$,1) = "Y" GOTO
     600
500  END
600 Z$ = "N":T$ = "N":K$ = "N"
610  INPUT "DO YOU WANT TO USE TH
     E CURRENT BACKGROUND DATA FI
     LE?(Y/N)";T$: PRINT
620  INPUT "DO YOU WANT TO KEEP T
     HE CURRENT PEAK DATA FOR REC
     ALCULATIONS OF THEIR LODS?(Y
     /N)";Z$: PRINT
625  IF  LEFT$ (T$,1) = "N" GOTO
     18
630  INPUT "DO YOU WANT THE SAME
     BACKGROUND POINTS FOR LOD CA
     LCULATIONS?(Y/N)";K$: PRINT

640  GOTO 45
1000  REM  DETERMINE THE MEAN OF
     THE NOISE
1005 SU = 0
1010 FP = 8210 + FI * 2
1015 NM = NU * 2
1020  FOR I = 2 TO NM STEP 2
1030 J = I / 2
1040 X(J) =  PEEK (FP + I - 2) +
      PEEK (FP + I - 1) * 256
1050 SU = SU + X(J)
1060  NEXT I
1070 MN = SU / NU
1080  RETURN
1500  REM  DETERMINE THE STD OF T
     HE NOISE
1510 SS = 0
1520  FOR K = 1 TO NU
1530 SS = SS + (X(K) - MN) ^ 2
1540  NEXT K
1550 SD =  SQR (SS / NU)
1560  RETURN
```

peak. When ISAAC chromatography module version #1.1.0 was used, the background corrected peak height obtained by the ISAAC-Apple IIe system was multiplied by 100 before the height was inputted into the LODS program. The computer program printed out the background points, the mean, standard deviation, and relative standard deviation of the background points; the concentration of the element in the solution for each peak; and the background corrected height and LOD for each peak.